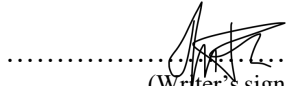




University of
Stavanger

Faculty of Science and Technology

MASTER'S THESIS

Study program/ Specialization: Offshore Technology/Marine and Subsea	Spring semester, 2017 Open
Writer: Thomas Ole Messelt Fadnes	 (Writer's signature)
Faculty supervisor: Prof. Ove Tobias Gudmestad and Prof. Jasna Bogunovic Jakobsen External supervisor(s): Mathias Eidem	
Thesis title: A Full-Scale Study on Traffic Induced Vibrations of a Suspension Bridge	
Credits (ECTS): 30	
Key words: Lysefjorden Bridge Traffic-induced Vibrations Damping Estimation Impact Loading Spectral Analysis	Pages: 111 + enclosure: 81 (192 total) Stavanger, 15/06/2017

A Full-Scale Study on Traffic Induced Vibrations of a Suspension Bridge

Thomas Ole Messelt Fadnes

June 2017

MASTER THESIS

Department of Mechanical and Structural Engineering and Materials Science

University of Stavanger

Supervisor 1: Ove Tobias Gudmestad

Supervisor 2: Jasna Bogunovic Jakobsen

Abstract

This thesis focuses on the traffic-induced vibrations of a suspension bridge, and the modal properties embedded in the traffic-induced response data.

Traffic has been observed at Lysefjorden bridge for five different days with low wind speeds. Observations were synchronized with the acceleration and wind data continuously acquired on the bridge. The purpose of the work has been to study the impact load response from heavy vehicles and estimate the modal damping ratios of the bridge.

In an experiment performed in cooperation with truck driver Anette Ravndal, a 50 tonne truck has crossed the bridge with different velocities from different directions. Findings from this experiment suggest that impact load response is present, but with different magnitude and cause for different vibration modes. For the first modes, response appears to be relatively similar for both exiting and entering the bridge at high velocities, while for higher modes with, frequencies over 1Hz, the impact effect for the vehicle entering the bridge at high velocity appears to be more significant.

Eight modal damping ratios for the bridge have been estimated using viscous damping assumption. This is done by isolating the free decay of the bridge after heavy vehicles have excited and exited the bridge. The results have relatively large variations, but are reasonable compared to other methods used for estimating modal damping ratio for Lysefjorden bridge as well as similar structures in existing literature. These large variations can be explained by variations in wind and temperature, but are also likely due to inaccuracies in filtering of the data.

A spectral analysis of the acceleration time series has been performed using Frequency Domain Decomposition. The findings agree with results from previous studies which show that response from vehicles consists of a combination of both low and higher frequency modes. Also, all identified frequencies agree with those found previously both using analytical methods and the full-scale response measurements with very little deviation.

Acknowledgements

This thesis is the final work of my Master's degree at the University of Stavanger. The work has been challenging, but all in all very interesting and educational.

The work has been supported by the Norwegian Public Road Administration, with Mathias Eidem as the main contact person.

I would like to thank the Norwegian Public Road Administration for giving me the opportunity to write for them, and my advisors Jasna Bogunovic Jakobsen and Ove Tobias Gudmestad for steady guidance, motivation and inspiration from the beginning to the end of the writing process. I would also like to thank Anette Ravndal at Bjørn Hansen AS for the cooperation when crossing the bridge on May 5th.

A very special thanks goes to Etienne Cheynet for his time and expert advice and guidance with any MATLAB related questions as well as general inputs to the Thesis throughout the entire process.

Thomas Ole Messelt Fadnes

Stavanger, 15th June 2017

Contents

Abstract	i
Acknowledgements	ii
Abbreviations	xii
1 Introduction	1
1.1 Background	1
1.2 Problem Formulation	2
1.3 Literature Survey	3
1.3.1 Ambient Vibration Measurements (AVM) of Traffic Induced Vibrations on Suspension Bridges	3
1.3.2 Field Measurements and Structural Analysis on Lysefjorden Bridge	3
1.3.3 Full-Scale Estimation of Structural Damping on Suspension Bridges	4
1.3.4 Analytical Methods for Traffic Induced Vibrations and Impact Loading on Suspension Bridges	5
1.4 Suspension Bridges	6
1.4.1 General	6
1.4.2 Towers	7
1.4.3 Anchors	8
1.4.4 Main Cables	8
1.4.5 Hanger Cables	8
1.4.6 Stiffening Girder and Bridge Deck	9
1.5 Structure of the Report	9

2	Theory	10
2.1	Dynamics	10
2.1.1	Mode Shapes and Frequencies	10
2.1.2	Modal Analysis	11
2.1.3	Damping	14
2.2	Time and Frequency Domain	19
2.3	Frequency Domain Decomposition	20
2.3.1	FDD Theoretical Background	20
2.3.2	FDD Algorithm	22
2.4	Vehicle Induced Vibrations	23
2.4.1	Impact Loading	23
2.4.2	Analytical Prediction of Impact Loading on Suspension Bridges	23
2.4.3	Equation of Motion for Vehicle	24
2.4.4	Coupled Systems	28
2.4.5	Simulation	29
3	Analysis and Results	30
3.1	Lysefjorden Bridge	30
3.2	Data Acquisition	32
3.2.1	Monitoring Equipment	32
3.2.2	Method for Vehicle Registration	34
3.2.3	Acquired Data	37
3.3	Thesis Limitations	40
3.4	Spectral Analysis	41
3.4.1	Traffic Induced Frequencies	41
3.4.2	Modes Excited by Individual Vehicles	48
3.4.3	Response Frequencies in Individual Sensors	50
3.4.4	Signal Processing/Filtering	51
3.5	Response Amplitude and Characteristics	53
3.5.1	Vertical Acceleration Response	55

3.5.2	Horizontal and Torsional Acceleration Response	67
3.5.3	Displacement	67
3.6	Impact Loading	70
3.6.1	Condition of Bridge Deck	70
3.6.2	Impact Loading “Experiment”	73
3.6.3	Quality of Experiment Measurements	74
3.6.4	Acceleration Response	75
3.6.5	Significance of the Vehicle-induced Response	86
3.7	Damping	87
3.7.1	Analysis process	91
3.7.2	Damping Ratio as Function of Frequency (Mode)	100
3.7.3	Modal Damping Ratio as Function of Mean Wind Speed and Temperature	101
3.7.4	Modal Damping Ratio as Function of Amplitude	105
4	Conclusion and Further Work	106
4.1	Conclusion	106
4.2	Further Work	108
	Bibliography	109
A	Mode Shapes	112
B	Matlab Functions	116
B.1	Evolutionary Power Spectral Density Function - by Etienne Cheynet	117
B.2	Frequency Domain Decomposition function - by Mohammad Farshchin and simplified by Etienne Cheynet	119
B.3	Filtering function based on Butterwoth filter - by Chad A. Greene	121
B.4	PSD for all individual sensors - based on MATLAB function “pwelch”	125
B.5	Exponential Decay Fit function	129
C	Impact Response	131
C.1	Impact Acceleration Response	132
C.2	Impact Displacement Response	138

D Damping Estimation Plots

List of Figures

1.1	Illustration of Golden Gate Bridge suspension bridge located in San Francisco . . .	7
2.1	Illustration of the relationship between time and frequency domain. Image credit: Pinsdaddy (nd)	19
2.2	Illustration of degrees of freedom for vehicle Equation of Motion (EOM). Source: Liu et al. (2017)	25
2.3	Illustration of simulated “excellent” road roughness. Source: Liu et al. (2017)	27
2.4	Illustration of simulated “good” road roughness. Source: Liu et al. (2017)	27
2.5	Illustration of simulated “normal” road roughness. Source: Liu et al. (2017)	28
3.1	Blueprint of Lysefjorden bridge	30
3.2	Map showing Lysefjorden inlet and Lysefjorden Bridge. Source: Google Maps (nd)	31
3.3	Positioning of accelerometer pairs	33
3.4	Positioning of all monitoring equipment on Lysefjorden Bridge	33
3.5	Recording setup for vehicle registration	34
3.6	Screenshot from recorded video of bridge April 17th	35
3.7	Screenshot from excel worksheet of vehicle registration April 17th	36
3.8	Time series of wind measurements at mid span from March 7th, May 2nd and May 3rd. “Normal” and “longitudinal” direction represents measured wind normal to and along with the bridge deck, respectively.	39
3.9	Evolutionary Power Spectral density (EPSD) for vertical (top), torsional (middle) and horizontal (bottom) acceleration data, Sensor position H9, March 7th	42

3.10 PSD used for peak picking March 7th for vertical (top), torsional (middle) and horizontal (bottom) 44

3.11 PSD peak picking for small truck crossing from south at 12.56.10 on March 7th with mean wind speed of 2,5 m/s 48

3.12 PSD of all sensor positions for a single crossing truck at 12.56.10 on March 7th with mean wind speed of 2,5 m/s 51

3.13 Overview of unfiltered vertical acceleration response at mid span for the cases illustrated in Table 3.8 on March 7th 55

3.14 Unfiltered vertical data for all 4 accelerometers for truck crossing from the North (case 1) 56

3.15 Unfiltered vertical acceleration data for all 4 accelerometers for truck crossing from the South (case 10) 57

3.16 Acceleration response band-pass filtered around 0,22 Hz (VA1) for case 1 - from North 59

3.17 Acceleration response band-pass filtered around 0,22 Hz (VA1) for case 2 - from South 60

3.18 Acceleration response band-pass filtered around 0,86 Hz (VS3) for case 1 - from North 62

3.19 Acceleration response band-pass filtered around 0,86Hz (VS3) for case 2 - from South 63

3.20 Acceleration response band-pass filtered around 1,55Hz for case 1 - from North - from South 65

3.21 Acceleration response band-pass filtered around 1,55 Hz for case 2 - from South 66

3.22 Acceleration and displacement response at mid span for case 1 68

3.23 PSD of displacement response at mid span for case 1 69

3.24 General pavement condition 71

3.25 71

3.26 Expansion joint on the South side of the bridge 71

3.27 Bump in pavement by entrance to bridge on the South side of the bridge 72

3.28 50 tonnes truck entering bridge from the South at 23 km/h with a total cargo of 50 Tonnes	74
3.29 Unfiltered acceleration response for 50 tonne truck entering bridge from South doing 55 km/h (trip 1)	75
3.30 Unfiltered acceleration response for 50 tonne truck entering bridge from North accelerating from 30 to 50 km/h (trip 2)	76
3.31 Unfiltered acceleration response for 50 tonne truck entering bridge from South doing 23 km/h (trip 3)	77
3.32 PSD functions for vertical acceleration for trip 1 (top), trip 2 (middle) and trip 3 (bottom)	79
3.33 PSD functions for vertical displacement for trip 1 (top), trip 2 (middle) and trip 3 (bottom)	80
3.34 Filtered response VA1 for trip 1(top), trip 2 (middle) and trip 3 (bottom)	81
3.35 Filtered response VS3 for trip 1(top), trip 2 (middle) and trip 3 (bottom)	82
3.36 Filtered response VA3 for trip 1(top), trip 2 (middle) and trip 3 (bottom)	83
3.37 Taramakau River bridge located in New Zealand with speed limitation for heavy vehicles. Image credit: Bernard Spragg (nd)	86
3.38 Acceleration response March 7th with chosen cases for damping analysis	88
3.39 Acceleration response May 2nd with chosen cases for damping analysis	89
3.40 Acceleration response May 3rd with chosen cases for damping analysis	90
3.41 Unfiltered acceleration data for all sensors case 1 -	92
3.42 PSD FDD case 1	93
3.43 PSD individual sensors case 1	94
3.44 “good” filtered modal acceleration response for VS3 (0,854 Hz) for case 1	95
3.45 “Poor” filtered modal acceleration response for F8 (1,92 Hz) for case 2	96
3.46 Exponential decay function fitted to free vertical modal acceleration oscillations from sensor H18 for VS3 for case 1. Free oscillations starting at 12.40.55 on March 7th. <i>zeta</i> in the title represents estimated damping ratio, ξ	97

3.47 Exponential decay function fitted to free vertical modal acceleration oscillations from sensor H18 for 1,92 Hz for case 2. *zeta* in the title represents estimated damping ratio, ξ 98

3.48 Whisker diagram illustrating spread in estimated torsional vertical modal damping ratios 100

3.49 Vertical damping ratio, ξ , as function of wind speed for all measured vertical modes 102

3.50 Torsional damping ratio, ξ , as function of wind speed for TS1 103

3.51 Vertical damping ratio, ξ , as function of Temperature for all measured vertical modes 104

3.52 Torsional damping ratio, ξ , as function of Temperature for TS1 105

List of Tables

3.1	Scale showing power ratios x , amplitude ratios \sqrt{x} , and dB equivalents $10 \log_{10} x$.	41
3.2	Identified vertical modal frequencies	45
3.3	Identified torsional modal frequencies	45
3.4	Identified horizontal modal frequencies	46
3.5	Comparison of the eigen-frequencies identified in previous work on Lysefjorden Bridge	47
3.6	Identified vertical frequencies from individual small truck crossing from south at 12.56.10 on March 7th	49
3.7	Identified torsional frequencies from individual small truck crossing from south at 12.56.10 on March 7th	49
3.8	Vehicle crossings for response analysis	53
3.9	Identified vertical displacement frequencies FDD case 1	69
3.10	Overview of three bridge crossings by Anette Ravndal on May 5th	73
3.11	Overview of maximum unfiltered acceleration amplitudes for all three trips driven by Anette Ravndal on May 5th	77
3.12	Overview of maximum vertical modal acceleration response and position for trips 1, 2 and 3	85
3.13	Vehicle crossings identified as potentially suitable for free oscillations analysis	87
3.14	Identified frequencies FDD case 1	93
3.15	Estimated vertical modal frequencies for each case for the first 9 identified frequencies	99
3.16	Estimated torsional modal frequencies for TS1	99

Abbreviations

AVM Ambient Vibration Measurements

DFT Discrete Fourier Transform

DLF Dynamic Load Factor

EOM Equation of Motion

FFT Fast Fourier Transform

FVT Forced Vibration Test

GNSS Global Navigation Satellite System

MEM Micro Electro-Mechanical

PSD Power Spectral Density

RTK-GPS Real-Time Kinematic-Global Positioning System

SVD Single Value Detriment

Chapter 1

Introduction

1.1 Background

Norway's coastline consists of long and deep fjords amongst rocky terrain. This leads to challenges within road and transportation systems along the coast. Ferry transportation has been the solution for crossing fjords such as Sognefjorden (3,7 km wide and 1300 m deep), Bjørnafjorden (5 km wide and 500 m deep) as well as several other similar fjords. However, in 2012 the Norwegian Parliement agreed on a goal towards a ferry free coastline road (E39) between Kristiansand and Trondheim by 2030 ([Norwegian Ministry of Transport and Communication \(2012\)](#)). Suspension bridges are amongst the suggested solution for crossing these wide fjords, which means that the world record for the longest central span will likely be broken, currently held by the Akashi Kaikyo Bridge in Japan (1991 m). In order to achieve such a feat, a detailed understanding of loading and structural parameters for bridges of this type is required.

Research work on monitoring of existing suspension bridges has therefore been supported by the Norwegian Public Roads Administration. In 2014 the Lysefjorden suspension bridge was equipped with accelerometers, anemometers, weather station and a GPS system, in a sense making it a full-scale laboratory for research on the bridges dynamic behavior and the wind characteristics in complex terrain. A “full scale laboratory” of this kind at a location like Lysefjorden opens up for the opportunity to study characteristics and effects from wind in complex terrain, and also allows for a detailed study on loading effects and response from individual,

heavy vehicles, which is the focus of the present work.

Using full-scale measurements and studying response from traffic opens up for a few opportunities. First, the response in the bridge from heavy vehicles during days of low wind speed can be used as a type of forced vibration test in order to estimate the modal damping ratios in the bridge. After heavy vehicles cross the bridge, the bridge is left to swing freely without any other significant external loading, and by filtering out the modal free vibrations the damping ratio can be estimated. Second, response from heavy vehicles entering and exiting the bridge at high velocities can be used to look at dynamic amplification from impact loading. Due to the geometry and varying pavement quality on certain areas of the bridge, the bridge likely experiences dynamic amplification effects from traffic loads. The nature of this response is known to be dependent several parameters, both in the bridge and in the vehicle. Studying the response from different vehicles at different velocities can potentially lead to a better understanding of the magnitude of dynamic amplification and the importance of the variable parameters. The current measurements at Lysefjorden bridge are not ideal for such analysis, but there is still a potential for drawing some conclusions on the magnitude and causes of this phenomena.

1.2 Problem Formulation

By observing traffic and analyzing vehicle induced acceleration and displacement response data of Lysefjorden bridge the goal of the present work is to

1. Estimate modal structural damping ratios for different modes by analyzing the decay oscillations excited by vehicles crossing the bridge at low wind speeds
2. Study impact response from vehicles by looking at response from vehicles with varied mass and velocity

In order to achieve the goals stated above, a detailed understanding of the response characteristics in the bridge from different vehicles is needed. A chapter on spectral analysis of the response as well as a general analysis of response the from different vehicles is therefore also performed.

1.3 Literature Survey

1.3.1 Ambient Vibration Measurements (AVM) of Traffic Induced Vibrations on Suspension Bridges

AVM vibration measurements is a (relatively) common method in monitoring bridge dynamics, and there have been published numerous studies on traffic induced vibrations in full-scale using similar methods of AVM on suspension bridges, including studies done on Bosphorus bridge in Turkey ([Erdoğan and Güral \(2013\)](#) and [Apaydin et al. \(2012\)](#)).

However, the common objective of the field investigations reported in the existing literature is finding and validating natural frequencies of the structures/bridges. [Kim et al. \(2003\)](#) studies the effect of vehicle mass from heavy traffic on eigenfrequencies on three types of bridges, including a long span suspension bridge, and concludes that vehicle mass has little effect on natural frequencies. To the authors knowledge there is no literature on full-scale studies from effect of individual vehicles on suspension bridges.

1.3.2 Field Measurements and Structural Analysis on Lysefjorden Bridge

Monitoring instrumentation for both wind and structural vibrations were installed on Lysefjorden suspension bridge in 2013, and several studies have been done using the recorded data. However, the focus has been directed mainly towards structural response from wind.

The PhD on “Wind induced vibrations of a suspension bridge” ([Cheynet \(2016\)](#)) by Etienne Cheynet is an extensive, detailed study of full-scale analysis of vibrations on Lysefjorden suspension bridge. This work focuses mainly on wind flow conditions in the complex terrain of Lysefjorden bridge, full-scale and computational modal analysis of the bridge, and an evaluation of the buffeting response of the bridge. Traffic induced vibrations are studied, but mainly in order to explain discrepancies/deviations in the buffeting response theory.

[Snæbjørnsson et al. \(2016\)](#) have also done some further work on studying the frequency content of traffic induced vibrations of Lysefjorden Bridge. However, here the focus is mainly on

methods of filtering out response dominated by traffic in order to improve results of buffeting analysis.

Master Thesis by [Steigen \(2011\)](#), [Tveiten \(2012\)](#) and [Thoresen \(2014\)](#) analyze wind response on this particular suspension bridge using finite element model in ABAQUS, and [Lunder \(2014\)](#) compares these analytical results to measured data.

In other words, extensive dynamic analysis on Lysefjorden Bridge has been performed both computationally and in full-scale, but detailed analysis focusing on traffic induced vibrations is still relatively unexplored.

The results from the above references will be further discussed in Chapter [3.4](#) for comparison and verification of measured eigenfrequencies and modes from the present analysis.

1.3.3 Full-Scale Estimation of Structural Damping on Suspension Bridges

In general, damping is still a field with limited theoretical understanding, and most analytical methods for damping are based on physical experiments. One of the reasons for the complexity is that energy dissipation is understood as being a combination of several mechanisms, some of which are not well understood. A few of these mechanisms and their analytical approximations will be further discussed in Chapters [2.1.3](#) and [3.7](#)

[Brownjohn \(1994\)](#) explores and summarizes research done on estimating damping in suspension bridges. Different damping mechanisms and methods of analyzing physical test data and related accuracy is discussed in order to rationalize choice of damping values for use in dynamic analysis of suspension bridges of different designs and span lengths. According to [Brownjohn \(1994\)](#) Forced Vibration Tests (FVT's) is considered to produce the best in terms of quality of experimental data.

One method for FVT used for relatively short span suspension bridges is described in [Selberg \(1950\)](#), where 15 - 20 men jumped continuously in rhythm with a given natural frequency, and coming to an immediate stop as the amplitude had reached its maximum and the free decay oscillations were measured to estimate damping.

As described in the earlier, the idea of the present Thesis is to use traffic-induced vibration as a form of FVT, and to the authors knowledge there is no existing literature or experiments using traffic as FVT for damping estimation.

For Lysefjordsbrua, aerodynamic damping ratio is estimated from the buffeting response in the PhD [Cheynet \(2016\)](#). Here, structural damping ratio is assumed constant at the design ratio of 0.005 for every mode, but the analysis suggests some deviations from this value. Further discussion and comparison on the results from Etiennes work on modal damping will be performed in Chapter [3.7](#).

1.3.4 Analytical Methods for Traffic Induced Vibrations and Impact Loading on Suspension Bridges

Analytical methods for estimating traffic induced vibrations are widely explored in the literature. [Liu et al. \(2017\)](#) and [Bryja and Śniady \(1998\)](#) are two examples of publications that present mathematical and statistical analytical models for traffic induced response in suspension bridges and looks at effects on bridge response from vehicle parameters such as damping and spring force in the suspension system as well as vehicle velocity. [Bryja and Śniady \(1998\)](#) simulates moving vehicles as two axled moving oscillators along the bridge deck. [Liu et al. \(2017\)](#) simulates vehicle bridge interaction through force and displacement coupling through the surface roughness of the bridge with 5 degrees of freedom.

The bridge parameters presented in [Liu et al. \(2017\)](#) are considered comparable to the bridge analyzed in the present work, and will be used as basis for theoretical comparison to the full-scale measurements in regards to impact loading. Relevant theory is presented in Chapter [3.6](#).

Impact factors are also studied and discussed in [Eurocode \(2003\)](#) and [Sanpaolesi and Croce \(2005\)](#). Here, it is stated that impact factors “depends on several parameters, like type, static scheme and span of bridge, the natural frequency, the damping coefficient, the dynamic characteristic and speed of the lorries, the roughness of the road pavement etc..” and that “Generally, impact results are greater when the natural frequency of the bridge is close to the natural frequencies of axles (10 - 12Hz) and lorries (1 - 2 Hz)” ([Sanpaolesi and Croce \(2005\)](#)).

1.4 Suspension Bridges

1.4.1 General

Suspension bridges are a common type of cable supported bridge. They vary in length, with the longest main span 2000 meters at present.

The main load carrying principle of suspension bridges is to transfer the weight of the bridge itself and external loads through hangers, main cables and towers to tower foundations and cable anchors, blocks or a rock.

The bridge is relatively light per unit length and allows for long spans that can be arched upward to allow for additional clearance under the bridge. As the concept is proven and fairly well understood, it is one of the most feasible alternatives for developments such as the coastal highway E39 project along the west coast of Norway, where several fjords are planned to be crossed.

Generally speaking, there are 5 main components that makes up a suspension bridge.

1. Towers
2. Anchor bolts
3. Main cables
4. Stiffening girder with bridge deck
5. Hanger cables

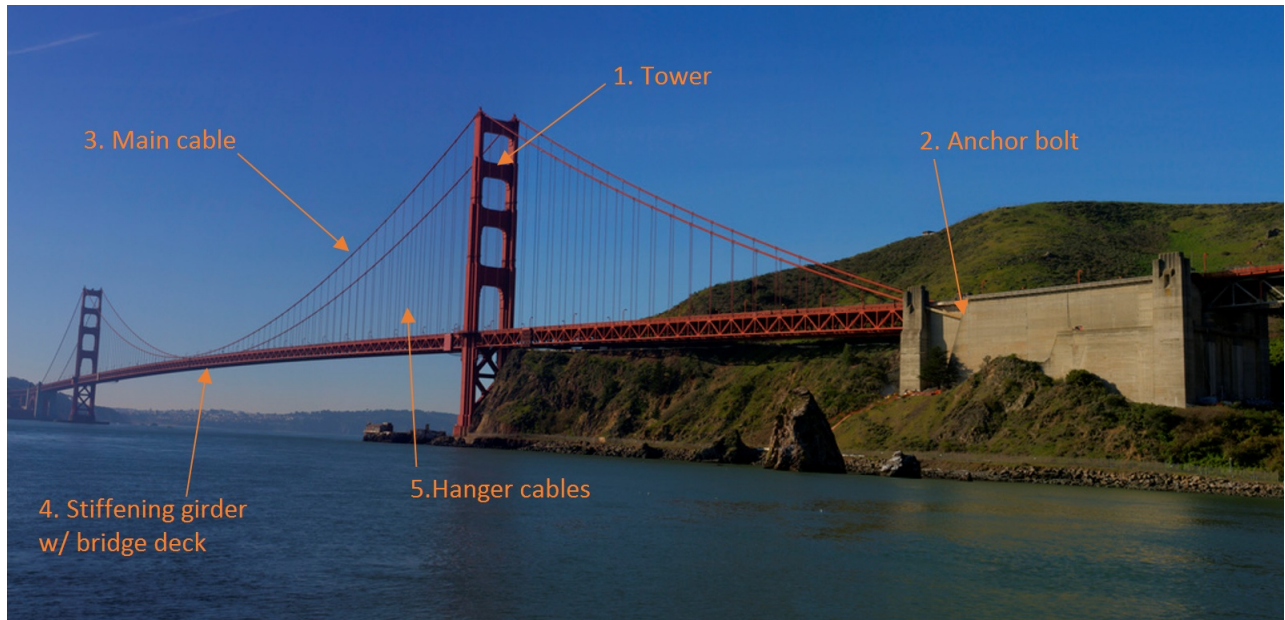


Figure 1.1: Illustration of Golden Gate Bridge suspension bridge located in San Francisco

As illustrated above in Figure 1.1, towers and anchor blocks connect the structure through the foundation, and all loads are transferred through these connections. The stiffening girder is suspended from the main cables by hanger cables, but is frequently also supported on the tower cross beam through expansion joints which allows for thermal expansion and displacements of the free span of the bridge.

1.4.2 Towers

As mentioned, the towers support the weight of the structure (main cables, stiffening girder with deck, hanger cables). The operational design forces/factors are therefore mainly compression, but the external forces such as wind and in some cases earthquakes can also cause bending and torsion in the towers. Traditionally, Suspension bridges have two main towers, and the height of the towers are decided by the desired or required geometry of the bridge. The materials used in the towers can vary, and depend on parameters such as type of design loads and soil conditions. For bridges in Norway with little risk of seismic activity, reinforced concrete is commonly used.

1.4.3 Anchors

Anchors are located at each end of the suspension bridge and is the second area in which the loads from suspension bridges are transferred to the soil/ground. Anchoring points are designed to withstand the axial forces from the main cables, often directly into solid rock.

1.4.4 Main Cables

The main cables of a suspension bridge are designed to carry the weight of the bridge as well as external loads on the bridge. The idea behind a suspension bridge of this type is to transfer the loads from the bridge girder to tension in the main cables. The main design factor for such cables are therefore tension forces, although there can also be considerable compression and bending in the contact areas of the main cables and towers, as well as local bending in the hanger connection joints. Cables on suspension bridges differ from most cables used in lifting or other dynamic operations due to their relatively static operational design and little to no torsional stresses. The geometrical consideration of the main cables is the sag ratio in the wire, which is defined as $k = f/L$, where L is the length of the span and f is the distance from the highest to the lowest point in the wire (the sag). Lower sag ratio means higher initial tension in the wire. This can be beneficial for dynamic stability, but will at the same time require higher design load for the cable. On the other hand, high sag ratio requires higher towers.

1.4.5 Hanger Cables

The hanger cables connect the main cables to the stiffening girder with the bridge deck. As these are vertical and connected only on each end, the design factor is pure tension. Depending on the specific design of the bridge, the spacing of each hanger cable can vary quite significantly from one bridge to another. The connection between the main cable and hanger cables is often through a jointed hanger attachment.

1.4.6 Stiffening Girder and Bridge Deck

The stiffening girder design and characteristics are important factors in bridge design. Historically, accidents in suspension bridges have often been related to poorly designed stiffening girders. The stiffening girder and deck is exposed to the majority of all external loads on bridges, which are mainly loads from traffic and wind. Torsional and bending stiffness as well as aerodynamic properties are therefore the main design considerations. This is in order to avoid excessive bending and displacement from static or dynamic loading as well as potential resonance from vortex induced vibrations or other periodic loading.

1.5 Structure of the Report

The Thesis consists of 5 main chapters with respective sub-chapters

Chapter 1 - Introduction

Introduction of the problem definitions and summary of existing literature.

Chapter 2 - Theory

Relevant theory for the subjects addressed in the report. This includes theory that will be applied in the analysis as well as theory included in order to increase the understanding of the subjects discussed in the Thesis.

Chapter 3 - Analysis and Results

Calculations and critical analysis is performed for all relevant subjects. Results are also discussed and compared to theory and existing literature.

Chapter 4 - Summary and Conclusion

Summary of findings in the Thesis as well as suggestions for future work.

Chapter 2

Theory

2.1 Dynamics

As far as bridges go, suspension bridges are relatively flexible structures, and external forces such as wind, waves or traffic can result in severe response. On long span suspension bridges subjected to strong winds, or in some cases heavy traffic, the oscillations of the bridge is noticeable even to the human eye (personal experience) and the motions can often be felt by a person on the bridge.

The study of dynamics of suspension bridges is therefore interesting from an engineering point of view, but also important, as flexible structures are more susceptible to vibrations from environmental loads. The Tacoma Narrows collapse in 1940 is one example where improper design lead to complete collapse of the bridge due to excitation from wind.

2.1.1 Mode Shapes and Frequencies

As described earlier, analysis of modal frequencies and shapes on Lysefjorden bridge is done in full scale in the works of [Lunder \(2014\)](#) and [Cheynet \(2016\)](#). Results from these analysis as well as hand calculations and computational finite element modeling in ABAQUS and Alvsat will be used as a basis for comparison of eigen-frequencies and shapes where it is applicable.

The methods for hand calculations of eigenfrequencies used in [Lunder \(2014\)](#) [Steigen \(2011\)](#) is based on theory from [Steinman \(1959\)](#) and [Bleich \(1950\)](#), which is commonly accepted theory for hand calculations of both torsional and vertical modes. Computational analysis of eigenfrequencies and is also performed by use of finite element software such as ABAQUS and Alvsat, based on widely explored and accepted methods for finite element analysis.

2.1.2 Modal Analysis

The present analysis will consist of analyzing modal response through spectral analysis of measurement data, but in order to illustrate the relevance of analyzing individual modes it is useful to recall the basics of *modal analysis*.

The dynamic behaviour of a bridge deck can be expressed by the *equation of motion* in matrix form

$$\ddot{\mathbf{r}}\mathbf{m} + \dot{\mathbf{r}}\mathbf{c} + \mathbf{r}\mathbf{k} = \mathbf{F}(t) \quad (2.1)$$

$\mathbf{r}(t)$ is the displacement vector containing key motion components, the so-called *Degrees of Freedom* (DOF). \mathbf{m} , \mathbf{c} and \mathbf{k} are the associated mass, damping and stiffness matrices, respectively, and $\mathbf{F}(t)$ is the load vector. Due to the orthogonality of eigenvectors $\boldsymbol{\phi}$ with respect to \mathbf{m} and \mathbf{k} , a multi-degree of freedom system can be reduced to a number of decoupled single degree of freedom (SDOF) systems with a few simple mathematical steps. This procedure is part of *modal analysis*

The damping matrix, \mathbf{c} , is only orthogonal in the case of “ideal damping” or “Rayleigh damping” ([Adhikari and Woodhouse \(2001\)](#)). In practice damping, c_i is estimated directly in modal analysis by making

$$c_i = 2\xi_i + \omega_i m_i \quad (2.2)$$

According to the modal expression theorem \mathbf{r} can be expressed by its modal displacement, $x_i(t)$, and eigenvectors $\boldsymbol{\phi}_i$

$$\mathbf{r}(t) = \sum_{i=1}^n x_i(t)\phi_i = \mathbf{x}_{nx1}(t)\boldsymbol{\phi}_{nxn} \quad (2.3)$$

and

$$\dot{\mathbf{r}}(t) = \sum_{i=1}^n \dot{x}_i(t)\phi_i = \dot{\mathbf{x}}_{nx1}(t)\boldsymbol{\phi}_{nxn} \quad (2.4)$$

$$\ddot{\mathbf{r}}(t) = \sum_{i=1}^n \ddot{x}_i(t)\phi_i = \ddot{\mathbf{x}}_{nx1}(t)\boldsymbol{\phi}_{nxn} \quad (2.5)$$

Substitution into Equation 2.1 gives

$$\mathbf{m}\ddot{\mathbf{x}}(t)\boldsymbol{\phi} + \mathbf{c}\dot{\mathbf{x}}(t)\boldsymbol{\phi} + \mathbf{k}\mathbf{x}(t)\boldsymbol{\phi} = \mathbf{Q}(t) \quad (2.6)$$

Pre-multiplication of the transpose of the eigenvector, $\boldsymbol{\phi}^T$, into Equation 2.6 gives

$$\boldsymbol{\phi}^T \mathbf{m} \boldsymbol{\phi} \ddot{\mathbf{x}}(t) + \boldsymbol{\phi}^T \mathbf{c} \boldsymbol{\phi} \dot{\mathbf{x}}(t) + \boldsymbol{\phi}^T \mathbf{k} \boldsymbol{\phi} \mathbf{x}(t) = \boldsymbol{\phi}^T \mathbf{F}(t) \quad (2.7)$$

Orthogonality of mode shapes with respect to \mathbf{m} and \mathbf{k} gives

$$\boldsymbol{\phi}_i^T \mathbf{m} \boldsymbol{\phi}_j = 0, \quad (2.8)$$

$$\boldsymbol{\phi}_i^T \mathbf{k} \boldsymbol{\phi}_j = 0, \quad (2.9)$$

for modes i and j , when $i \neq j$.

Modal mass and stiffness, m_i and k_i can then be expressed as following for each independent mode, i

$$\phi_i^T \mathbf{m} \phi_i = m_i, \quad (2.10)$$

$$\phi_i^T \mathbf{k} \phi_i = k_i, \quad (2.11)$$

$$(2.12)$$

These modal parameters can be obtained by working with the diagonal matrices of eigenvectors, \mathbf{M} and \mathbf{K}

$$\boldsymbol{\phi}^T \mathbf{m} \boldsymbol{\phi} = \mathbf{M} = \begin{bmatrix} m_1 & 0 & \dots & 0 \\ 0 & m_2 & \dots & 0 \\ \vdots & \vdots & \ddots & \vdots \\ 0 & 0 & \dots & m_i \end{bmatrix} \quad (2.13)$$

$$\boldsymbol{\phi}^T \mathbf{k} \boldsymbol{\phi} = \mathbf{K} = \begin{bmatrix} k_1 & 0 & \dots & 0 \\ 0 & k_2 & \dots & 0 \\ \vdots & \vdots & \ddots & \vdots \\ 0 & 0 & \dots & k_i \end{bmatrix} \quad (2.14)$$

This transformation finally results in a set of n uncoupled differential equations that can each be solved separately.

$$\mathbf{M}\ddot{\mathbf{x}}(t) + \mathbf{C}\dot{\mathbf{x}}(t) + \mathbf{K}\mathbf{x}(t) = \boldsymbol{\phi}^T \mathbf{F}(t) = \mathbf{Q}(t) \quad (2.15)$$

where each uncoupled differential equation is in the form

$$m_i \ddot{x}_i(t) + c_i \dot{x}_i(t) + k_i x_i = Q_i(t) \quad (2.16)$$

In terms of modal parameters, this thesis will focus on damping. A general introduction to the concept of damping and estimation of damping is therefore explained in the next section.

2.1.3 Damping

Damping is a generalized term describing the dissipation of kinetic energy, and is present in different forms in all structures. Kinetic energy dissipates through transformation to other forms of energy such as heat or (forms of) radiation. This dissipation of energy will force an oscillating structure to rest as long as no additional energy is added to the system. Accurate modelling of damping in a structure can be quite complex ([Langen and Sigbjørnsson \(1979\)](#) and [Adhikari and Woodhouse \(2001\)](#)), as the actual damping mechanisms are a combination of different types of damping, some of which are not well understood.

[Brownjohn \(1994\)](#) describes the damping ratio, ξ , to be the sum of several effects, including material damping, friction damping, hysteretic damping, radiation and more.

Viscous damping is very unlikely to be the only damping mechanism in suspension bridges, but can often lead to satisfactory analytical approximations. More complex analytical methods are explored in the literature, but for the present work the assumption of viscous damping will be applied. Methods/discussion concerning the validity of this assumption, or if other damping models can prove more accurate, will be presented in Chapter [3.7](#).

Below is a description of the theory behind viscous damping and estimation of damping ratio from measurement data.

Viscous Damping

The assumption of viscous damping is the most common model for energy dissipation, as it provides relatively simple mathematical solutions and is often accepted as providing sufficiently accurate solutions for many applications [Langen and Sigbjørnsson \(1979\)](#).

The viscous damping forces are proportional and in phase with velocity as described below.

$$F_D(t) = c\dot{x}(t) \tag{2.17}$$

Here, c is the damping coefficient and F_D is the damping force.

If we consider free vibration of a single degree of freedom system, the equation of motion with viscous damping yields

$$m\ddot{x}(t) + c\dot{x}(t) + kx(t) = 0 \quad (2.18)$$

The damping ratio, ξ , is defined as the ratio between actual damping coefficient, c , and critical damping, c_c

$$\xi = c/c_c \quad (2.19)$$

This non-dimensional number allows for comparison of damping of different structural systems.

Critical damping is defined as

$$c_c = 2m\omega_n \quad (2.20)$$

where ω_n is the natural frequency and defined as

$$\omega_n = \sqrt{k/m} \quad (2.21)$$

The equation can be rewritten as

$$\ddot{x}(t) + 2\xi\omega_n\dot{x}(t) + \omega_n^2x(t) = 0 \quad (2.22)$$

The general solution to this differential equation is

$$x(t) = D_1e^{s_1t} + D_2e^{s_2t} \quad (2.23)$$

where we assume exponential decay of the oscillations (characteristic of viscous damping)

$$s_{1,2} = -\omega_n(\xi \pm \sqrt{1 - \xi^2}) \quad (2.24)$$

D_1 and D_2 are integration constants and depend on initial conditions.

Structures such as suspension bridges are known to be under-damped, $\xi < 1$, which results in two complex roots

$$s_{1,2} = -\omega_n \xi \pm i\omega_d, \quad (2.25)$$

where ω_d is the damped frequency, defined as

$$\omega_d = \omega_n \sqrt{1 - \xi^2} \quad (2.26)$$

The displacement response can finally be written as

$$x(t) = e^{-\xi\omega_n t} (A \sin(\omega_d t) + B \cos(\omega_d t)) \quad (2.27)$$

The damped period, T_d can be written as

$$T_d = \frac{2\pi}{\omega_d} = \frac{2\pi}{\omega_n} \frac{1}{\sqrt{1 - \xi^2}} \quad (2.28)$$

In order to be able to estimate damping in a freely oscillating system, it can be useful to look at the relationship between consecutive amplitudes. From Equation 2.27 we can write this equation as

$$\frac{x(t)}{x(t + T_d)} = \frac{e^{-\xi\omega_n t}}{e^{-\xi\omega_n(t+T_d)}} = e^{-\xi\omega_n T_d} \quad (2.29)$$

The natural logarithm of this ratio, δ , is known as the *logarithmic detriment*

$$\delta = \ln \frac{x(t)}{x(t + T_d)} = \xi\omega_n T_d \quad (2.30)$$

By substituting T_d with Equation 2.28 we get

$$\delta = \ln \frac{x(t)}{x(t+T_d)} = \frac{2\pi\xi}{\sqrt{1-\xi^2}} \quad (2.31)$$

Damping in a suspension bridge is $\ll 0$. Analysis on damping by [Cheynet \(2016\)](#) suggest that the highest modal structural damping ratio at around 1,3%. This means that the equation can be fairly accurately simplified to

$$\delta = 2\pi\xi \quad (2.32)$$

By denoting the peak as X_i , the damping ratio can be estimated by analyzing decaying oscillations of a freely oscillating system from two consecutive peaks

$$\xi = \frac{\ln \frac{X_i}{X_{i+1}}}{2\pi} \quad (2.33)$$

or for the n'th peak

$$\xi = \frac{1}{n} \frac{\ln \frac{X_i}{X_{i+n}}}{2\pi} \quad (2.34)$$

By analyzing several peaks we can check for consistency in the measured damping ratio. If consistent, this can indicate that the viscous damping assumption is reasonable.

Structural and Nonlinear Viscous Damping

Other damping models are in many cases considered more accurate than viscous assumption, depending on materials, structure type, and also load type and loading conditions. These methods are more complex mathematically and will not be explored in detail in this thesis. However, the general theory behind these methods are described below.

The theoretical differences between linear viscous damping and other models is the dependency on the parameters in the equation of motion.

One such example is *structural damping*, where the damping force is proportional to displace-

ment *and* in phase with velocity

$$F_D(t) = i\mu kx(t) \quad (2.35)$$

Where μ is the structural damping coefficient and k is structural stiffness. Another example is *nonlinear viscous damping*, where the damping force is proportional with velocity squared

$$F_D(t) = c_N|\dot{x}(t)|\dot{x}(t) \quad (2.36)$$

2.2 Time and Frequency Domain

Response in structures such as suspension bridges is often a combination of response in several of its modal frequencies. In structural analysis it is therefore necessary to analyze response both in the time and frequency domain. Time series such as acceleration data from Lysefjorden Bridge can be converted from its original domain (time) to the frequency domain through Fourier Transformations. The specific method often applied in computer programs are Fast Fourier Transform (FFT) algorithms.

Typical outputs from Fourier transformations are presented as Power Spectral Density functions (PSD), which describes the distribution of energy along the frequency domain.

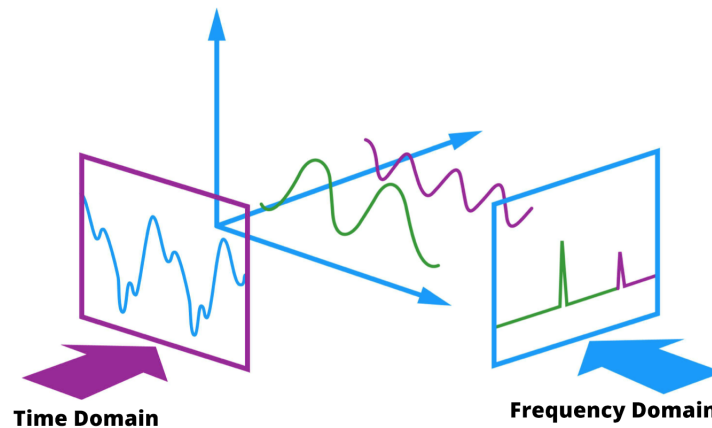


Figure 2.1: Illustration of the relationship between time and frequency domain. Image credit: [Pinsdaddy \(nd\)](#)

As mentioned, FFT is a common method of transforming from time to frequency domain, but there are few limitations that have lead to the development of methods which are more accurate for the specific applications. For modal analysis of structures such as suspension bridges, there can be limitations due to the frequency domain resolution, and also the fact that modal frequencies are too close to be detected. A method presented in [Brincker et al. \(2000\)](#) claims to “remove all the disadvantages with the classical approach (FFT), but keeps its user friendliness.” This method is called Frequency Domain Decomposition (FDD), and is used for modal analysis in the present work.

2.3 Frequency Domain Decomposition

FDD is an output-only method for identifying modal parameters where the input exciting the system is unknown. FDD is suggested as removing all disadvantages with classical Fourier Transformation methods. FDD is a method for finding modal parameters such frequency, mode shapes as well as damping. For the present work, the method is used mainly for identifying modal eigenfrequencies.

2.3.1 FDD Theoretical Background

The description of the governing theory behind FDD is illustrated below as presented in [Brincker et al. \(2000\)](#).

First, the relationship between the unknown inputs $x(t)$ and the responses $y(t)$ is expressed as a $r * r$ power spectral density matrix, $G_{yy}(j\omega)$

$$G_{yy}(j\omega) = \bar{H}(j\omega)G_{xx}(j\omega)H(j\omega)^T. \quad (2.37)$$

G_{yy} is the $m * m$ PSD matrix for the responses for m number of responses. $\bar{H}(j\omega)$ and $H(j\omega)^T$ are the complex conjugate and transpose Frequency Response Functions (FRF), respectively.

$H(j\omega)$ can also be written in partial form for n modes,

$$H(j\omega) = \sum_{k=1}^n \frac{R_k}{j\omega - \lambda_k} + \frac{\bar{R}_k}{j\omega - \bar{\lambda}_k} \quad (2.38)$$

Where λ_k and R_k is the pole and residue, respectively. The residue is defined as

$$R_k = \phi_k \gamma_k^T \quad (2.39)$$

where ϕ_k and γ_k^T is the mode shape vector and the mode participation vector, respectively.

The FDD method assumes white noise excitation, which gives an additional, constant, PSD ma-

trix $G_{xx}(j\omega) = C$. substitution into Equation 2.37 gives

$$G_{yy}(j\omega) = \sum_{k=1}^n \sum_{s=1}^n \left[\frac{R_k}{j\omega - \lambda_k} + \frac{\bar{R}_k}{j\omega - \bar{\lambda}_k} \right] C \left[\frac{R_s}{j\omega - \lambda_s} + \frac{\bar{R}_s}{j\omega - \bar{\lambda}_s} \right]^H \quad (2.40)$$

Here, superscript H denotes the complex conjugate and transpose. Through use of Heaviside fraction theorem and some mathematical manipulations, multiplying these two partial fraction factors reduces the output PSD to a pole/residue form as follows

$$G_{yy}(j\omega) = \sum_{k=1}^n \frac{A_k}{j\omega - \lambda_k} + \frac{\bar{A}_k}{j\omega - \bar{\lambda}_k} \frac{B_k}{-j\omega - \lambda_k} + \frac{\bar{B}_k}{-j\omega - \bar{\lambda}_k}. \quad (2.41)$$

The Residue matrix is an $m * m$ hermitian matrix as the output PSD itself given by

$$A_k = R_k C \left(\sum_{s=1}^n \frac{\bar{R}_s^T}{-\lambda_k - \bar{\lambda}_s} + \frac{R_s^T}{-\lambda_k - \bar{\lambda}_s} \right) \quad (2.42)$$

this residue contribution, A_k , can also be written as

$$A_k = \frac{R_k C \bar{R}_k^T}{2\alpha_k} \quad (2.43)$$

α_k is minus the real part of the pole $\lambda_k = -\alpha_k + j\omega_k$, and therefore becomes dominating in the case of light damping. This leads to the residue, A_k becoming proportional to the mode shape vector

$$A_k \propto R_k C \bar{R}_k = \phi_k \gamma_k^T C \gamma_k \phi_k^T = d_k \phi_k \phi_k^T \quad (2.44)$$

where d_k is a scalar constant. Only a limited number of modes (one or two) contributes significantly to each frequency. These modes are denoted by $Sub(\omega)$. This way the response spectral density for the k th mode can be written as

$$G(j\omega) = \sum_{k \in Sub(\omega)} \frac{d_k \phi_k \phi_k^T}{j\omega - \lambda_k} + \frac{\bar{d}_k \bar{\phi}_k \bar{\phi}_k^T}{j\omega - \bar{\lambda}_k} \quad (2.45)$$

2.3.2 FDD Algorithm

In short, the logical process of FDD is to apply the Single Value Detriment (SVD) technique to the PSD by assuming white noise excitation. If desired, damping and undamped natural frequencies can then be obtained by taking the single degree of freedom back to the time domain by applying inverse Fourier transform. For the present work, a MATLAB function attached in Appendix B is used for identifying the modal frequencies in the bridge using the FDD method.

2.4 Vehicle Induced Vibrations

As discussed in the introduction, analytical methods for estimating traffic induced vibrations are widely explored in the literature. For the present work, simulations of vehicle response will not be performed. However, theory behind analytical methods is presented to gain understanding of the underlying causes of vehicle induced vibrations.

2.4.1 Impact Loading

Impact loading is defined as “The dynamic effect on a stationary or mobile body as imparted by the short, forcible contact of another moving body” [Dictionary of Construction \(nd\)](#), and the impact factor or Dynamic Load Factor (DLF), is often defined as the ratio between the maximum dynamic response and the maximum static response.

$$DLF = \max_{dyn} / \max_{stat} \quad (2.46)$$

As indicated by Equation 2.46 one of the manifestations of the dynamic impact effects is an increase in response. Impact loading is therefore relevant for bridge design as it directly affects ultimate limit states, serviceability limit state and fatigue assessment of a bridge.

Dynamic response is also a function of the *load application duration* (load as a function of time) relative to the natural frequencies. However, for load application from a moving vehicle on a suspension bridge, the load application function is very complex, and will not be investigated in detail in the present work.

2.4.2 Analytical Prediction of Impact Loading on Suspension Bridges

Eurocode EN-1991-2 ([Eurocode \(2003\)](#)) is a European standard used as a guideline for bridge design. The framework for this code has performed several simulations on different schemes in order to determine global local impact factors and has found the impact factor as high as 1,7 in cases with medium pavement condition. The standard also states that even more unfavourable

values can be reached with poorer pavement quality. The code recommends analysis for the individual project for bridges with lengths greater than 200 meters and is therefore not directly applicable to longer span suspension bridges discussed in the present work.

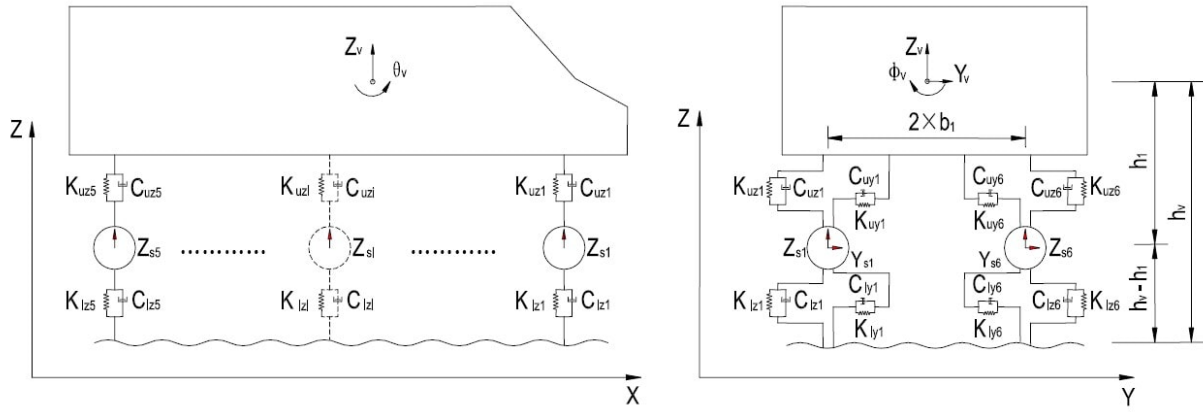
According to [Sanpaolesi and Croce \(2005\)](#), a “Development of Skills Facilitating Implementation of Eurocodes”, impact loading on bridges also depends on several parameters such as natural frequency of vehicle and bridge, roughness of pavement and velocity of vehicles. Due to the many factors affecting impact loading, it is difficult to accurately predict analytically.

[Liu et al. \(2017\)](#) presents a numerical method simulating vehicle-bridge response on long span suspension bridges by varying parameters such as vehicle velocity, parameters of the vehicle suspension (c and k) and surface roughness of bridge deck. This paper presents analytical/theoretical effects of the impact loading from varying the parameters which are expected to affect dynamic amplification from vehicles. The underlying theory used in [Liu et al. \(2017\)](#) is presented below.

2.4.3 Equation of Motion for Vehicle

Vehicles consist of a minimum of two axles, each with two or more wheels each with its own damper. Depending on the weight distribution and the positioning of the axles, the vehicle mass is distributed through each of the wheels. A vehicle model with five degrees of freedom as illustrated below in [Figure 2.2](#). Also, the dampers are considered linear and the vehicle centroid is in the geometrical center of the vehicle. Rotation around vertical direction φ_v (yaw) is included but is not depicted below. The response in the longitudinal direction (along *X axis*) is neglected as velocity is assumed constant, but will in practice be introduced through displacement from the surface roughness function which will be further explained below.

Figure 2.2: Illustration of degrees of freedom for vehicle Equation of Motion (EOM). Source: Liu et al. (2017)



Two of the five degrees of freedom for vehicle centroid are displacements in vertical and lateral direction, Z_V and Y_V , respectively. The remaining three are angular displacements, Θ_V, ϕ_V and φ_V , around y, x and z , respectively.

Each i^{th} wheel has two degrees of freedom; displacements in vertical and lateral directions, Z_{sn} and Y_{sn} . s, l and u are notations for *center, lower* and *upper* position in vertical direction, respectively, relative to the wheel center. Each wheel has a lateral distance from the center of the vehicle, b_1 . The vertical distance from the center of mass of the vehicle, M_v , to the bridge deck surface is h_v , and the distance from the center of mass of the wheel, M_{si} (for the i^{th} wheel) to M_v is h_1 . The distance from the M_{si} to the bridge deck is $h_v - h_1$.

The equation of motion for vehicle displacements in directions y and z for the vehicle body can then be expressed as

$$M_V \ddot{Y}_V + C_Y \dot{Y}_V + K_Y Y = F_{VYW} \quad (2.47)$$

$$M_V \ddot{Z}_V + C_Z \dot{Z}_V + K_Z Z = F_{VZW} \quad (2.48)$$

where $C_{Y,Z}$ and $K_{Y,Z}$ are damping and stiffness matrices in directions Y and Z , respectively, and $F_{VYW, VZW}$ are forces in directions Y and Z , respectively.

The mass moments of inertia for directions x, y and z are denoted I_{xv}, I_{yv} and I_{zv} , respectively. The equations of motion for vehicle body rotation around x, y and z axis, described by Θ_V, ϕ_V

and φ_V can then be expressed as

$$I_{XV}\ddot{\phi}_V + C_z\dot{Z}_v b_1 + C_Y\dot{Y}_V h_1 + K_z Z_V b_1 + K_Y Z_V h_v = M_{VXW} \quad (2.49)$$

$$I_{YV}\ddot{\Theta}_V + C_Y\dot{Y}_V L + K_Y Y_V L = M_{VYW} \quad (2.50)$$

$$I_{ZV}\ddot{\phi}_V + C_Z\dot{Z}_V L + K_Z Z_V L = M_{VZW} \quad (2.51)$$

where M_{VXW} , M_{VYW} and M_{VZW} are rotating moments around x , y and z , respectively.

Each wheel, i , has its own equation of motion for both degrees of freedom (displacement in z and y directions), and can be expressed as

$$\begin{aligned} M_{si}\ddot{Y}_{si} - C_{uyi}(\dot{Y}_V + h_1\dot{\phi}_V + L_i\dot{\phi}_V - \dot{Y}_{si}) \\ - K_{uyi}(Y_V + h_1\phi_V + L_i\phi_V - Y_{si}) + C_{lyi}\dot{Y}_{si} + K_{lyi}Y_{si} = 0 \end{aligned} \quad (2.52)$$

for Y direction, and

$$\begin{aligned} M_{si}\ddot{Z}_{si} - C_{uzi}(\dot{Z}_V + L_i\dot{\Theta}_V + b_1\dot{\phi}_V - \dot{Z}_{si}) \\ - K_{uzi}(Z_V + L_i\Theta_V + b_1\phi_V - Z_{si}) + C_{lzi}(\dot{Z}_{si} - \dot{Z}_{ci}) + K_{lzi}(Z_{si} - Z_{ci}) = 0 \end{aligned} \quad (2.53)$$

for Z direction. Z_{ci} is a displacement term for each i 'th wheel which can be described through pavement roughness and bridge surface “geometry”. As long as the wheel is in contact with the pavement, the acceleration, velocity and displacement of the contact point between the wheel and bridge can be described by the 2nd, 1st and 0th derivative of the surface roughness function when expressed as function of time.

“Surface roughness” can be described in both space and time coordinates as a simply plotting the vertical position of the surface relative to a reference point on the vertical axis along any horizontal axis of either space or vehicle position at a given time. This is often simulated mathematically as a random Gaussian process, with varying constants depending on surface conditions/pavement quality. The complete process and variables for this simulation are given in [Wang et al. \(2015\)](#), [Oliva et al. \(2013\)](#) and [Liu et al. \(2017\)](#), and will not be described in detail here. Typical results of such simulations are depicted below, as simulated by [Liu et al. \(2017\)](#). These are simulated as “Excellent”, “good” and “normal” conditions, as per ISO provisions ([Wang et al.](#)

(2015)) along a 1000 meter long bridge as illustrated in Figures 2.3, 2.4 and 2.5.

Figure 2.3: Illustration of simulated “excellent” road roughness. Source: Liu et al. (2017)

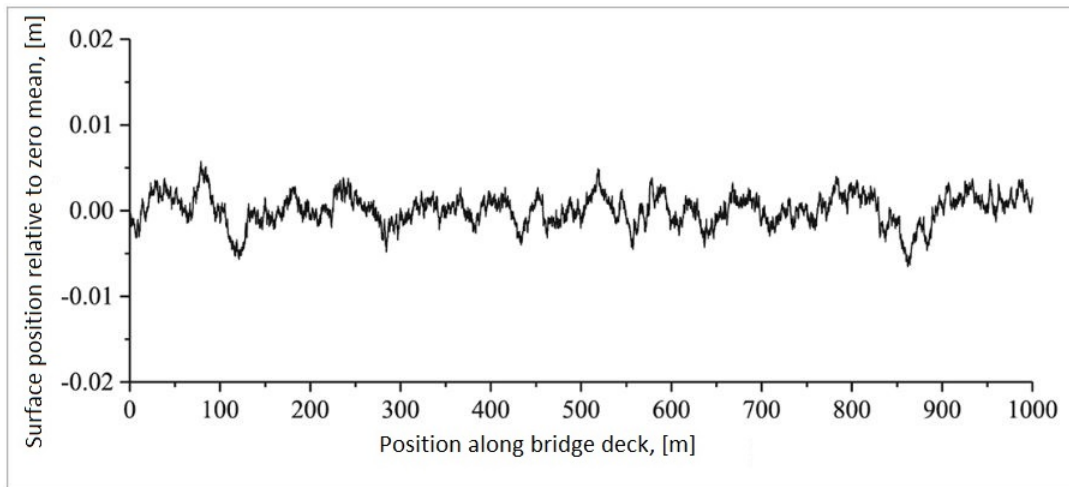


Figure 2.4: Illustration of simulated “good” road roughness. Source: Liu et al. (2017)

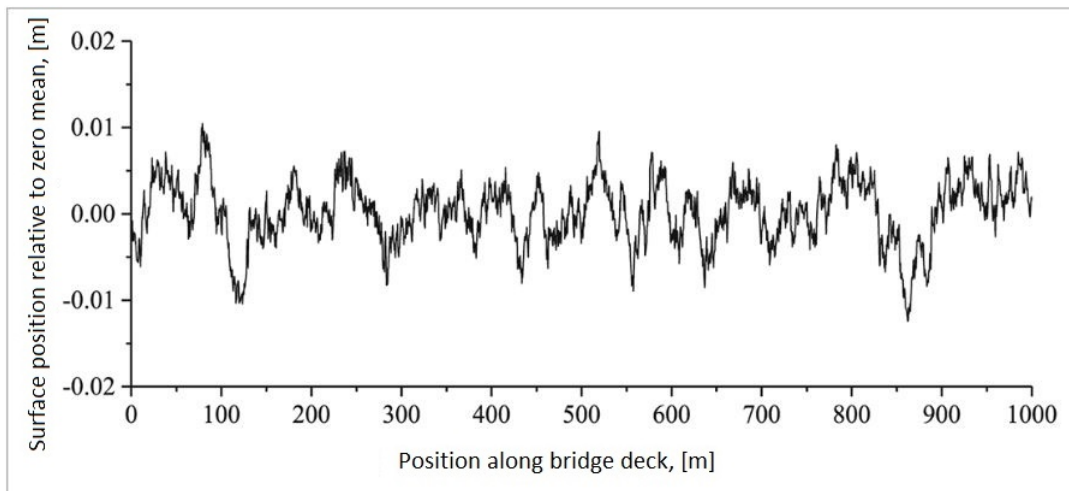
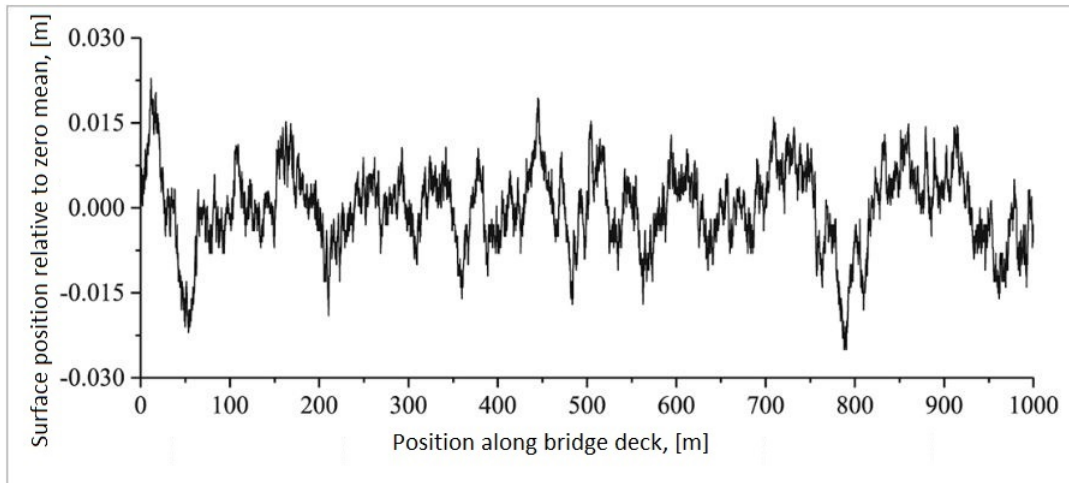


Figure 2.5: Illustration of simulated “normal” road roughness. Source: Liu et al. (2017)



2.4.4 Coupled Systems

The dynamic behaviour of a suspension bridge has already been discussed, and is quite complex with several degrees of freedom in both lateral, vertical and torsional (rotation around x-axis) direction. The equation of motion can be expressed as simple as

$$M_b \ddot{r}_b + C_b \dot{r}_b + K_b r = F \quad (2.54)$$

Where F is the load vector for external load, and M_b , C_b and K_b are the modal mass, damping and stiffness matrices for the bridge structure, respectively.

As mentioned earlier, when a vehicle is travelling along the bridge deck, surface irregularities cause displacement in the contact point of the wheel and deck initiating motion in the entire vehicle sub-system as described in its EOM. These displacements will further affect the bridge subsystem due to action – reaction (newtons 3rd law). The coupling between the two sub-systems have on each other can be modelled through the geometrical displacement as well as Force coupling. In other words, we can couple the two sub-systems through both force and displacement relationships. The result is the following equation, where each EOM consists of

individual matrices for Mass, Damping and Stiffness.

$$\mathbf{M}_b \ddot{\mathbf{r}}_b + \mathbf{C}_b \dot{\mathbf{r}}_b + \mathbf{K}_b \mathbf{r}_b = \mathbf{F}_{bv} + \mathbf{F}_{bg} \quad (2.55)$$

$$\mathbf{M}_v \ddot{\mathbf{r}}_v + \mathbf{C}_v \dot{\mathbf{r}}_v + \mathbf{K}_v \mathbf{r}_v = \mathbf{F}_{vb} + \mathbf{F}_{vg} \quad (2.56)$$

2.4.5 Simulation

Simulations for analytical methods such as the one presented above is typically done using finite element modelling programs such as ANSYS. For the present work, the theory presented above is included in order to illustrate which factors contribute to vehicle induced vibrations of a bridge. Simulations will therefore not be performed.

Chapter 3

Analysis and Results

3.1 Lysefjorden Bridge

The Lysefjorden bridge was completed in 1997, and crosses the inlet of Lysefjorden between Forsand and Oanes. The bridge is a two-lane suspension bridge with a main span of 446 meters approximately 55 meters above sea level, and towers ranging approximately 102 meters tall.

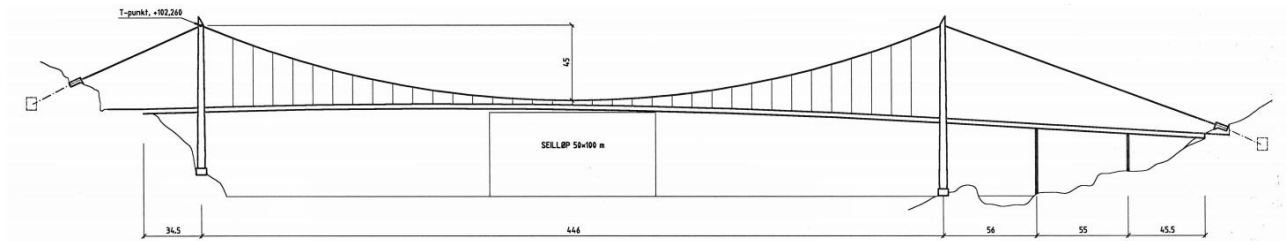


Figure 3.1: Blueprint of Lysefjorden bridge



Figure 3.2: Map showing Lysefjorden inlet and Lysefjorden Bridge. Source: [Google Maps \(nd\)](#)

3.2 Data Acquisition

3.2.1 Monitoring Equipment

The monitoring system was installed on Lysefjorden bridge starting in November 2013 as a collaboration project between the University of Stavanger (UIS) and the Norwegian Public Road Administration. The initial system consists of three types of sensors installed at different points along the span of the bridge; anemometers for measuring wind conditions, accelerometers for measuring displacements of the bridge deck and a weather station for measuring parameters such as wind, air pressure and temperature. In June 2015, a GPS system was installed to measure static and quasi-static displacement.

Anemometers and Weather Station

Six sonic anemometers of the type 3D WindMaster Pro and a Vaisala weather station are installed on the west side of the bridge different locations as illustrated in Figure 3.4. Five of the anemometers and the weather station are positioned 6 meters above deck, either directly mounted to the hangers or separate on steel poles where main cables are below 6 meters, and the sixth anemometer is fixed 10 meters above deck.

Accelerometers

Four pairs of triaxial Micro Electro Mechanical (MEM) silicon accelerometers from Canterbury Seismic Instruments Ltd. are installed at four different locations on the bridge. The sensors are installed inside the bridge deck. Each pair has a sensor positioned near the hangers/edge of the deck, one on the east and one on the west side of the bridge, in order to capture torsional response in the bridge. The positioning of the pairs relative to each other is as illustrated below in Figures 3.3 and 3.4, and enables the possibility to capture both symmetrical and non symmetrical horizontal and vertical modes. The set sampling rate of the accelerometers is 50Hz, which is further decimated in post-processing of the data.

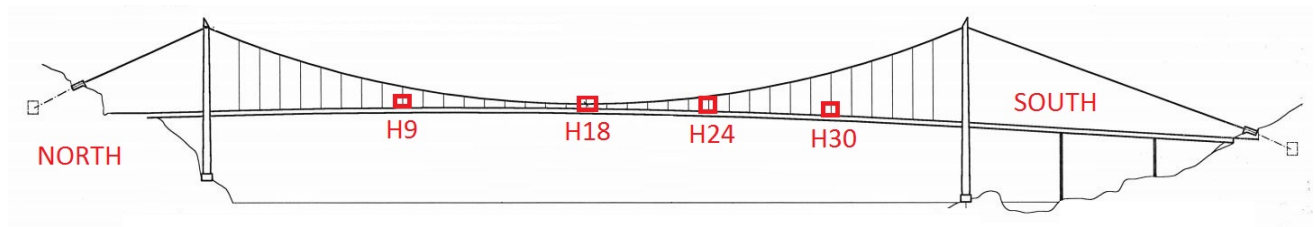


Figure 3.3: Positioning of accelerometer pairs

GPS

The GPS system is a Real-Time Kinematic-Global Positioning System (RTK-GPS) consisting of a set of Trimble BD930 Global Navigation Satellite System (GNSS) receivers coupled to Trimble AV33 GNSS antennas. The system is installed with one "measuring" station located on the longitudinal center of the bridge and one "reference" station positioned at a stationary position relative to the bridge deck as illustrated below in Figure 3.4.

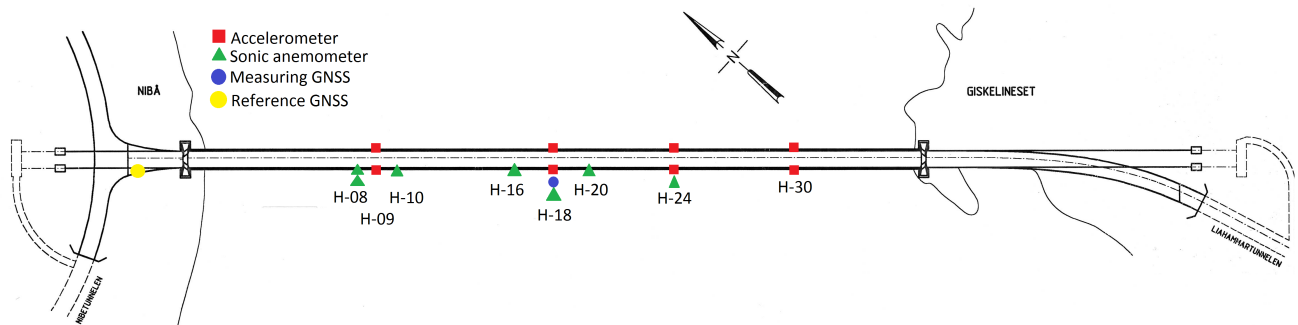


Figure 3.4: Positioning of all monitoring equipment on Lysefjorden Bridge

Sampling Rates

The sampling data from weather and accelerations are collected locally to two CUSP units, and transmitted via mobile network for storage and access. The GPS sensors can handle a sampling rate of 20Hz, and the sampling rate from accelerometers is 50Hz. However, this is reduced during post processing of data due to practical and mathematical limitations (issues using band-pass filtering with high frequency sampling rates).

3.2.2 Method for Vehicle Registration

As the purpose of this thesis is to look at traffic induced vibrations, data collection is limited to time periods of low wind speeds. It also requires the observer to be present at the location to register the vehicles passing during the relevant time period of data collection. Due to these practical limitations, data in the present thesis is limited to approximately 7 hours of relevant data, recorded during 4 days. The quality of the data is also varied due to these limitations, as some wind is inherently present in a location such as Lysefjorden inlet. Variations in temperature can also contribute to variations in the result. That being said, varied wind and temperatures in the different observations can potentially be practically beneficial as this can allow for comparing the response and damping effects from wind and varied temperatures.

During all observations of the bridge, a video camera is used to constantly monitor the bridge span with vehicles as illustrated below in Figure 3.5.



Figure 3.5: Recording setup for vehicle registration

This allows for accurate timing of the vehicles entering and exiting the bridge, as well as a means to double check if there are vehicles present on the bridge at any time of the recordings. Figure 3.6 below is a screen grab from the recording taken on April 17th, showing a semi truck passing the bridge from the south side of the bridge.

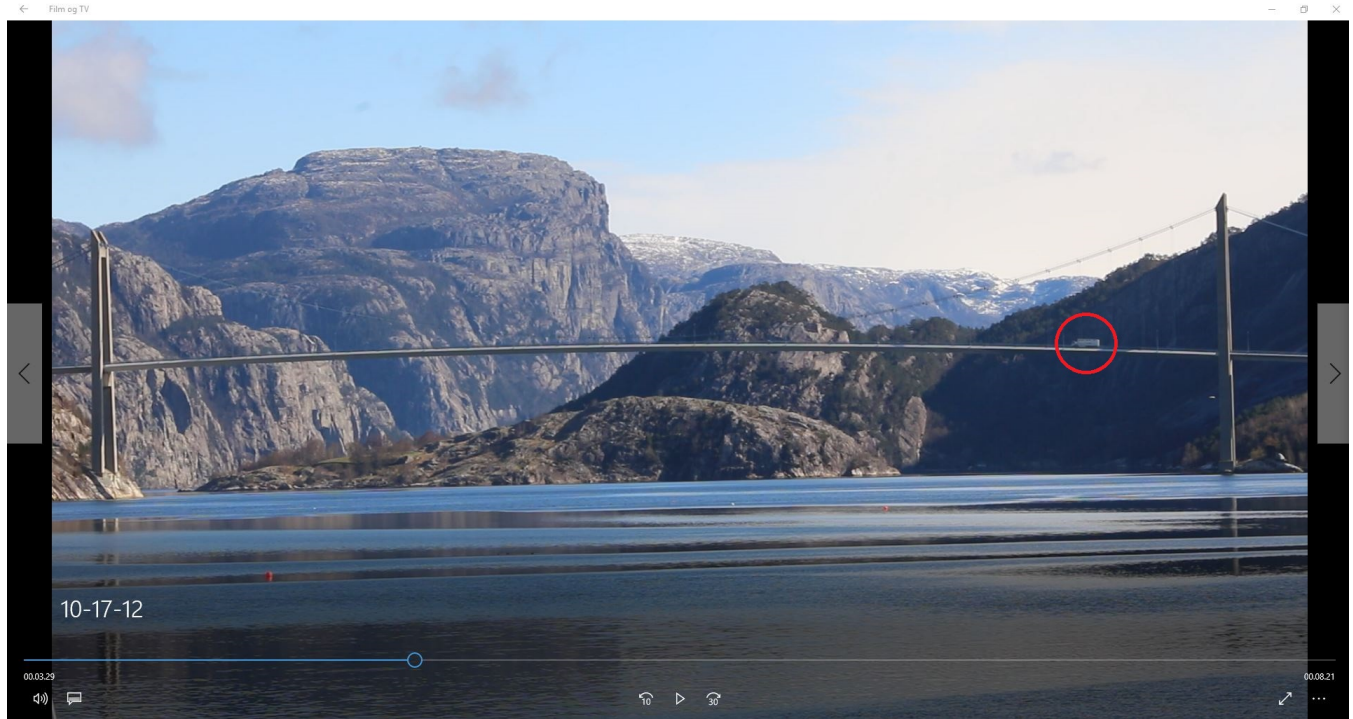


Figure 3.6: Screenshot from recorded video of bridge April 17th

After recording, the videos are thoroughly reviewed. The individual recordings are calibrated to a wrist watch during recording, which is later calibrated to the time of the recorded data from the monitoring instrumentation using the excel spreadsheet attached in in a separate electronic file. The measured bridge response can then accurately be correlated and compared to the videos of the vehicles crossing the bridge. Figure 3.7 below is a screenshot from the excel worksheet illustrating logging of recorded traffic from April 17th.

	A	B	C	D	E	F	G	H	I	J	K	N
1	start tid video	from direction	Time in video		Time on watch			Time (data)		vehicle type	comment	average velocity
2	Ref tid		fra	til	Time o	Time of	calit	Time	Time			[km/h]
3	13.35.12	North	00,28	00,50	13.35.40	13.36.02	2:02:47	11.32.53	11.33.15	truck	Small	73
4	13.35.12	North	03,50	04,17	13.39.02	13.39.29		11.36.15	11.36.42	personal car		59
5	13.35.12	North	05,00	05,28	13.40.12	13.40.40		11.37.25	11.37.53	Garbage truck		57
6	13.35.12	North	06,50	07,18	13.42.02	13.42.30		11.39.15	11.39.43	personal car	Several	57
7	13.35.12	South	08,31	09,01	13.43.43	13.44.13		11.40.56	11.41.26	truck	Small	54
8	13.35.12	North	09,03	09,38	13.44.15	13.44.50		11.41.28	11.42.03	truck		46
9	13.35.12	North	09,58	10,26	13.45.10	13.45.38		11.42.23	11.42.51	personal car		57
10	13.35.12	South	10,48	11,14	13.46.00	13.46.26		11.43.13	11.43.39	personal car		62
11	13.35.12	South	11,17	11,41	13.46.29	13.46.53		11.43.42	11.44.06	personal car		67
12	13.35.12	North	13,37	14,06	13.48.49	13.49.18		11.46.02	11.46.31	personal car		55
13	13.35.12	South	12,58	13,25	13.48.10	13.48.37		11.45.23	11.45.50	personal car		59
14	13.35.12	South	16,37	16,56	13.51.49	13.52.08		11.49.02	11.49.21	personal car		85
15	13.35.12	South	17,21	17,44	13.52.33	13.52.56		11.49.46	11.50.09	personal car		70
16	13.35.12	North	18,13	18,34	13.53.25	13.53.46		11.50.38	11.50.59	personal car		76
17	13.35.12	South	18,15	18,56	13.53.27	13.54.08		11.50.40	11.51.21	personal car		39
18	13.35.12	South	19,17	19,37	13.54.29	13.54.49		11.51.42	11.52.02	personal car		80
19	13.35.12	South	19,35	19,59	13.54.47	13.55.11		11.52.00	11.52.24	personal car		67
20	13.35.12	South	20,54	21,23	13.56.06	13.56.35		11.53.19	11.53.48	truck	small	55
21	13.35.12	North	21,49	22,13	13.57.01	13.57.25		11.54.14	11.54.38	personal car	2 vehicles	67

Figure 3.7: Screenshot from excel worksheet of vehicle registration April 17th

3.2.3 Acquired Data

The following sections provide an overview of the quality and extent of relevant data for the analysis. The bridge was observed for a varied amount of time (between 2 and 4 hours) during six different days; February 14th, March 7th, April 17th, May 2nd, May 3rd and May 5th. Recorded data from April 17th is not available for the analysis due to a storage problem at Lysefjorden bridge, but data for the remaining days is available and all sensors are considered to be synchronized and in working condition. Data from May 5th is only used for impact response analysis in Chapter 3.6, and February 14th only for spectral analysis in Chapter 3.4.

It is also important to mention that in order for the recorded data to vectors compatible with MATLAB, a MATLAB function created by Etienne Cheyney at UiS has been used to convert the raw data extracted from the bridge to MATLAB compatible vectors.

Sampling Frequency

As mentioned, the acceleration data is sampled at 50 Hz. This is reduced in post processing in MATLAB, and depending on the application, sampling frequency of either 25 or 10 Hz is used for the analysis.

Traffic and Vehicles

A complete overview of all vehicles observed and an overview of bridge acceleration response can be found in the spreadsheet attached in a separate electronic file. It is difficult to know which vehicles produce the best response for analysis before any analysis of the data is performed, and thorough inspection of both the acceleration data and the video recording of the bridge is therefore needed in order to identify the situations that cause the response which suits the analysis in question. For each analysis, the relevant cases which are potentially suitable for the analysis in question will be presented in tables for illustration.

For impact analysis, more information on vehicle and driving parameters are needed in order to come to any conclusion on what the impact load effects are. Cooperation with the drivers of

the heavy vehicles crossing the bridge has therefore been necessary, and is further explained in Chapter [3.6](#)

Temperature

Temperature is relatively constant for each day of vehicle observation, but varies quite significantly for the different days. For February 14th, March 7th, May 2nd and May 3rd, the average temperatures were around 0°C , -1°C , 10°C and 15°C , respectively.

Wind

The data collected for the present work is recorded during 5 separate days, all in which were predicted and hoped to be days with low wind velocity. As the bridge deck of Lysefjorden bridge is up to 55 meters above sea level at the start of a fjord on the western coast of Norway, it was difficult to find days without any noticeable dynamic effects from wind. This limited the amount of days in which data was collected. As illustrated in Figure [3.8](#), some of the days of recording also had some presence of what can be considered significant wind. Initially, this was considered not to be ideal, but it also opens up for the opportunity to look at aerodynamic damping effects by comparing free decay during different wind speeds.

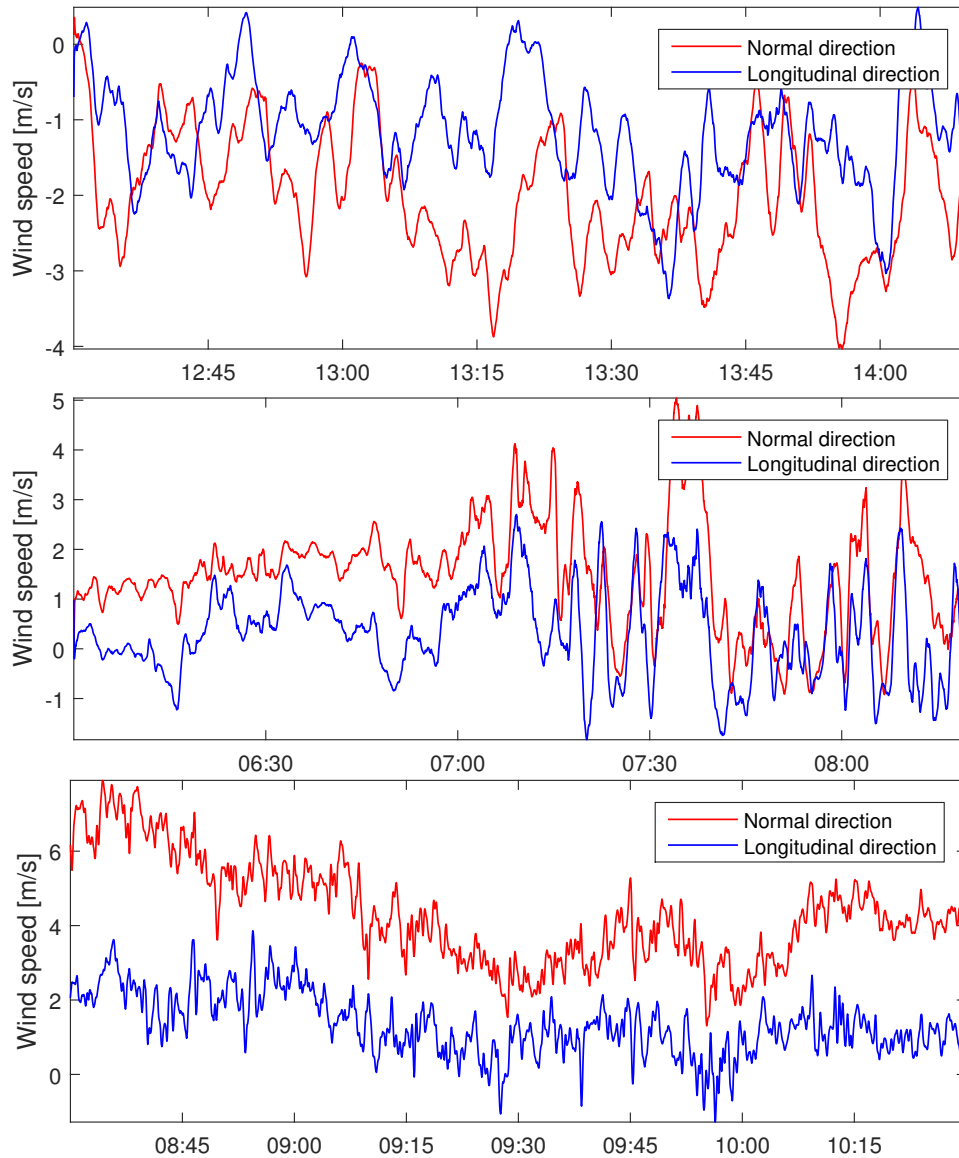


Figure 3.8: Time series of wind measurements at mid span from March 7th, May 2nd and May 3rd. “Normal” and “longitudinal” direction represents measured wind normal to and along with the bridge deck, respectively.

Figure 3.8 shows the wind measurements at mid-span for the time intervals of vehicle observation. Here, we see that wind varies quite significantly the different days of observation.

Mean wind speed for each specific time interval of interest will be considered in the analysis. Ideally, one should also consider other wind characteristics such as turbulence intensities, frequencies as well as wind in all directions. However, due to simplifications in the present work, only mean wind speeds for the time intervals of the vehicle crossings will be considered.

3.3 Thesis Limitations

The main limitations in the present work relate to the amount of data available for analysis. The method of using visual observations of the bridge is very time consuming as it requires a person to be present at the bridge while data is collected, before thoroughly reviewing and preprocessing the information from video recordings.

The complex terrain and geographical position of the bridge also limits the days with low wind speeds, which is one of the requirements for data collection for the present work.

For damping estimation, there are limitations within the accuracy of the applied method of filtering the acceleration data. Also, there are variations in wind and temperature that affect the results. However, this limitation can be reduced with larger and more comprehensive data sets. There are also limitations within the lack of theoretical understanding of damping mechanisms. The present work assumes viscous damping, but different damping mechanisms might also be present.

For impact analysis, the main limitations relate to the amount of unknown variables that theoretically contribute to impact effects. Without doing extensive and detailed research on vehicle suspension properties, weight distribution, tire pressure, tire roughness, surface roughness and condition of bridge (and more), no definite conclusion can be made on which specific factors contribute to impact loading response.

3.4 Spectral Analysis

The Power Spectral Density (PSD) function for the acceleration time series of vehicle crossings is estimated in order to identify the modal eigenfrequencies of the bridge. This is useful to understand which frequencies are excited by traffic, and is thereby also a necessary step in the damping and impact analysis performed in the present work.

Units for all the FDD spectral density functions used in the present work as well as the time-frequency plots displayed in Figure 3.9 are in decibel (db), a logarithmic unit used to express the ratio between to physical values. For the time-frequency plot, the units are fixed to a reference scale (see legend at bottom of Figure 3.9) using power ratio. For the FDD functions, the dominating frequency is the reference frequency at $0db = 1$ using amplitude ratio. The amplitude ratios and power ratios relative to db values are presented in Table 3.1 below

Table 3.1: Scale showing power ratios x , amplitude ratios \sqrt{x} , and dB equivalents $10 \log_{10} x$.

dB	Power Ratio	Amplitude Ratio
0	1	1
-10	0,1	0,316
-20	0,01	0,1
-30	0,001	0,0316
-40	0,0001	0,01
-50	0,00001	0,00316
-60	0,000001	0,001
-70	0,0000001	0,000316

3.4.1 Traffic Induced Frequencies

In order to illustrate how different, higher modes are excited by traffic, a time-frequency distribution for the time series of observation for both vertical, torsional and horizontal acceleration is displayed in Figure 3.9

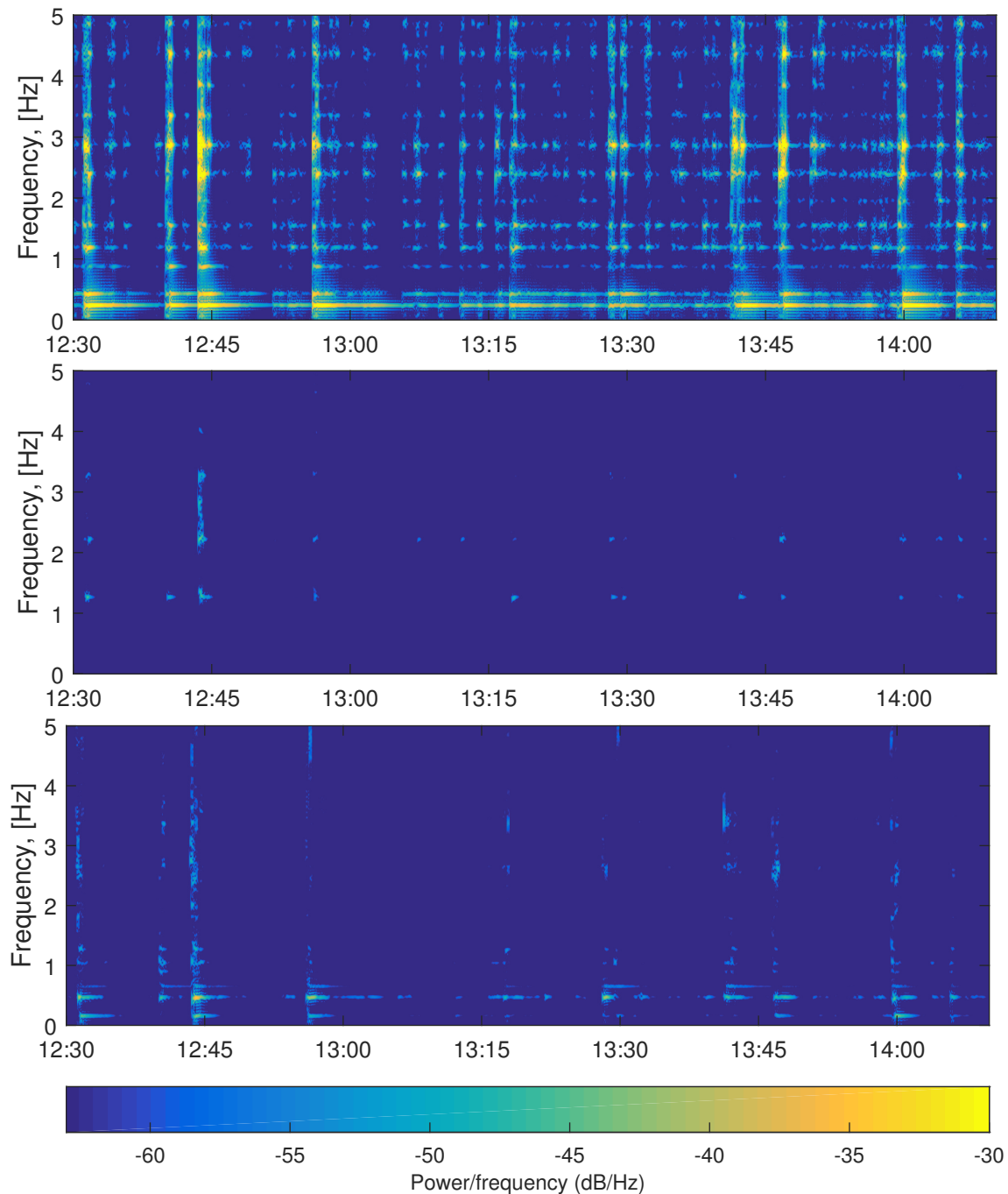


Figure 3.9: Evolutionary Power Spectral density (EPSD) for vertical (top), torsional (middle) and horizontal (bottom) acceleration data, Sensor position H9, March 7th

As shown in [Snæbjörnsson et al. \(2016\)](#) and [Cheynet \(2016\)](#), traffic induced vibrations are known to excite/cause vibrations in several modes, whereas wind induced vibrations mainly only excite the first few modes. Figure 3.9 is a time-frequency plot from March 7th, 2016, obtained

using a MATLAB function attached in Appendix B. Mean wind speed normal to the bridge is less than 2 m/s, and the majority of the vibrations can therefore be assumed to be induced by traffic. By comparing traffic observations during the time interval discussed above, all the peaks correspond with vehicles observed on the bridge.

For vertical acceleration, several frequencies appear to be excited by traffic. For torsional and horizontal acceleration, fewer modes are excited. Further analysis on the exact response frequencies will be performed below, and analysis on response characteristics for the different frequencies will be further explored in Chapter 3.5.

Peak Picking Method

In order to identify the modal frequencies of the bridge deck, the peak picking method of PSD functions is used. A Frequency Domain Decomposition function in MATLAB which combines data from all four sensor positions is used in the following analysis. Compared to using PSD for one sensor, this reduces the risk of overlooking modes and identifying measurement noise as modal vibration. See Appendix B for attached MATLAB code.

For simplicity, only the 12 first modes/visible peaks are picked for vertical and horizontal vibration, and 8 for torsional vibration.

PSD functions illustrated in Figure 3.10 are for the entire time series of observation from March 7th for vertical, torsional and horizontal acceleration.

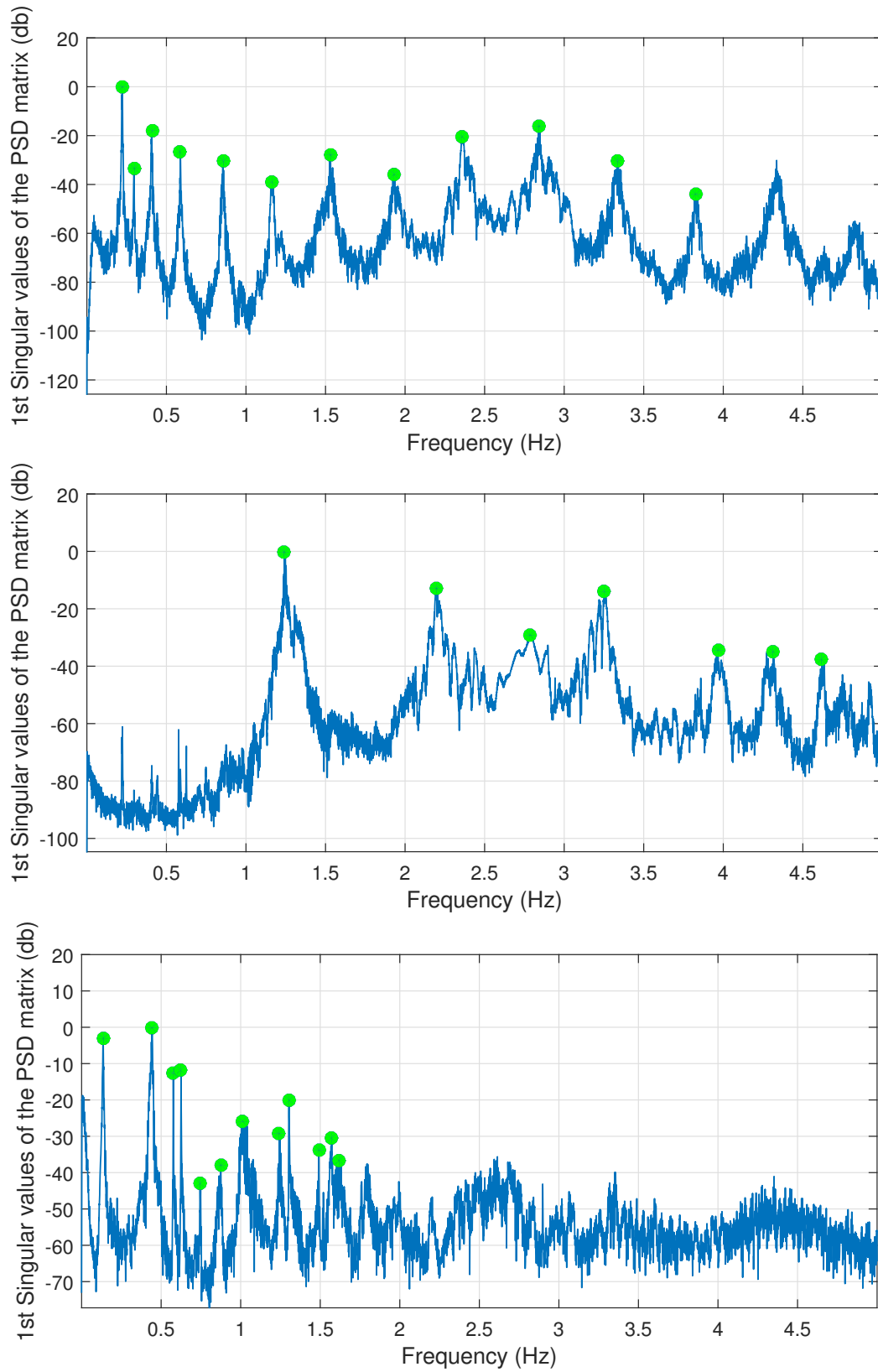


Figure 3.10: PSD used for peak picking March 7th for vertical (top), torsional (middle) and horizontal (bottom)

The results from all days of observation are summarized in Tables 3.2, 3.3 and 3.4 below.

Table 3.2: Identified vertical modal frequencies

Identified mode number	day of observation				maximum diff [Hz]
	February 14th [Hz]	March 7th [Hz]	May 2nd [Hz]	May 3rd [Hz]	
1	0,2243	0,2235	0,2220	0,2189	0,0053
2	0,2937	0,2960	0,2937	0,2929	0,0030
3	0,4135	0,4086	0,40436	0,4035	0,0099
4	0,5928	0,5882	0,5859	0,5828	0,0099
5	0,8651	0,8544	0,8468	0,84916	0,0183
6	1,1703	1,1665	1,1619	1,15806	0,0122
7	1,5350	1,5313	1,5113	1,5129	0,0236
8	1,9867	1,9288	1,9211	1,9149	0,0718
9	2,4163	2,3689	2,3720	2,3430	0,0732
10	2,8847	2,8381	2,8435	2,8015	0,0831
11	3,3706	3,3356	3,3134	3,2890	0,0816
12	3,8673	3,8239	3,8192	3,7811	0,0862

Table 3.3: Identified torsional modal frequencies

Identified mode number	day of observation				maximum diff [Hz]
	February 14th [Hz]	March 7th [Hz]	May 2nd [Hz]	May 3rd [Hz]	
1	1,2603	1,2428	1,2405	1,2321	0,0028
2	2,2339	2,1981	2,1889	2,1729	0,0610
3	-	2,7870	-	-	2,7870
4	3,2829	3,2509	3,2242	3,1967	0,0862
5	4,0077	3,9672	3,9344	3,9466	0,0732
6	4,3395	4,3159	4,2733	4,2724	0,0671
7	4,7783	4,7494	4,7341	4,7135	0,0648
8	5,1239	5,0803	5,0911	5,0736	0,0503
9	5,4153	-	5,3627	5,3429	0,0725

Table 3.4: Identified horizontal modal frequencies

Identified mode number	day of observation				maximum diff [Hz]
	Feburary 14th [Hz]	March 7th [Hz]	May 2nd [Hz]	May 3rd [Hz]	
1	0,1355	0,1349	0,1343	0,1335	0,0020
2	-	-	-	0,2190	-
3	0,4499	0,4437	0,4402	0,4364	0,0135
4	0,5779	0,5767	0,5768	0,5768	0,0012
5	0,6274	0,6255	0,6263	0,6248	0,0026
6	0,7483	0,7445	-	0,7393	0,0091
7	0,8814	0,8752	0,8552	0,8583	0,0262
8	1,0266	1,0150	1,0093	0,9986	0,0280
9	1,2604	1,2427	1,2383	1,2321	0,0283
10	1,3080	1,3037	1,3038	1,3015	0,0065
11	1,4961	1,4911	1,4855	1,4718	0,0243
12	1,5730	1,5722	-	1,5382	0,0348

As we see in Tables 3.2, 3.3 and 3.4, modal frequencies are quite consistent, only varying slightly depending on the day of observation. For torsional and horizontal directions, a few frequencies were not consistent over all days. This can be due to the fact that horizontal and torsional response from vehicles is not very significant as illustrated in Figure 3.10 as well as measurement noise or a specific situation (wind, vehicle) that caused response on this day only. Xia et al. (2012) states that higher temperatures decreases the modal frequencies. Cheynet (2016) also suggests a slight temperature dependency of eigenfrequencies on Lysefjorden Bridge. The deviations in the present measurements seem to agree with this, as the mean temperature February 14th was around 0 °C and around 15 °C on May 3rd. For the majority of the identified frequencies, these days are also the days with the highest and lowest frequencies, respectively. Higher frequencies also appear to have higher variations with variations in temperature, which agrees with Cheynet (2016).

Previous work on identifying modal frequencies using AVM measurement data on Lysefjorden bridge is performed for the first 6 vertical modes and 6 torsional modes in the work by Lunder (2014), and 6 vertical modes and 2 torsional modes in the work by Cheynet (2016). The results from these papers are displayed and compared to the mean modal frequencies identified in the present work in Table 3.5.

Table 3.5: Comparison of the eigen-frequencies identified in previous work on Lysefjorden Bridge

Mode name	Present work [Hz]	Cheynet (2016)		Lunder (2014)	
		SSI-COV [Hz]	deviation %	Peak picking [Hz]	deviation %
VA1	0,2221	0,223	0,05	0,224	-1,35
VS1	0,294	0,294	0	0,295	-0,34
VS2	0,407	0,408	-0,24	0,407	0
VA2	0,587	0,587	0	0,590	-0,5
VS3	0,854	0,853	0,12	0,894	-4,68
VA3	1,164	1,163	0,09	1,169	0,043
TS1	1,244	1,237	0,55	1,230	1,11
TA1	2,198	2,184	0,65	2,191	0,34
TS2	3,239	-	-	3,248	-0,29
TA2	3,964 or 4,300	-	-	3,954 or 4,335	0,25 or -0,81
TA3	5,092	-	-	5,072 or 6,480	0,40
TS3	4,744 or 5,374	-	-	4,752 or 5,423	-0,17 or -0,90
HS1	0,135	0,136	-1,09	0,132	1,883
HA1	0,443	0,444	-0,33	0,475	-7,335
HS2	0,577	0,577	0,007	0,5-0,6	13,351
HA2	0,626	0,626	0,003	0,5-0,6	4,156
HS3	0,744 or 0,868	0,742	0,27	0,874	-0,749
HA3	1,012	1,011	0,138	1,027	-1,441

The abbreviations “VA”, “VS”, “TA”, “TS”, “HA” and “HS” stands for “Vertical Asymmetric”, “Vertical Symmetric”, “Torsional Symmetric”, “Torsional Asymmetric”, “Horizontal Asymmetric” and “Horizontal Symmetric”, respectively, and refers to the shape and direction of the vibration as identified in [Cheynet \(2016\)](#) and [Lunder \(2014\)](#). The present work will not perform any further analysis on mode shapes, but findings from [Lunder \(2014\)](#) which illustrates the first six vertical, torsional and horizontal modes are presented in Appendix A in order to illustrate how different sensor positions (H9, H18, H24 and H30) respond differently for different modes.

When comparing the results of the vertical eigenfrequencies identified in the present work with those identified in [Cheynet \(2016\)](#) and [Lunder \(2014\)](#), it can be suggested that the modal frequencies are quite accurate. Without having any basis for comparisons for the higher modes 6

- 12, referred to as F7 - F12 in the present work for vertical frequencies, it seems reasonable to assume they are accurate as they are found using the same method as the first six modes.

3.4.2 Modes Excited by Individual Vehicles

For the present analysis, it is of interest to look at vibrations from individual vehicles. By using the video observations of traffic on the bridge, it is possible to identify PSD function peaks for each vehicle. An example illustrating (typical) response from an individual vehicle is illustrated below.

Vertical Response from Traffic

As seen in Figure 3.9, traffic appears to excite several vertical modes of the bridge. For small vehicles, only the higher modes are excited. The example displayed in Figure 3.11 and Table 3.6 shows a PSD function for vertical acceleration data used for peak picking for a small truck crossing from the South during relatively low wind speed. Here, mode VS1 is not visible in the PSD function.

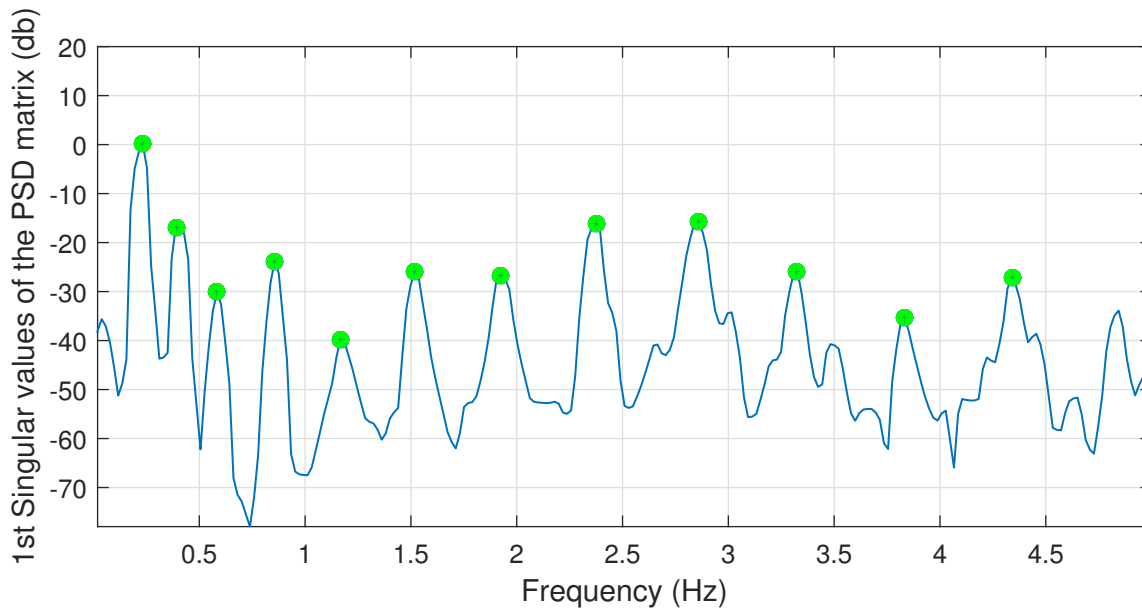


Figure 3.11: PSD peak picking for small truck crossing from south at 12.56.10 on March 7th with mean wind speed of 2,5 m/s

Table 3.6: Identified vertical frequencies from individual small truck crossing from south at 12.56.10 on March 7th

Mode name	identified frequency [Hz]
VA1	0,233
VS1	-
VS2	0,389
VA2	0,587
VS3	0,854
VA3	1,167
F7	1,517
F8	1,926
F9	2,373
F10	2,859
F11	3,326
F12	3,832

Torsional and Horizontal Response from Traffic

By looking at Figure 3.9, it can appear that torsional and horizontal response is not as significant from traffic, and in many cases it is hard to identify the modes from PSD functions. Table 3.7 lists the modes identified for the torsional response for the same vehicle as above. Here, the seventh identified mode is referred to as TF7.

Table 3.7: Identified torsional frequencies from individual small truck crossing from south at 12.56.10 on March 7th

Mode name	identified frequency [Hz]
TA1	1,262
TS1	2,242
TS2	3,319
TA2	3,901
TS3	4,290
TA3	4,775
TF7	5,085

The PSD function for the horizontal acceleration for the same vehicle does not give sufficient

response to identify the modal frequencies.

3.4.3 Response Frequencies in Individual Sensors

As mentioned, the modes in Table 3.2 are calculated by combining all sensors using an FDD method in MATLAB. For the analysis performed in the present work, it is also necessary to look at response at different locations along the bridge. This can be due to practical reasons such as quantifying the displacement or acceleration or as a means to better time and filter the signal around certain frequencies as seen below in Chapters 3.5, 3.6 and 3.7.

This is done with a MATLAB function with automatic peak picking of PSD functions for a given time interval attached in Appendix B, and can easily be performed for each individual case before analysis. Figure 3.12 illustrates the different response in the different sensors for the same, single crossing of a “small” truck entering the bridge at 12.56.10 on March 7th from the South. Here, different sensors identify different frequencies, and also have the same frequencies with different (relative) magnitude.

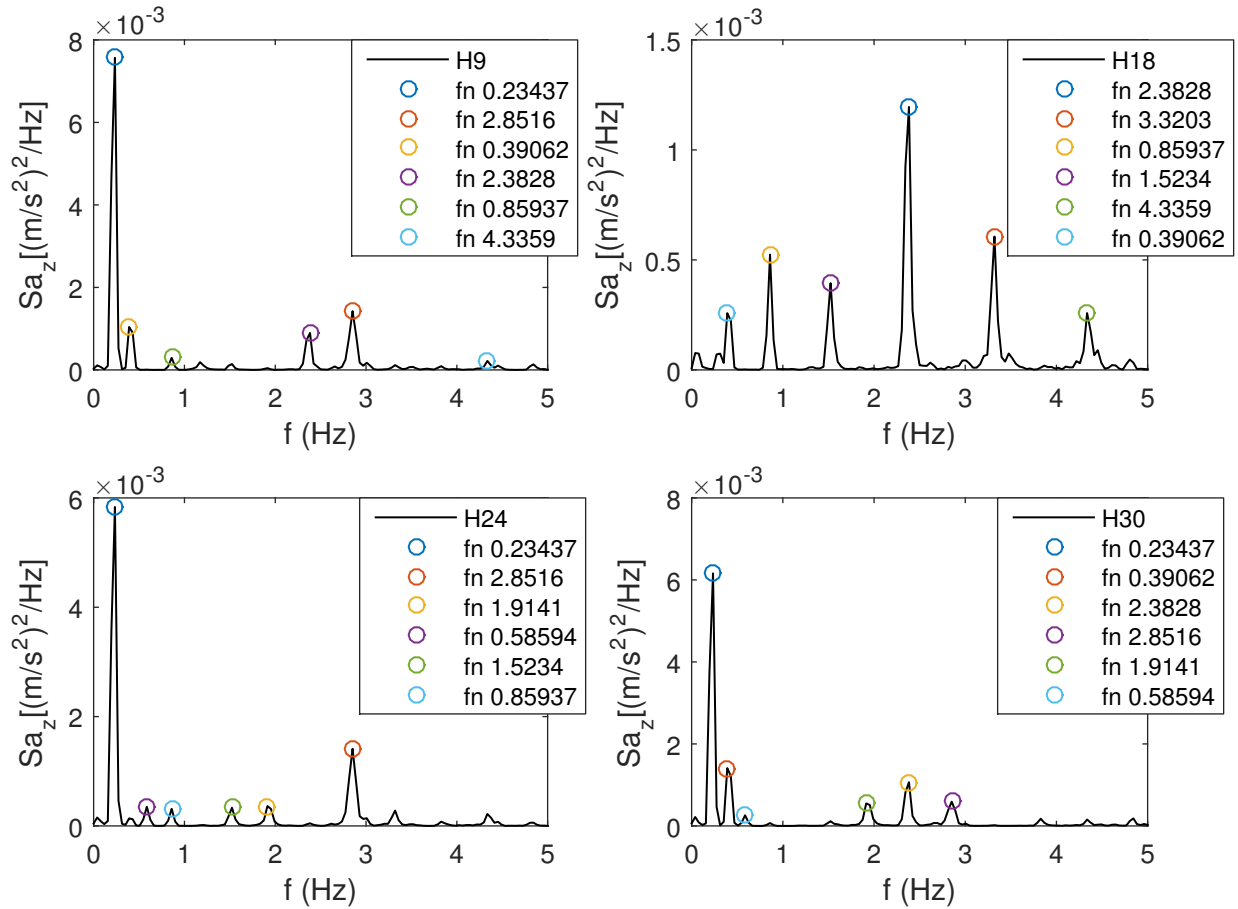


Figure 3.12: PSD of all sensor positions for a single crossing truck at 12.56.10 on March 7th with mean wind speed of 2,5 m/s

3.4.4 Signal Processing/Filtering

In order to analyze the individual modal parameters, it is convenient to filter out the frequencies of interest. In the present work, this is done with MATLAB functions attached in Appendix B based on the Butterworth filtering method either using high-pass and low-pass or band-pass filtering around the frequencies of interest.

When using high-pass and low-pass filtering, the acceleration data is first high-pass filtered with a cutoff frequency between 5 and 10 % over the target frequency, before the data is further low-pass filtered with a cut-off frequency between 5 and 10 % below the target frequency.

When using band-pass filtering, upper and lower cut-off frequencies are specified between 5 -

10 % higher and lower than the target frequency, respectively

The filtering order can also be specified between 1 and 8 in the MATLAB filter function used for the present work. The order specifies the *steepness* of the cutoff curve. Attempts have been made to improve filtering results by varying the order of the filter, but in most cases the best results were obtained with the 8th order filter.

3.5 Response Amplitude and Characteristics

Apart from looking at response frequencies analysed in Chapter 3.4, it is also necessary to look at the modal acceleration and displacement response *time series* for different vehicles from different directions. This can be done by filtering the acceleration data as described above in Chapter 3.4.4.

In the following, acceleration and displacement response from a set of chosen vehicle crossings will be analyzed and illustrated in order to increase the understanding of bridge response from vehicles. This is a necessary step before performing impact and damping analysis in Chapters 3.6 and 3.7.

Table 3.8 presents an overview of observed situations which will be used for response analysis. Here, a sampling frequency of 25Hz is used.

Table 3.8: Vehicle crossings for response analysis

Case number	Date [month,day]	Time on bridge [HH:MM:SS]	Time off bridge [HH:MM:SS]	From direction enters bridge	Vehicle type (rough description)
1	March 7th	12:40:18	12:40:46	North	Truck
2	March 7th	12:43:49	12:44:56	North and South	2 trucks
3	March 7th	12:56:12	12:56:41	South	Small Truck
4	March 7th	13:01:45	13:02:09	South	Small Truck
5	March 7th	13:12:08	13:12:28	South	Small buss
6	March 7th	13:17:32	13:18:04	South	Buss
7	March 7th	13:29:33	13:30:00	South	Truck
8	March 7th	13:42:11	13:42:41	North	Truck (15 s after another truck)
9	March 7th	13:46:40	13:47:13	North	Truck
10	March 7th	14:05:55	14:06:16	South	Truck

In order to illustrate the bridge response from vehicles, the following steps are presented for two a cases.

1. Unfiltered acceleration response for all sensors
2. Filtered acceleration response for each sensor for selected modes. (VA1 VS3 and F7 for vertical response and TA1 and TS1 for torsional response)

Cases 1 and 10 are selected as cases for illustration. These cases are chosen as they from an observers perspective appear to be similar vehicles, and illustrate differences in response from vehicles entering the bridge from different directions of the bridge and also how presence of smaller vehicles can affect the response.

case 1 - description

The truck is what appears to be a garbage truck entering the bridge from the North side. Due to the intersection right before the bridge, the truck enters the bridge at a relatively low velocity (approximately 30km/h), but accelerates to approximately 60 km/h during the first quarter span of the bridge. There are no vehicles on the bridge before, during or within 1 minute and 22 seconds after the vehicle has exited the bridge. Average wind speed normal to the bridge deck is 1 m/s.

case 2 - description

The truck is what appears to be a large postal truck that enters the bridge from the South side of the bridge. The vehicle enters the bridge at a velocity approximated at 73 km/h and keeps this velocity until it reduces its velocity quite significantly during the last 50 meters of the free span before it exits the bridge. There is one small vehicle on the bridge when the truck enters the bridge. Another small vehicle enters the bridge as the truck exits, and one more 20 seconds after.

3.5.1 Vertical Acceleration Response

Figure 3.13 presents unfiltered vertical acceleration response for all the cases along with the timing of each case.

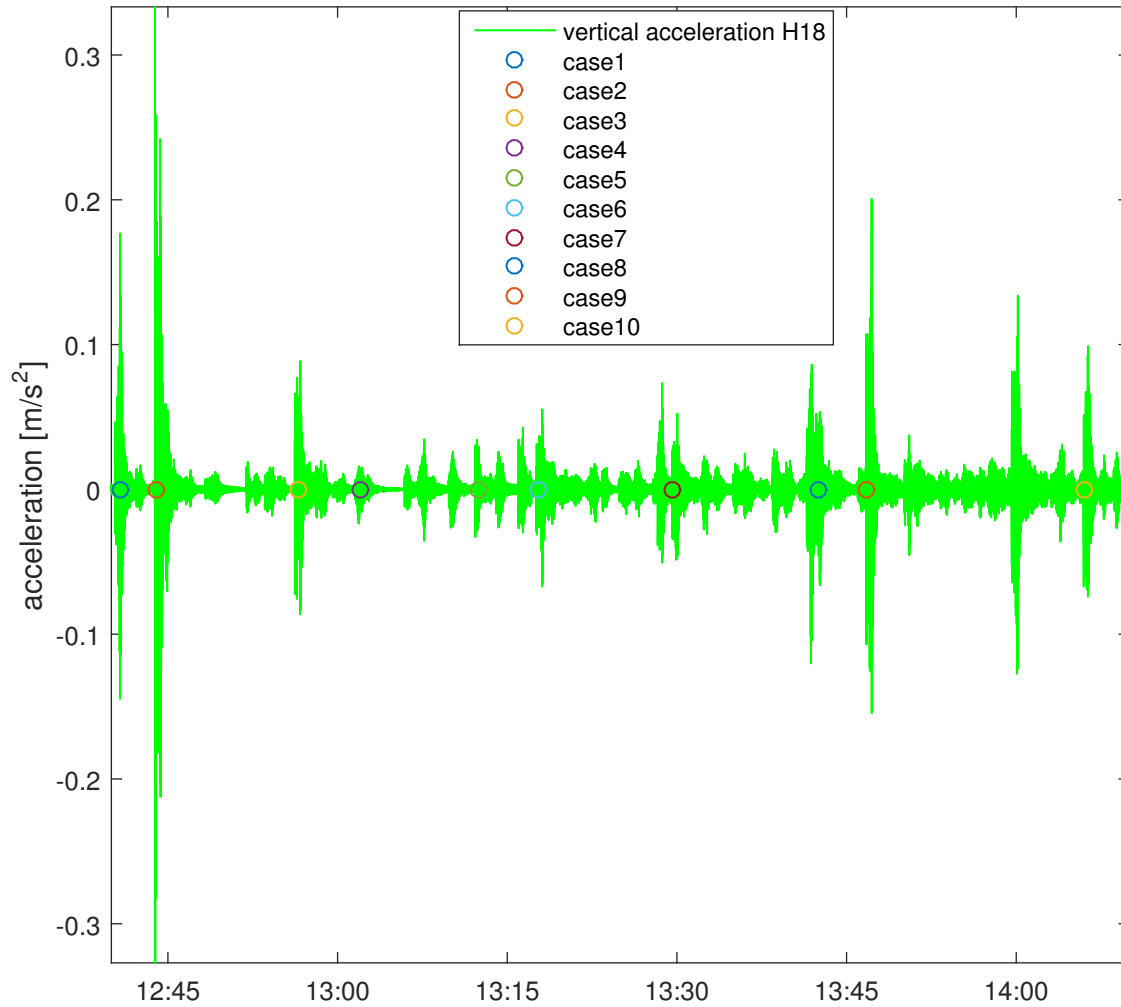


Figure 3.13: Overview of unfiltered vertical acceleration response at mid span for the cases illustrated in Table 3.8 on March 7th

Unfiltered Vertical Acceleration Response for All Sensors

Figures 3.14 and 3.15 illustrates unfiltered acceleration for case 1 and case 2, respectively.

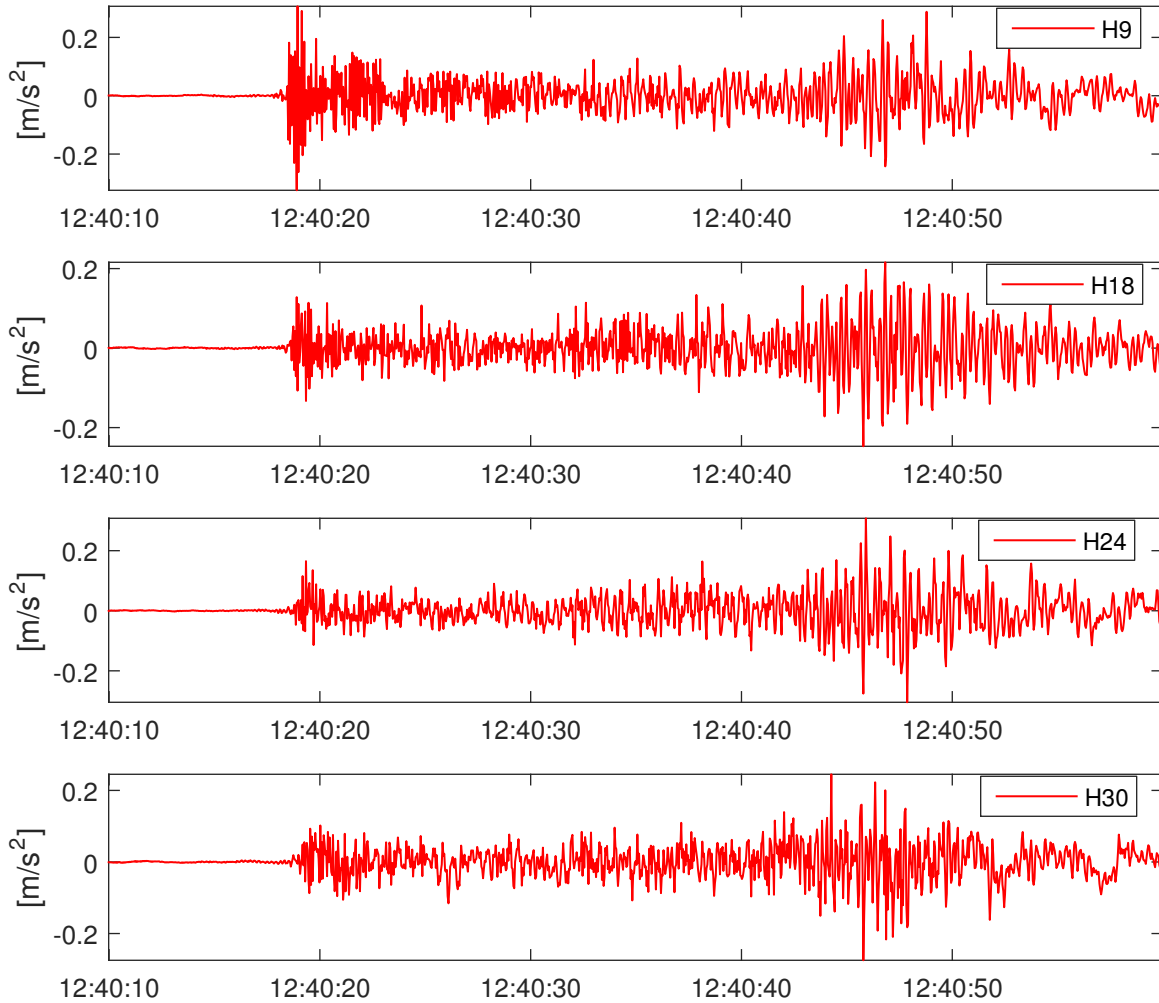


Figure 3.14: Unfiltered vertical data for all 4 accelerometers for truck crossing from the North (case 1)

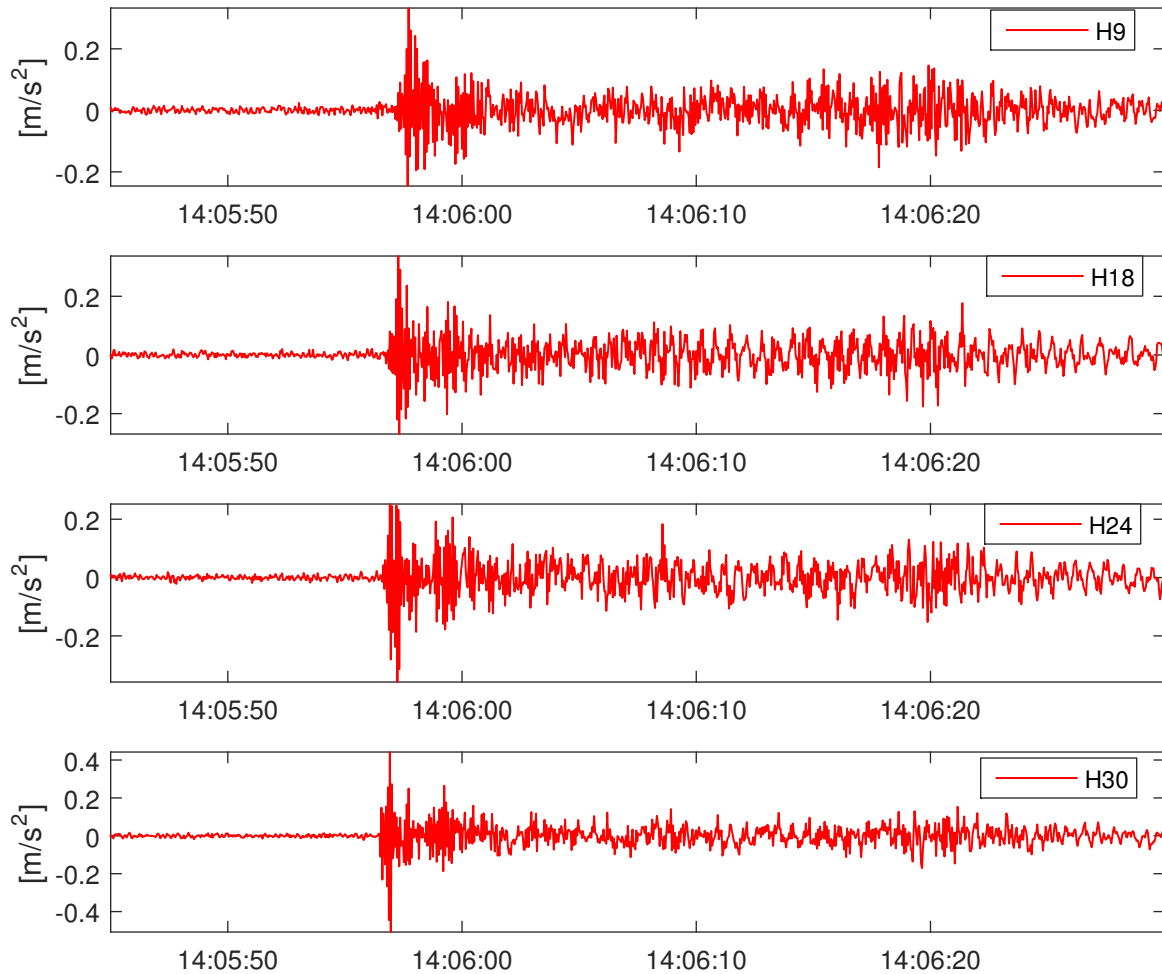


Figure 3.15: Unfiltered vertical acceleration data for all 4 accelerometers for truck crossing from the South (case 10)

By looking at the unfiltered acceleration data for cases 1 and 10 presented above in Figures 3.14 and 3.15 and assessing them qualitatively, one thing is worth mentioning; with the exception of sensor H9 in case 1, all sensors for both cases have their maximum response amplitude as the vehicle is located on the South entrance (or exit) of the bridge.

This phenomenon can be investigated in more detail by looking at the modal response for the individual sensors for the two cases.

Filtered Acceleration Response for All Sensors

For the following Figures, the dots “Case 1 on”, “Case 2 on”, “Case 1 off” and “Case 2 off” illustrates the time when case 1 and 2 enter and exit the bridge, respectively.

VA1 - 0,22 Hz

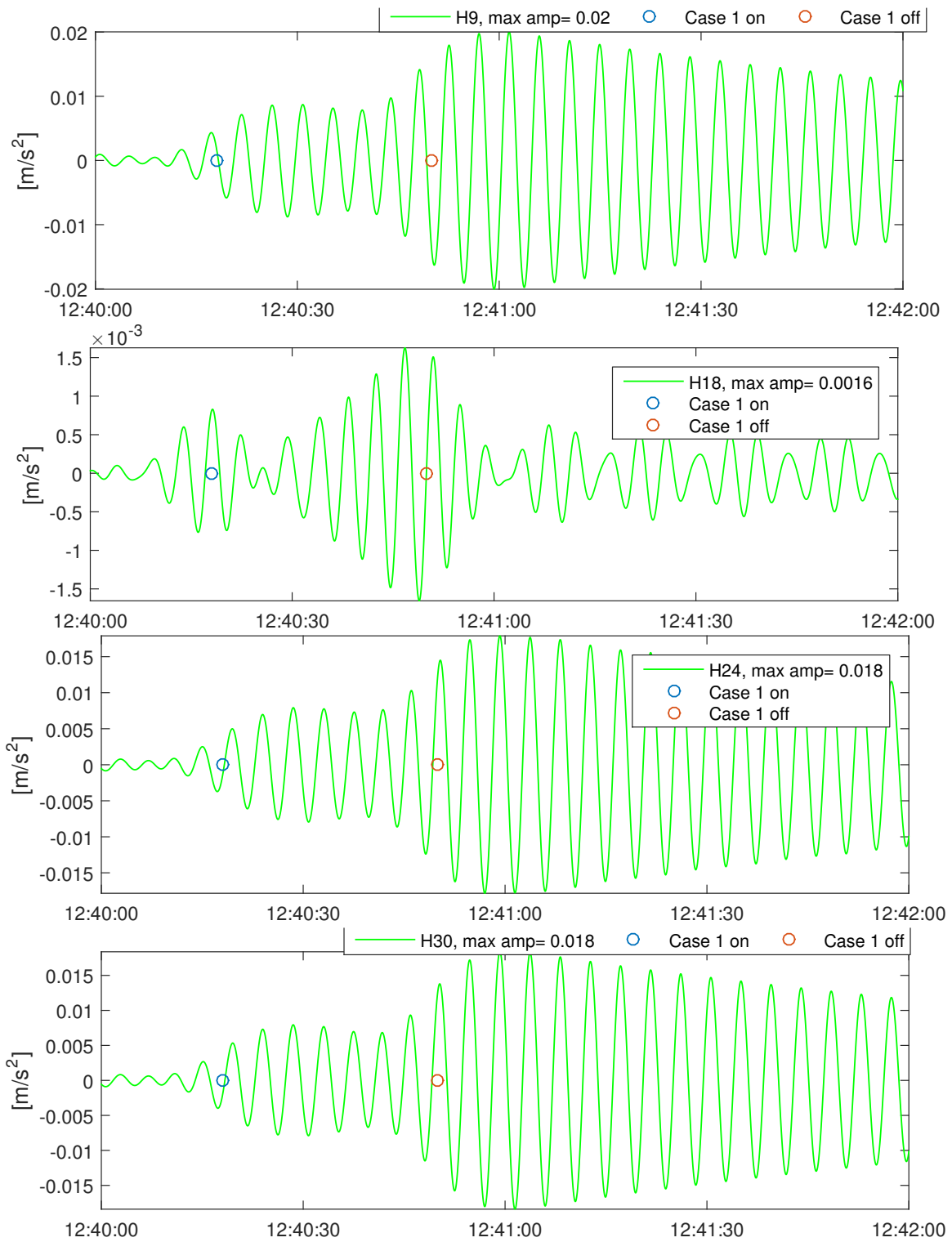


Figure 3.16: Acceleration response band-pass filtered around 0,22 Hz (VA1) for case 1 - from North

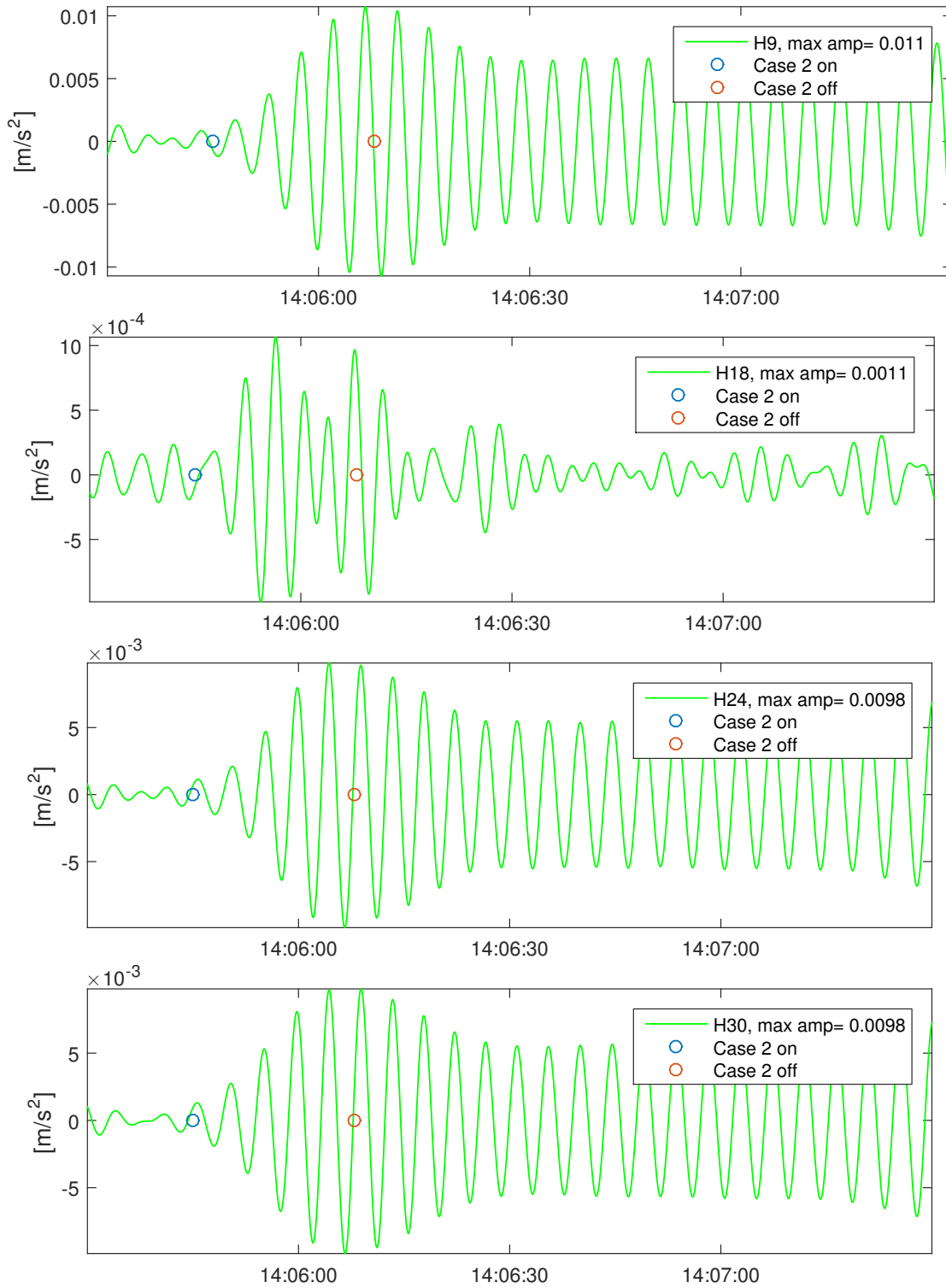


Figure 3.17: Acceleration response band-pass filtered around 0,22 Hz (VA1) for case 2 - from South

As we can expect from mode VA1, sensor H18 located at mid-span is relatively stationary, as is

expected for asymmetric modes (see Appendix A). Sensor H9 has the largest amplitude as this sensor is positioned at 1/4th of the bridge span. A more interesting observation is the timing of when the maximum amplitudes occur for the different sensors. As with the unfiltered acceleration data, the maximum modal acceleration peaks occur approximately when the vehicle is located on the South exit/entrance of the bridge. For each case, this is when the vehicles have the highest velocity, and along with bridge geometry and poor pavement condition here, this is an indication of impact response. It is difficult to determine how the different “impact” contributions (velocity, road roughness etc) affect the impact load individually, as this requires detailed information and about vehicle parameters along with controlled experiments. This will be further explored in an experiment performed in order to get an idea of the impact effect from velocity for heavy vehicles. This experiment is described in more detail below in Chapter 3.6.

VS3 - 0,86 Hz

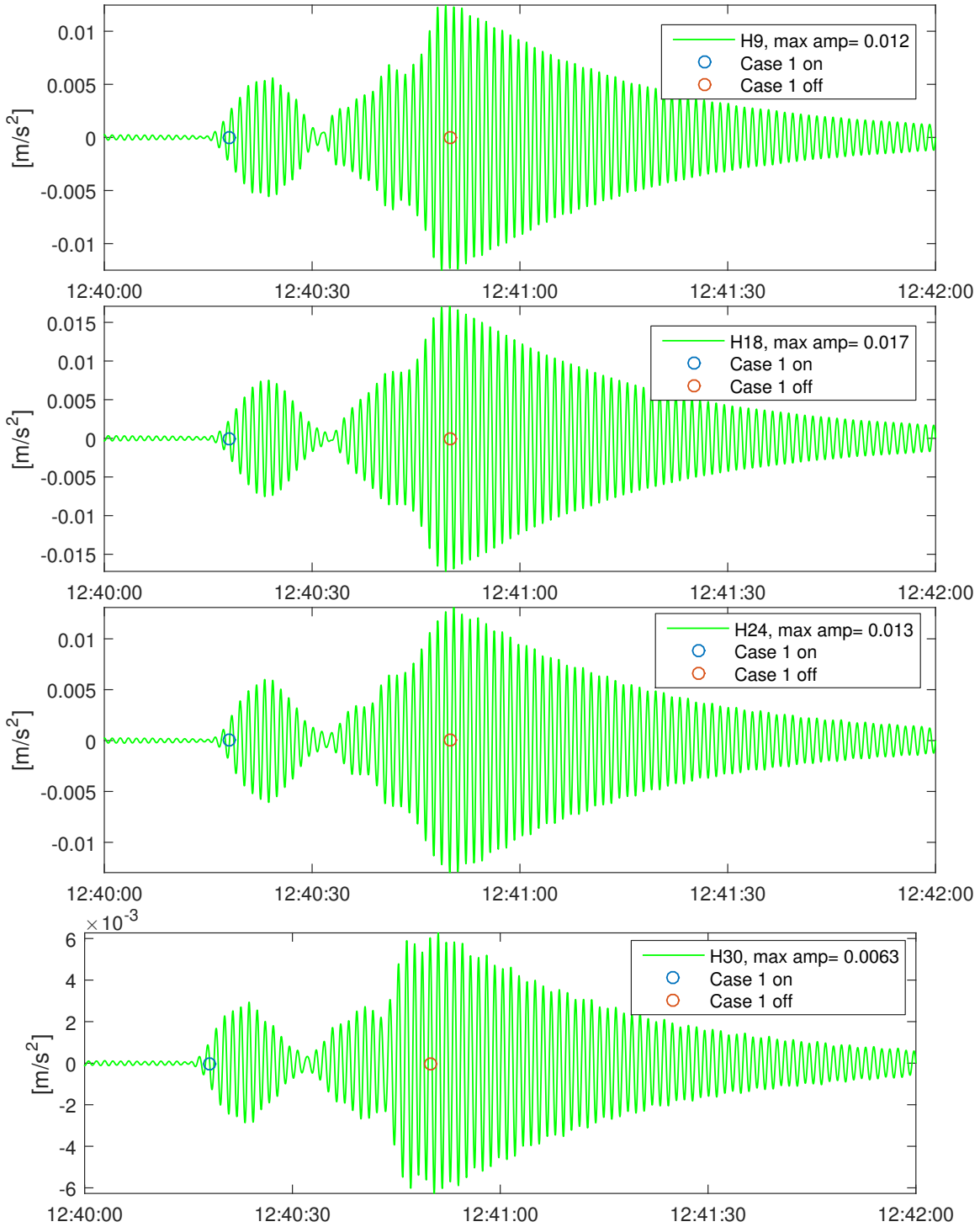


Figure 3.18: Acceleration response band-pass filtered around 0,86 Hz (VS3) for case 1 - from North

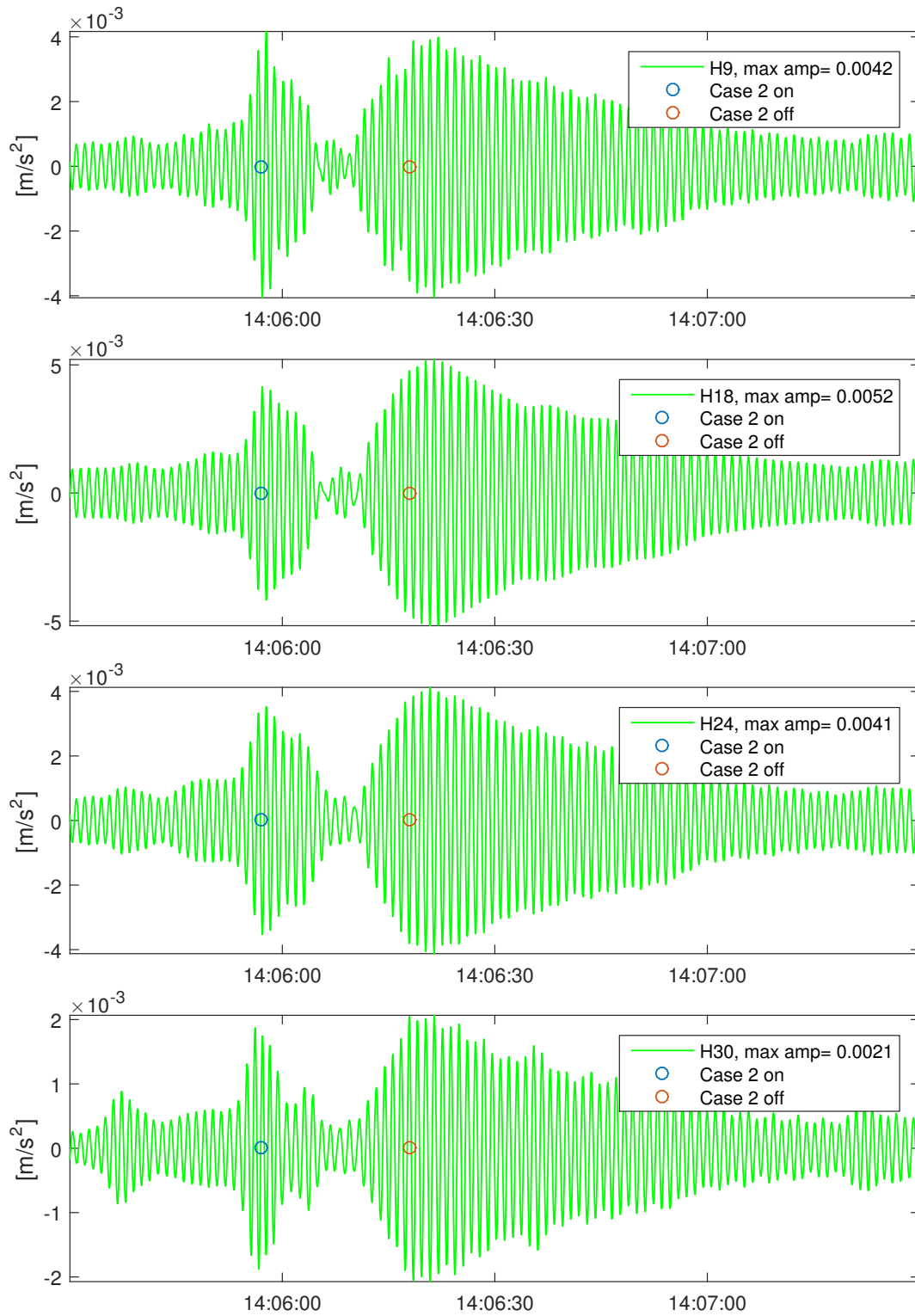


Figure 3.19: Acceleration response band-pass filtered around 0,86Hz (VS3) for case 2 - from South

For VS3, both cases illustrated in Figures 3.18 and 3.19 reach their maximum modal response as the vehicle exits the bridge. Another interesting observation here is how the oscillation seems to stop approximately as the vehicle is positioned at mid-span of the bridge. For both cases 1 and 10, the modal oscillations stop quite suddenly as the vehicle is crossing the bridge compared to the free vibrations after the vehicle has left the bridge. This can be an indication that the presence of the vehicle on the bridge increases damping as it passes a certain part of the bridge.

F7 - 1,55Hz

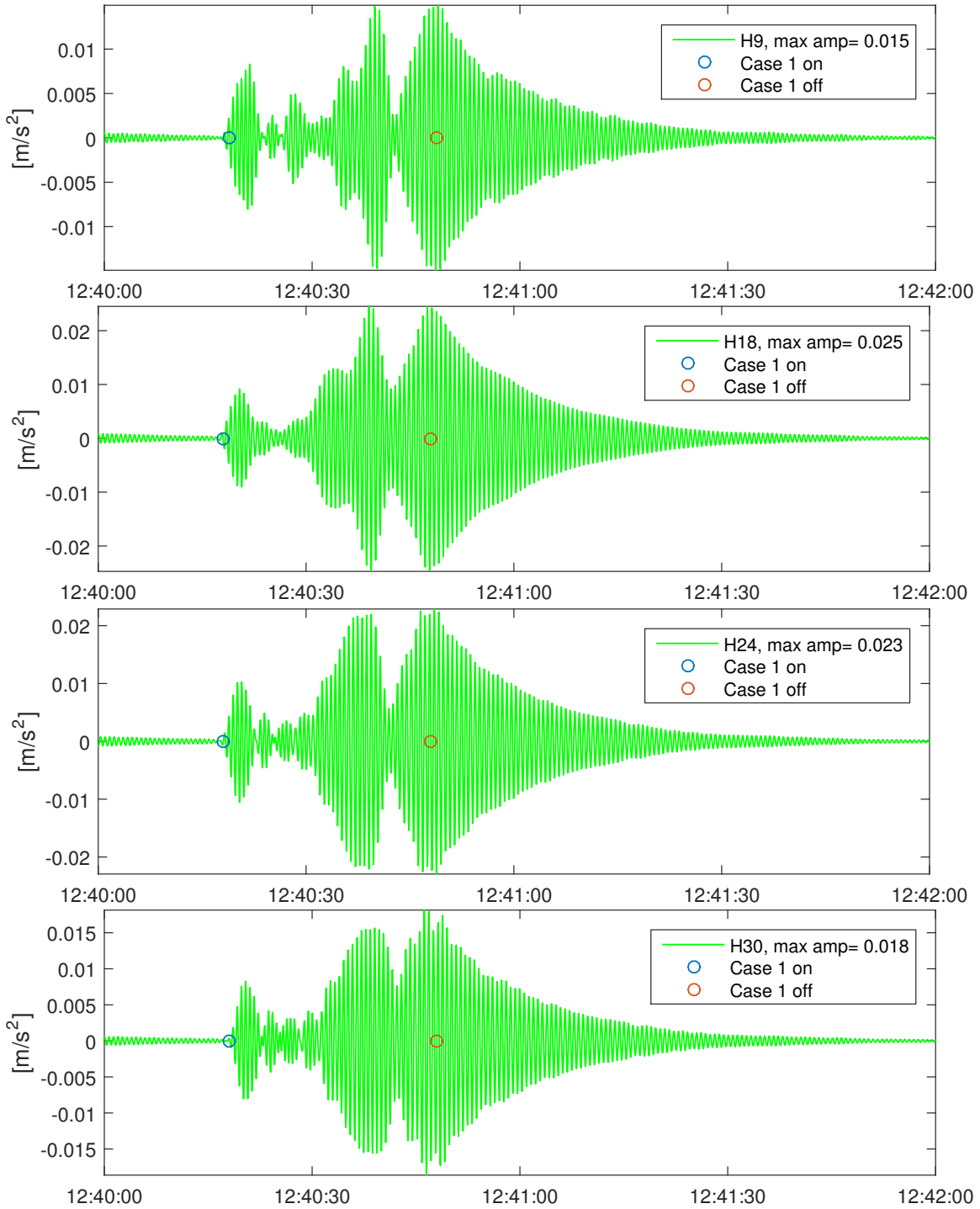


Figure 3.20: Acceleration response band-pass filtered around 1,55Hz for case 1 - from North - from South

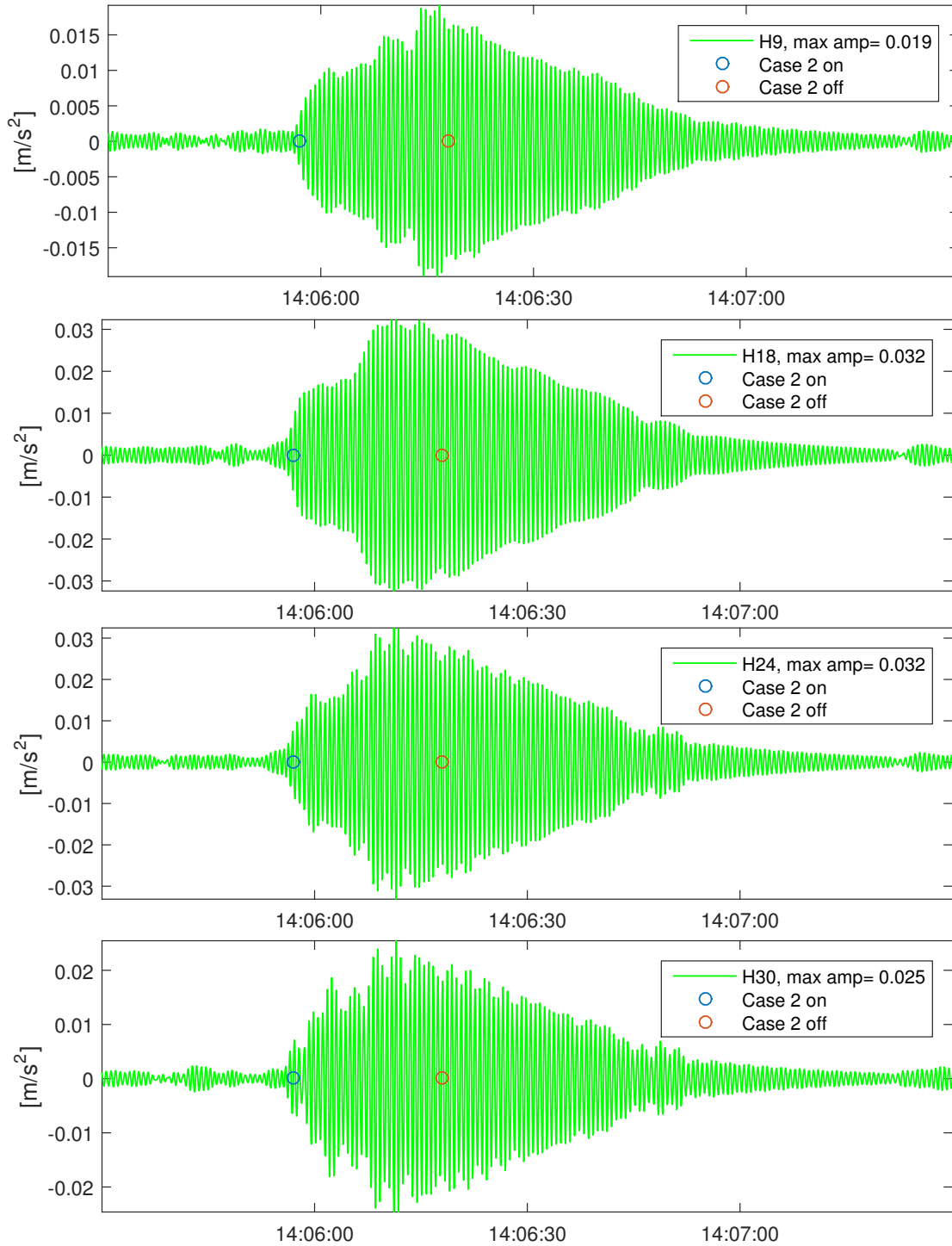


Figure 3.21: Acceleration response band-pass filtered around 1,55 Hz for case 2 - from South

For mode $F7$, illustrated in Figures 3.20 and 3.21, the two cases differ quite significantly in comparison to VA1 and VS3. Here, it appears that the presence of smaller vehicles affect the response quite significantly, as seen in Figure 3.21 as the bridge does not appear to swing freely. This is

an important observation in regards to Chapter 3.7, where free oscillations of the bridge will be used for damping estimation.

3.5.2 Horizontal and Torsional Acceleration Response

Results from horizontal and torsional response analysis will not be included in the main body of the present work due to practical limitations and the fact that the response is concluded to be more or less unsatisfactory for further analysis. However, results are included in a separate electronic file.

3.5.3 Displacement

In analyzing the response from vehicles in regards to both damping and impact analysis, it is not sufficient to look at the response from acceleration data only. For the purpose of structural health monitoring (fatigue and stress/strain analysis), it is ultimately displacement (magnitude and frequency) that is of interest. Displacement can be calculated from the acceleration data, as acceleration, a , by definition is the second time derivative of displacement, x .

$$a = \frac{d^2x}{dt^2} \quad (3.1)$$

Displacement can therefore be obtained from acceleration data by double integration of the acceleration vector. In the present work displacement response is obtained using a MATLAB function that calculates the displacement from acceleration data through integration in the frequency domain using Discrete Fourier Transform (DFT).

Figures 3.22 and 3.23 are included to illustrate the magnitude of displacement in the different modes.

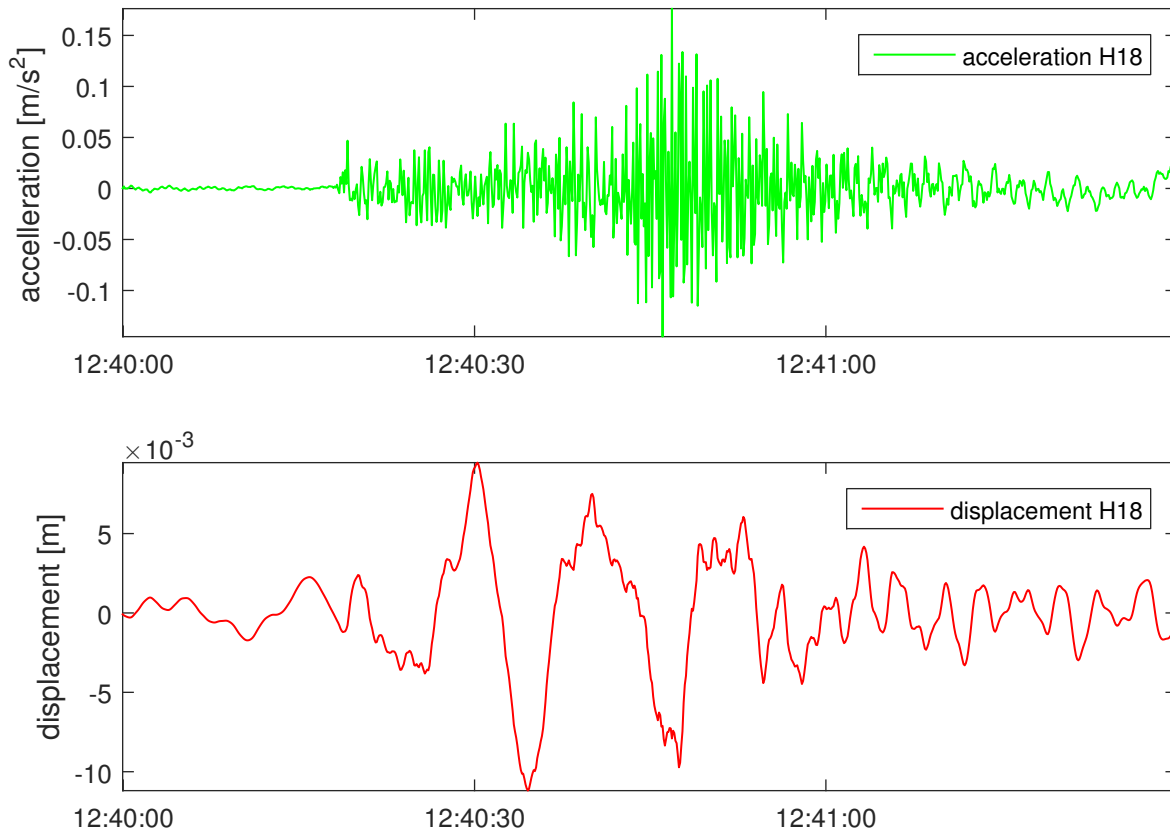


Figure 3.22: Acceleration and displacement response at mid span for case 1

Displacement in Figure 3.22 is filtered at 0,08 Hz in order to filter out static displacement at frequencies below 0,136 (HS1). By examining Figure 3.22, it is clear that the lower modes dominate the response. This is also clearly illustrated in the FDD power spectral density function for displacement as illustrated in Figure 3.23

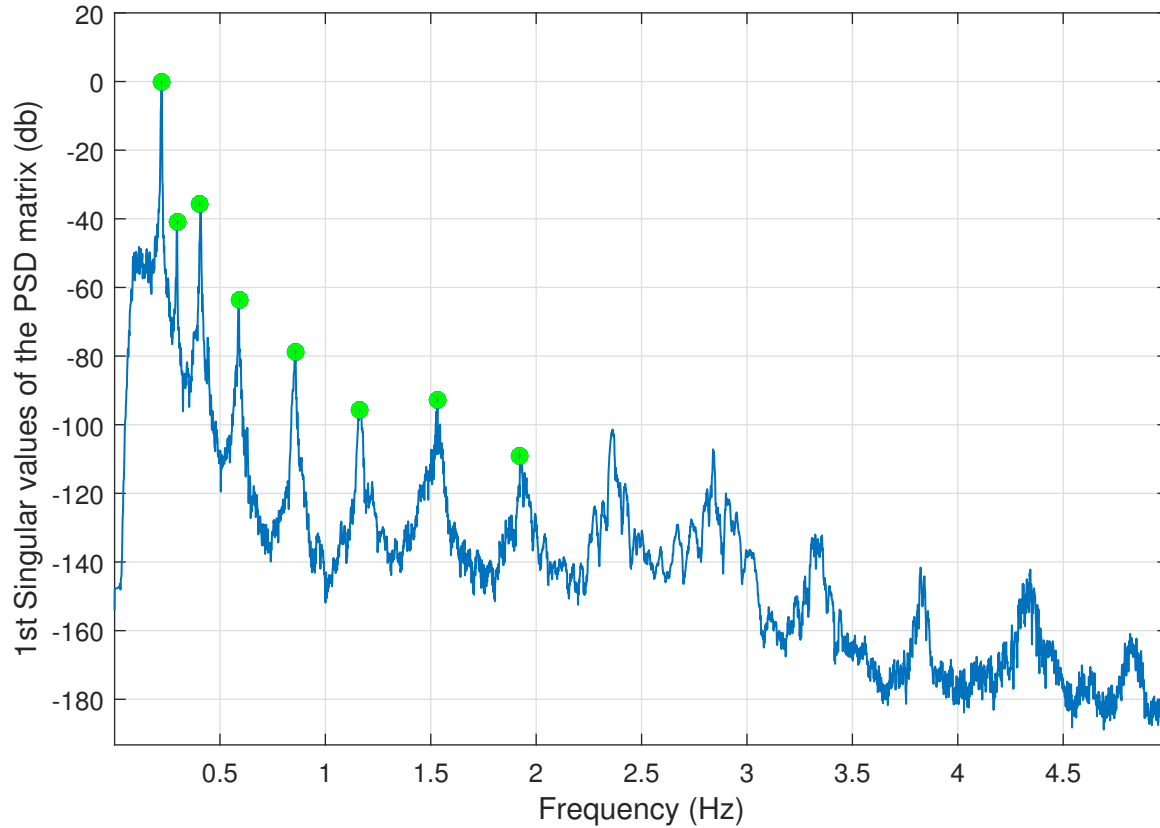


Figure 3.23: PSD of displacement response at mid span for case 1

The identified peaks in Figure 3.23 are listed in Table 3.9. Out of the 6 first modes, only VA2 is not visible, and modes VA1, VS2 and VS1 contain the most energy. This is as expected as sensor H18 is located at mid-span. The fact that displacement is within the same frequencies as acceleration is obvious due to the relationship between the two illustrated in Equation 3.1.

Table 3.9: Identified vertical displacement frequencies FDD case 1

	identified frequencies							
	VA1	VS1	VS2	VA2	VS3	VA3	F7	F8
Frequencies [Hz]	0,2233	0,2966	0,4076	-	0,8546	1,168	1,167	1,532

For simplification purposes, only acceleration data is used for damping analysis in the present work. For impact response, both acceleration and displacement is illustrated.

3.6 Impact Loading

As described earlier, impact loading is quite difficult to predict analytically, partly because of its dependence on several parameters. It is also quite difficult to analyze Impact loading from empirical data, due to the same reasons, as well as limitations with measurement equipment and methods.

In measured dynamic response of a single vehicle or traffic, it is hard to separate which parts of the response are due to impact loading effects, and which are due to regular response from a moving load.

By comparing response from different vehicles from different directions and with different velocities as done in Chapter 3.5 above, presence of impact loading is suggested. However, there are far too many unknowns to draw any conclusion on how much the individual factors contribute to impact loading. Below is a description of observed “factors” on the bridge deck which, in theory, can contribute to impact response from vehicles.

3.6.1 Condition of Bridge Deck

The present work will not focus on the condition of the bridge in terms of fatigue, corrosion and other wear factors. However, in relation to the impact and response analysis, it is of interest to investigate the condition of the bridge deck. This “investigation” is simply based on the authors qualitative assessment from a visual inspection of the deck. Figures 3.24, 3.26 and 3.27 illustrate some findings that are found to potentially contribute to the magnitude and significance of response in the bridge from vehicles.



Figure 3.24: General pavement condition



Figure 3.25

Figure 3.26: Expansion joint on the South side of the bridge



Figure 3.27: Bump in pavement by entrance to bridge on the South side of the bridge

Visual inspection of the areas illustrated in Figures, [3.24](#), [3.26](#) and [3.27](#), conclude that the condition of pavement is relatively uneven/“poor”. Bumps such as those seen in Figures [3.26](#) and [3.27](#) can cause oscillations as well as reaction force amplification from crossing vehicles. These assumptions are also supported by analytical theory described in Chapter [2.4](#), and increased response during and after vehicles cross these points can be expected in the impact analysis.

3.6.2 Impact Loading “Experiment”

In an attempt to fix some of the variable parameters inherent in the method of simply observing vehicles on Lysefjorden bridge, Bjørn Hansen AS and Forsand Betong AS, two concrete factories at Forsand, were contacted and asked to cooperate to set up an “experiment.” Both factories were willing to cooperate, but due to timing limitations and the dependency of relatively low wind speed, organizing the experiment proved quite difficult.

However, on May 5th, *Bjørn Hansen AS* driver Anette Ravndal agreed to drive at different given velocities while making trips between Forsand and Jørpeland carrying loads of 50 tonnes in both directions, for three different crossings.

As will be discussed below, getting usable results from such “experiments” or controlled crossings, is difficult, as it requires the bridge to be empty of any other traffic before, during and after the vehicle crosses the bridge.

The resulting experiment was three separate trips, summarized below in Table 3.10

Table 3.10: Overview of three bridge crossings by Anette Ravndal on May 5th

Trip #	Cargo [Tonnes]	Direction “from”	Velocity entering bridge [m/s]	velocity exiting bridge [m/s]	Wind speed [m/s]
1	50	South	55	25	4,6
2	50	North	30	60	4,3
3	50	South	23	25	4,1



Figure 3.28: 50 tonnes truck entering bridge from the South at 23 km/h with a total cargo of 50 Tonnes

3.6.3 Quality of Experiment Measurements

Ideally, all three crossings would be during low wind speed and without any presence of other cars or trucks before, during and after the experiment. For the present work, closing off the bridge for other traffic was not an option, and no presence of other vehicles is only a matter of chance/luck. For trip 1 and 2, the bridge was more or less empty from other traffic in the relevant time period, and the acceleration data appears to be free from vibration from other vehicles. On the other hand, for trip 3, a truck crossed the bridge approximately 1,5 minutes before Annette Ravndal crossed the bridge at 23 m/s. This truck caused significant response in the bridge, which leaves the response from Anette's crossing to be mixed or hidden with the free vibrations from this truck. See Figure 3.34 for illustration.

3.6.4 Acceleration Response

The unfiltered acceleration response for the three trips is illustrated below in Figures 3.29, 3.30 and 3.31

Trip 1 - 50 tonne truck from South going 55 km/h

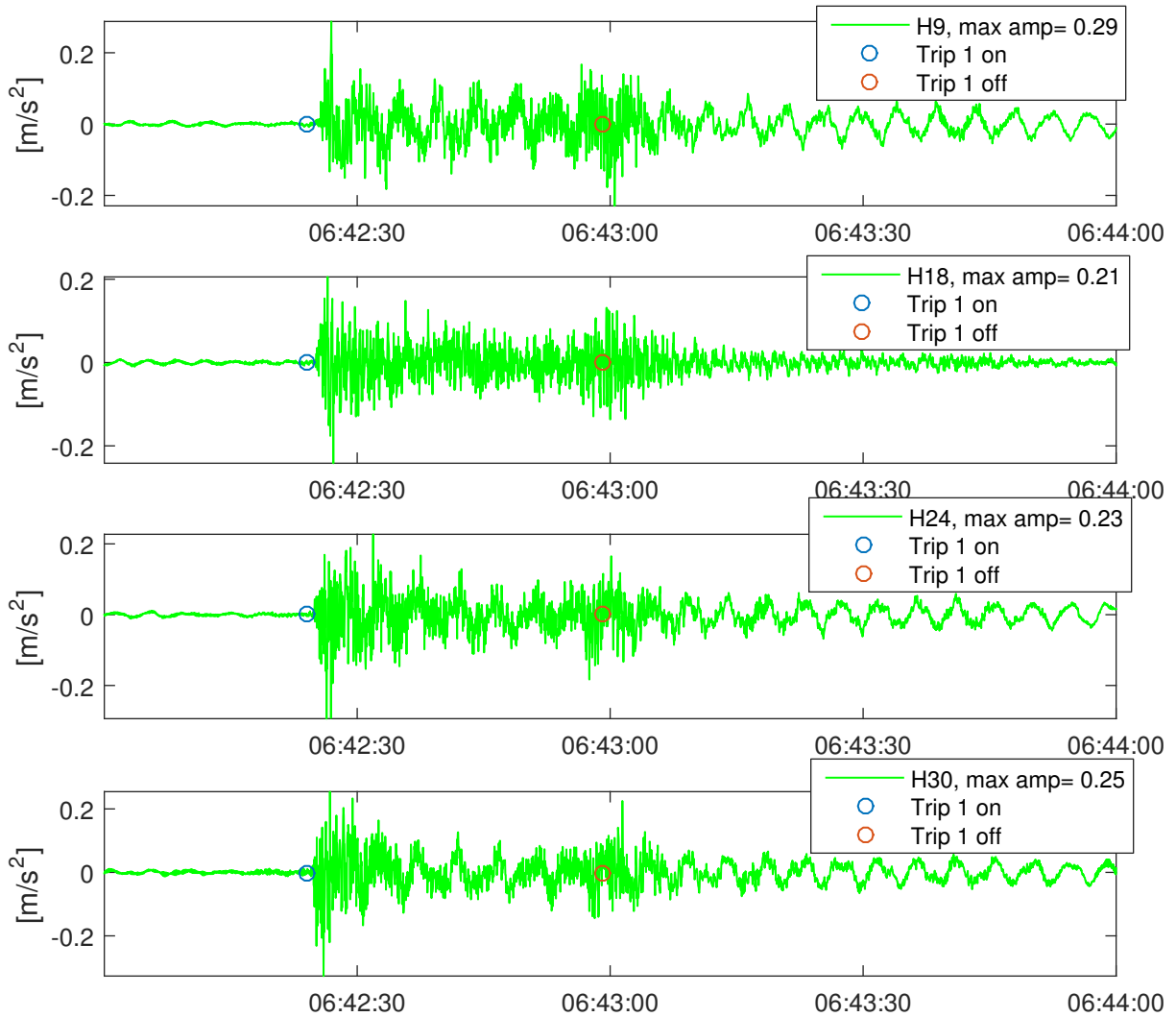


Figure 3.29: Unfiltered acceleration response for 50 tonne truck entering bridge from South doing 55 km/h (trip 1)

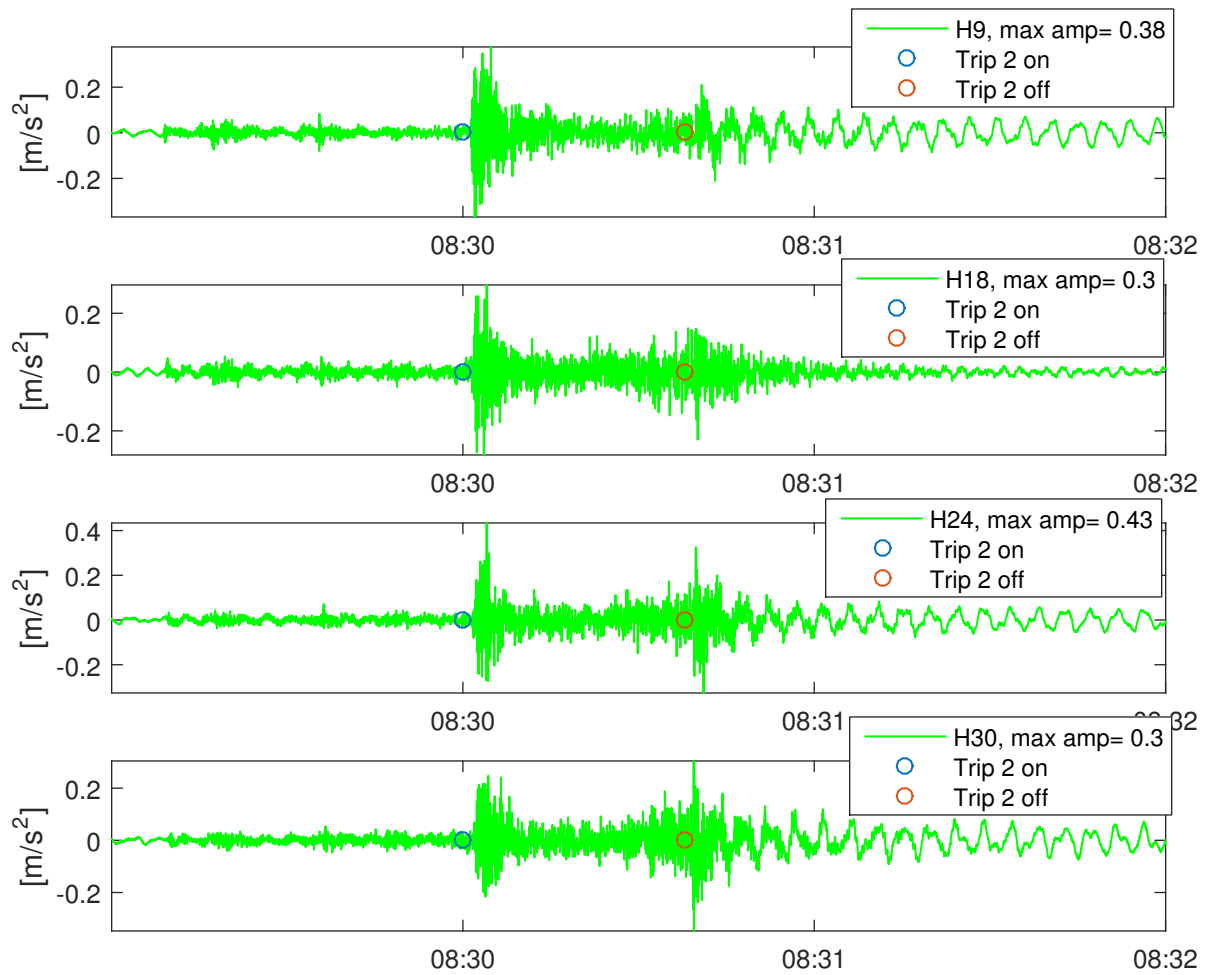
Trip 2 - 50 tonne truck from North going 30 km/h

Figure 3.30: Unfiltered acceleration response for 50 tonne truck entering bridge from North accelerating from 30 to 50 km/h (trip 2)

Trip 2 - 50 tonne truck from South going 23 km/h

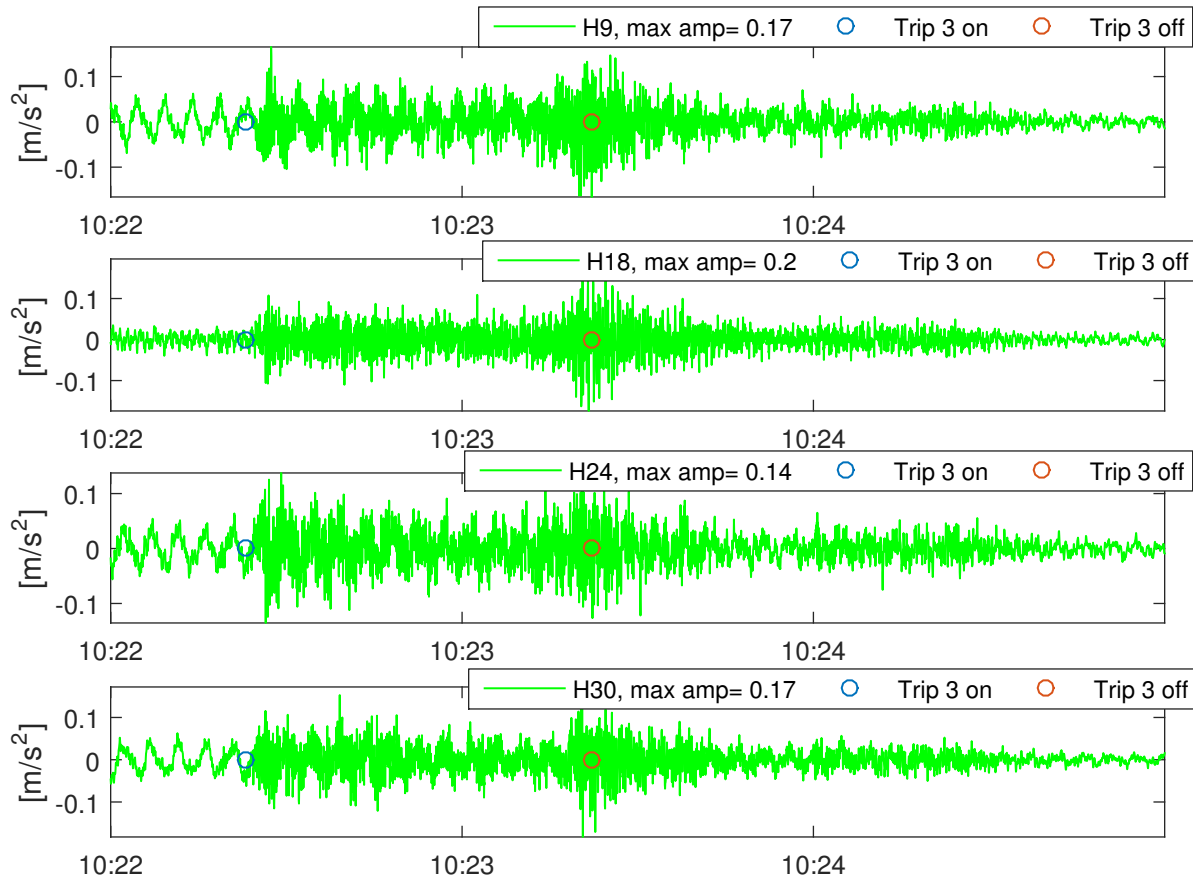


Figure 3.31: Unfiltered acceleration response for 50 tonne truck entering bridge from South doing 23 km/h (trip 3)

Table 3.11 summarizes the maximum acceleration values for unfiltered acceleration for the three separate trips.

Table 3.11: Overview of maximum unfiltered acceleration amplitudes for all three trips driven by Anette Ravndal on May 5th

Trip #	Maximum response/sensor			
	H9 [m/s ²]	H18 [m/s ²]	H24 [m/s ²]	H30 [m/s ²]
1	0,029	0,21	0,23	0,25
2	0,38	0,3	0,43	0,3
3	0,17	0,2	0,14	0,17

Even though unfiltered acceleration data does not say much about the impact response, it can appear that the second trip from the North has a more significant response than the both trips from the South, and that the difference in velocity only has a small effect on the response. These differences are further explored by looking at how modal acceleration and displacement response and is affected. Before filtering the response, the PSD functions for the three cases are analyzed.

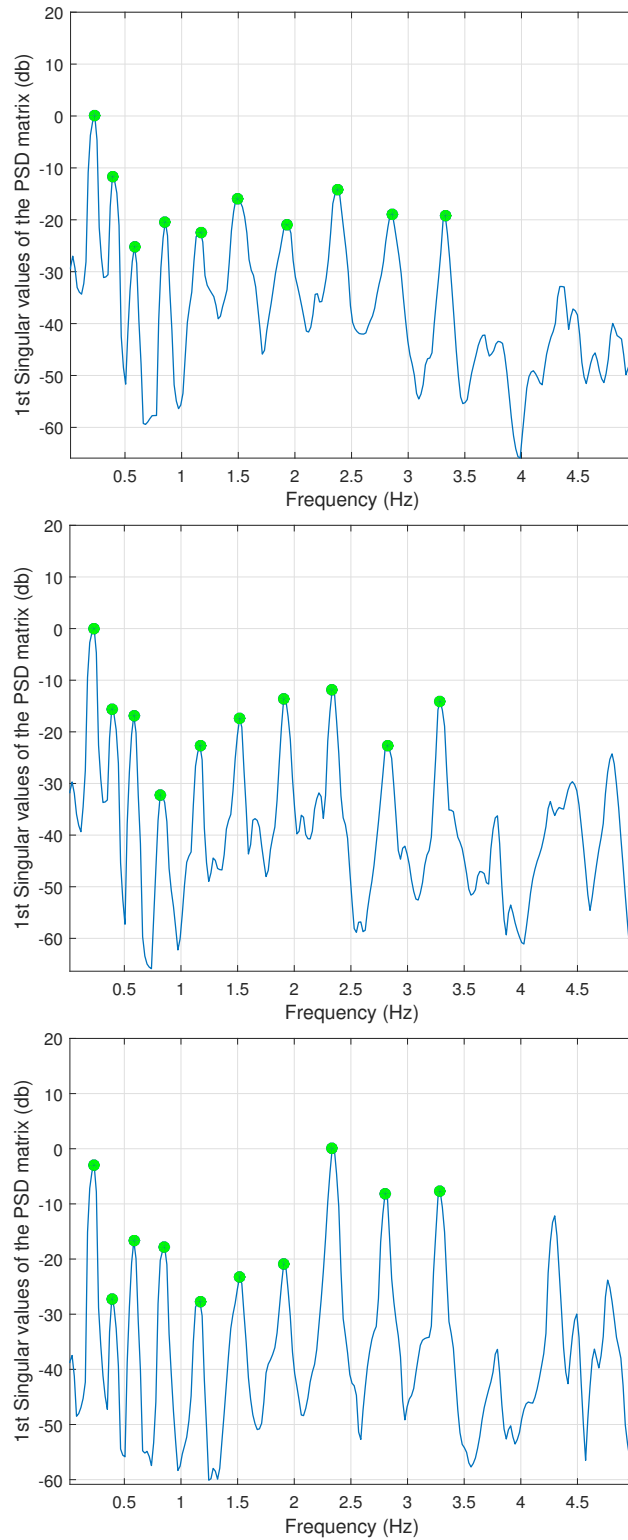


Figure 3.32: PSD functions for vertical acceleration for trip 1 (top), trip 2 (middle) and trip 3 (bottom)

And for displacement in Figure 3.33.

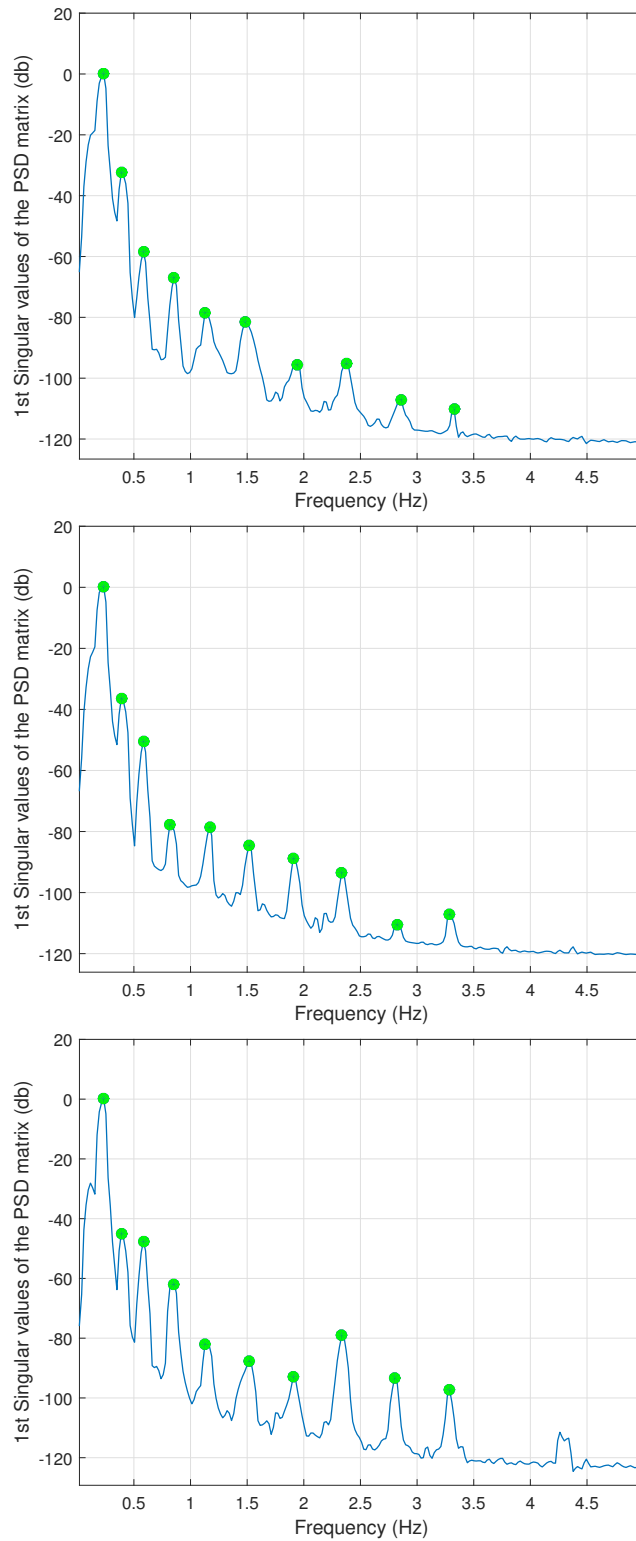


Figure 3.33: PSD functions for vertical displacement for trip 1 (top), trip 2 (middle) and trip 3 (bottom)

The PSD functions for the three cases differ slightly from one another, which indicates that the “average” response differs for the three cases. For trip 1 and 2, mode VA1 appears to be more dominating relative to the other modes than that of trip 3. Also, for trip 2, the relative response for higher modes (between 2 and 3,5Hz) are more dominating, which is also slightly evident in the PSD function for displacement. Displacement and acceleration response for the three cases will be compared for modes VA1, VA2, VS3,VA3, F7 (1,5 Hz) and F8 (1,91 Hz) in the following. Modes VA1, VS3 and VA3 are illustrated below in Figures 3.34, 3.35 and 3.36, respectively. Results for all modes are summarized in Table 3.12.

Displacement plots are not presented below, but are attached in Appendix C.

VA1 - sensor H9

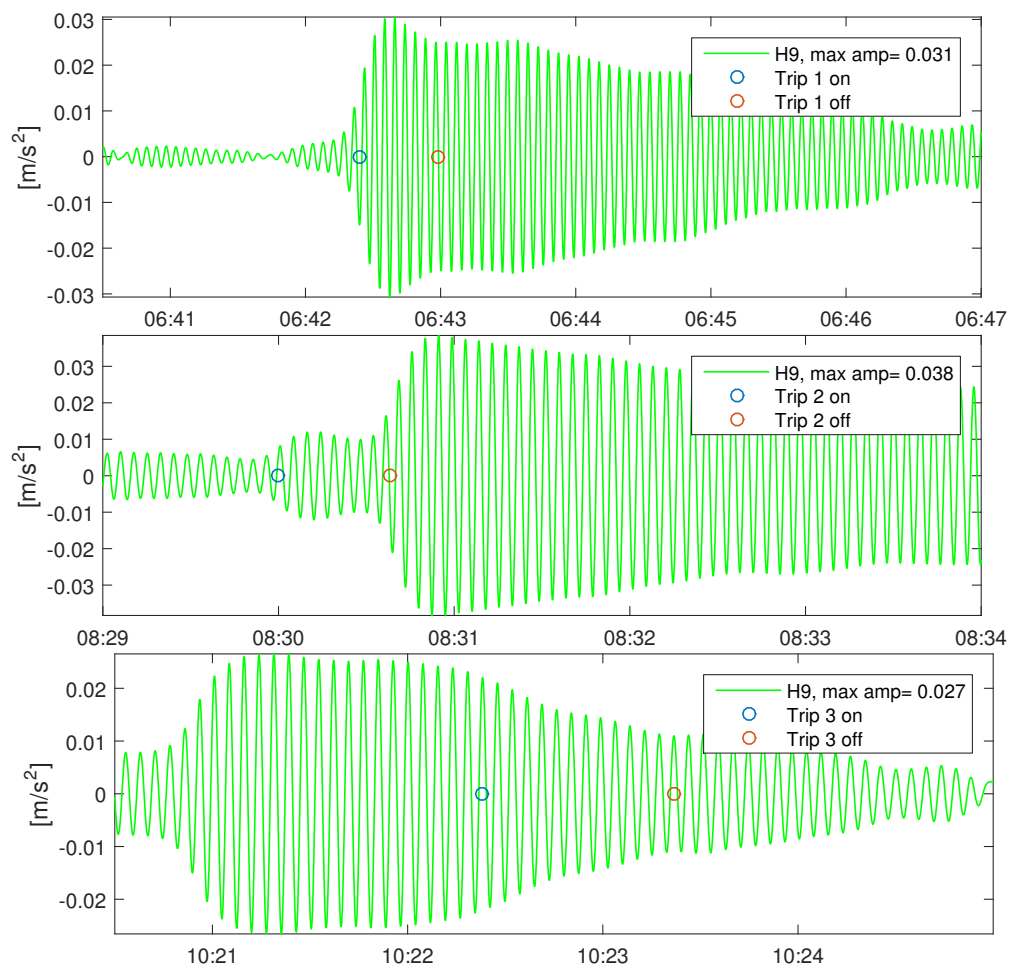


Figure 3.34: Filtered response VA1 for trip 1(top), trip 2 (middle) and trip 3 (bottom)

VS3 - sensor H18

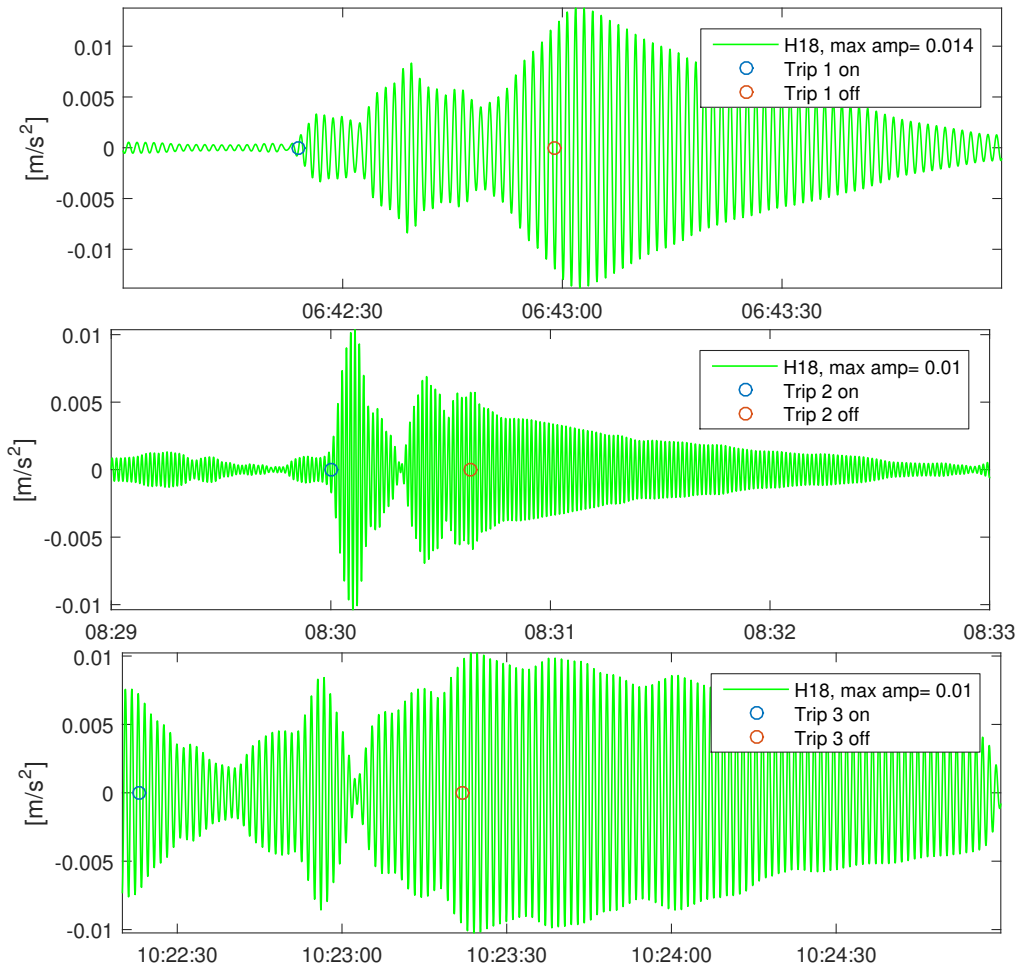


Figure 3.35: Filtered response VS3 for trip 1(top), trip 2 (middle) and trip 3 (bottom)

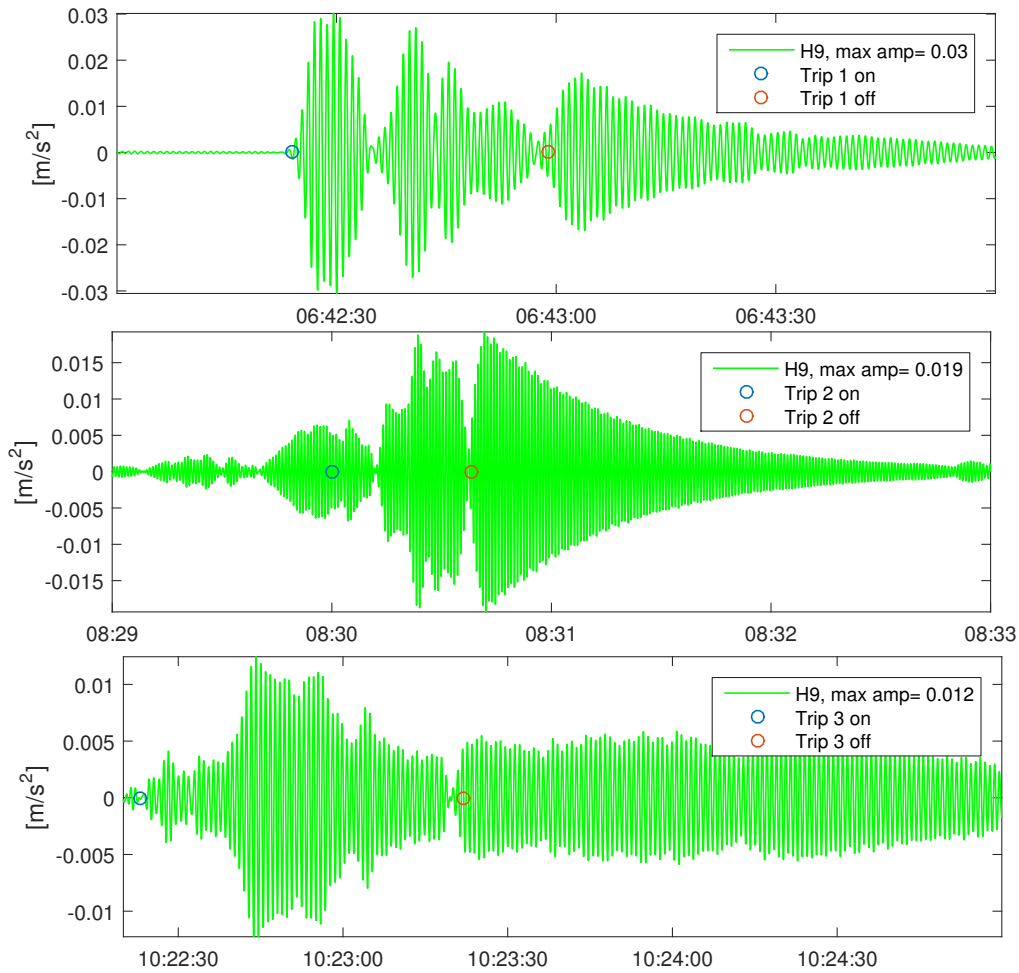
VA3 - sensor H9

Figure 3.36: Filtered response VA3 for trip 1 (top), trip 2 (middle) and trip 3 (bottom)

Figures 3.34, 3.35 and 3.36 illustrate that different modes respond differently for the different trips.

For VA1 illustrated in Figure 3.34, there is a clear difference in the response characteristics between trip 1, trip 2 and trip 3. Response from trip 3 is hidden and mixed with the free decay of a previous vehicle, and results from this mode are therefore unsatisfactory for any analysis. For trip 1 there appears to be an impact response in this specific mode when Anette Ravndal enters the bridge, but interestingly, there also seems to be a sudden response of even greater magnitude when the truck exits the bridge in trip 2. The timing of the observations made for the present work are not accurate enough to say if the response for trip 2 occurs right before the

truck has left the bridge or right after. This timing matters as one indicates impact response, and the other one does not. If the response is immediately after the truck leaves the bridge, this is not due to impact loading response (per definition), as the bridge simply appears to swing freely after suddenly being released from a static/dynamic load. If this is true this is an indication that the impact effect which could be expected in case 1, is not very significant for this mode. The other possibility for the relatively large response in mode VA1 as the truck is leaving the bridge in trip 2, is that the truck itself oscillates due to the the poor pavement condition as the majority of the truck is still on the bridge span, before it suddenly leaves the bridge span. If these oscillations cause the peak in response in the bridge for mode VA1, this could be classified as impact response as seen in the theory presented in [Liu et al. \(2017\)](#) caused by road roughness/condition.

For VS3 illustrated in Figure 3.35, trips 1 and 2 have their maximum response opposite to that of VA1 in terms of position, where the maximum response is at its highest for trip 1 as it leaves the bridge, and trip 2 as it enters the bridge. In this case, as with VA1 mentioned above, the response is at its highest for the case when the vehicle leaves the bridge (trip 1 for VS3 and trip 2 for VA1). For both trip 1 and trip 2, velocities are different when exiting the bridge compared to entering the bridge (see Table 3.11).

As velocity changes, the surface irregularities and roughness relative to the vehicle also changes as illustrated in [Liu et al. \(2017\)](#), which can explain why different velocities causes response in bridge in different frequencies.

For VA3 illustrated in Figure 3.36, trip 1 has the highest acceleration response with a magnitude of $0,03 \text{ m/s}^2$. This is more than 50 % higher than trip 2 with its maximum response as the truck exits the bridge at $0,019 \text{ m/s}^2$, and 250% more than for trip 3 which has its maximum response of only $0,012 \text{ m/s}^2$. This indicates that the magnitude of impact response as vehicle enters the bridge is dependent on velocity for this mode. In fact, this is the case for all higher modes analyzed in the present work, as illustrated in Table 3.12.

For Table 3.12, "*Position*" indicates the location of the vehicle at the time of maximum response. "*S*" is for "*Start*" of bridge - as the vehicle enters the free span of the bridge. "*M*" is for "*Middle*" of the bridge - when the vehicle is positioned near the middle of the free span. "*E*" is for "*End*"

of bridge - when the vehicle exits the free span of the bridge.

Table 3.12: Overview of maximum vertical modal acceleration response and position for trips 1, 2 and 3

		Trip					
		1 - from South (fast)		2 - from North		3 - from South (slow)	
		Maximum amplitude					
Mode name	sensor	magnitude	position	magnitude	position	magnitude	position
[Hz]		[m/s^2]	S/M/E	[m/s^2]	S/M/E	[m/s^2]	S/M/E
VA1 - 0,22	H9	0,031	S	0,038	E	0,027	N/A
VA2 - 0,57	H24	0,0093	S	0,015	E	0,0096	E
VS3 - 0,86	H18	0,014	E	0,01	S	0,01	E
VA3 - 1,16	H9	0,03	S	0,019	E	0,012	M
F7 - 1,5	H18	0,04	S	0,022	E	0,01	M/E
F8 - 1,91	H30	0,051	S	0,037	E	0,025	E

In conclusion, there are potential indications of impact effects for all modes, although different modes appear to be affected differently from different phenomena. Modes VA1, VA2 and VS3 in the present work are not dominated by the response from the impact of the vehicle at high velocity when the vehicle enters the bridge, but rather have their maximum response when the vehicle leaves the bridge. On the other hand, for the higher modes, the impact effect from vehicle velocity as the bridge enters the bridge seems to have a significant effect. When comparing the 3 trips for modes VS3, F7 and F8, response as the vehicle enters the bridge in trip 1 is significantly larger than for the other two trips.

As stated in [Sanpaolesi and Croce \(2005\)](#), lorries (trucks) often have natural frequencies between 1 and 2 Hz, and the impact response observed for the frequencies within this range can be due to the fact that natural frequencies of the vehicle suspension are close to these modal frequencies. This theory is also strengthened by the bumps and unevenness in the bridge deck, which likely causes the vehicle to oscillate at its natural frequency. It is also likely that the *load application duration* from the vehicle discussed in Chapter 2.4 plays a role the impact response observed at high velocities for these frequencies, although this is difficult to prove from the information available in the present work. For a large and relatively flexible structure such as Lysefjorden bridge, the magnitude of the response from impact in this frequency range is not considered significant ([Cheynet \(2016\)](#)), but this is not necessarily the case for all bridges. Smaller bridges such

as the Bridge in Figure 3.37 can have their fundamental modal frequencies within this range. As these bridges most likely also have lower allowable design loads than large suspension bridges, the impact effects from the velocity of heavy vehicles entering and exiting the bridge such as those illustrated for the higher frequency modes in Table 3.12, should be considered.



Figure 3.37: Taramakau River bridge located in New Zealand with speed limitation for heavy vehicles. Image credit: [Bernard Spragg \(nd\)](#)

3.6.5 Significance of the Vehicle-induced Response

A detailed analysis of the significance of the bridge response from heavy vehicles in terms of limit states will not be performed in the present work. However, to the authors knowledge, there are no indications that impact loading from heavy vehicles is significant, although [Cheynet \(2016\)](#) suggests that traffic induced vibrations such as those on Lysefjorden bridge may have to be included in structural health monitoring of long-span suspension bridges.

3.7 Damping

One of the main advantages of Lysefjorden bridge is its relatively remote location and the fact that heavy vehicles cross the bridge several times daily, often with no other traffic on the bridge. As seen in the previous chapter the response from certain vehicles is quite significant/noticeable. The idea in this chapter is therefore to use this vehicle induced response for modal damping analysis. The situations of interest is when the bridge is excited by heavy vehicle or traffic, before suddenly no vehicles are present on the bridge. This opens for the opportunity to measure the free decay or energy dissipation in the structure in the different frequencies/modes identified in Chapter 3.4.

By comparing acceleration response plots with written observations on the bridge, a number of potential cases have been identified as having potential for free oscillation damping estimation. These cases are presented in Table 3.13 and Figures 3.38, 3.39 and 3.40.

Table 3.13: Vehicle crossings identified as potentially suitable for free oscillations analysis

Case number	Date [month,day]	Time on bridge [HH:MM:SS]	Time off bridge [HH:MM:SS]	Time before next vehicle enters bridge	Vehicle type (rough description)
1	March 7th	12:40:18	12:40:46	00:01:22	Truck
2	March 7th	12:44:21	12:44:56	00:00:20	Truck
3	March 7th	12:56:12	12:56:41	00:00:26	Small Truck
4	March 7th	13:01:45	13:02:09	00:00:15	Truck
5	March 7th	13:12:08	13:12:28	00:00:33	Small buss
6	March 7th	13:17:32	13:18:04	00:00:26	Buss
7	March 7th	13:29:33	13:30:00	00:00:15	Truck
8	March 7th	13:42:11	13:42:41	00:00:26	Truck
9	March 7th	13:59:32	14:00:07	00:00:20	Truck
10	May 2nd	06:24:55	06:25:23	00:01:20	Truck+traffic
11	May 2nd	06:29:54	06:30:28	00:00:44	Truck
12	May 2nd	06:42:32	06:43:09	00:00:35	Truck
13	May 2nd	06:43:44	06:44:16	00:01:10	Truck
14	May 2nd	06:55:58	06:56:24	00:02:43	Truck+traffic
15	May 2nd	07:31:59	07:32:27	00:01:31	Truck
16	May 2nd	07:34:12	07:34:53	00:02:03	Truck
17	May 3rd	08:30:30	08:30:54	00:01:41	2 Trucks+traffic
18	May 3rd	09:05:41	09:06:11	00:00:31	Truck
19	May 3rd	09:06:42	09:07:09	00:01:59	Truck
20	May 3rd	09:16:12	09:16:49	00:01:30	Truck
21	May 3rd	10:04:08	10:04:43	00:01:06	Truck

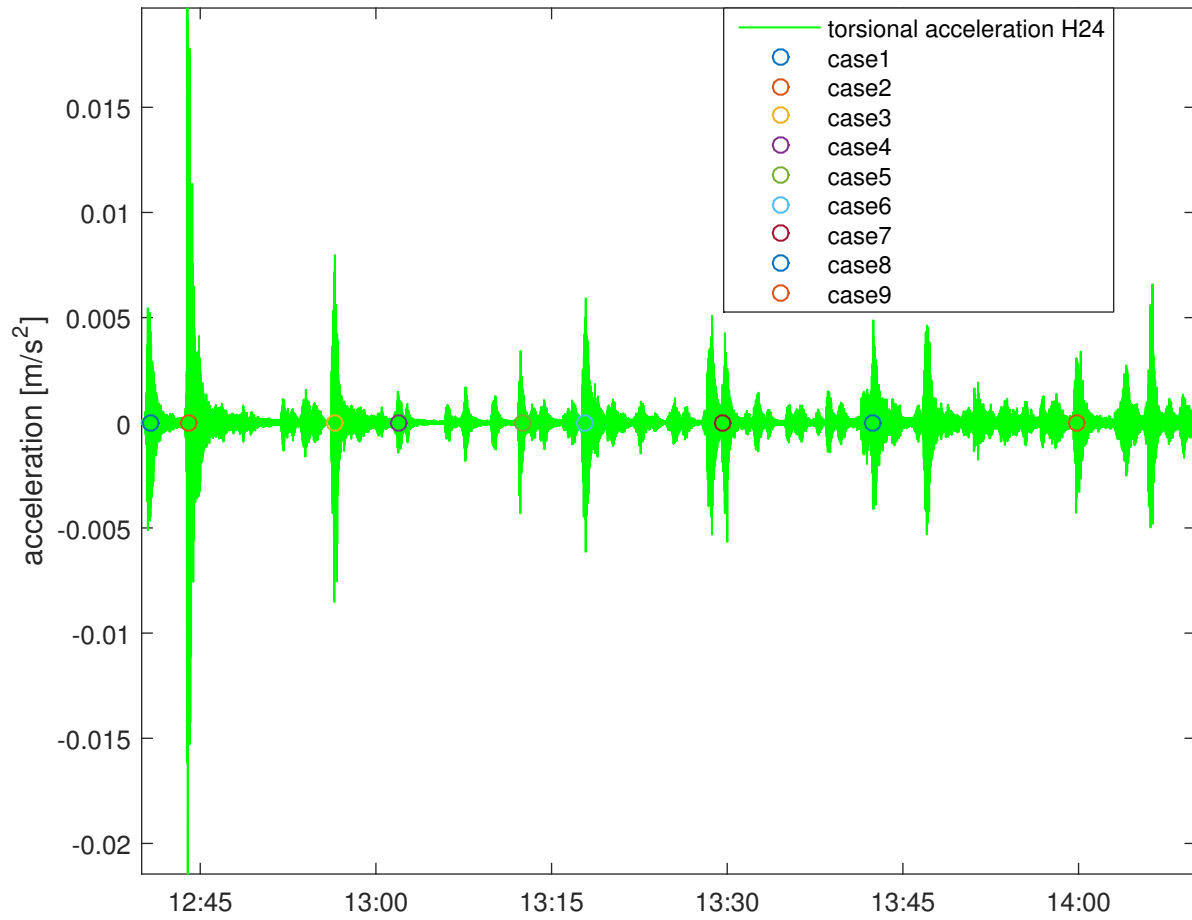


Figure 3.38: Acceleration response March 7th with chosen cases for damping analysis

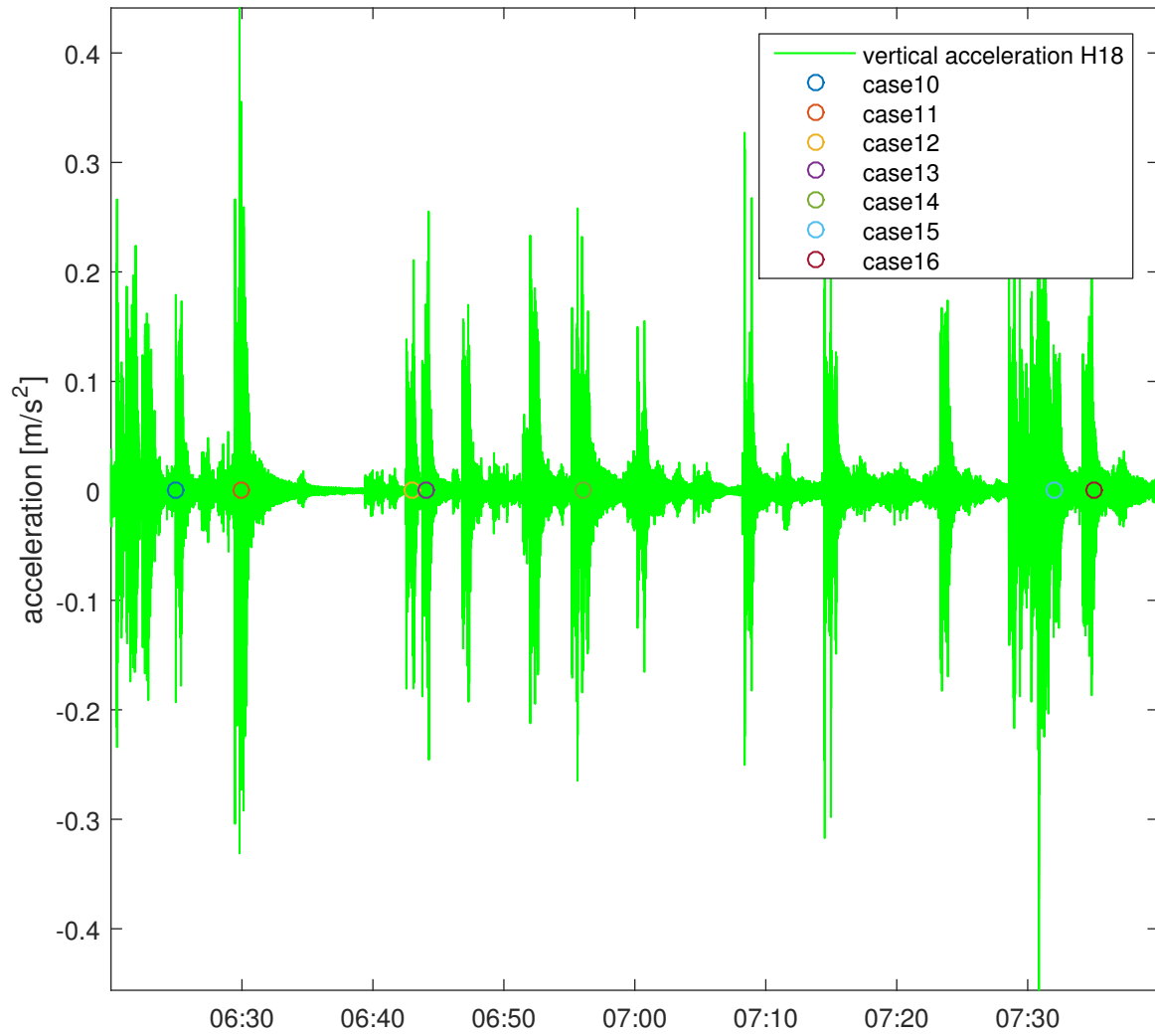


Figure 3.39: Acceleration response May 2nd with chosen cases for damping analysis

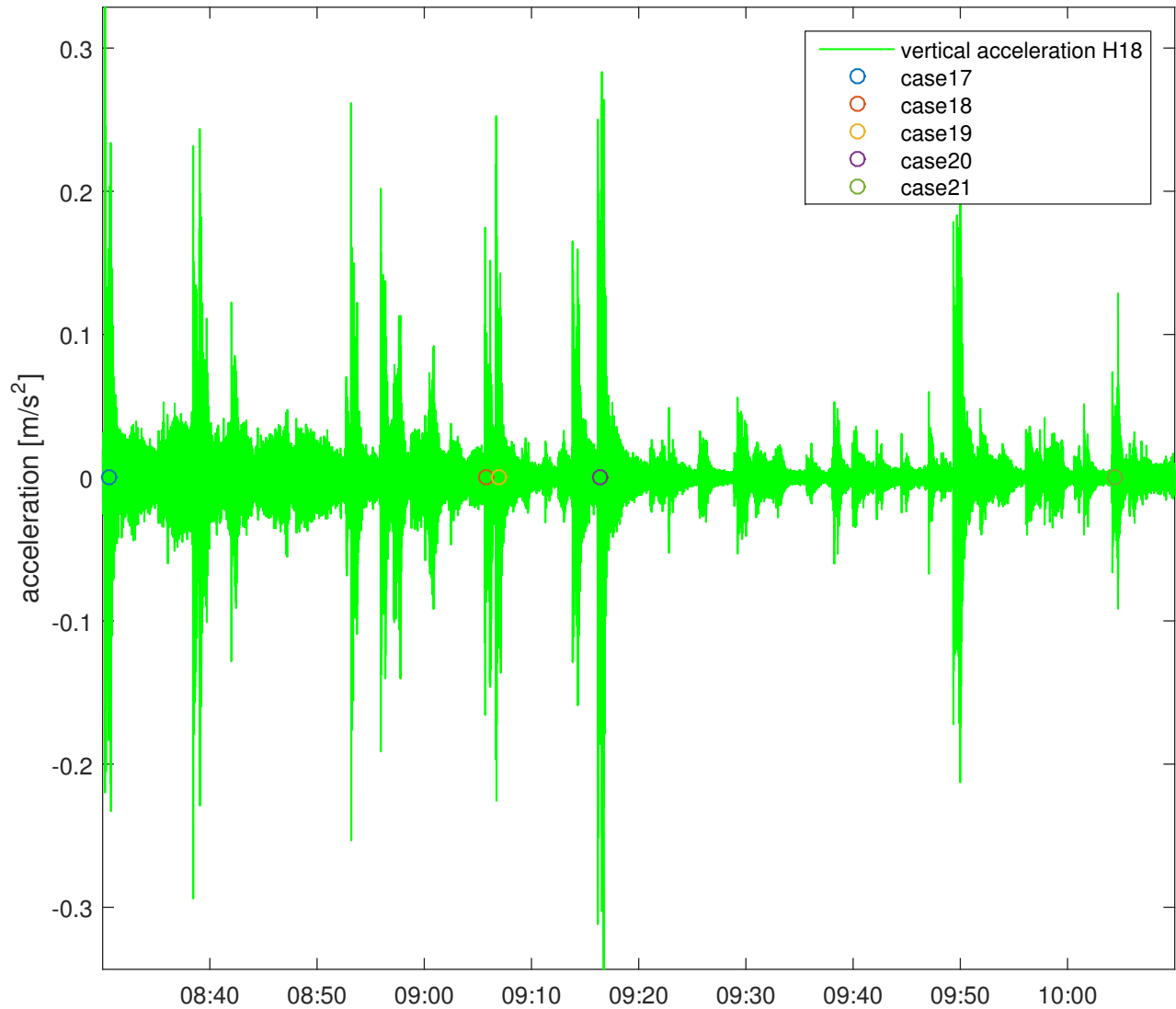


Figure 3.40: Acceleration response May 3rd with chosen cases for damping analysis

As discussed in Chapters 2.1.3 and 1.3.3, damping mechanisms are relatively unknown, and energy dissipation is often assumed to be a combination of several mechanisms each with their own physical properties as well as theoretical approximations. In the present work, the damping ratio, ξ , is estimated using viscous damping assumption (exponential decay). This is done using a MATLAB function which “fits” an exponential decay curve to the peaks of the filtered and timed free oscillations (MATLAB Function attached in Appendix B). The varied wind and temperatures in the data also opens for the opportunity to look at the modal damping ratio as a function of wind velocity and temperature.

3.7.1 Analysis process

In each case listed in Table 3.13, the following steps are performed in order to estimate the modal damping ratios for each of the vehicles.

1. Identify response frequencies
2. Find the best method to filter out the frequencies through trial and error
3. Find exact timing when free oscillation starts
4. Fit exponential decay function to peaks of free oscillation
5. Evaluate filtering and exponential decay fitting results.

The process is illustrated for *case 1* below.

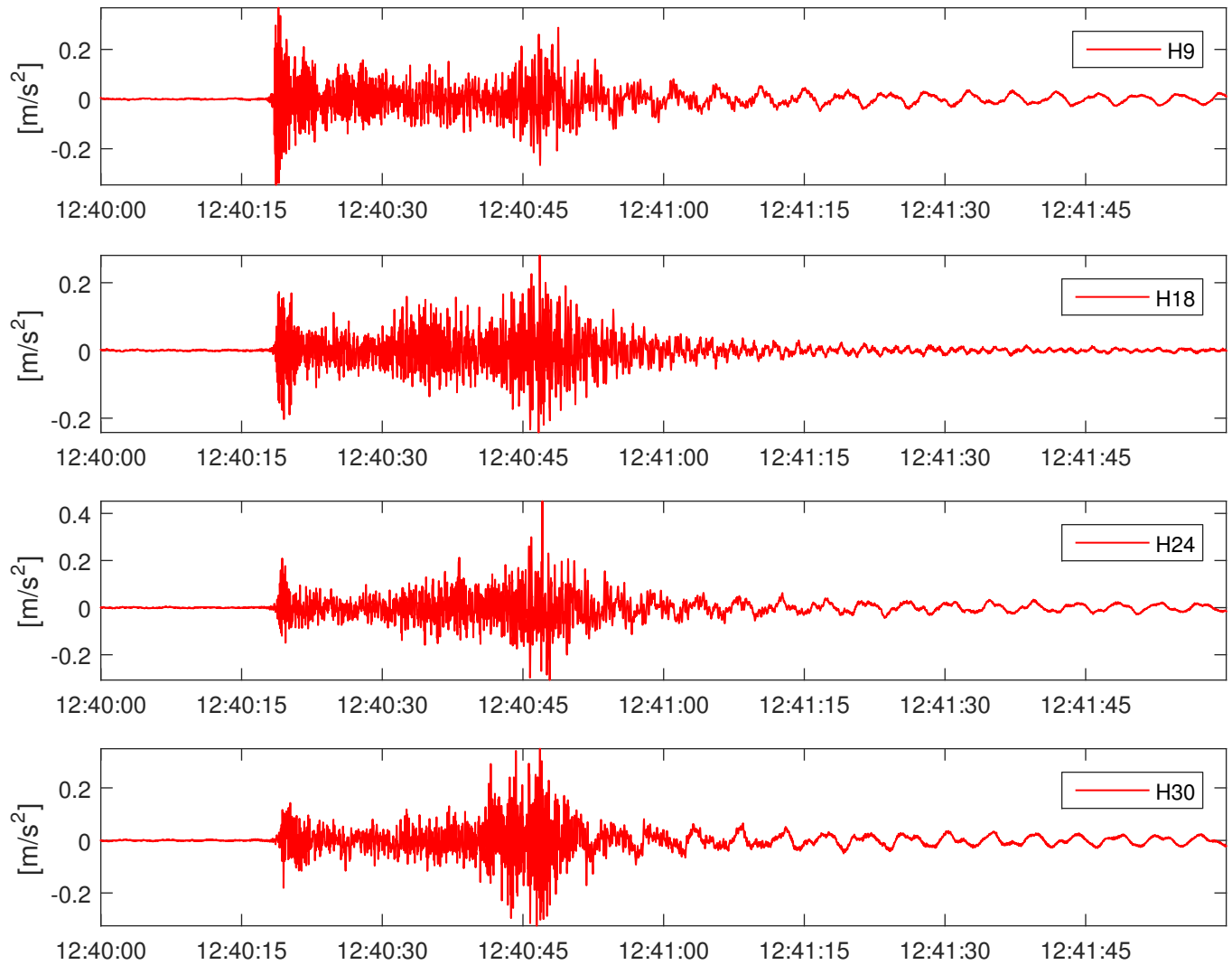


Figure 3.41: Unfiltered acceleration data for all sensors case 1 -

The unfiltered acceleration data in Figure 3.41 shows immediate response in the bridge when the vehicle enters bridge from 12:40:18. The vehicle exits the bridge around 12:46:46, where we can expect the free oscillations of the bridge to start.

Identify response frequencies

Vibration frequencies are identified using both modal acceleration (FDD), as presented in Figure 3.42 and Table 3.14, and for each sensor individually, as presented in Figure 3.43.

Table 3.14: Identified frequencies FDD case 1

identified frequencies											
Frequencies [Hz]	0,233	0,428	0,583	0,856	1,167	1,517	1,926	2,431	2,840	3,326	4,338

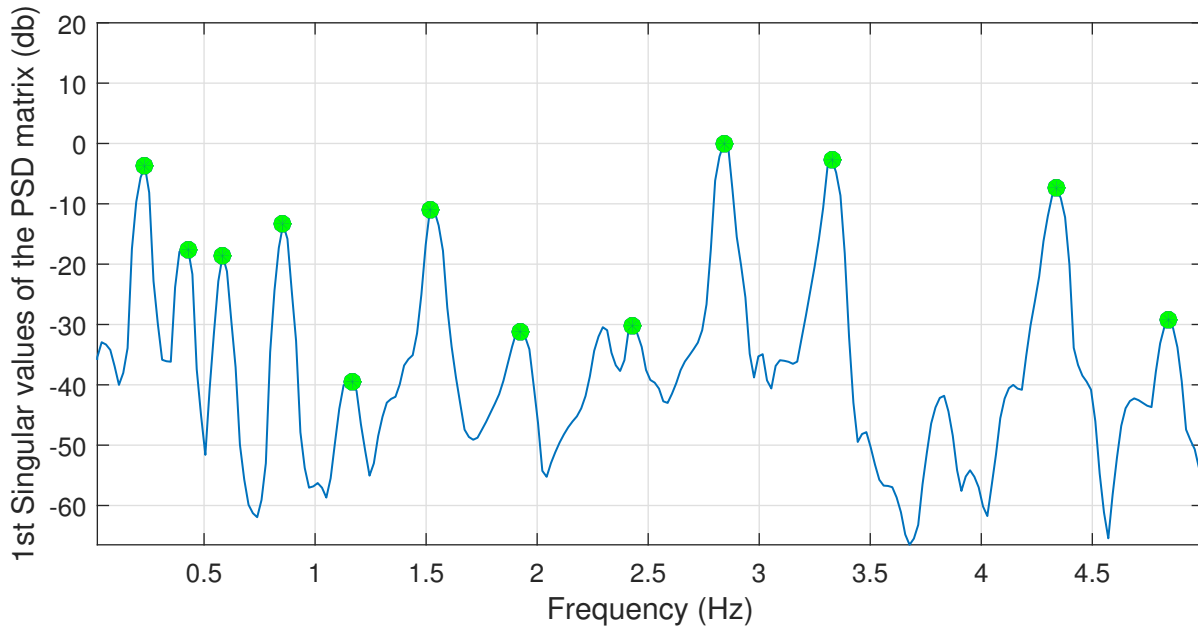


Figure 3.42: PSD FDD case 1

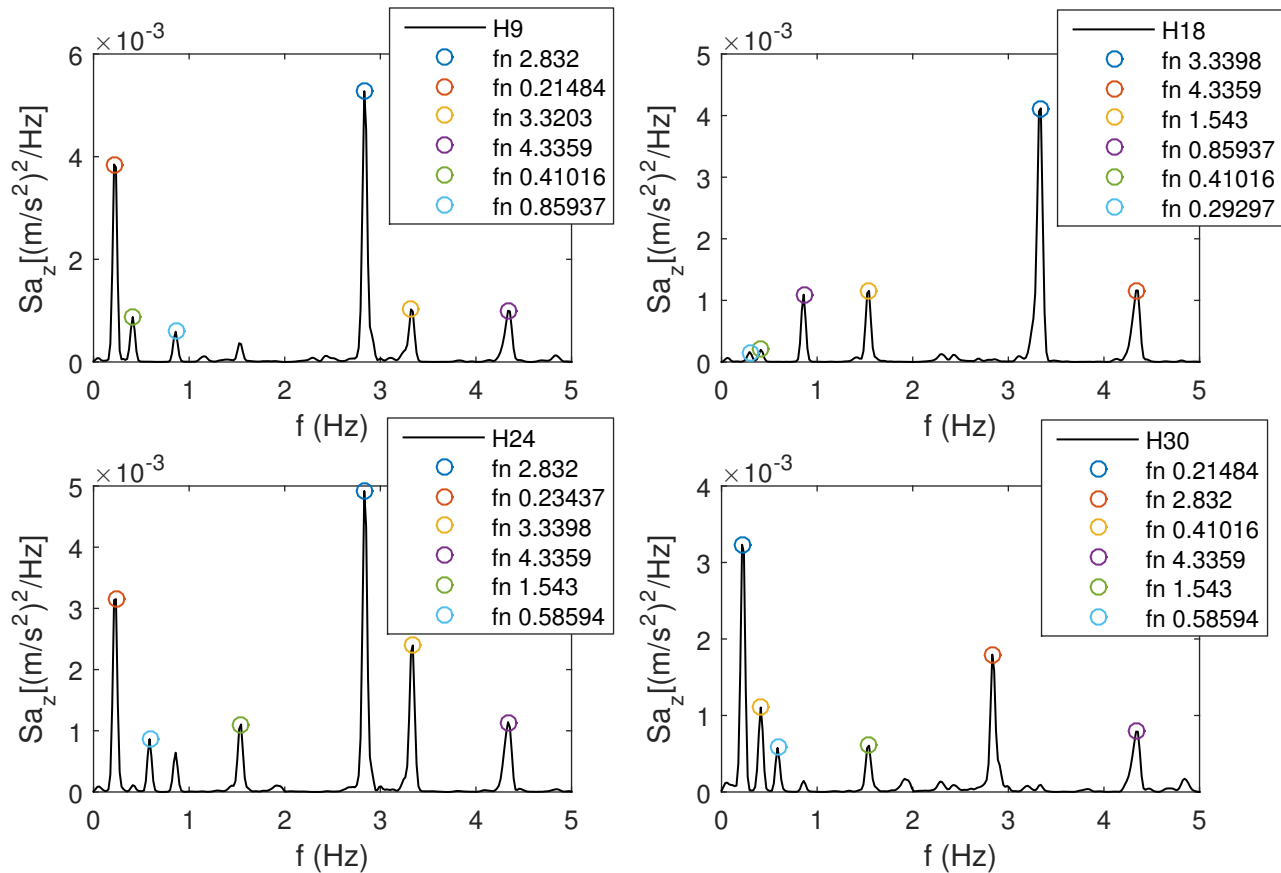


Figure 3.43: PSD individual sensors case 1

All modal frequencies identified in Chapter 3.4 are interesting in terms of damping estimation, although mainly the first, lower modes are relevant in regards to response from wind. The information found in the spectral analysis of the case discussed in Figures 3.42 and 3.43 is further used for isolating the frequencies in the next step.

Filter frequencies, find exact timing of free oscillations and evaluate quality of filter

For the identified frequencies, trial and error of different filtering methods is performed in order to best isolate the frequency in question. Both low-pass high-pass filtering and band-pass filtering is applied to the data. Filtering is applied to individual sensors as well as a method related to FDD known as Time Domain Decomposition (TDD)¹ For simplification reasons, only the re-

¹In short, TDD is similar to FDD, where it further converts the power spectral density functions from all sensors back to time domain, resulting in an acceleration time series that combines all sensors.

sults from individual sensors are applied to the analysis, but all results from fitting exponential decay function to TDD free decay are attached in a separate electronic folder.

The quality of the filtered modal acceleration response varies from case to case. One indication of “good” filtering is that the free oscillations after the vehicle has left the bridge looks relatively smooth, and not affected by other frequencies (beating) or vehicles. Results vary from case to case, and for some cases none of the modes are filtered “well enough” to where free oscillations can be estimated. Judging which modal filters are acceptable is qualitative, with consideration of the free decay oscillations as well as a quantitative mean error function between the oscillation peaks and the fitted exponential decay function.

Examples of “good” and “poor” filtering results are illustrated in Figures 3.44 and 3.45 below.

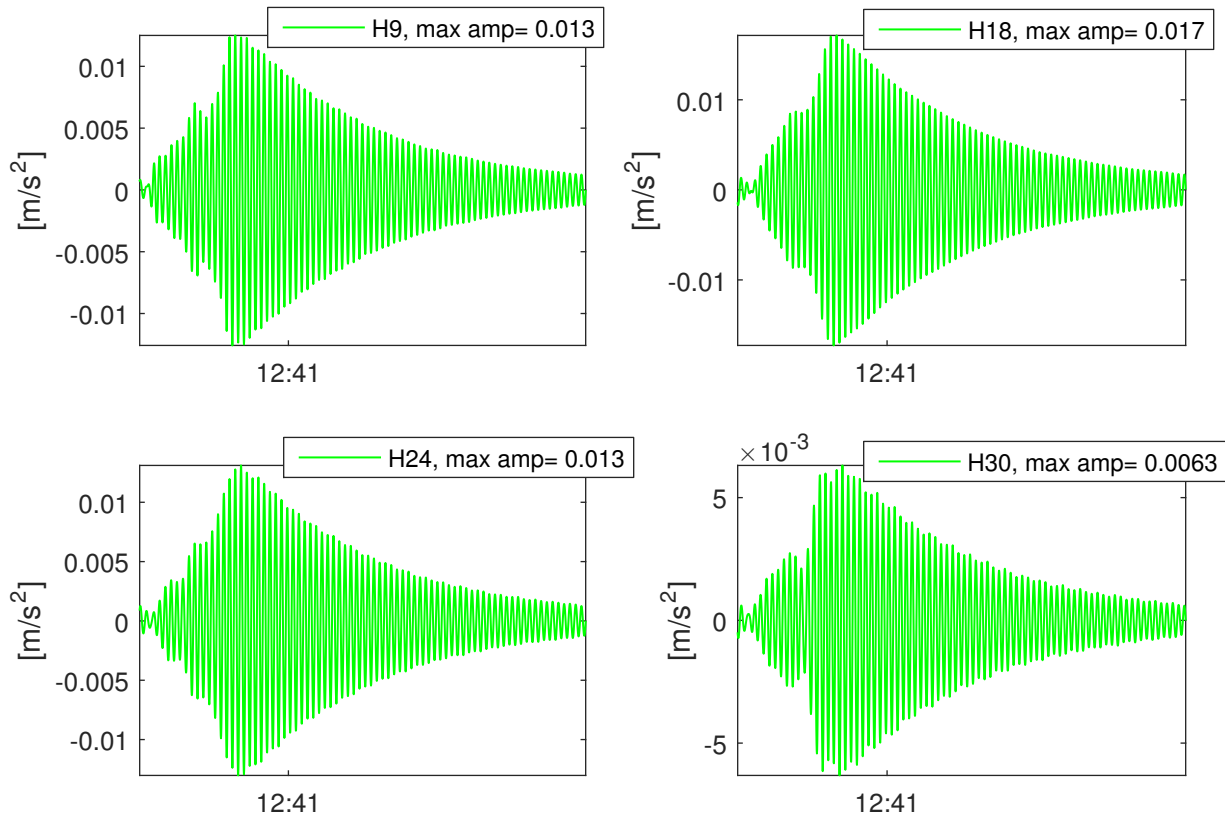


Figure 3.44: “good” filtered modal acceleration response for VS3 (0,854 Hz) for case 1

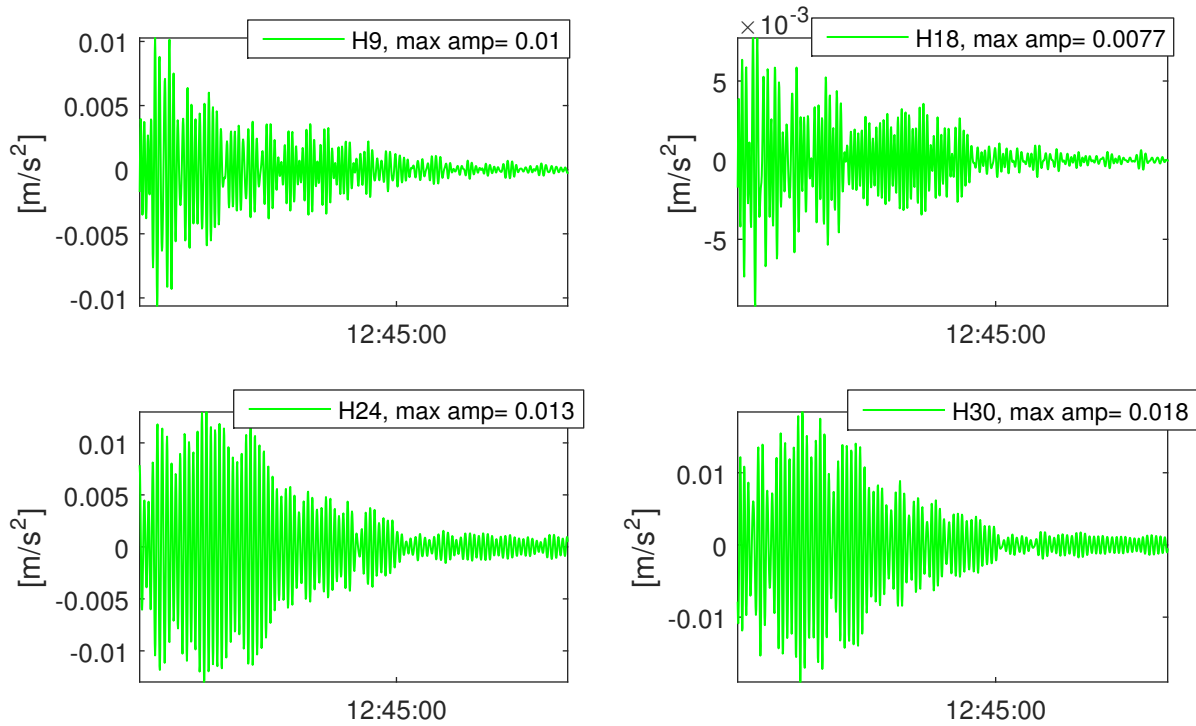


Figure 3.45: “Poor” filtered modal acceleration response for F8 (1,92 Hz) for case 2

The acceleration response illustrated in Figure 3.44 appears to be filtered quite well, and the free oscillations start at around 12:40:55 in the time series, which is reasonable in regards to the observations in Table 3.13. An exponential decay function is fitted to the free oscillations as illustrated in Figure 3.46. Figure 3.47 illustrates an attempt to apply exponential decay fit to a “poorly” filtered frequency. The red and green curves visible in Figure 3.47 are the exponential decay fit used for estimating ξ and the curve used for quantifying the error of the fit of the exponential decay, respectively.

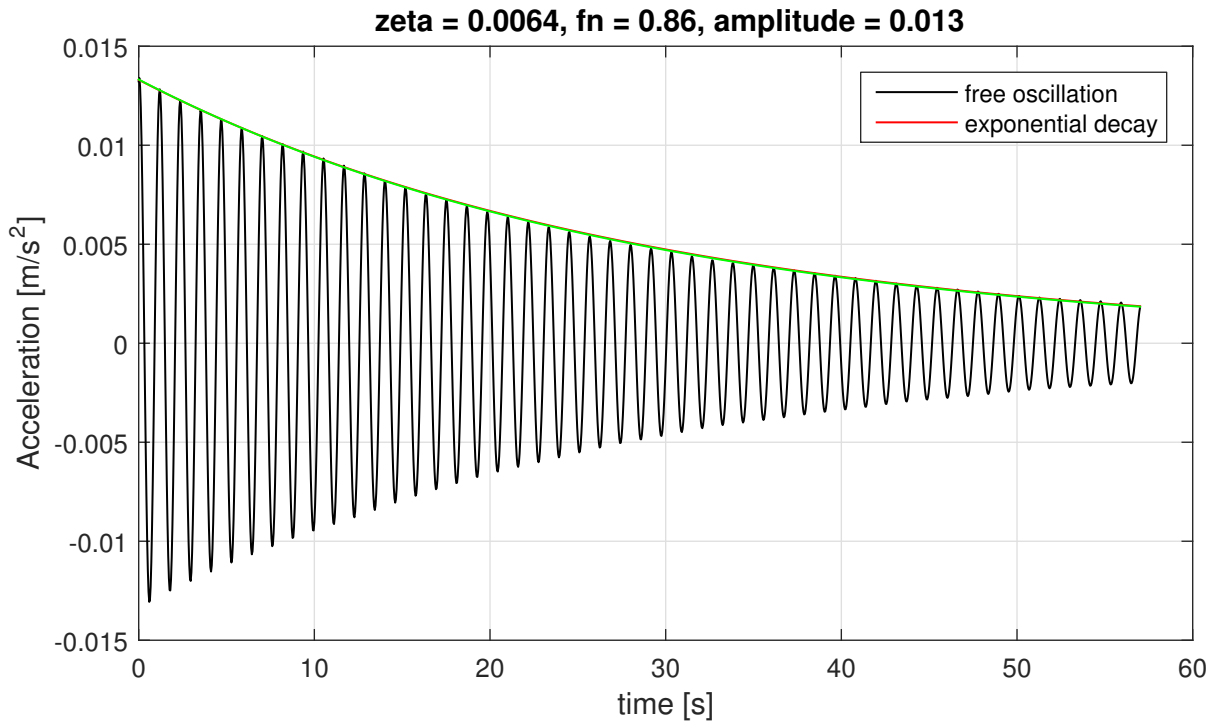
Fitting exponential decay curve to free oscillations

Figure 3.46: Exponential decay function fitted to free vertical modal acceleration oscillations from sensor H18 for VS3 for case 1. Free oscillations starting at 12.40.55 on March 7th. ζ in the title represents estimated damping ratio, ξ .

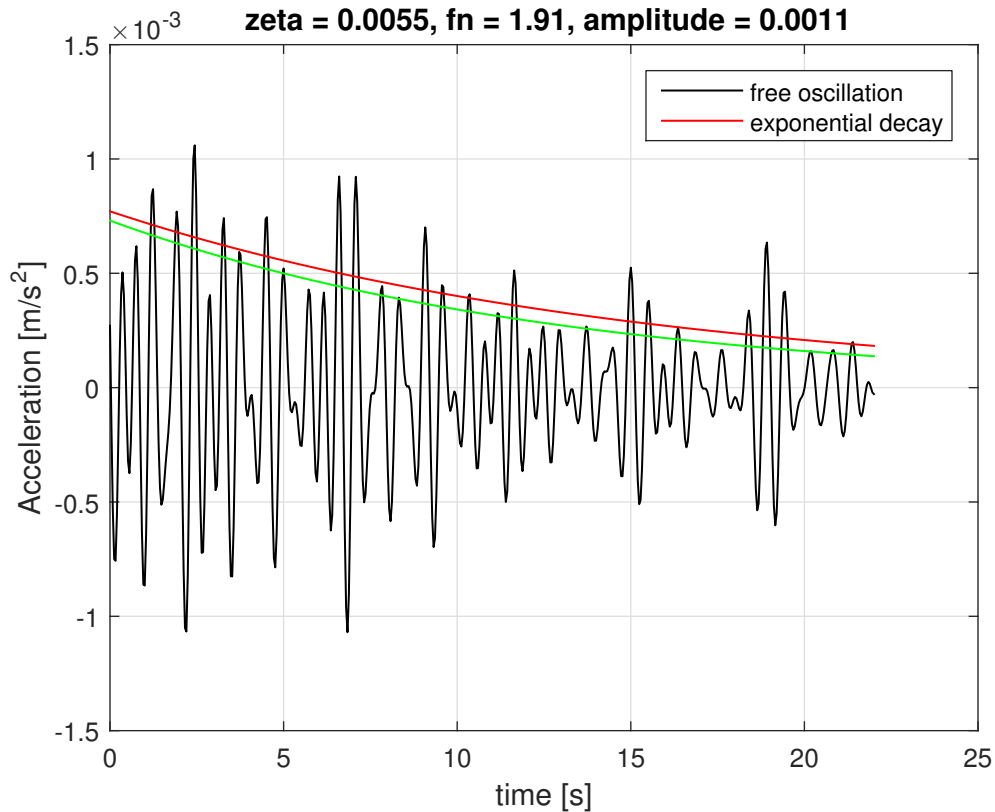


Figure 3.47: Exponential decay function fitted to free vertical modal acceleration oscillations from sensor H18 for 1,92 Hz for case 2. *zeta* in the title represents estimated damping ratio, ξ

For the example discussed in Figure 3.46, the exponential decay curve appears to fit the free oscillations quite perfectly, which indicates that the viscous damping assumption is reasonable. As illustrated in Figure 3.47, this is not always the case. The “poor” results are very likely due to issues with filtering the individual modes, but in some cases it can also be due to different damping mechanisms. The process is performed for all frequencies and all cases, and the results which are considered acceptable are used as data for further analysis. Results are illustrated in Tables 3.15 for vertical response and 3.16 for torsional response. Results such as in Figure 3.47 are considered too poor to qualify as an accepted result. Plots for all frequencies and cases are attached in Appendix D.

Table 3.15: Estimated vertical modal frequencies for each case for the first 9 identified frequencies

case #	wind [m/s]	Temp °C	Modal damping ratio, ξ								
			VA1 %	VS1 %	VS2 %	VA2 %	VS3 %	VA3 %	F7 %	F8 %	F9 %
1	1	-1,4	0,56		0,76	0,65	0,63	0,68	0,75	0,56	0,72
2	1,9	-1,4								0,66	0,72
3	1,8	-1,3			1,3		0,43	0,91	0,94	0,92	0,58
4	0,5	-1,2									
5	3,0	-1,1									
6	2,4	-1,1					0,83	0,67	0,61	0,75	0,6
7	2,8	-1,1									
8	2,6	-1,0					0,72	0,88	0,63	0,79	0,69
9	2,6	-1,0									
10	1,5	8,0			0,41	0,57		0,69	0,62	0,50	0,56
11	1,2	8,9			0,51	0,51	0,52		1,20	1,20	0,80
12	1,7	9,3					0,67	0,56		1,20	0,96
13	1,9	10,0			0,43	0,56	0,54	0,63	0,97	0,85	0,52
14	1,2	10,2			0,40	0,53	0,40	1,00		0,65	0,64
15	0,4	11,5	0,62			0,80		0,45	0,41	0,49	0,48
16	4,1	11,5					0,40	0,45	0,48	0,47	0,51
17	4,8	14,1	0,11		0,46			0,41	0,40		0,52
18	5,7	14,8						0,33	0,32	0,51	0,38
19	5,3	14,8			0,56			0,27	0,21	0,35	0,34
20	4,0	15,0	0,26				0,41	0,29	0,30		0,38
21	3,0	16,5			0,18	0,18	0,19	0,23	0,26		0,23

Table 3.16: Estimated torsional modal frequencies for TS1

Case #	wind [m/s]	Temp °C	Modal damping ratio,
			TS1 %
1	1,0	-1,4	0,52
6	2,4	-1,1	0,66
11	1,5	8,9	0,53
12	1,7	9,3	0,45
13	1,9	10,0	0,45
14	1,2	10,2	0,43
16	4,1	11,5	0,39
20	4,0	15,0	0,28
21	3,0	16,5	0,19

3.7.2 Damping Ratio as Function of Frequency (Mode)

As seen above in Tables 3.15 and 3.16, there are quite a few cases that did not produce satisfactory results for damping estimation. All cases and frequencies left blank or not included are due to either poor filtering results, noise, or some other disturbance that caused unsatisfactory free vibrations. The results that were qualified as acceptable are summarized in the whisker diagram below in Figure 3.48

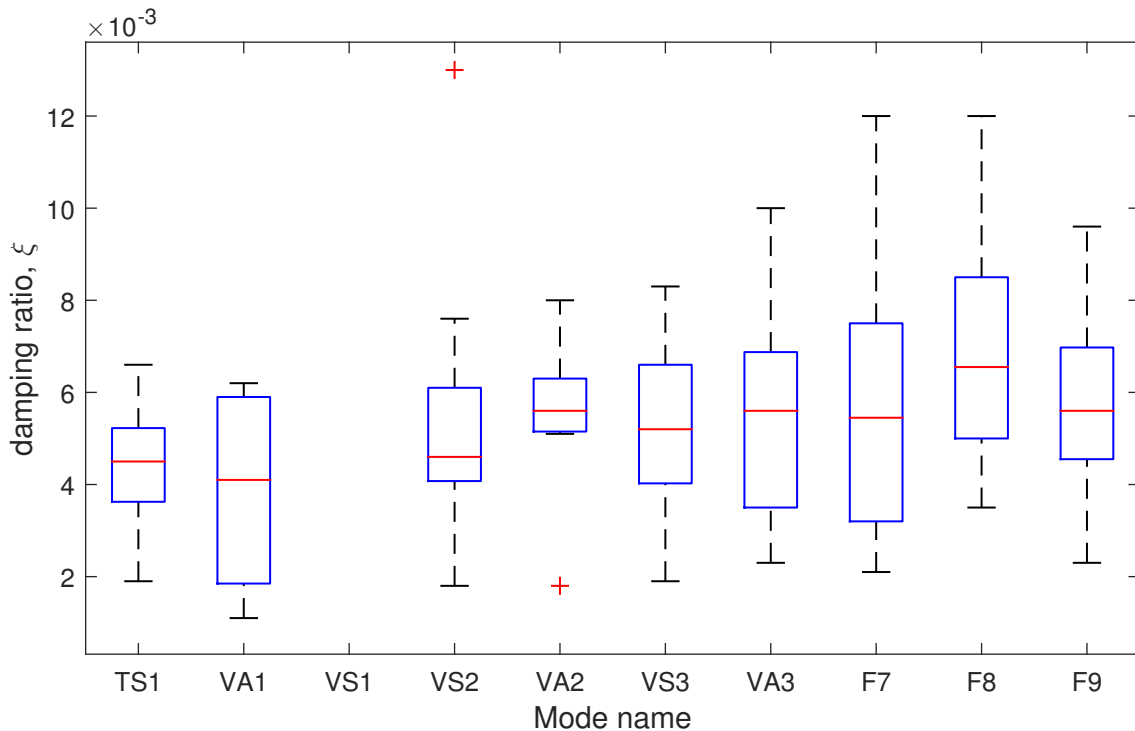


Figure 3.48: Whisker diagram illustrating spread in estimated torsional vertical modal damping ratios

The wide spread in the modal damping ratio is likely to be at least partly due to varied accuracy of the exponential fitting to the filtered free oscillations. However, the damping ratio is also known to be dependent on parameters such as wind, temperature and perhaps also amplitude of oscillations, all of which will be addressed below.

3.7.3 Modal Damping Ratio as Function of Mean Wind Speed and Temperature

Wind is known to have considerable effect on response and vibrations in flexible structures such as suspension bridges, but it also affects properties such as damping. According to theory and full scale measurements ([Cheynet \(2016\)](#)), damping ratio is expected to increase with increased wind velocity. Figures [3.49](#) and [3.50](#) illustrates estimated damping ratios and their respective mean wind speeds for all measured modal frequencies.

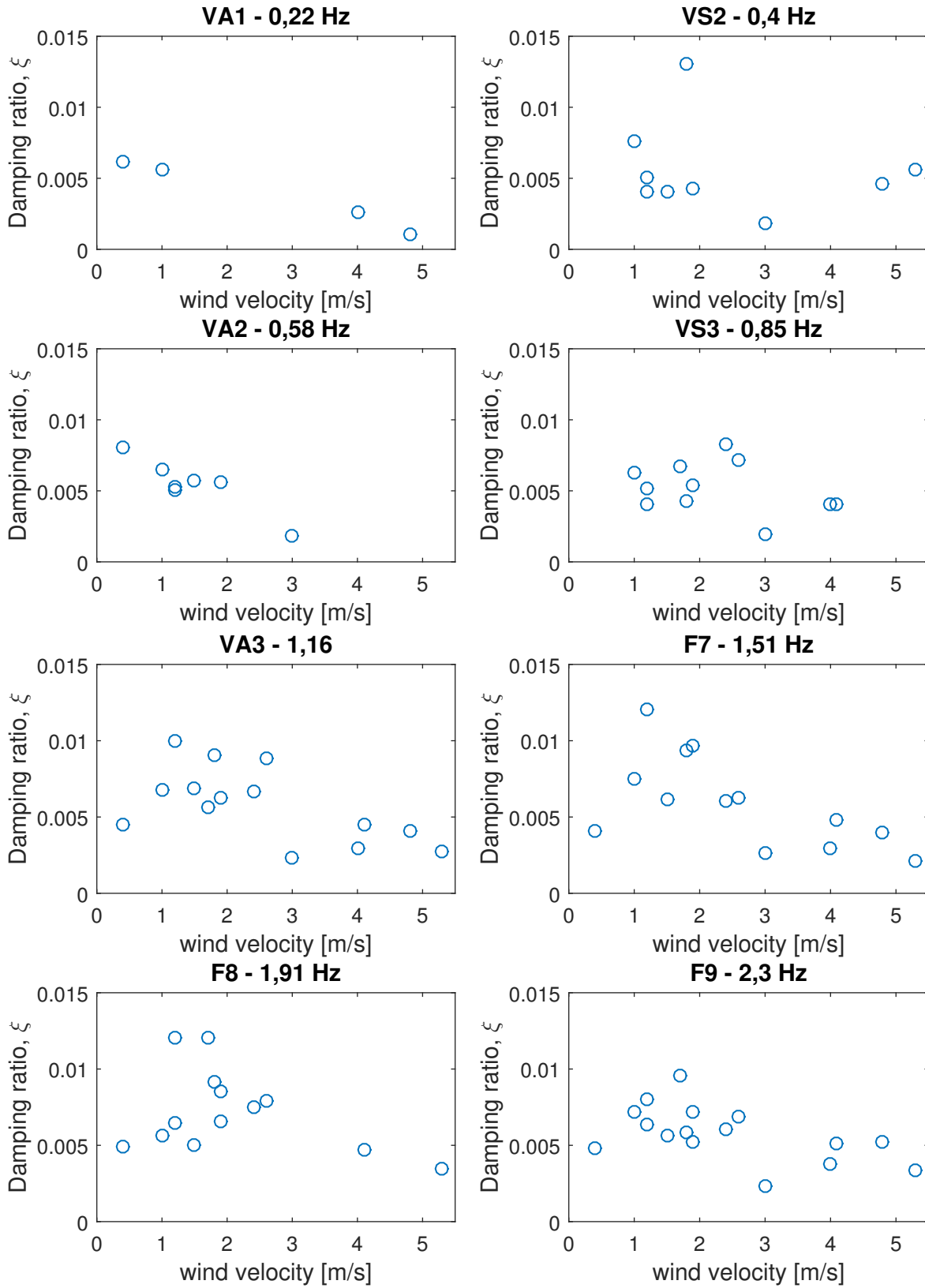


Figure 3.49: Vertical damping ratio, ξ , as function of wind speed for all measured vertical modes

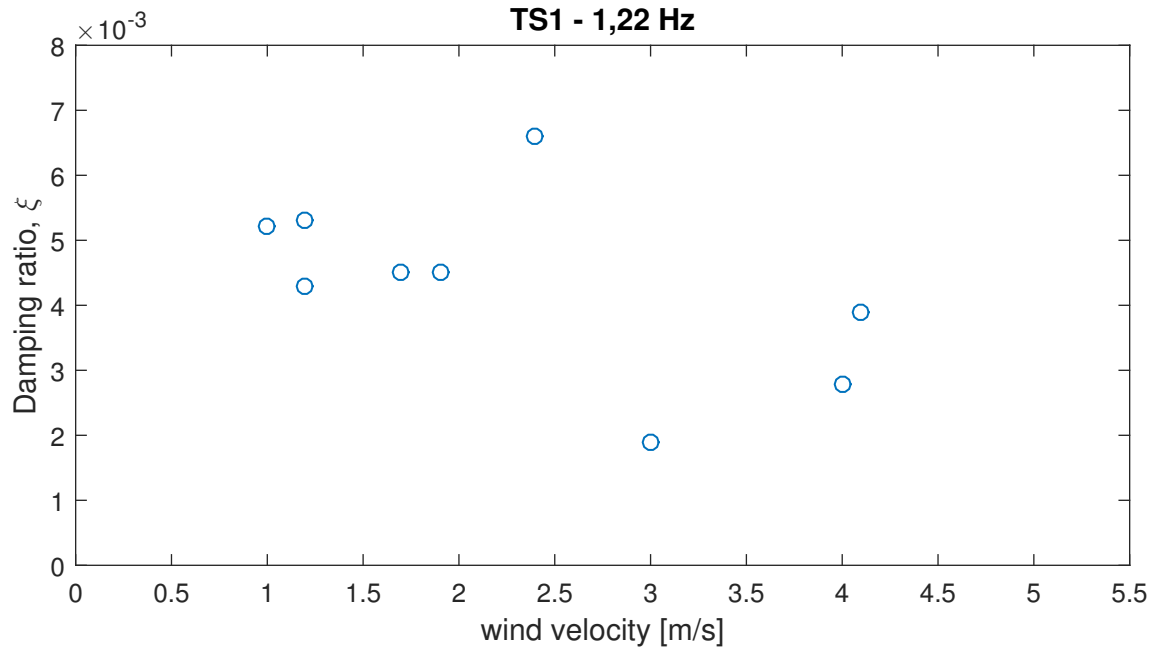


Figure 3.50: Torsional damping ratio, ξ , as function of wind speed for TS1

For most of the plots above in Figures 3.49 and 3.50, there appears to be an inverse relationship between wind speed and modal damping ratio, which is the opposite of what existing literature suggests. However, a maximum mean wind velocity of $5,7\text{ m/s}$ is not very significant, and there are other factors that perhaps have a larger effect on the damping ratio for the data for the present work, such as temperature. Higher temperatures are known to be negatively correlated to damping ratio (Cheynet (2016)), and for the recorded data in the present work there is a relatively large spread in temperature. Also, coincidentally, the days with the highest temperatures are the days with the highest wind speeds. The negative correlation between wind speed and damping ratio can therefore possibly be explained by the temperature variations. Estimated damping ratios and the respective temperatures during the oscillations are illustrated below in Figures 3.51 and 3.52 for all measured modal frequencies.

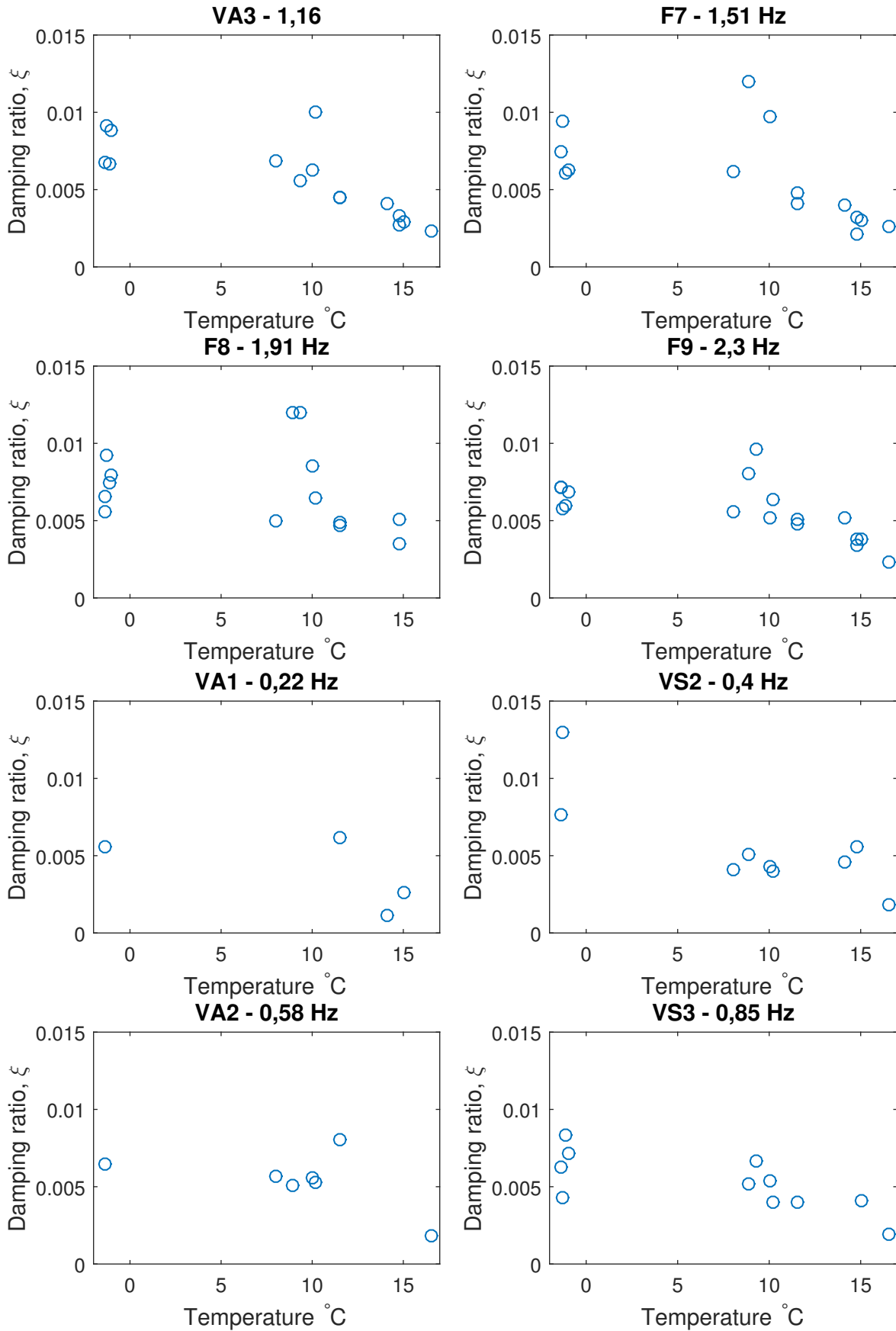


Figure 3.51: Vertical damping ratio, ξ , as function of Temperature for all measured vertical modes

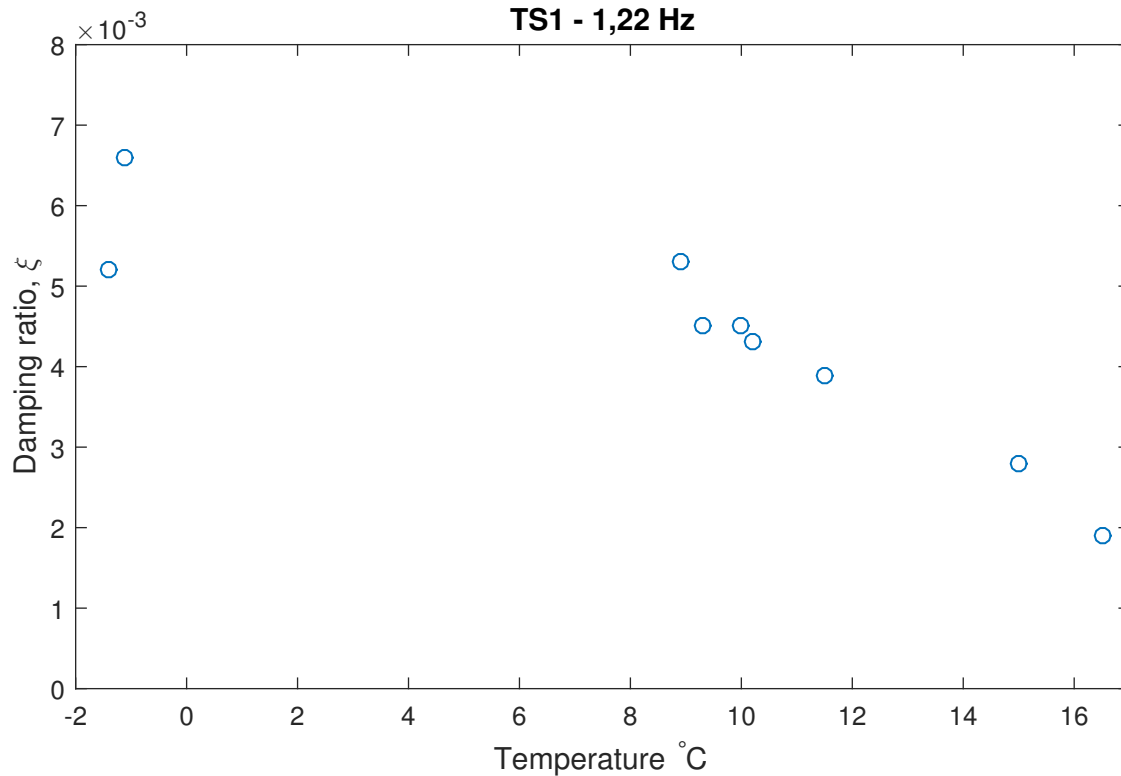


Figure 3.52: Torsional damping ratio, ξ , as function of Temperature for TS1

For all modes above in Figure 3.51 and 3.52, there appears to be a negative correlation between the damping ratio, ξ , and temperature, which agrees with theory and existing literature.

3.7.4 Modal Damping Ratio as Function of Amplitude

One method to check for potential amplitude dependency of damping ratio is to simply compare the exponential decay function (damping ratio) for the first few oscillations of free oscillations of large amplitude vibrations with the oscillations of smaller amplitude vibrations. However, due to the variation in quality in the filtered oscillations, there are quite significant uncertainties regarding the accuracy in estimated modal damping ratios. The filtered free vibrations are therefore not considered accurate enough to draw any conclusions using this method, as the filtered free vibrations can falsely indicate this²

²This conclusion is a strictly qualitative opinion drawn by the author after carefully examining all results

Chapter 4

Conclusion and Further Work

4.1 Conclusion

The present work has been a full-scale study of traffic-induced vibrations of the Lysefjorden bridge. By observing and logging vehicles crossing the bridge on days with low wind speed and correlating the observations with ambient vibration measurements from the bridge, modal damping ratios and impact effects from heavy vehicles have been estimated.

The location of the bridge along with the measurement equipment installed has presented this unique opportunity as traffic is relatively low, and often consists of heavy vehicles transporting concrete modules from factories located in Forsand.

As a means of gaining understanding of the bridge response from vehicles, a spectral analysis of the acceleration time series has been performed. The findings agree with the results from previous studies showing that the response to vehicles consists of a combination of both low and higher frequency modes. Also, all identified frequencies agree with those found previously both using analytical methods and full-scale measurements with very little deviation.

As expected, drawing a definitive conclusion for the magnitude of impact response from different contributing factors such as surface roughness, mass and velocity has proven quite difficult. However, through cooperation with Anette Ravndal, a truck driver for Bjørn Hansen AS, an ex-

periment to study impact load response from heavy vehicles has been performed. The findings in this particular experiment suggest impact load response from heavy vehicles at high velocities while entering and exiting the bridge. For the first modes, response appears to be relatively similar for both exiting and entering the bridge at high velocities. For higher modes of frequencies over 1Hz, the impact load response for the heavy vehicle entering the bridge at high velocity appears to be significant. The magnitude of this impact response from the 50 tonne vehicle is not considered severe/critical for a large structure such as Lysefjorden bridge. However, for bridges with higher fundamental frequencies and lower design loads the findings in the present work suggest that impact effects from high velocities of heavy vehicles entering the bridge should be taken into account.

Damping ratios have been estimated for eight vertical modes and one torsional mode with the assumption of viscous damping for energy dissipation. By isolating the modal free decay oscillation after large vehicles leave the bridge a MATLAB code is used to fit an exponential decay function to the peaks. All in all the method is considered successful, and damping ratios identified seem reasonable in comparison to existing literature and the damping values estimated from the bridge ambient vibration data. However, the variations in the results are quite significant, and are likely largely due to inaccuracies in the filtering of the free decay.

Varying wind and temperatures for the days of vehicle observation can also explain the variations in the modal damping ratio results. By plotting estimated damping ratio as a function of velocity and/or temperature, these relationships are explored. Separating the two (wind and temperature) proved difficult as the days of “high” temperatures also happened to be the days of “high” wind speeds. According to existing literature and theory, increased wind speeds increase the modal damping ratios, and increased temperatures decrease the modal damping ratios. This means that the two variables theoretically affect the damping ratios in different directions in the measurements for the present work. However, out of the two variables the difference in temperature appears to be dominating. This seems reasonable as the relative variations in temperatures are larger than the variations in wind speed encountered during the period considered.

4.2 Further Work

There are several limitations within the methods used in the present work as discussed in Chapter 3.3, but the main limitation lies within the amount of data used for analysis. One of the main suggestions for further work is therefore to increase the amount of data for the analysis. For damping analysis, the method of bridge observation used in the present work should be sufficient. However, if more work is to be performed on impact effects, several controlled experiments need to be performed with different velocities, masses, axle types, and perhaps most importantly with *known* eigenfrequency of the vehicle and with no other vehicles on the bridge.

There are also improvements that can be done using the data collected for the present work, some of which are presented below.

1. Increase understanding of which vehicle situations (direction and velocity) give the best results for free decay analysis. This can be done by thoroughly reviewing and comparing available data and videos from the present work with free decay plots.
2. The present work has perhaps been too lenient in including exponential fits that don't fit properly in the analysis. A review and re-evaluate the exponential decay plots should therefore be performed, removing those considered to "poor" to include in the analysis.
3. More work on different filtering methods and MATLAB functions should be performed in order to try to obtain better filtration of the individual modes.
4. Perform static displacement calculations for a 50 tonne truck in order to estimate Dynamic Load Factor from impact responses found in the present work.
5. Further investigation in severity/significance of the response from heavy vehicles observed.

Bibliography

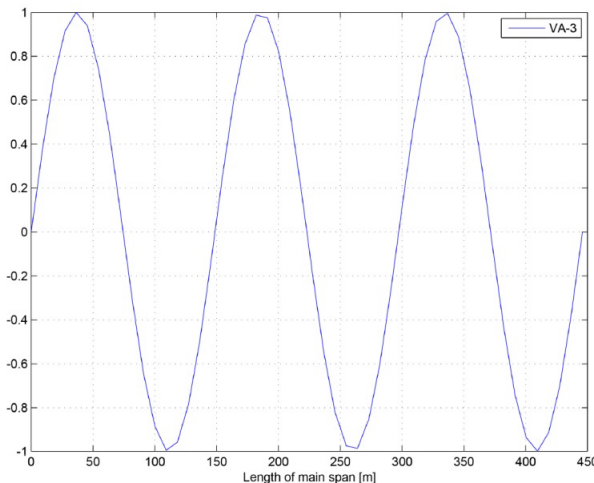
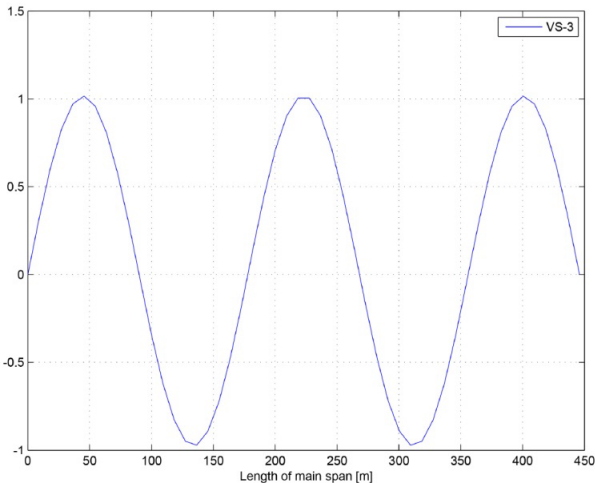
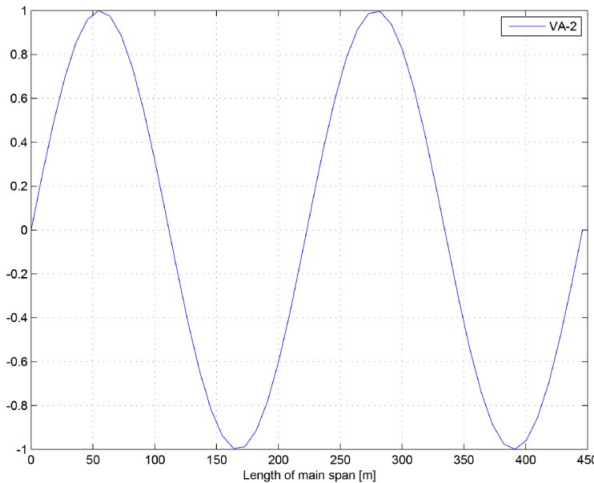
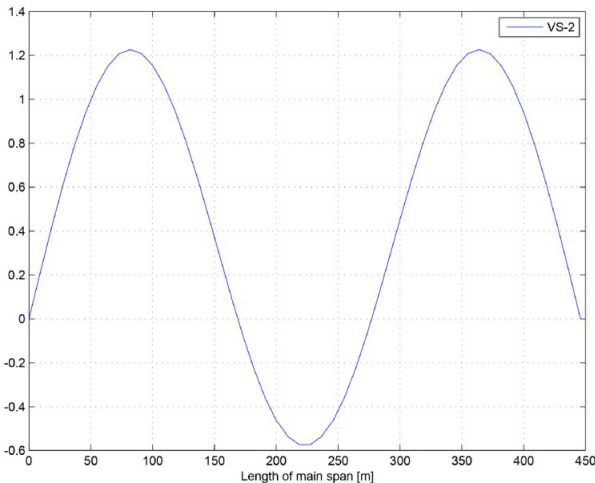
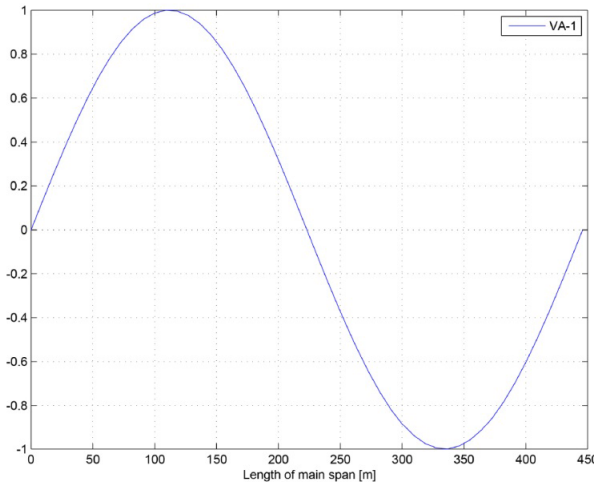
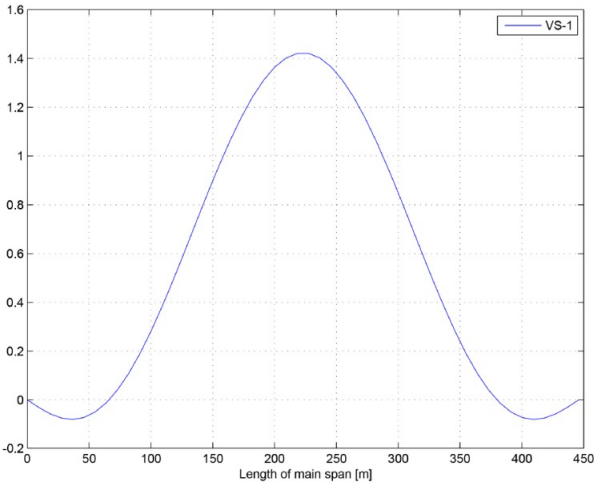
- Adhikari, S. and Woodhouse, J. (2001). Identification of damping: Part 1, viscous damping. *Journal of Sound and Vibration*, 243(1):43–61.
- Apaydın, N. M., Kaya, Y., Şafak, E., and Alçık, H. (2012). Vibration characteristics of a suspension bridge under traffic and no traffic conditions. *Earthquake Engineering & Structural Dynamics*, 41(12):1717–1723.
- Bernard Spragg (n.d.). Taramakau River bridge [Picture]. Available at: <https://www.flickr.com/photos/volvob12b/16460722631/> Accessed [June 2nd 2016].
- Bleich, F. (1950). *The Mathematical Theory of Vibration in Suspension Bridges: A Contribution to the Work of the Advisory Board on the Investigation of Suspension Bridges*.
- Brincker, R., L. Zhang, N., and Andersen, P. (2000). Modal identification from ambient responses using frequency domain decomposition. In *2000 IMAC XVIII – 18th International Modal Analysis Conference*.
- Brownjohn, J. M. W. (1994). Estimation of damping in suspension bridges. *Proceedings of the Institution of Civil Engineers - Structures and Buildings*, 104(4):401–415.
- Bryja, D. and Śniady, P. (1998). Stochastic non-linear vibrations of highway suspension bridge under inertial sprung moving load. *Journal of Sound and Vibration*, 216(3):507 – 519.
- Cheyne, E. (2016). *Wind-Induced vibrations of a suspension bridge*. phd thesis, University of Stavanger.

- Dictionary of Construction (n.d.). Definition of Impact load [Online]. Available at: [<http://www.dictionaryofconstruction.com/definition/impact-load.html>] Accessed [March 9th 2017].
- Erdoğan, H. and Güral, E. (2013). Ambient vibration measurements of the bosphorus suspension bridge by total station and gps. *Experimental Techniques*, 37(3):16–23.
- Eurocode (2003). Eurocode 1: Actions on structures - part 2: Traffic loads on bridges. EN 1991-2.
- Google Maps (n.d.). Map of Lysefjorden inlet [Online]. Available at: [<https://www.google.no/maps/@58.9247512,6.0990762,8384m/data=!3m1!1e3?hl=no>] Accessed [May 20th, 2017].
- Kim, C.-Y., Jung, D.-S., Kim, N.-S., Kwon, S.-D., and Feng, M. Q. (2003). Effect of vehicle weight on natural frequencies of bridges measured from traffic-induced vibration. *Earthquake Engineering and Engineering Vibration*, 2(1):109–115.
- Langen, I. and Sigbjørnsson, R. (1979). *Dynamisk Analyse av Konstruksjoner*. Tapir.
- Liu, Y., Kong, X., Cai, C., and Wang, D. (2017). Driving effects of vehicle-induced vibration on long-span suspension bridges. *Structural Control and Health Monitoring*, 24(2):e1873–n/a. e1873 STC-15-0118.R1.
- Lunder, H. (2014). Dynamic properties of a suspension bridge; comparison of monitored and theoretically estimated response. Master's thesis, University of Stavanger.
- Norwegian Ministry of Transport and Communication (2012). *National Transport Plan 2014 – 2023*.
- Oliva, J., Goicolea, J. M., Antolín, P., and Astiz, M. . (2013). Relevance of a complete road surface description in vehicle–bridge interaction dynamics. *Engineering Structures*, 56:466 – 476.
- Pinsdaddy (n.d.). Time And Frequency Domain [Picture]. Available at: [<https://willianjusten.com.br/frontinsampa-16/img/time-frequency-domain.png>] Accessed [May 2nd 2016].
- Sanpaolesi, L. and Croce, P. (2005). *Handbook 4 - Development of Skills Facilitating Implementation of Eurocodes - Desing of Bridges*.

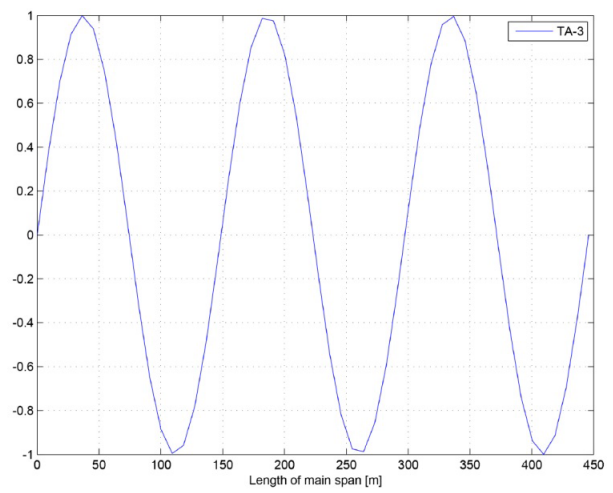
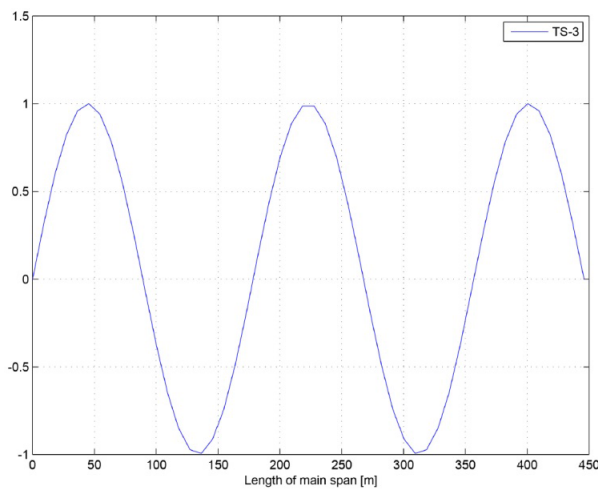
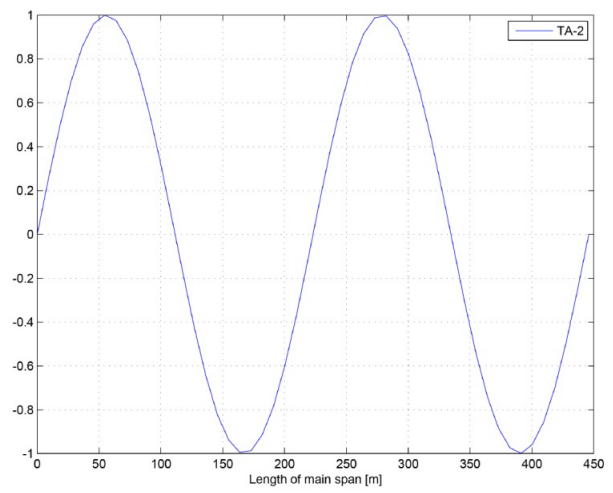
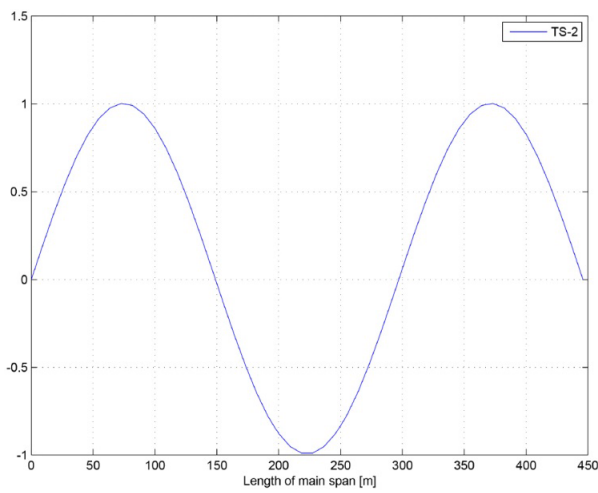
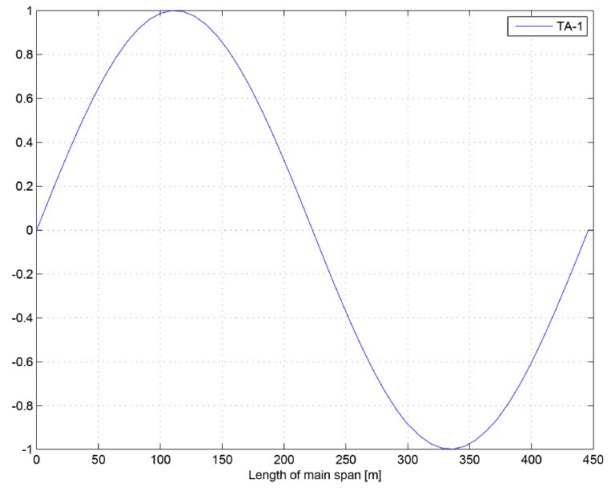
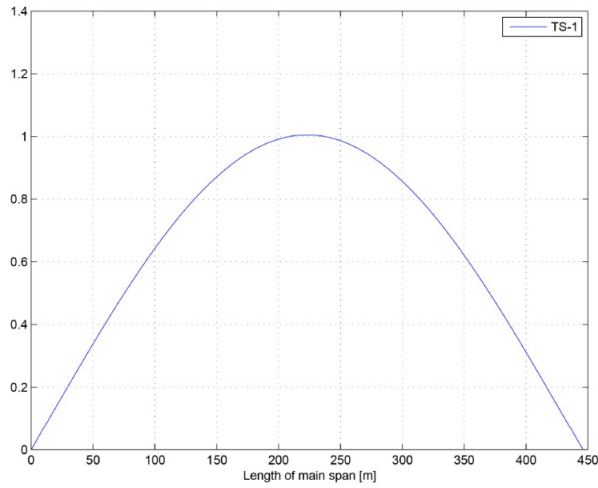
- Selberg, A. (1950). Damping effects in suspension bridges. *IABSE publications = Mémoires AIPC = IVBH Abhandlungen*.
- Snæbjörnsson, J., Cheynet, E., and Jakobsen, J. B. (2016). Performance evaluation of a suspension bridge excited by wind and traffic induced action. In *8th European Workshop On Structural Health Monitoring (EWSHM 2016), At Bilbao, Spain*.
- Steigen, R. O. (2011). Modeling and analyzing a suspension bridge in light of deterioration of the main cable wires. Master's thesis, University of Stavanger.
- Steinman, D. (1959). Modes and natural frequencies of suspension bridge oscillations. *Journal of the Franklin Institute*, 268(3):148 – 174.
- Thoresen, K. (2014). Wind loads and wind effects on suspension bridge. Master's thesis, University of Stavanger.
- Tveiten, J. (2012). Dynamic analysis of a suspension bridge. Master's thesis, University of Stavanger.
- Wang, D., Deng, Y., and Liu, Y. (2015). Influence of central buckle on suspension bridge dynamic characteristics and driving comfort. *Journal of Central South University*, 22(8):3108–3115.
- Xia, Y., Chen, B., Weng, S., Ni, Y.-Q., and Xu, Y.-L. (2012). Temperature effect on vibration properties of civil structures: a literature review and case studies. *Journal of Civil Structural Health Monitoring*, 2(1):29–46.

Appendix A

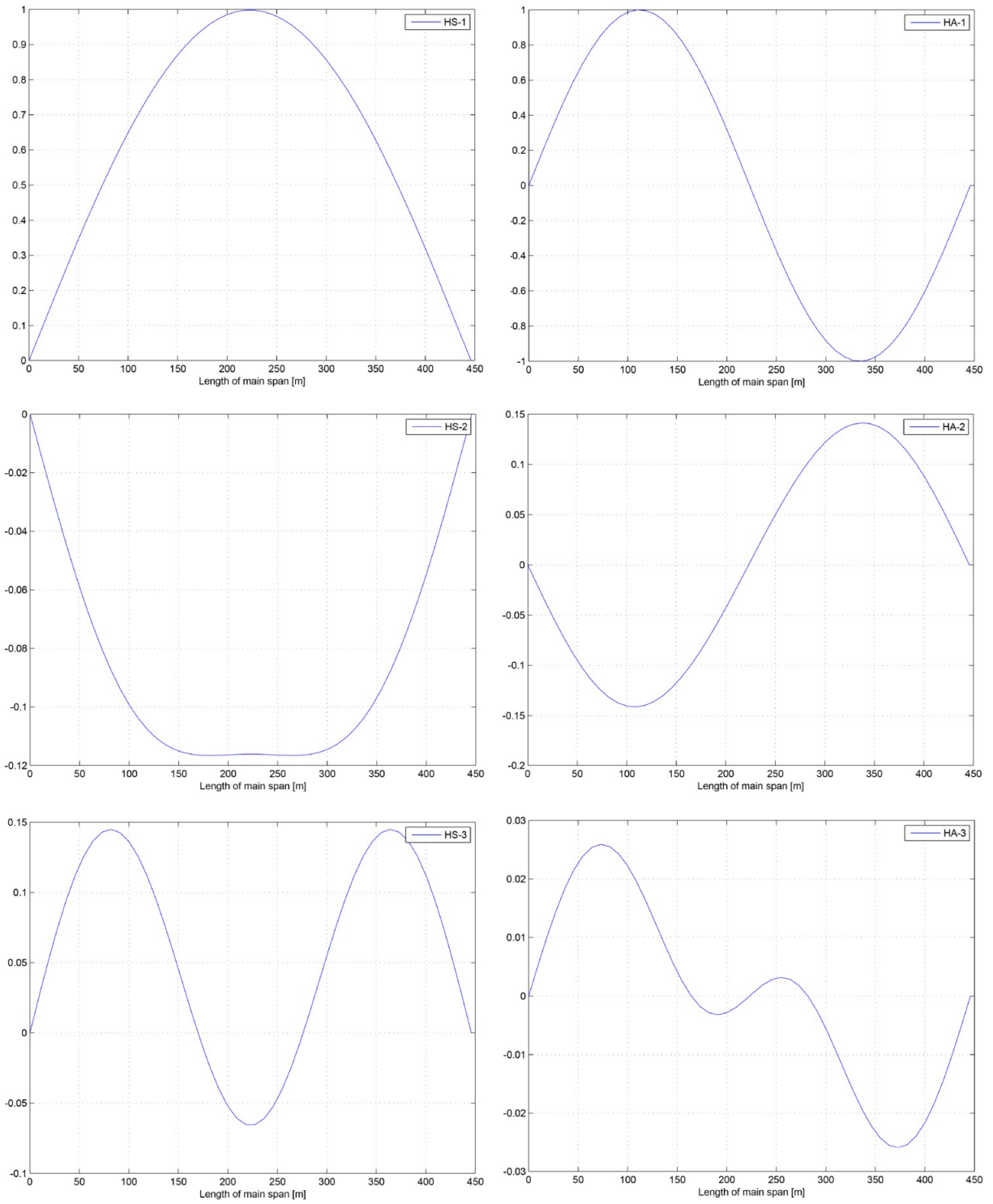
Mode Shapes



Vertical mode shapes as presented in [Lunder \(2014\)](#)



Torsional mode shapes as presented in [Lunder \(2014\)](#)



Horizontal mode shapes as presented in [Lunder \(2014\)](#)

Appendix B

Matlab Functions

B.1 Evolutionary Power Spectral Density Function - by Etienne Cheynet

```

function [Sp,freq,t] = EPSD(x,fs,Nfreq,varargin)
% [Sp,freq] = EPSD(H,T,NFFT,N,x,tmax,scale) compute the Evolutaionary
% Power Spectral Density (EPSD) of a vector x based on the study of Priestley
% [1]
%
%% Input
% x: vector [1 x N] or [N x 1]: time series of a random process
% fs : scalar: sampling frequency
% Nfreq: scalar: number of frequency step.
%
% Varargin: contains additional optaional parameters:
% 'H': scalar : weighting function
% 'T': scalar: window length
% 'scale': string: 'lin' or 'log' to define the frequency vector with
% linspace or logspace respectively.
%
%% Output:
% Sp: matrix [N x Nfreq] : EPSP of the signal x.
% freq: vector [1 x Nfreq]: frequency vector
% t: vector [1 x N]: time vector
%
%% Syntax:
% [Sp,freq,t] = EPSD(x,fs,Nfreq)
% [Sp,freq,t] = EPSD(x,fs,Nfreq,'H',1,'T',10,'scale','lin')
% [Sp,freq,t] = EPSD(x,fs,Nfreq,'scale','log')
% [Sp,freq,t] = EPSD(x,fs,Nfreq,'dataPlot',0)
%
%% Example
% t = 0:0.001:2;
% dt = median(diff(t));
% fs=1/dt;
% x = chirp(t,100,1,200,'quadratic');
% [Sp,freq,t] = EPSD(x,fs,Nfreq,'scale','lin','H',50*dt,'T',1.01*dt );
% caxis([-50,-20])
% ylim([0,500])
% xlim([0.1,1.9])
% title('EPSP')

%% Author info
% E. Cheynet, Universitetet i Stavanger, norway.
% last modified 08/08/2016
%
%% References
% [1] Priestley, M. B. (1965). Evolutionary spectra and non-stationary
% processes. Journal of the Royal Statistical Society.
% Series B (Methodological), 204-237.
%
% see also spectrogram

%% Inputparser
p = inputParser();
p.CaseSensitive = false;
p.addOptional('H',10./fs);
p.addOptional('T',10./fs);
p.addOptional('scale','log');
p.addOptional('dataPlot',1);
p.parse(varargin{:});

```

```

% shorten the variables name
H = p.Results.H ;
T = p.Results.T ;
scale = p.Results.scale ;
dataPlot = p.Results.dataPlot;
%%
N=numel(x);
x = x(:)';
tmax = N/fs;
t0 = linspace(-tmax/2,tmax/2,N);
dt = median(diff(t0));
fs = 1/dt;
fmin = 1/tmax;

if strcmpi(scale,'log'),
    freq=logspace(log10(fmin),log10(fs/2),Nfreq);
elseif strcmpi(scale,'lin'),
    freq=linspace(0,fs/2,Nfreq);
else
    error(' 'scale' must be 'lin' or 'log' ');
end

% window and weigthing function
g = zeros(1,N);
h = zeros(1,N);
for ii=1:N,
    if abs(t0(ii))<=H,
        g(1,ii) = 1/(2*sqrt(H.*pi));
    else
        g(1,ii)=0;
    end
    if abs(t0(ii))<=T/2,
        h(1,ii) = 1/T;
    else
        h(1,ii)=0;
    end
end
end
Sp = nan(Nfreq,N);
for ii=1:Nfreq,
    U0 = conv(g,x.*exp(-1i*2*pi.*freq(ii)*t0),'same');
    Sp(ii,:) = conv(h,abs(U0).^2,'same').*2*(dt).^3;
end
t = linspace(0,tmax,N);

if dataPlot==1,
    imagesc(t,freq,pow2db(Sp));
    axis('xy')
    axis tight
    xlabel('time (s)')
    ylabel('frequency (Hz)')
    c=colorbar('Eastoutside');
    ylabel(c,'Power/frequency (dB/Hz)')
end
end

```

B.2 Frequency Domain Decomposition function - by Mohammad Farshchin and simplified by Etienne Cheynet

```

function [newS,newF,fn] = getS_from_FDD(Az,t,M,Nmodes)
%% Pre-processing
[Nyy,N] = size(Az);
fs = 1/median(diff(t));
if M>numel(t), error('M must be less than numel(t)');end
%% Computation of the spectral matrix G
% size(G) is [N x Nyy x Nyy]
if rem(M,2),
    G = zeros(Nyy,Nyy,round(M/2));
else
    G = zeros(Nyy,Nyy,round(M/2)+1);
end
for ii=1:Nyy,
    for jj=1:Nyy,
        [G(ii,jj,:),f] = cpsd(Az(ii,:),Az(jj,:),M,round(M/2),M,fs);
    end
end
%% Application of SVD to G
% U =zeros(size(G));
S =zeros(Nyy,size(G,3));
% V =zeros(size(G));
for ii=1:size(G,3),
    [~,diagMat,~] = svd(G(:,:,ii));
    S(:,ii) = diag(diagMat);
end

S = S(1,:);

% interpolation to improve accuracy of peak picking and damping estimation
Ninterp=2;
newF = linspace(f(1),f(end),Ninterp*numel(f));
newS = interp1(f,S(1,:),newF,'pchip');
newS = newS./max(newS); % normalized power spectral density

indMax = manualPickPeaking(newF,newS,Nmodes);
fn = newF(indMax);

function [Fp] = manualPickPeaking(f,S,Nmodes)
    % original author: Mohammad Farshchin
    % FileExchange submission:
https://se.mathworks.com/matlabcentral/fileexchange/50988-frequency-domain-decomposition--fdd-/content/FDD.m
    %%
    display('Peak selection procedure')
    display('a: Draw rectangles around peaks while holding left click')
    display('b: Press "Space" key to continue the peak selection')
    display('c: Press "any other key" if you have selected a peak by
mistake and want to ignore it')

    clf

```

```

plot(f,mag2db(S))
grid on
xlim([f(2),f(end)])
ylim([min(mag2db(S)),max(mag2db(10*S))])
hold on
set(gcf,'color','w');
xlabel('Frequency (Hz)')
ylabel('1st Singular values of the PSD matrix (db)')
Fp=[];% Frequencies related to selected peaks
while numel(Fp)<Nmodes
    myRec=getrect;
% Draw a rectangle around the peak
    [~,P1]=min(abs(f-myRec(1)));
    [~,P2]=min(abs(f-(myRec(1)+myRec(3))));
    [~,P3]=max(S(P1:P2));
    indPeak=P3+P1-1;
% Frequency at the selected peak

scatter(f(indPeak),mag2db(S(indPeak)),'MarkerEdgeColor','b','MarkerFaceColor',
'b')    % Mark this peak
    pause;
    key=get(gcf,'CurrentKey');
    if strcmp(key,'space'),
        % Press space to continue peak selection
        Fp=[Fp,indPeak];

scatter(f(indPeak),mag2db(S(indPeak)),'MarkerEdgeColor','g','MarkerFaceColor',
'g')    % Mark this peak as green
        else
            % Press any other key to ignore this peak

scatter(f(indPeak),mag2db(S(indPeak)),'MarkerEdgeColor','r','MarkerFaceColor',
'r')    % Mark this peak as red
        end
    end
    % Number selected peaks, respectively
    Fp=sort(Fp);
    pause(0.01);
end
end
end

```


B.3 Filtering function based on Butterworth filter - by Chad A. Greene

```

function [yfilt,filtb,filta] = filter1(filtertype,y,varargin)
% filter1 performs frequency or wavelength filtering on a 1D array
% using zero-phase Butterworth filtering.
%
%% Syntax
%
% yfilt = filter1(filtertype,y,'fc',Fc)
% yfilt = filter1(filtertype,y,'lambdac',lambdac)
% yfilt = filter1(...,'fs',Fs)
% yfilt = filter1(...,'x',x)
% yfilt = filter1(...,'Ts',Ts)
% yfilt = filter1(...,'order',FilterOrder)
% [yfilt,filtb,filta] = filter1(...)
%
%% Description
%
% yfilt = filter1(filtertype,y,'fc',Fc) filters 1D signal y
% using a specified filtertype and cutoff frequency Fc. For
% high-pass or low-pass filters Fc must be a scalar. For band-
% pass and band-stop filters Fc must be a two-element array. The
% filtertype can be
%
% * 'hp' high-pass with scalar cutoff frequency Fc
% * 'lp' low-pass with scalar cutoff frequency Fc
% * 'bp' band-pass with two-element cutoff frequencies Fc
% * 'bs' band-stop with two-element cutoff frequencies Fc
%
% yfilt = filter1(filtertype,y,'lambdac',lambdac) specifies cutoff
% wavelength(s) rather than cutoff frequencies. This syntax assumes
% lambda = 1/f.
%
% yfilt = filter1(...,'fs',Fs) specifies a sampling frequency Fs.
% If neither 'fs', 'x', nor 'Ts' are specified, Fs = 1 is assumed.
%
% yfilt = filter1(...,'x',x) specifies a vector of monotonically-
% increasing, equally-spaced sampling times or x locations corresponding
% to y, which is used to determine sampling frequency. If neither 'fs',
% 'x', nor 'Ts' are specified, Fs = 1 is assumed.
%
% yfilt = filter1(...,'Ts',Ts) specifies a sampling period or sampling
distance
% such that Fs = 1/Ts. If neither 'fs', 'x', nor 'Ts' are specified,
% Fs = 1 is assumed.
%
% yfilt = filter1(...,'order',FilterOrder) specifies the order (sometimes
% called rolloff) of the Butterworth filter. If unspecified, FilterOrder = 1
is assumed.
%
% [yfilt,filtb,filta] = filter1(...) also returns the filter numerator
% filta and denominator filtb.
%
%% Example
% % For this example we'll use the built-in train whistle example file and
we'll add
% % a little gaussian random noise to make things interesting.
%
% load train

```

```

%     y = y+0.1*randn(size(y));
%
% % High-pass filter the train whistle, keeping only frequencies above 750 Hz:
%
%     yhp = filter1('hp',y,'fs',Fs,'fc',750);
%
% % Lowpass filter the train whistle, keeping only frequencies below 1100 Hz
% % and specify a sharp 5th order rolloff. Also reference y to a time vector
% % instead of the sampling rate we specified above:
%
%     t = (0:length(y)-1)/Fs;
%     ylp = filter1('lp',y,'x',t,'fc',1100,'order',5);
%
% % Bandstop filter the train whistle from 750 Hz to 1000 Hz to eliminate the
886 Hz
% % middle frequency.
%
%     ybs = filter1('bs',y,'fs',Fs,'fc',[750 1000],'order',5);
%
% % Use plotpsd (available on File Exchange) to show original and
% % bandstop-filtered signals:
%
%     plotpsd(y,Fs,'b')
%     hold on
%     plotpsd(ybs,Fs,'r')
%
%% Author Info
% The filter1 function was written by Chad A. Greene of the University of
% Texas at Austin's Institute for Geophysics (UTIG), October 2015.
% http://www.chadagreene.com
%
% See also butter and filtfilt.

%% Initial error checks:

assert(license('test','signal_toolbox')==1,'The filter1 function requires
Matlab's Signal Processing Toolbox.')
assert(nargin>3,'Not enough input arguments.')
assert(sum(strcmpi({'hp';'lp';'bp';'bs';'high';'low';'bandpass';'stop'},filter
type))==1,'Filter type must be 'hp', 'lp', or 'bp'.'),
assert(sum([strcmpi(varargin,'fc') strcmpi(varargin,'lambdac')])==1,'Must
declare a cutoff frequency (or frequencies) 'fc', or cutoff wavelength(s)
'lambdac'.')
assert(isvector(y)==1,'Input y must be a vector.')

%% Define defaults:

order = 1;
Fs = 1;

%% Parse Inputs:

% Replace filtertype string if necessary:
filtertype = strrep(filtertype,'hp','high');
filtertype = strrep(filtertype,'lp','low');
filtertype = strrep(filtertype,'bp','bandpass');

```

```

filtertype = strcmp(filtertype, 'bs', 'stop');

% Is a sampling frequency defined?
tmp = strcmpi(varargin, 'fs');
if any(tmp)
    Fs = varargin{find(tmp)+1};
end

% Define sampling period:
tmp2 = strcmp(varargin, 'Ts');
if any(tmp2)
    Fs = 1/varargin{find(tmp2)+1};
end

% Define sampling vector:
tmp3 = strcmp(varargin, 'x');
if any(tmp3)
    x = varargin{find(tmp3)+1};
    assert(isvector(x)==1, 'Input x must be a vector.')
    assert(length(x)==length(y), 'Dimensions of input vector x must match
dimensions of input signal vector y.')

    Ts = unique(diff(x));
    assert(all([isscalar(Ts) isfinite(Ts)])==1, 'Input vector x must be equally
spaced.')
```

Fs = 1/Ts;

```

end

% Make sure user didn't try to define a sampling frequency AND a sampling
period:
assert(any(tmp)+any(tmp2)+any(tmp3)<2, 'I am confused. It looks like you have
attempted to define a sampling frequency and a sampling period. Check inputs
of filter1.')
```

```

% Cutoff Frequency:
tmp = strcmpi(varargin, 'fc');
if any(tmp)
    cutoff_freqs = varargin{find(tmp)+1};
end

tmp2 = strncmpi(varargin, 'lambdac', 4);
if any(tmp2)
    cutoff_freqs = 1./varargin{find(tmp2)+1};
end
assert(any(tmp)+any(tmp2)<2, 'I am confused. It looks like you have attempted
to define a cutoff frequency and a cutoff period. Check inputs of filter1.')
```

```

% Filter order:
tmp = strncmpi(varargin, 'order', 3);
if any(tmp)
    order = varargin{find(tmp)+1};
end

%% Error checks on inputs:

```

```
assert(isscalar(Fs)==1,'Input error: Undefined sampling frequency or period.')

switch filtertype
    case {'low','high'}
        assert(isscalar(cutoff_freqs)==1,'Low-pass and High-pass filters
require a scalar cutoff frequency.')

        case {'stop','bandpass'}
            assert(numel(cutoff_freqs)==2,'Bandpass and bandstop filters require a
low and high frequency.')
            cutoff_freqs = sort(cutoff_freqs);

        otherwise
            error('Unrecognized filter type.')
end

%% Construct filter:

nyquist_freq = Fs/2;           % Nyquist frequency

if cutoff_freqs>nyquist_freq,
    warning('the cut off frequency specified is larger than the Nyquist
frequency.');
```

```
    yfilt=nan;
    filtb=nan;
    filta=nan;
    return
end
Wn=cutoff_freqs/nyquist_freq; % non-dimensional frequency
[filtb,filta]=butter(order,Wn,filtertype); % construct the filter
yfilt=filtfilt(filtb,filta,y); % filter the data with zero phase

end
```

B.4 PSD for all individual sensors - based on MATLAB function

“pwelch”

```

clearvars;close all;clc;
load('C:\Users\Eier\OneDrive - Universitetet i
Stavanger\master\matlab\ANALYSE_Test\dataAnalysed\StatsResult_2017_03_07_10Hz.
mat','U','V','W','Aox','Aoz','Aot','t','time','GPS')

% Select starting time and ending time
dt = median(diff(t)); % time step
fs = 1/dt; % sampling frequency

% %% INPUT Time selection
% tStart = datenum(2017,03,07,12,40,00); % start time
% tEnd = datenum(2017,03,07,12,42,00); % stop time

tStart = datenum(2017,03,07,12,40,00); % start time
tEnd = datenum(2017,03,07,12,42,00); % stop time

name = '6.png';

% Get acceleration between tStart and tEnd vertical
[Az1,newTime] = getTimeSeries(tStart,tEnd,squeeze(Aoz(1, :, :)),time,fs);
[Az2,newTime] = getTimeSeries(tStart,tEnd,squeeze(Aoz(2, :, :)),time,fs);
[Az3,newTime] = getTimeSeries(tStart,tEnd,squeeze(Aoz(3, :, :)),time,fs);
[Az4,newTime] = getTimeSeries(tStart,tEnd,squeeze(Aoz(4, :, :)),time,fs);
[Vx1,newTime] = getTimeSeries(tStart,tEnd,squeeze(U(4, :, :)),time,fs);
%[U2,newTime] = getTimeSeries(tStart,tEnd,squeeze(U(5, :, :)),time,fs);
[Vy1,newTime] = getTimeSeries(tStart,tEnd,squeeze(V(4, :, :)),time,fs);
%Umean = mean(U2);

% Get acceleration between tStart and tEnd Torsional
[At1,newTime] = getTimeSeries(tStart,tEnd,squeeze(Aot(1, :, :)),time,fs);
[At2,newTime] = getTimeSeries(tStart,tEnd,squeeze(Aot(2, :, :)),time,fs);
[At3,newTime] = getTimeSeries(tStart,tEnd,squeeze(Aot(3, :, :)),time,fs);
[At4,newTime] = getTimeSeries(tStart,tEnd,squeeze(Aot(4, :, :)),time,fs);

%%
%Filter acc data HP

Dz1 = iomega(Az1,dt,3,1);
Dz2 = iomega(Az2,dt,3,1);
Dz3 = iomega(Az3,dt,3,1);
Dz4 = iomega(Az4,dt,3,1);

%Dz1 = filter1('hp',Dz1,'fs',fs,'fc',0.03,'order',4); %H9 North
%Dz2 = filter1('hp',Dz2,'fs',fs,'fc',0.03,'order',4); %H18
%Dz3 = filter1('hp',Dz3,'fs',fs,'fc',0.03,'order',4); %H24
%Dz4 = filter1('hp',Dz4,'fs',fs,'fc',0.03,'order',4); %H30 South

%Vertical

Az1h = filter1('hp',Az1,'fs',fs,'fc',0.03,'order',4); %H9 North
Az2h = filter1('hp',Az2,'fs',fs,'fc',0.03,'order',4); %H18
Az3h = filter1('hp',Az3,'fs',fs,'fc',0.03,'order',4); %H24
Az4h = filter1('hp',Az4,'fs',fs,'fc',0.03,'order',4); %H30 South

%Torsional

```

```

%Az1h = filter1('hp',At1,'fs',fs,'fc',0.03,'order',4); %H9 North
%Az2h = filter1('hp',At2,'fs',fs,'fc',0.03,'order',4); %H18
%Az3h = filter1('hp',At3,'fs',fs,'fc',0.03,'order',4); %H24
%Az4h = filter1('hp',At4,'fs',fs,'fc',0.03,'order',4); %H30 South

%% Some useful tools
% figure
% subplot(311)
% plot(newTime,Az2h,'g')%,newTime,Az3h,'b',newTime,Az2h,'g',newTime,Az1h,'y')
% datetick('x')
% axis tight
% ylabel('acceleration')
% legend ('H18')%, 'H24', 'H18', 'H9')
% title('Vertical Accelleration H18')
%
% subplot(312)
% plot(newTime,At2,'r')%,newTime,Az3h,'b',newTime,Az2h,'g',newTime,Az1h,'y')
% datetick('x')
% axis tight
% ylabel('acceleration')
% legend ('H18')%, 'H24', 'H18', 'H9')
% title('Tortional Accelleration H18')
%
% subplot(313)
% plot(newTime,Vx1,'b')%,newTime,U2,'r')
% datetick('x')
% axis tight
% ylabel('Wind velocity')
% title('wind velocity normal to bridge H18')

%%
% PSD with pwelch algorithm - FOR AZ
[Sz1,f1]=pwelch(detrend(Az1h),[],[],[],fs);
[Sz2,f2]=pwelch(detrend(Az2h),[],[],[],fs);
[Sz3,f3]=pwelch(detrend(Az3h),[],[],[],fs);
[Sz4,f4]=pwelch(detrend(Az4h),[],[],[],fs);

figure
plot(f1,Sz1,'k',f2,Sz2,'b',f3,Sz3,'g',f4,Sz4,'y')%plotter med log på y og
vanlig på x - lettere å se tall på egenfrekvenser
xlabel('f (Hz)')
ylabel('Sa_z [(m/s^2)^2/Hz]')
legend ('H9', 'H18', 'H24', 'H30')
title('PSD acceleration')

%Finding the frequency values of the peaks of the PSD for acceleration
%and sorting lowest to highest
%Eigenfrequencies H9
[x1,freqPeak1] = findpeaks(Sz1,f1);
peaks1 = [x1 freqPeak1];
peaksSorted1 = sortrows(peaks1);

```

```

%Eigenfrequencies H18
[x2,freqPeak2] = findpeaks(Sz2,f2);
peaks2 = [x2 freqPeak2];
peaksSorted2 = sortrows(peaks2);

%Eigenfrequencies H24
[x3,freqPeak3] = findpeaks(Sz3,f3);
peaks3 = [x3 freqPeak3];
peaksSorted3 = sortrows(peaks3);

%Eigenfrequencies H30
[x4,freqPeak4] = findpeaks(Sz4,f4);
peaks4 = [x4 freqPeak4];
peaksSorted4 = sortrows(peaks4);

peaksSorted1num = numel(peaksSorted1(:,2));
peaksSorted2num = numel(peaksSorted2(:,2));
peaksSorted3num = numel(peaksSorted3(:,2));
peaksSorted4num = numel(peaksSorted4(:,2));

allpeaksSorted = zeros(6,4);

%Sorts 6 highest PSD peaks for all four sensors in 6 x 4 matrix

for ii=1:6,
allpeaksSorted(ii,:) = [peaksSorted1((peaksSorted1num-(ii-1)),2),peaksSorted2((peaksSorted2num-(ii-1)),2),peaksSorted3((peaksSorted3num-(ii-1)),2),peaksSorted4((peaksSorted4num-(ii-1)),2)];
end

%Displays
allpeaksSorted(:, :)

Umean = mean(Vx1)
Vmean = mean(Vy1)

figure('units','normalized','outerposition',[0,0,.6,.6])
set(gcf,'color','w');
subplot(221)
plot(f1,Sz1,'k',peaksSorted1(peaksSorted1num,2),peaksSorted1(peaksSorted1num,1),
'0',peaksSorted1(peaksSorted1num-1,2),peaksSorted1(peaksSorted1num-1,1),
'0',peaksSorted1(peaksSorted1num-2,2),peaksSorted1(peaksSorted1num-2,1),
'0',peaksSorted1(peaksSorted1num-3,2),peaksSorted1(peaksSorted1num-3,1),
'0',peaksSorted1(peaksSorted1num-4,2),peaksSorted1(peaksSorted1num-4,1),
'0',peaksSorted1(peaksSorted1num-5,2),peaksSorted1(peaksSorted1num-5,1),
'0')
xlabel('f (Hz)')
ylabel('Sa_z [(m/s^2)^2/Hz]')
legend('H9',[ 'fn ' num2str(peaksSorted1(peaksSorted1num,2)) ], [ 'fn '
num2str(peaksSorted1(peaksSorted1num-1,2)) ], [ 'fn '
num2str(peaksSorted1(peaksSorted1num-2,2)) ], [ 'fn '
num2str(peaksSorted1(peaksSorted1num-3,2)) ], [ 'fn '
num2str(peaksSorted1(peaksSorted1num-4,2)) ], [ 'fn '
num2str(peaksSorted1(peaksSorted1num-5,2)) ])

```

```

subplot(222)
plot(f2,Sz2,'k',peaksSorted2(peaksSorted2num,2),peaksSorted2(peaksSorted2num,1),
'0',peaksSorted2(peaksSorted2num-1,2),peaksSorted2(peaksSorted2num-1,1),
'0',peaksSorted2(peaksSorted2num-2,2),peaksSorted2(peaksSorted2num-2,1),
'0',peaksSorted2(peaksSorted2num-3,2),peaksSorted2(peaksSorted2num-3,1),
'0',peaksSorted2(peaksSorted2num-4,2),peaksSorted2(peaksSorted2num-4,1),
'0',peaksSorted2(peaksSorted2num-5,2),peaksSorted2(peaksSorted2num-5,1),
'0')
xlabel('f (Hz)')
ylabel('Sa_z[(m/s^2)^2/Hz]')
legend('H18',[ 'fn ' num2str(peaksSorted2(peaksSorted2num,2)) ],[ 'fn '
num2str(peaksSorted2(peaksSorted2num-1,2)) ],[ 'fn '
num2str(peaksSorted2(peaksSorted2num-2,2)) ],[ 'fn '
num2str(peaksSorted2(peaksSorted2num-3,2)) ],[ 'fn '
num2str(peaksSorted2(peaksSorted2num-4,2)) ],[ 'fn '
num2str(peaksSorted2(peaksSorted2num-5,2)) ])
%title('PSD acceleration H18')

subplot(223)
plot(f3,Sz3,'k',peaksSorted3(peaksSorted3num,2),peaksSorted3(peaksSorted3num,1),
'0',peaksSorted3(peaksSorted3num-1,2),peaksSorted3(peaksSorted3num-1,1),
'0',peaksSorted3(peaksSorted3num-2,2),peaksSorted3(peaksSorted3num-2,1),
'0',peaksSorted3(peaksSorted3num-3,2),peaksSorted3(peaksSorted3num-3,1),
'0',peaksSorted3(peaksSorted3num-4,2),peaksSorted3(peaksSorted3num-4,1),
'0',peaksSorted3(peaksSorted3num-5,2),peaksSorted3(peaksSorted3num-5,1),
'0')
xlabel('f (Hz)')
ylabel('Sa_z[(m/s^2)^2/Hz]')
legend('H24',[ 'fn ' num2str(peaksSorted3(peaksSorted3num,2)) ],[ 'fn '
num2str(peaksSorted3(peaksSorted3num-1,2)) ],[ 'fn '
num2str(peaksSorted3(peaksSorted3num-2,2)) ],[ 'fn '
num2str(peaksSorted3(peaksSorted3num-3,2)) ],[ 'fn '
num2str(peaksSorted3(peaksSorted3num-4,2)) ],[ 'fn '
num2str(peaksSorted3(peaksSorted3num-5,2)) ])
%title('PSD acceleration H24')

subplot(224)
plot(f4,Sz4,'k',peaksSorted4(peaksSorted4num,2),peaksSorted4(peaksSorted4num,1),
'0',peaksSorted4(peaksSorted4num-1,2),peaksSorted4(peaksSorted4num-1,1),
'0',peaksSorted4(peaksSorted4num-2,2),peaksSorted4(peaksSorted4num-2,1),
'0',peaksSorted4(peaksSorted4num-3,2),peaksSorted4(peaksSorted4num-3,1),
'0',peaksSorted4(peaksSorted4num-4,2),peaksSorted4(peaksSorted4num-4,1),
'0',peaksSorted4(peaksSorted4num-5,2),peaksSorted4(peaksSorted4num-5,1),
'0')
xlabel('f (Hz)')
ylabel('Sa_z[(m/s^2)^2/Hz]')
legend('H30',[ 'fn ' num2str(peaksSorted4(peaksSorted4num,2)) ],[ 'fn '
num2str(peaksSorted4(peaksSorted4num-1,2)) ],[ 'fn '
num2str(peaksSorted4(peaksSorted4num-2,2)) ],[ 'fn '
num2str(peaksSorted4(peaksSorted4num-3,2)) ],[ 'fn '
num2str(peaksSorted4(peaksSorted4num-4,2)) ],[ 'fn '
num2str(peaksSorted4(peaksSorted4num-5,2)) ])
%title('PSD acceleration H30')

```


B.5 Exponential Decay Fit function

```

function [zeta,varargout] = expoFit(y,t1,wn,optionPlot,py)
%
% [zeta] = expoFit(y,t,wn) returns the damping ratio calculated by fitting
% an exponential decay to the envelop of the Impulse Response Function.
%
% y: envelop of the IRF: vector of size [1 x N]
% t: time vector [ 1 x N]
% wn: target eigen frequencies (rad/Hz) : [1 x 1]
% zeta: modal damping ratio: [1 x 1]
% optionPlot: 1 to plot the fitted function, and 0 not to plot it.
%%
% Initialisation
guess = [1,1e-2];
% simple exponential decay function
myFun = @(a,x) a(1).*exp(-a(2).*x);
% application of nlinfit function
coeff1 = nlinfit(t1,y,myFun,guess);
fprintf('coeff1 = \n')
disp(coeff1)
% modal damping ratio:
zeta = abs(coeff1(2)./wn);

if nargout>1,
    varargout{1} = coeff1 ;
end
% alternatively: plot the fitted function
if optionPlot== 1

    plot(t1,myFun(coeff1,t1),'r')

end

%Y = abs(hilbert(y));

[py2,indP] = findpeaks(py);

% pycount = numel(py2);
% tlnew = linspace(1,pycount,pycount)
coeff2 = nlinfit(t1(indP),py(indP),myFun,guess);
nyExpo = myFun(coeff2,t1);
fprintf('coeff2 = \n')
disp(coeff2)

hold on;box on; grid on; grid minor;
plot(t1,nyExpo,'g')%,t1(indP),py(indP),'ko')

%method file exchange
[gf] = gfit(t1(indP),py(indP))

%method mathworks
cost_func = 'MSE';

X = py(indP);

```

```
XREF = myFun(coeff2,t1(indP));
% fit = goodnessOfFit(X,Xref,cost_func);

%err = immse(X,XREF)

%fit = nanmean((X-XREF).^2)/XREF

%OWN
fit1 = abs(X-XREF)/XREF

%OWN2
for i=1:numel(X)
    fit2(i)=abs((X(i)-XREF(i))/XREF(i));
end

fit2 = nanmean(fit2);

%fit2 = goodnessOfFit(X,XREF,cost_func)

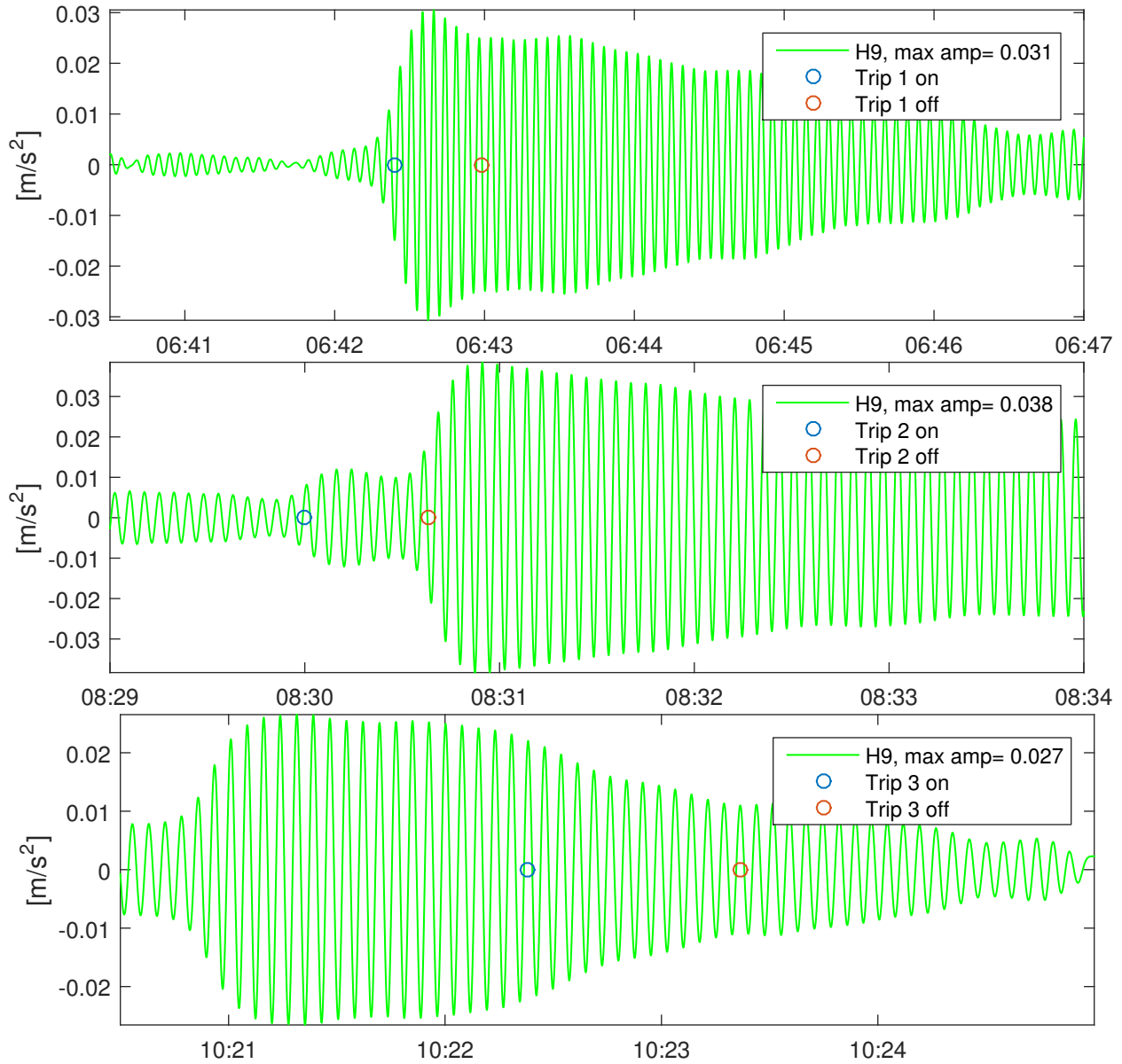
fprintf(['fit 1 error is :',num2str(fit1,3),' \n','fit 2 error is
',num2str(fit2,3),'\n']);
end
```

Appendix C

Impact Response

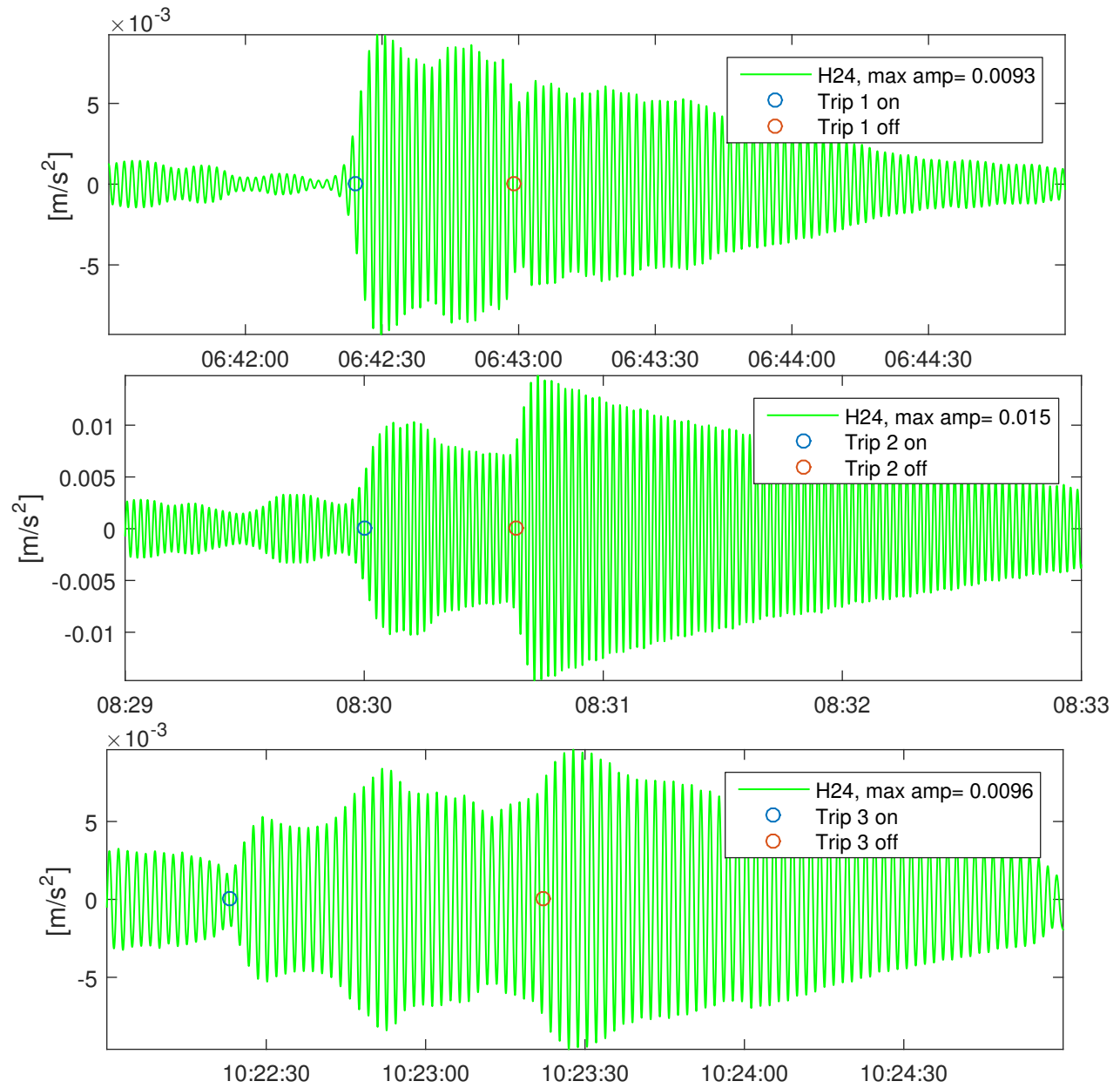
C.1 Impact Acceleration Response

VA1 - sensor H9



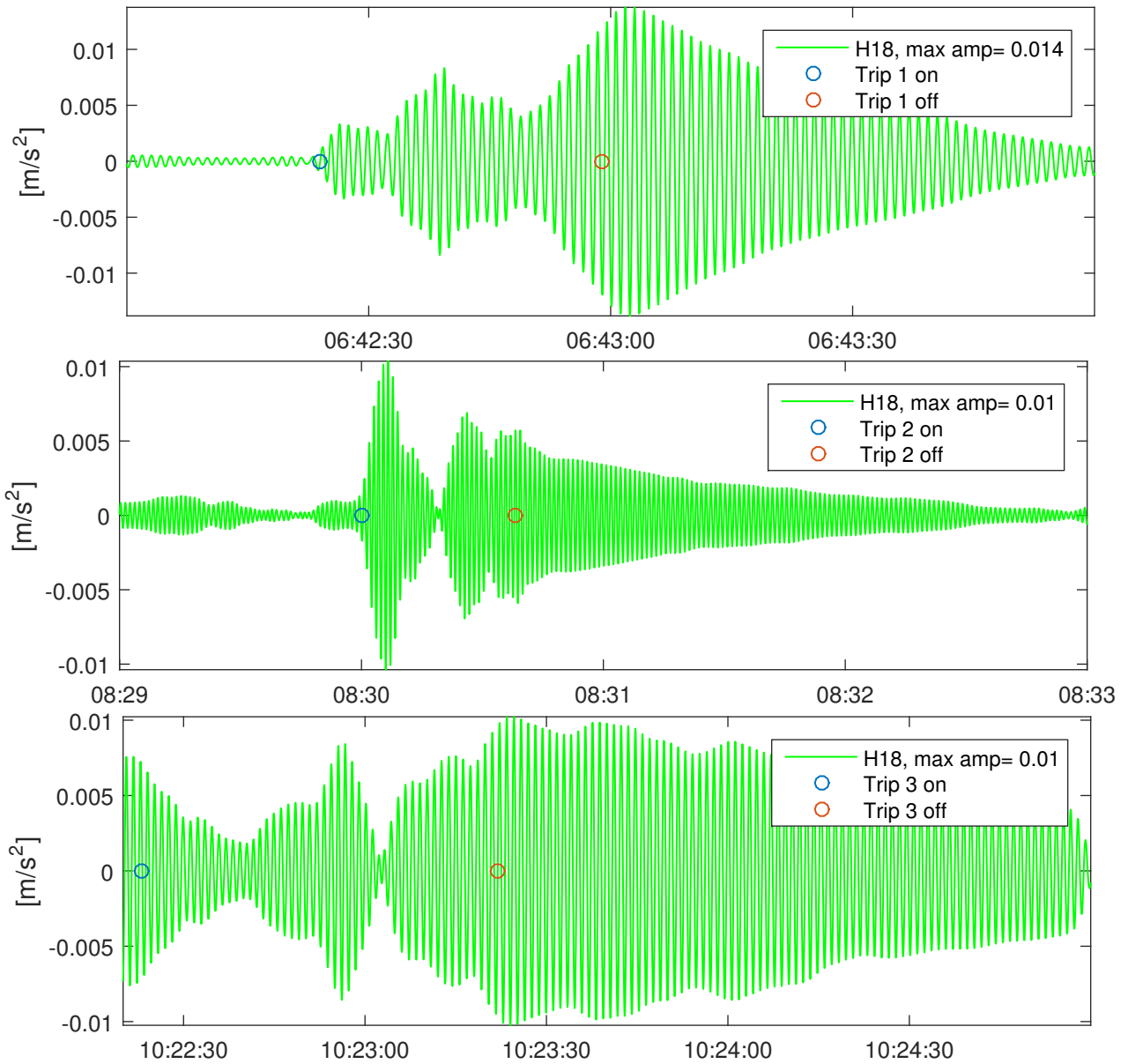
Filtered response VA1 for trip 1(top), trip 2 (middle) and trip 3 (bottom)

VA2 - sensor H24



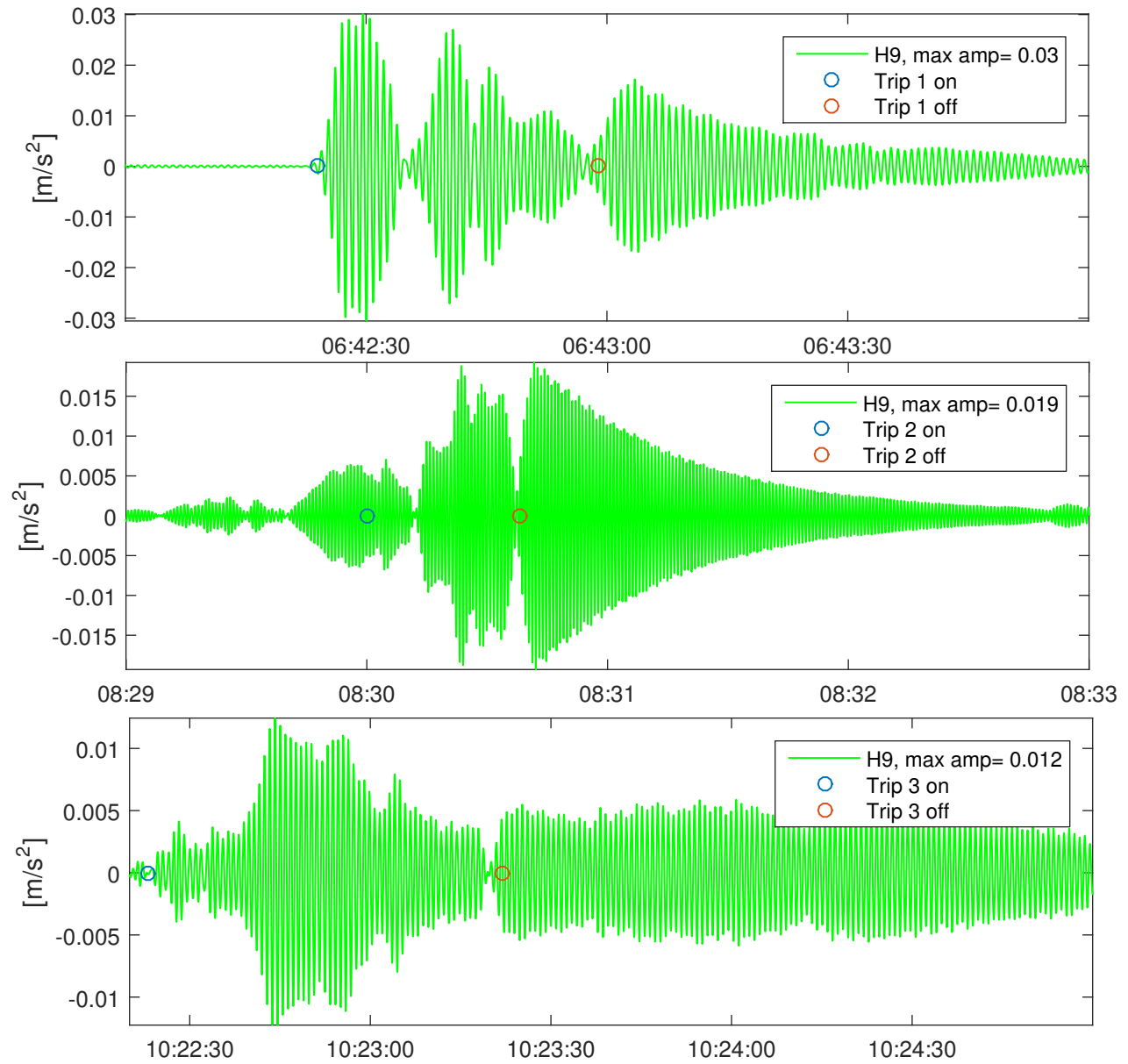
Filtered response VA2 for trip 1(top), trip 2 (middle) and trip 3 (bottom)

VS3 - sensor H18



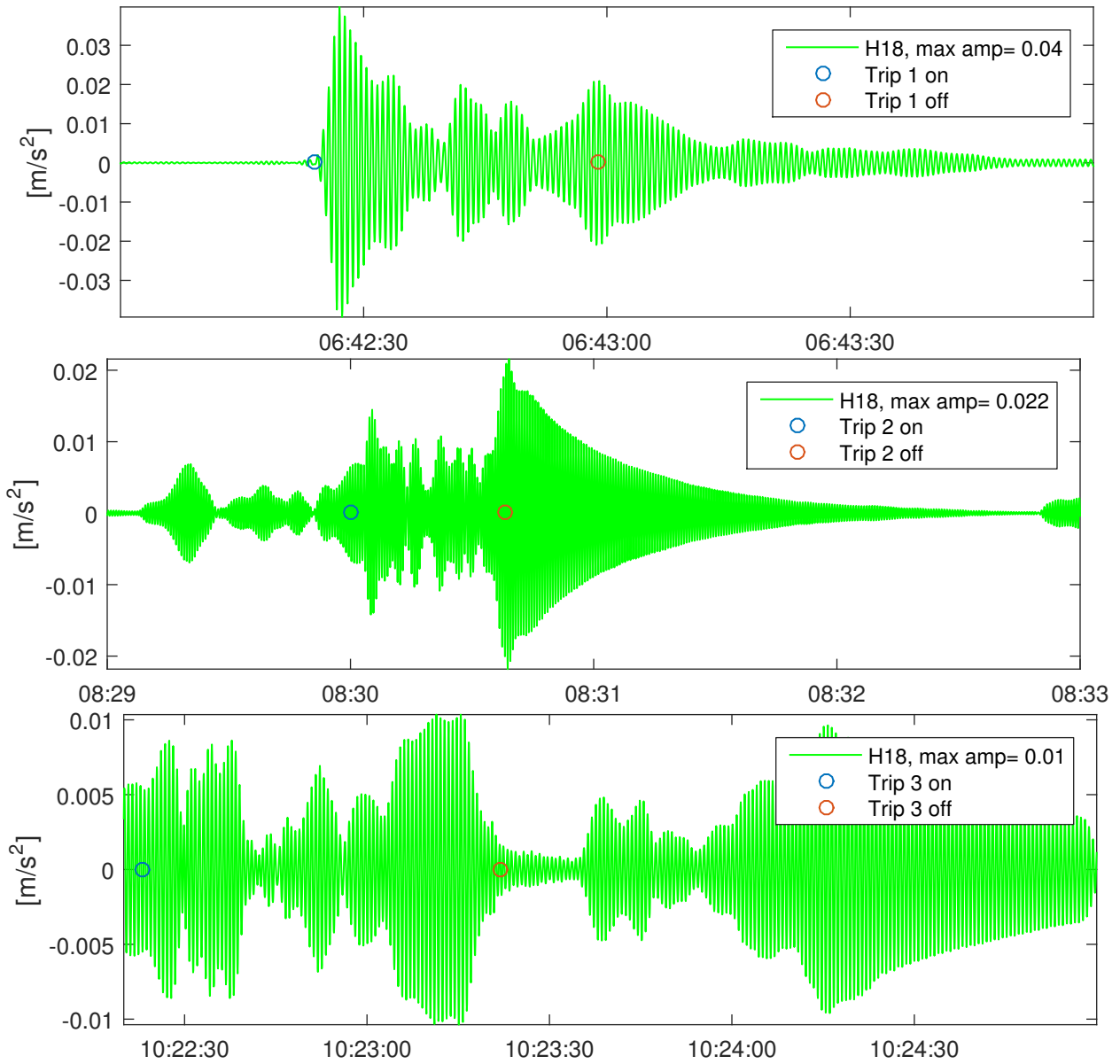
Filtered response VS3 for trip 1(top), trip 2 (middle) and trip 3 (bottom)

VA3 - sensor H9



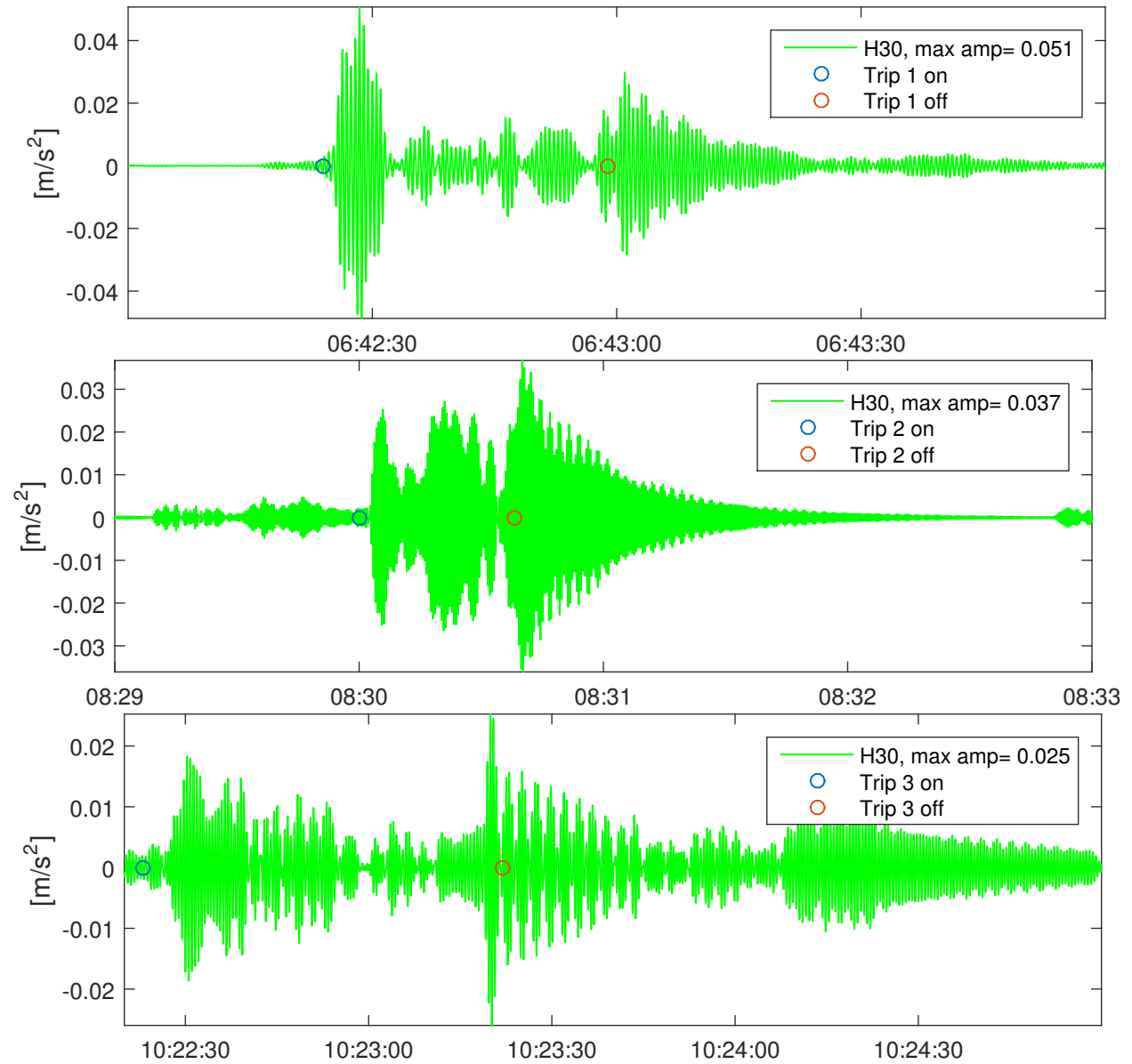
Filtered response VA3 for trip 1(top), trip 2 (middle) and trip 3 (bottom)

1,5Hz - sensor H18



Filtered response 1,5Hz for trip 1(top), trip 2 (middle) and trip 3 (bottom)

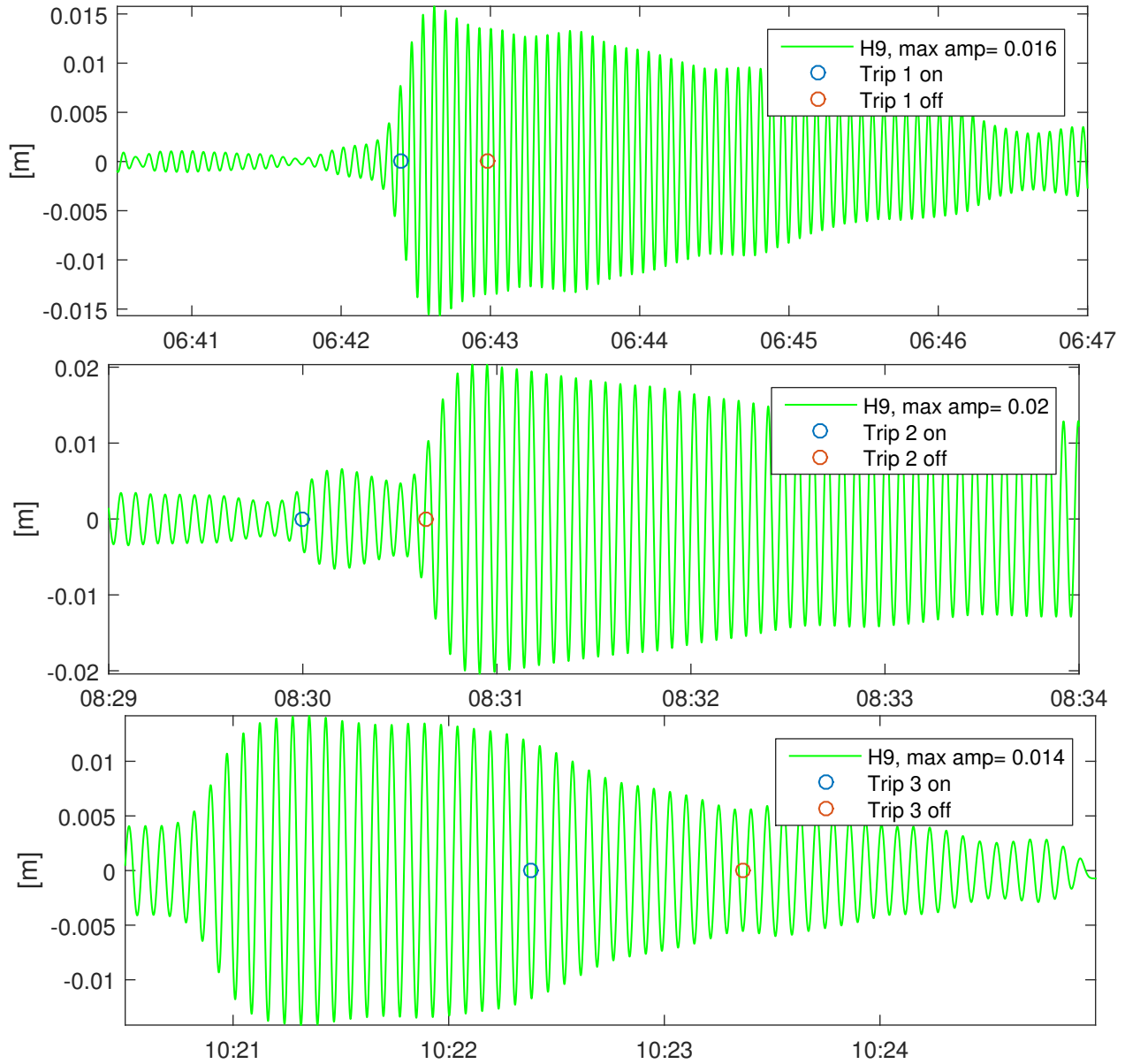
1,91Hz - sensor H30



Filtered response 1,91Hz for trip 1(top), trip 2 (middle) and trip 3 (bottom)

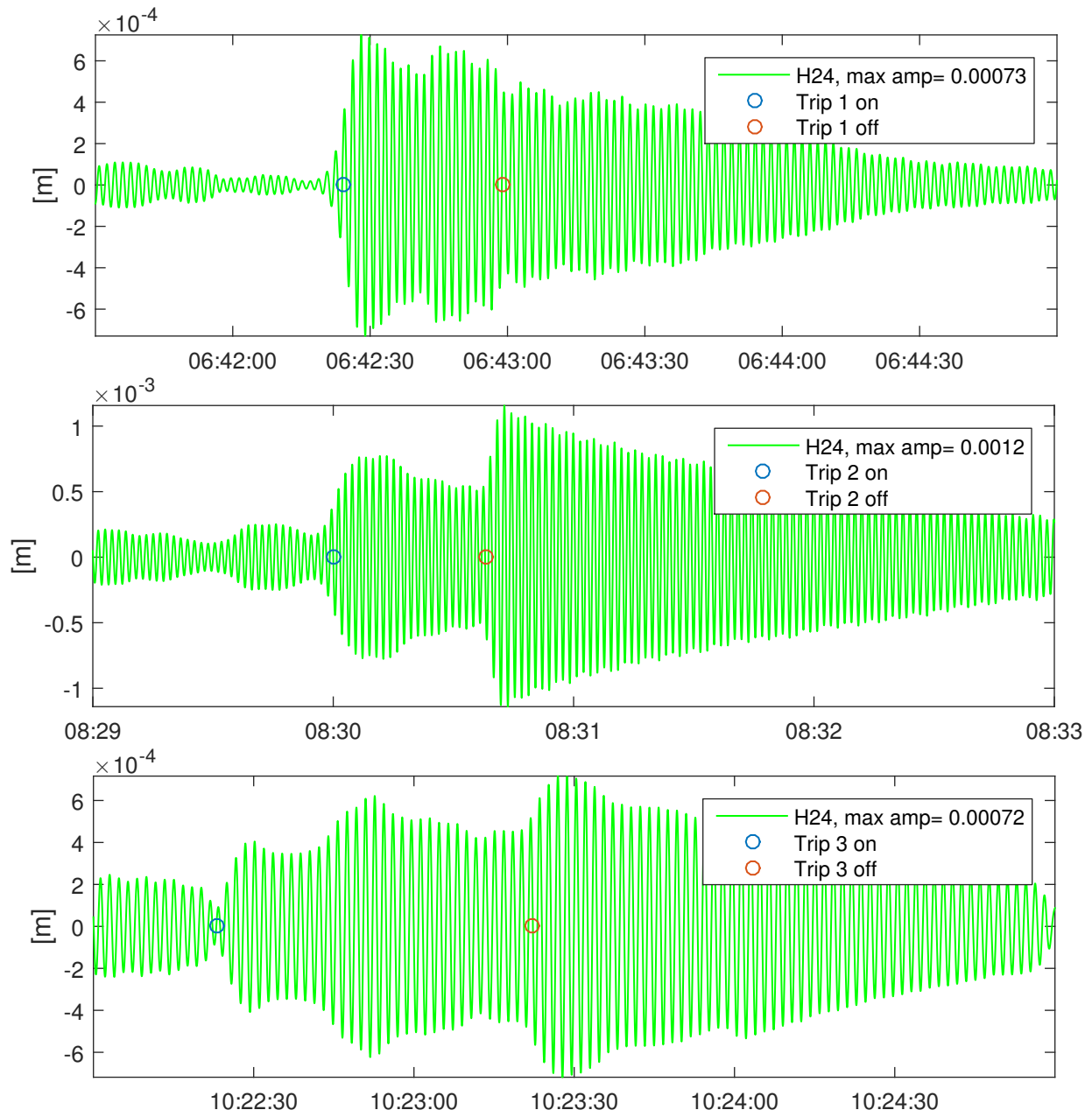
C.2 Impact Displacement Response

VA1 - sensor H9



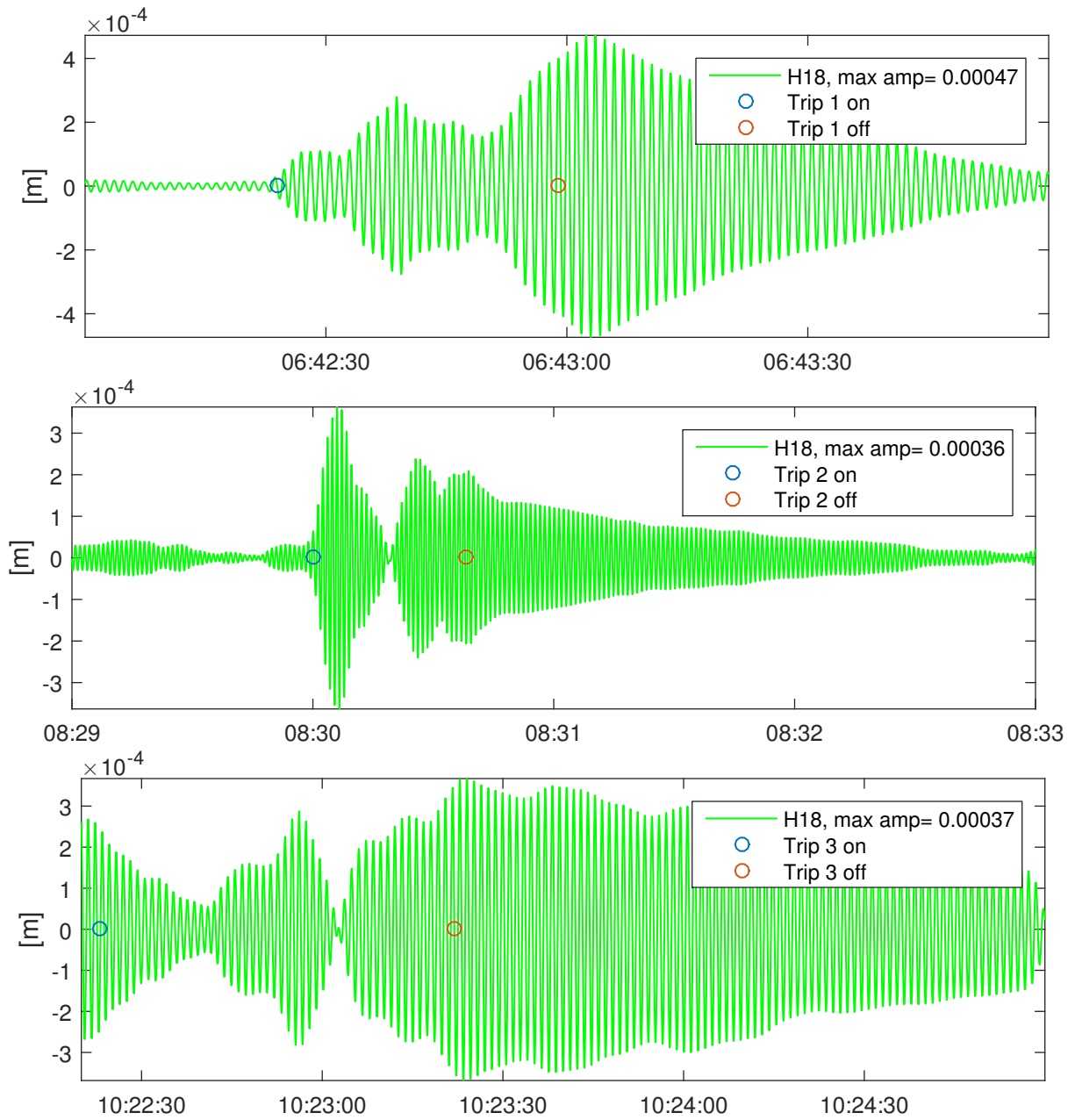
Filtered response VA1 for trip 1(top), trip 2 (middle) and trip 3 (bottom)

VA2 - sensor H24



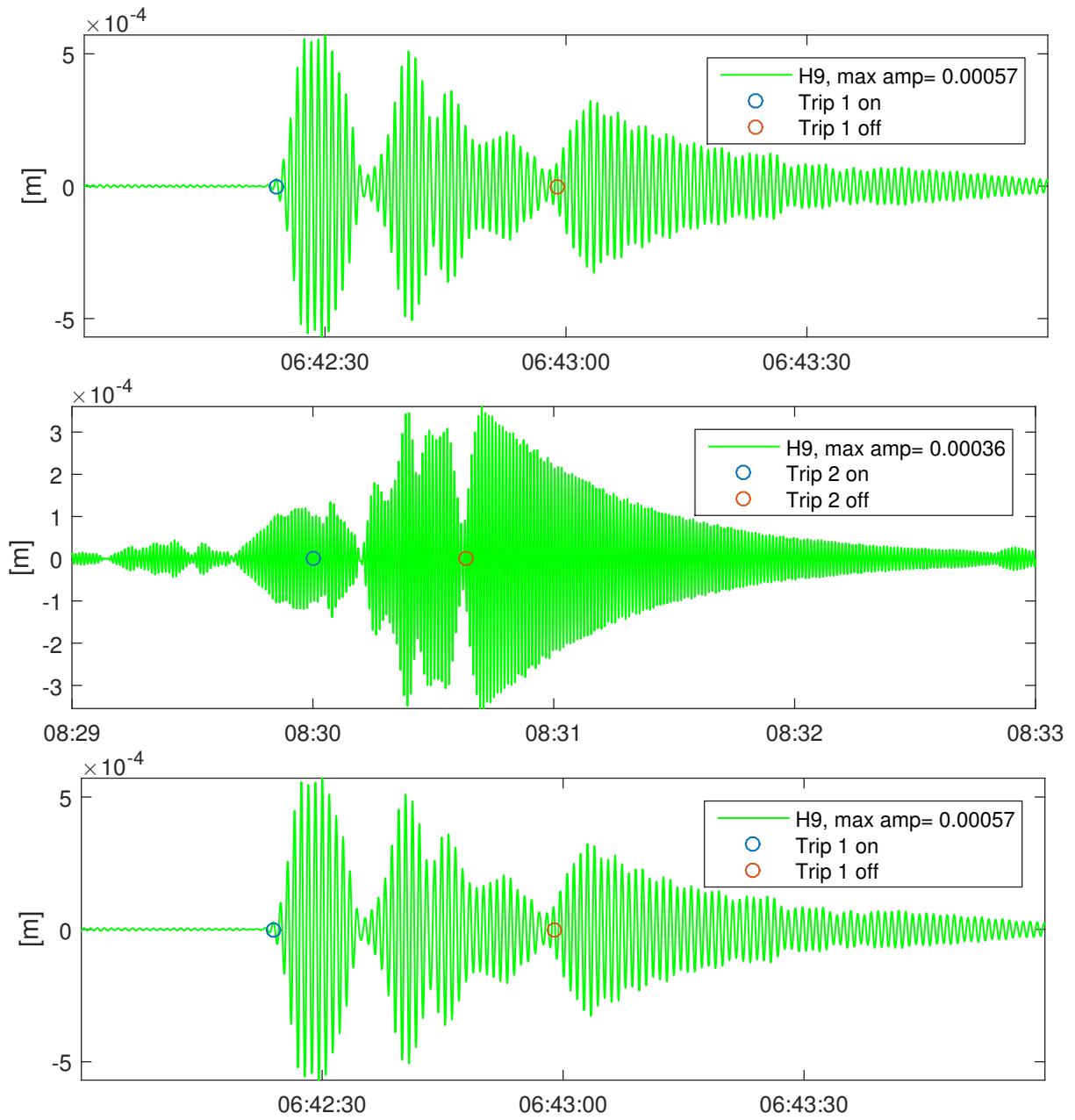
Filtered response VA2 for trip 1(top), trip 2 (middle) and trip 3 (bottom)

VS3 - sensor H18



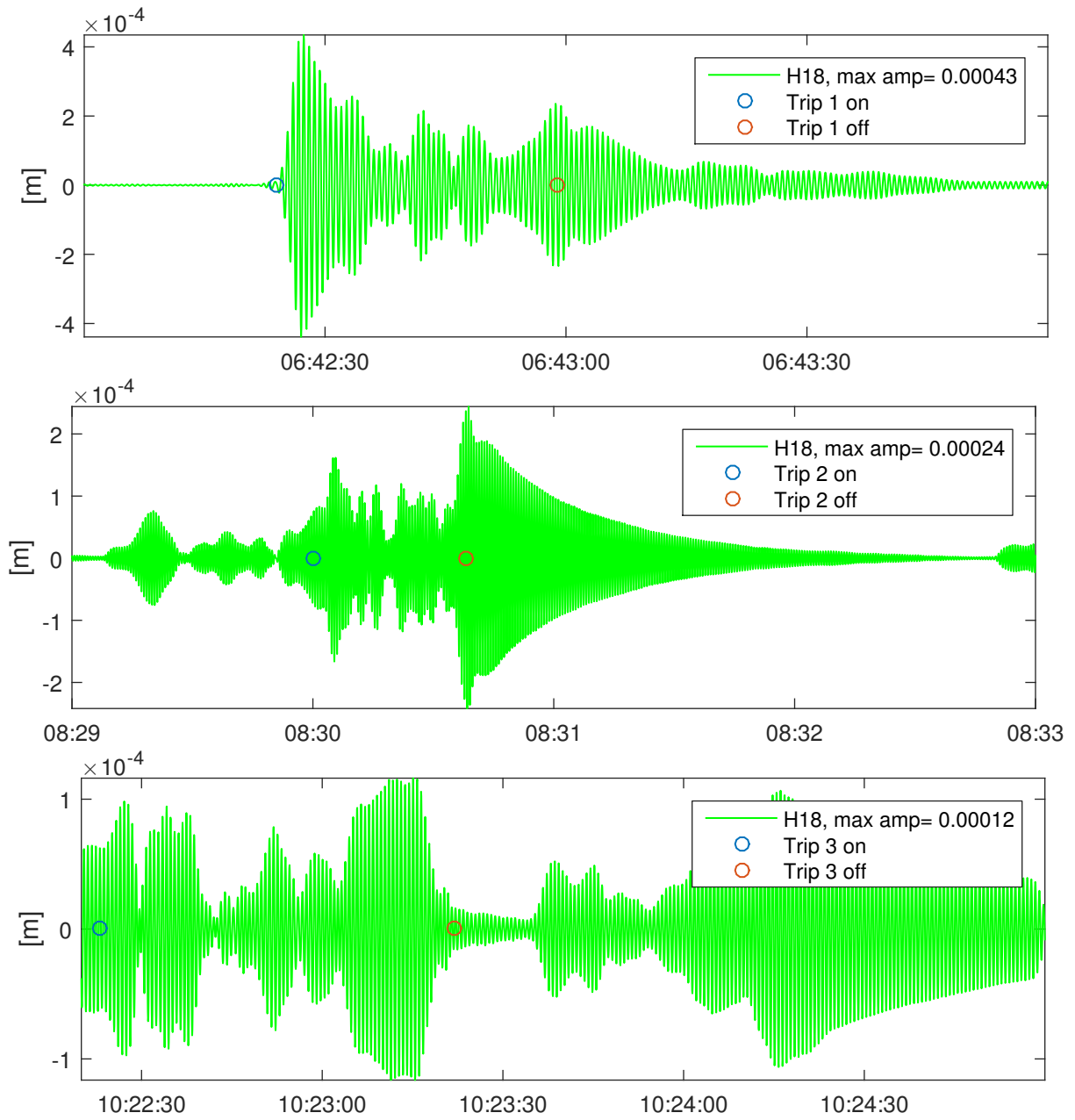
Filtered response VS3 for trip 1(top), trip 2 (middle) and trip 3 (bottom)

VA3 - sensor H9



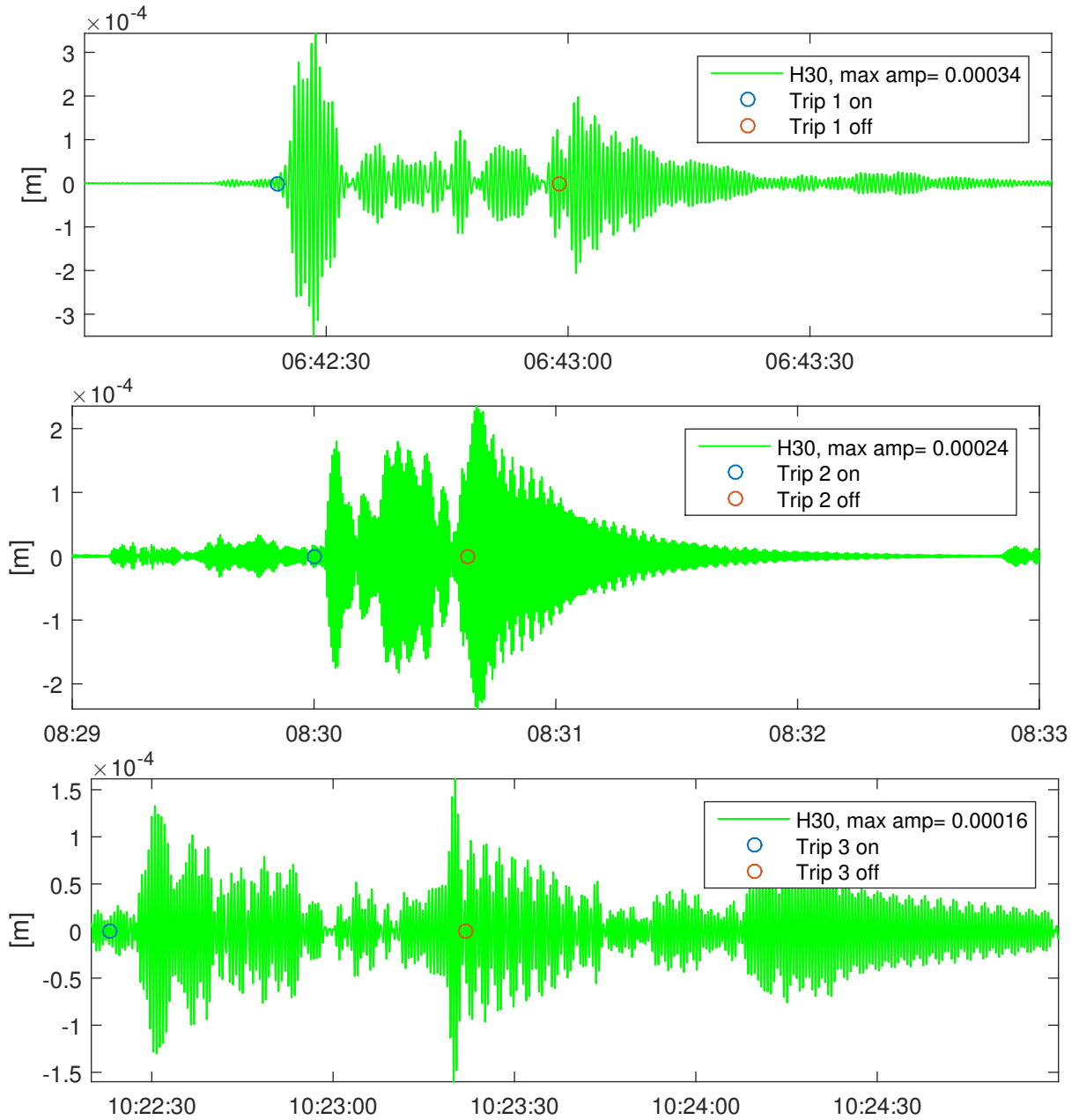
Filtered response VA3 for trip 1(top), trip 2 (middle) and trip 3 (bottom)

1,5Hz - sensor H18



Filtered response 1,5Hz for trip 1(top), trip 2 (middle) and trip 3 (bottom)

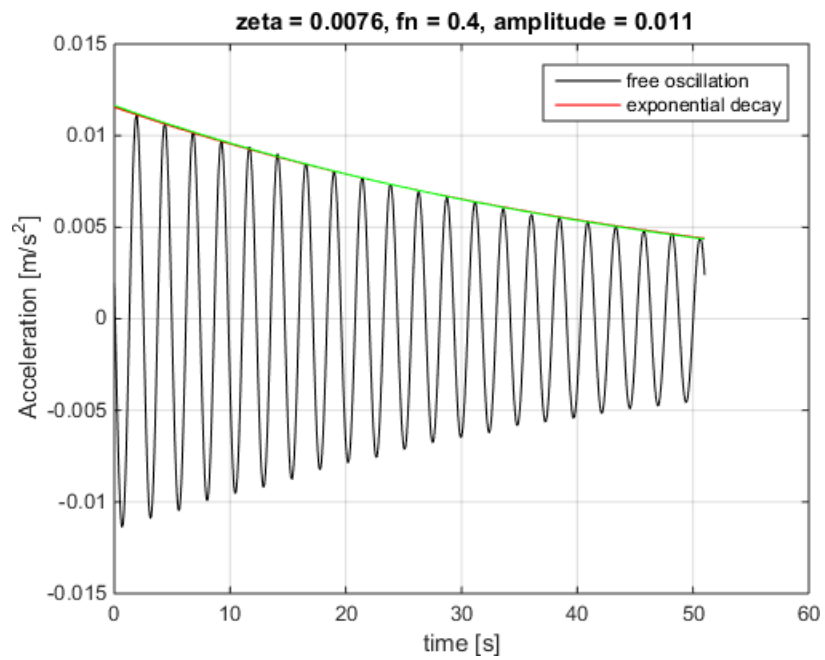
1,91Hz - sensor H30



Filtered response 1,91Hz for trip 1(top), trip 2 (middle) and trip 3 (bottom)

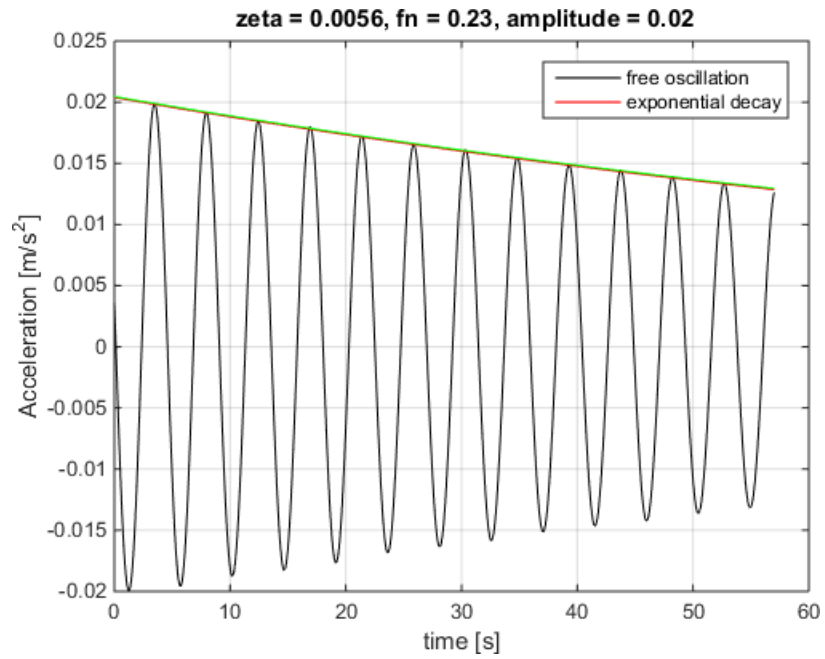
Appendix D

Damping Estimation Plots

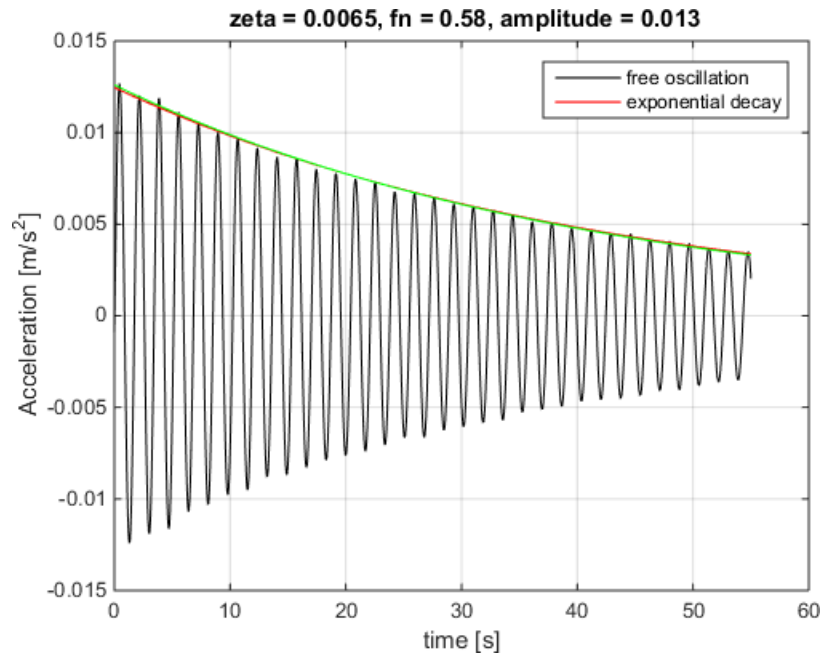


*

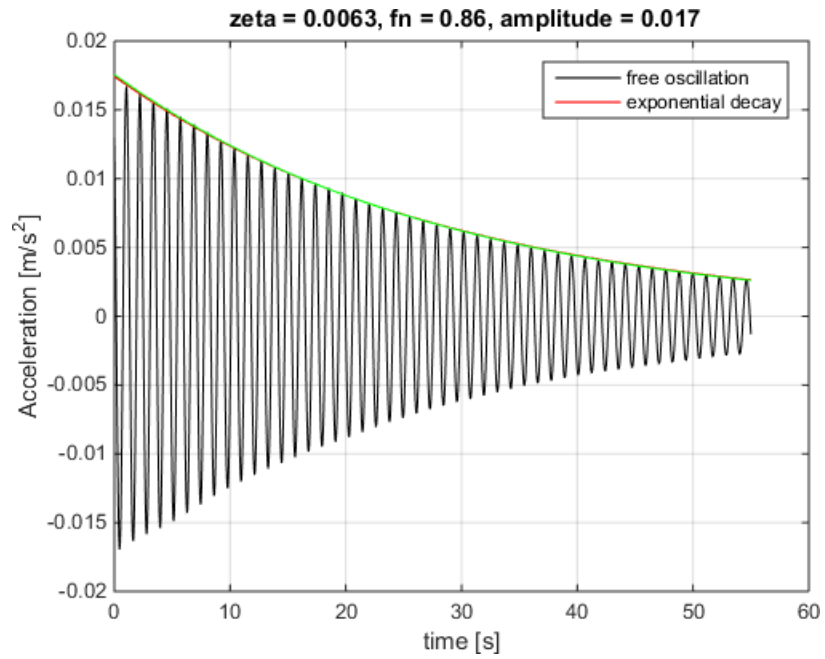
case 1, fn = 0.4, sensor 1



case 1, fn = 0.23, sensor 1

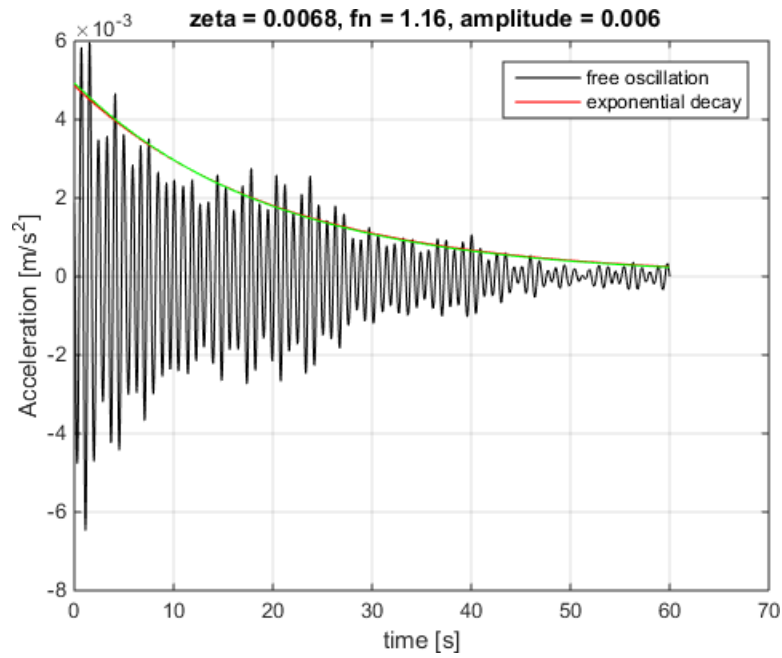


case 1, fn = 0.58, sensor 3



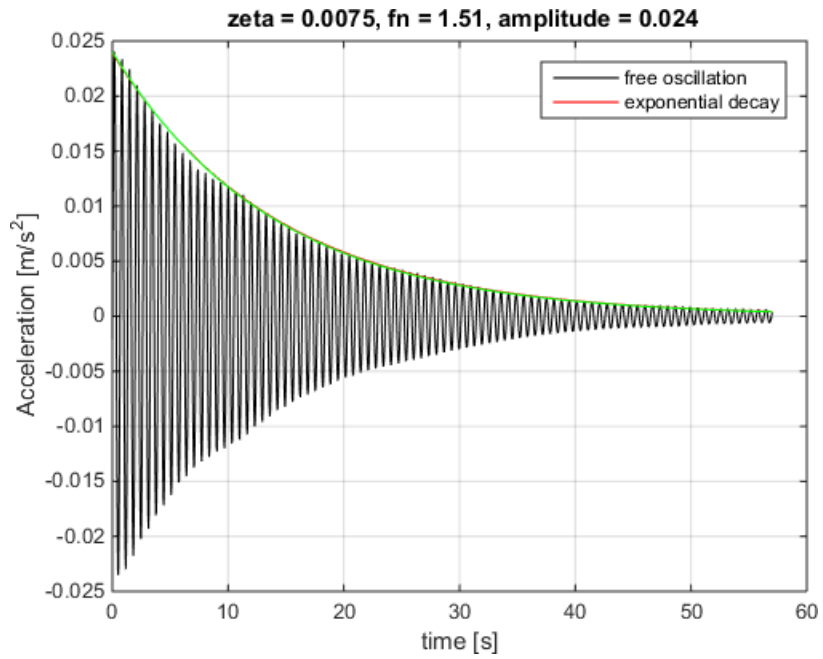
*

case 1, fn = 0.86, sensor 2



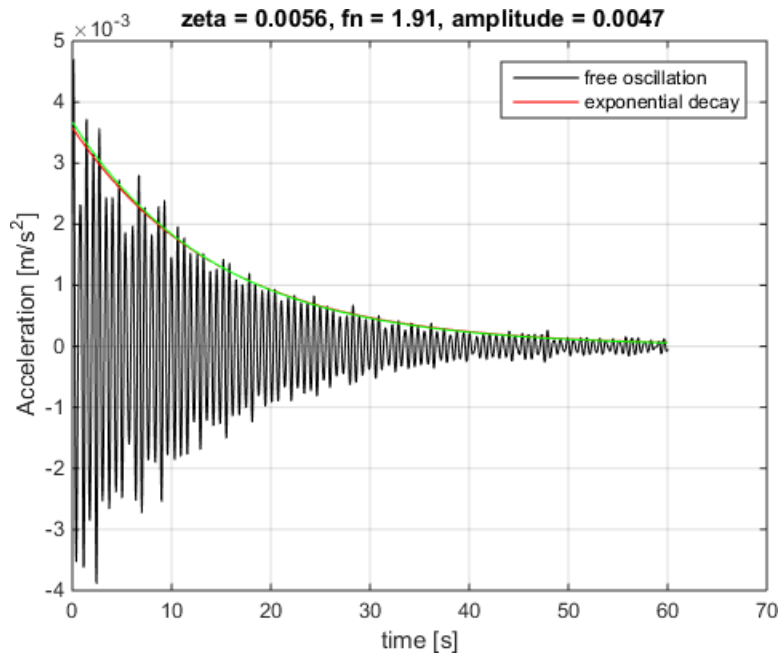
*

case 1, fn = 1.16



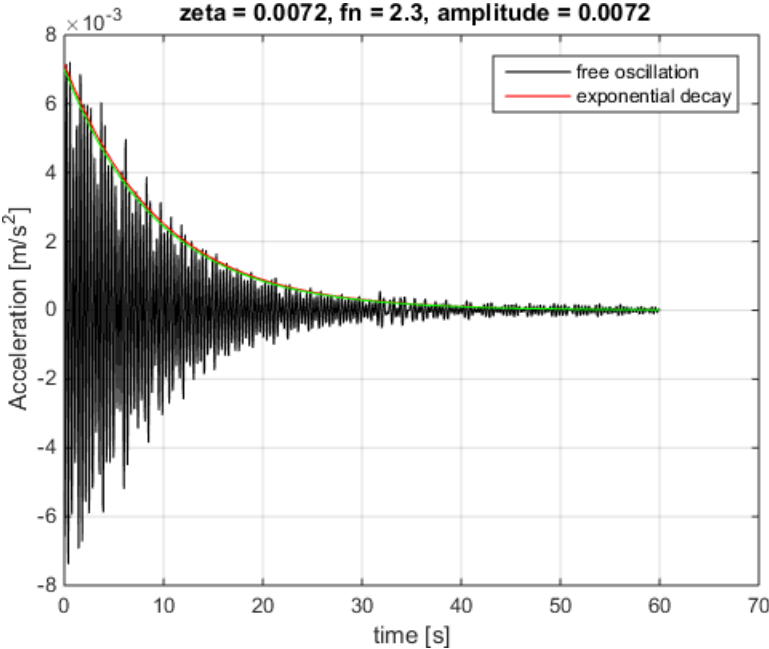
*

case 1, fn = 1.51, sensor 2

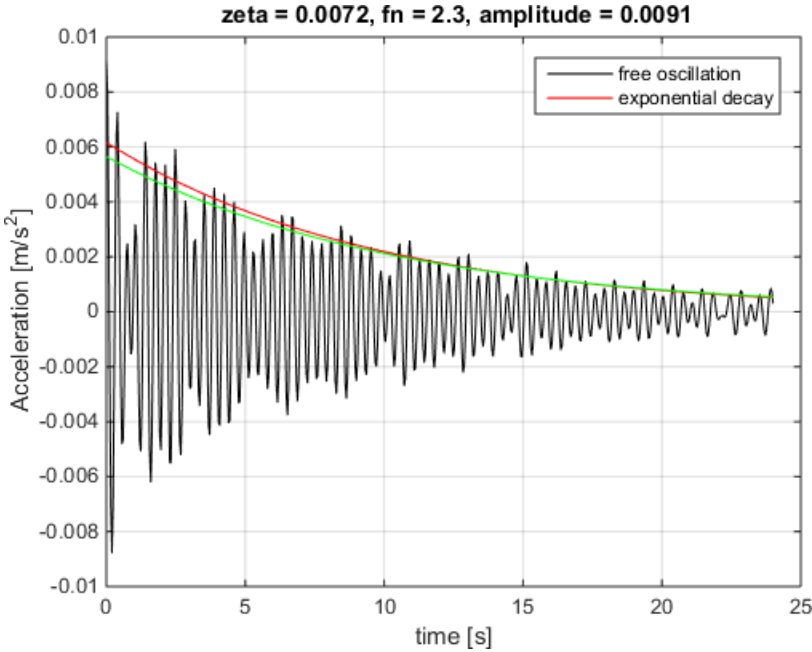


*

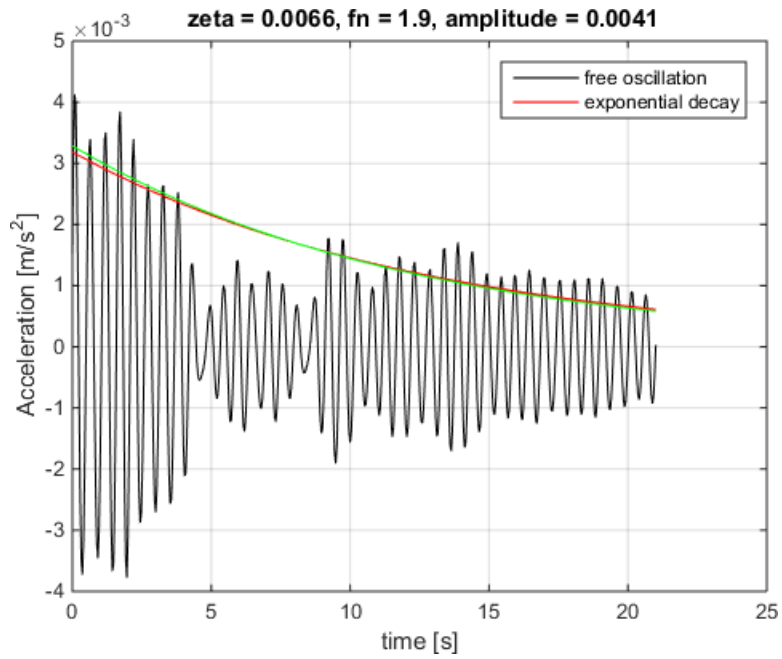
case 1, fn = 1.91



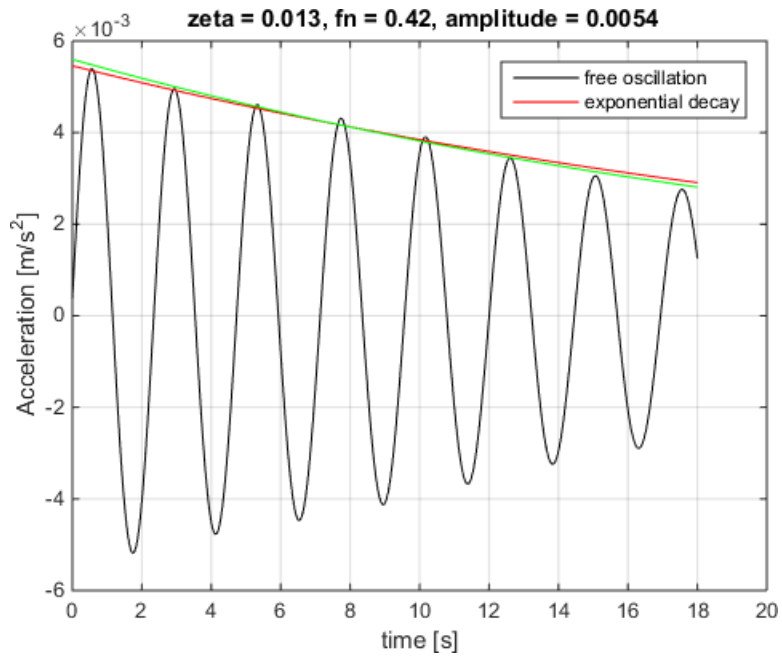
*
case 1, fn = 2.3



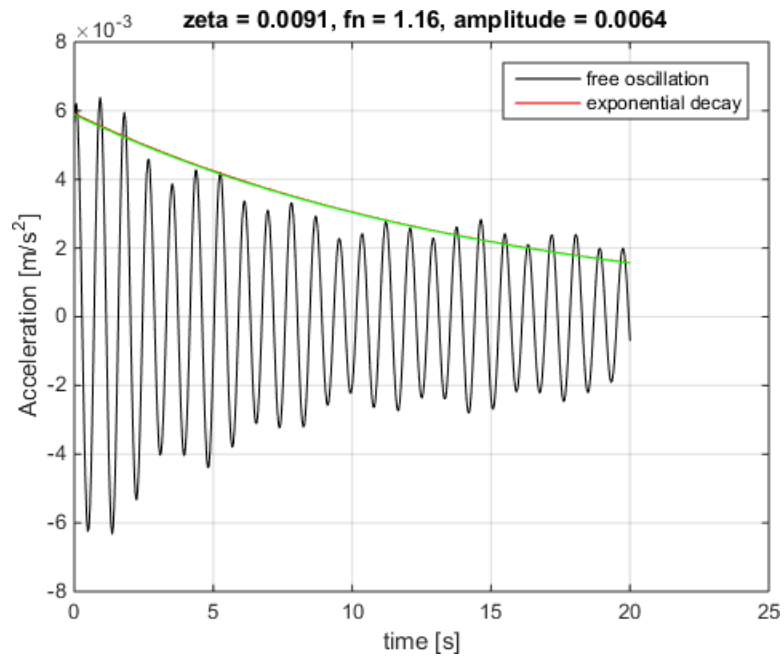
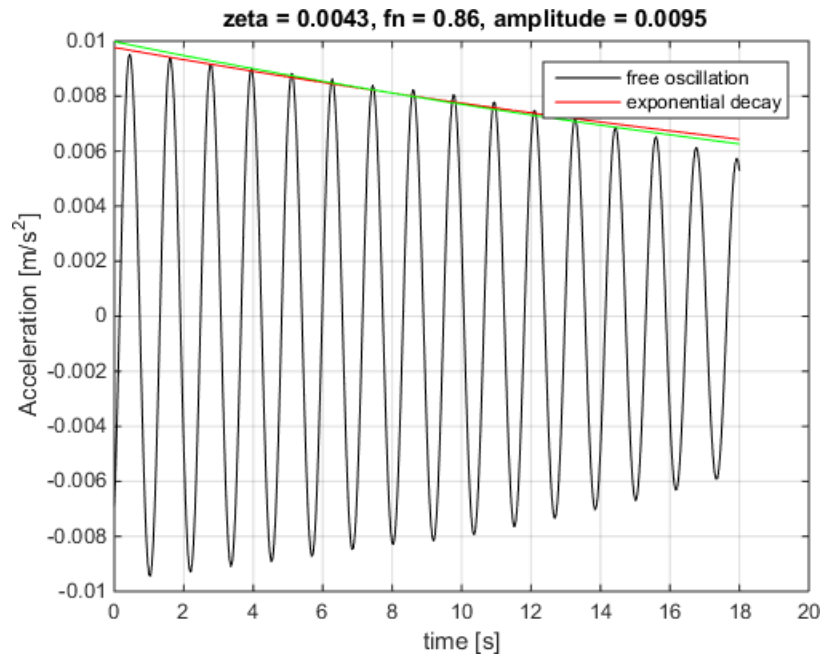
*
case 2, fn = 2.3

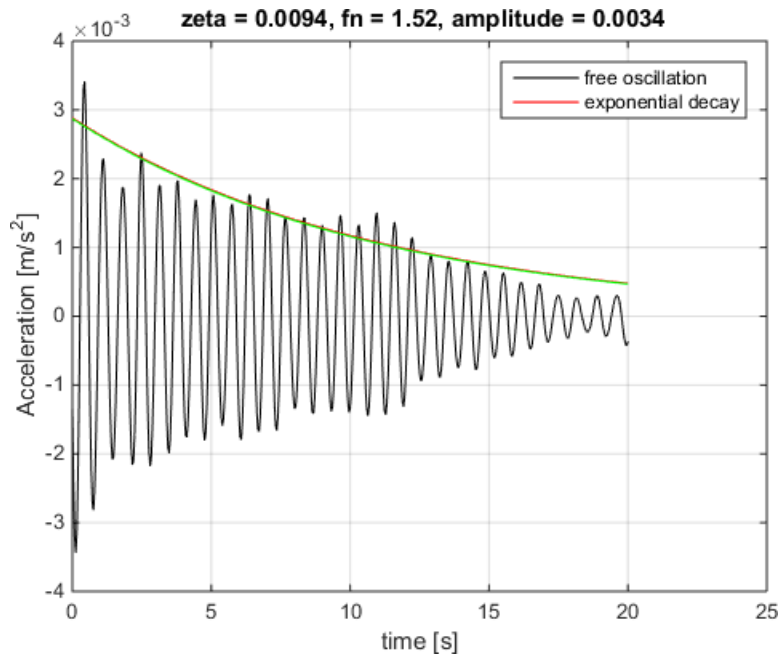


case 2, fn = 1.9

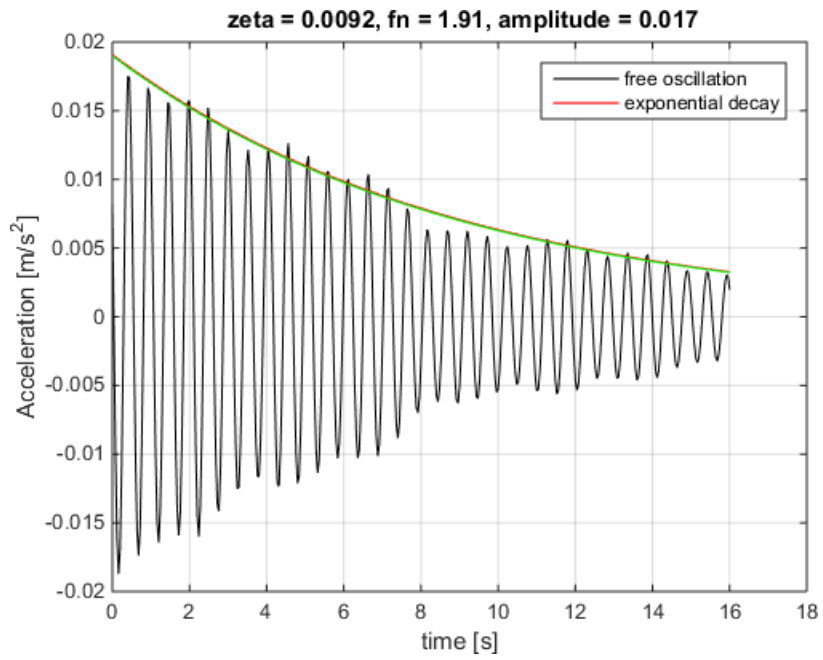


case 3, fn = 0.42

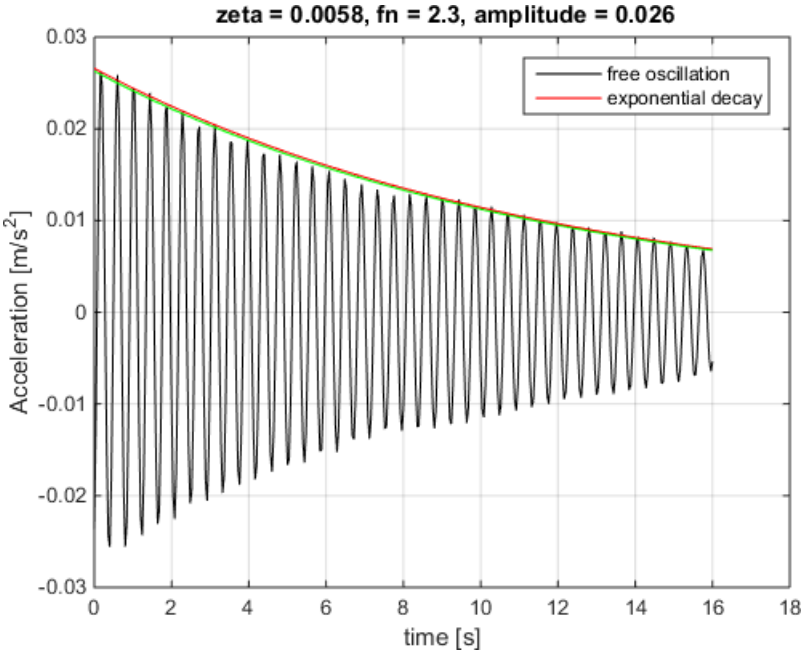




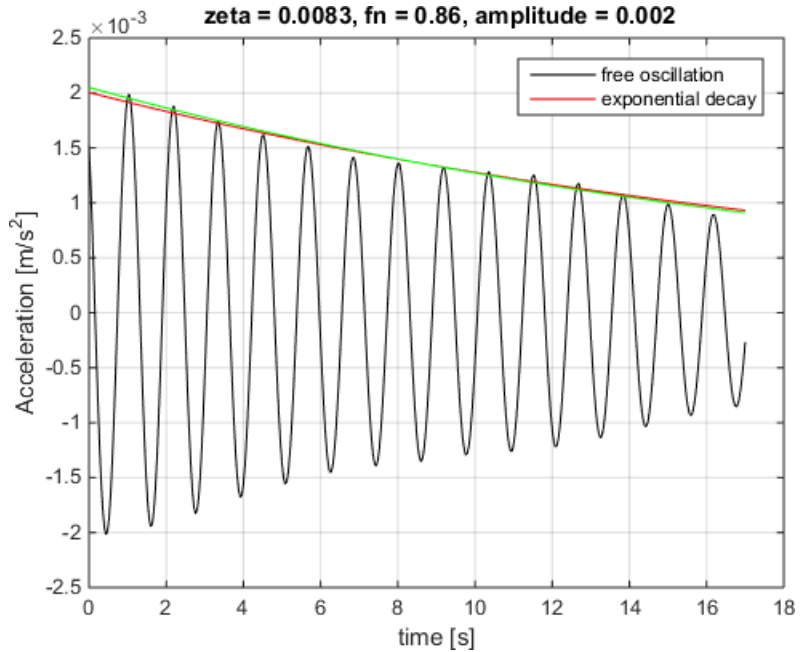
case 3, $f_n = 1.52$



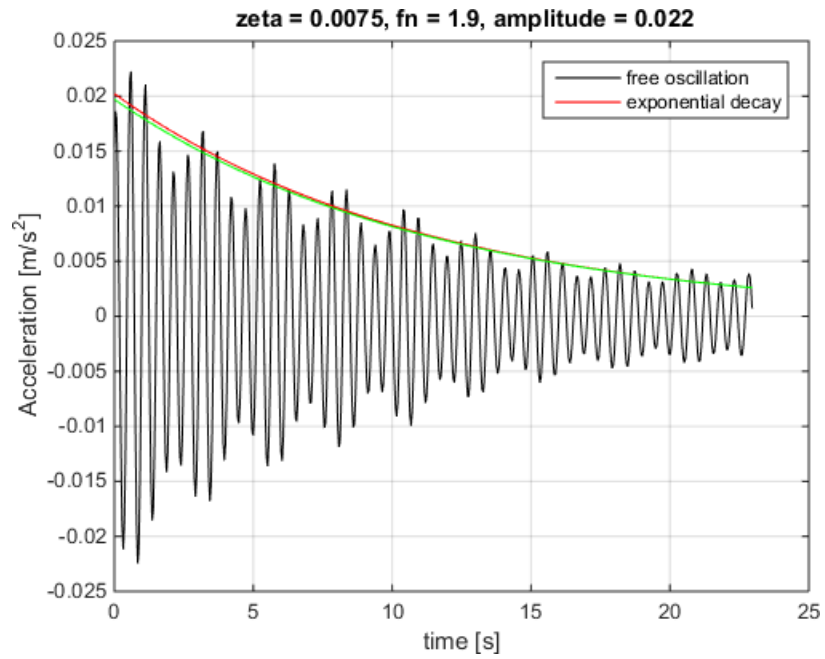
case 3, $f_n = 1.91$



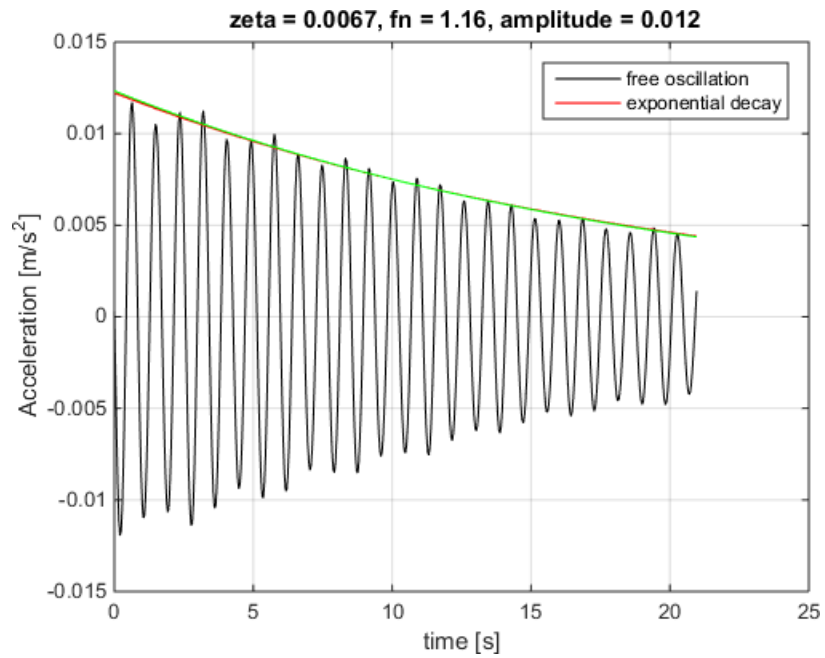
case 3, fn = 2.3



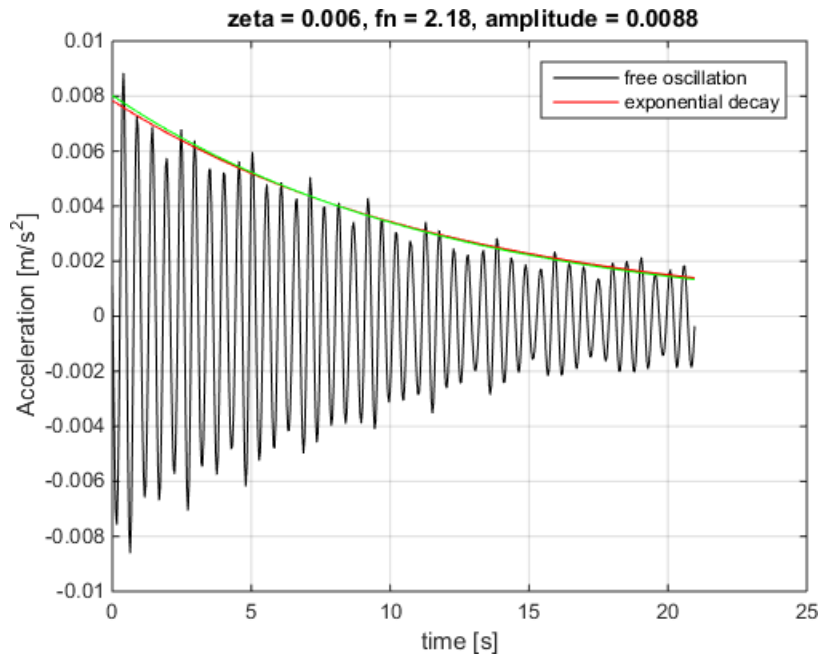
case 6, fn = 0.86, sensor 2



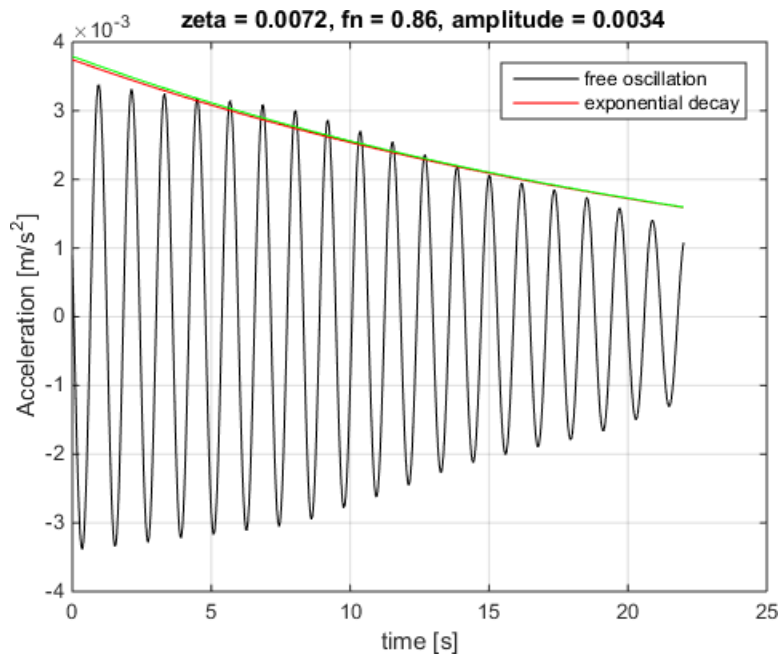
case 6, fn = 1.9, sensor 4



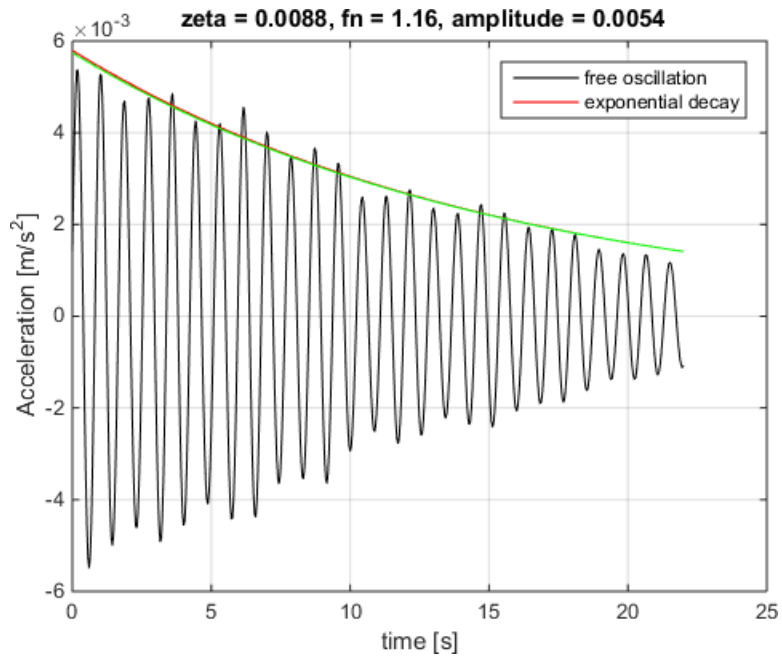
case 6, fn = 1.16, sensor 1



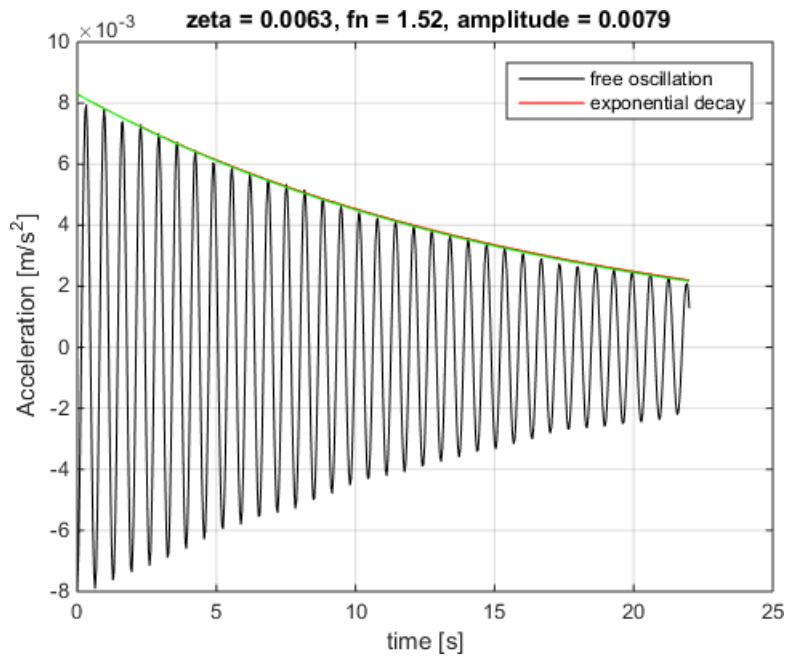
case 6, fn = 2.18, sensor 3



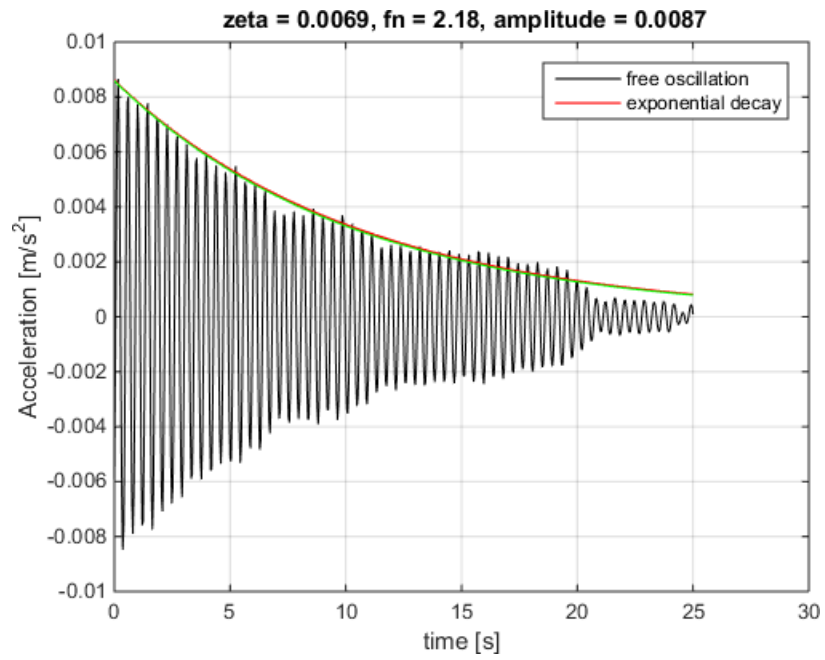
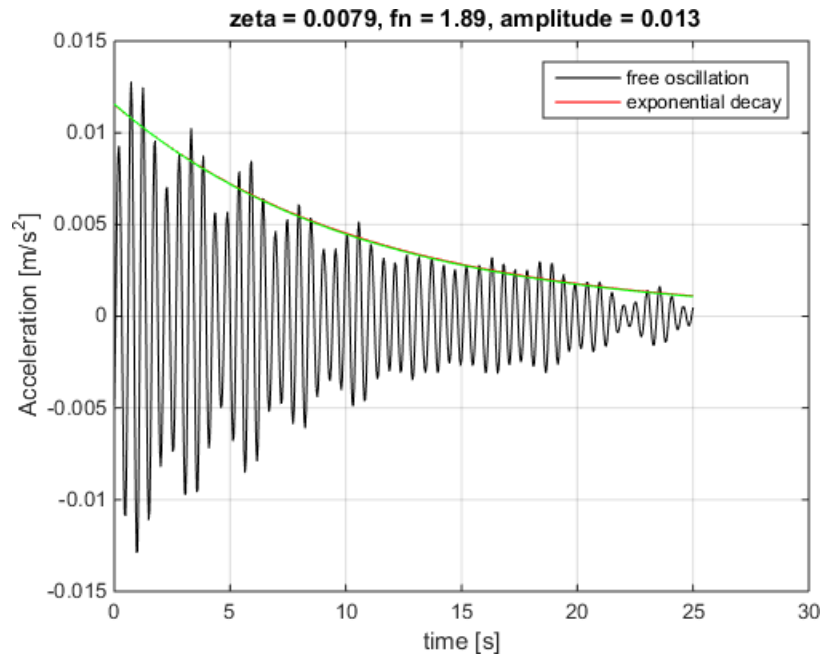
case 8, fn = 0.86, sensor 2

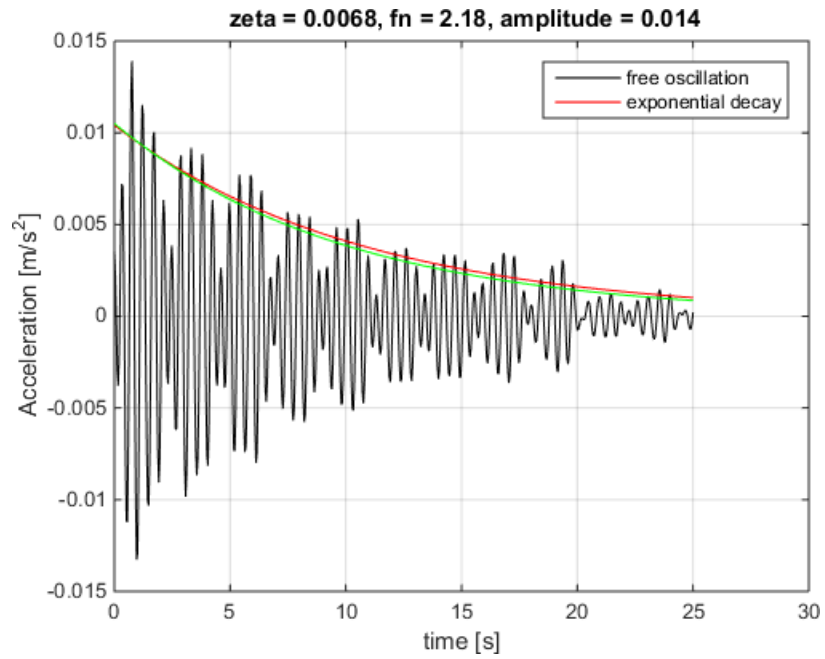


case 8, fn = 1.16, sensor 1

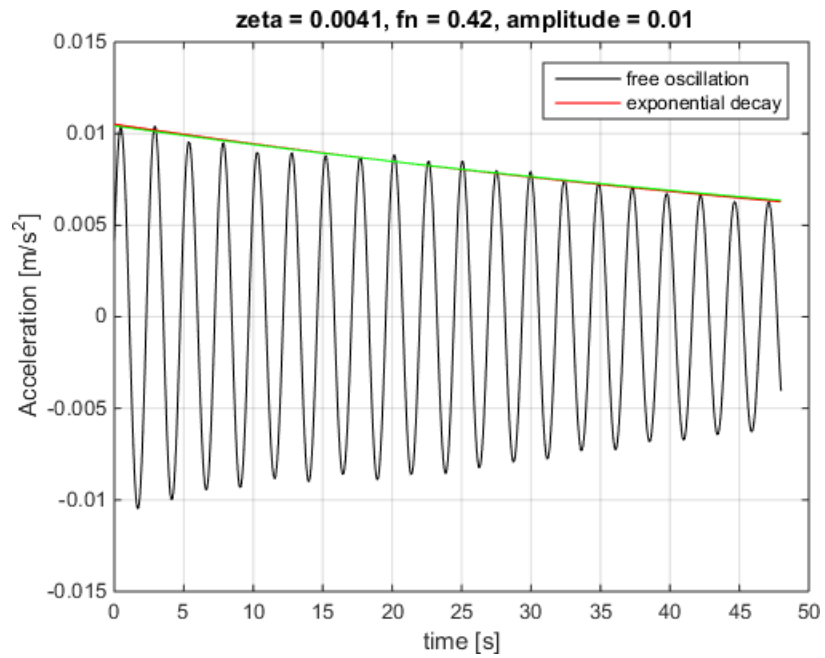


case 8, fn = 1.52, sensor 2

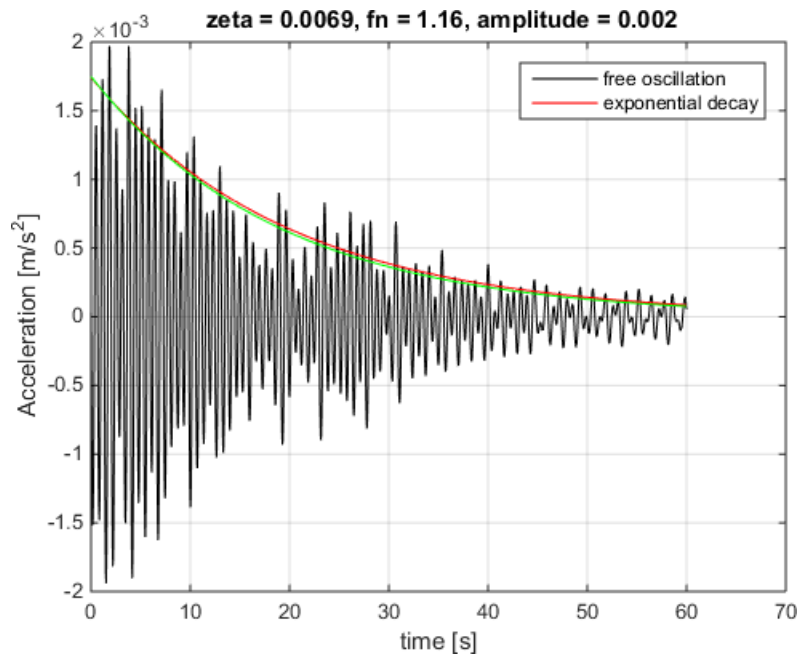
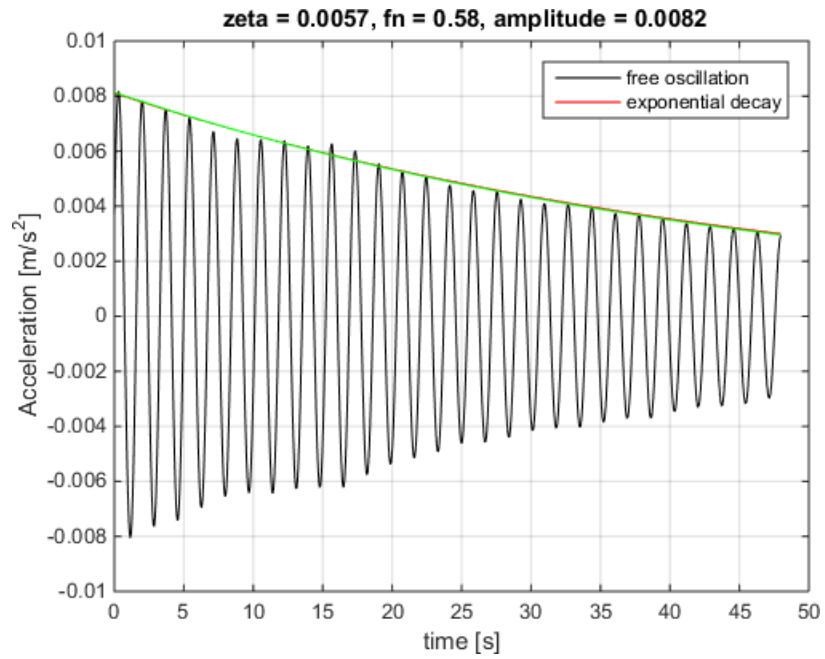


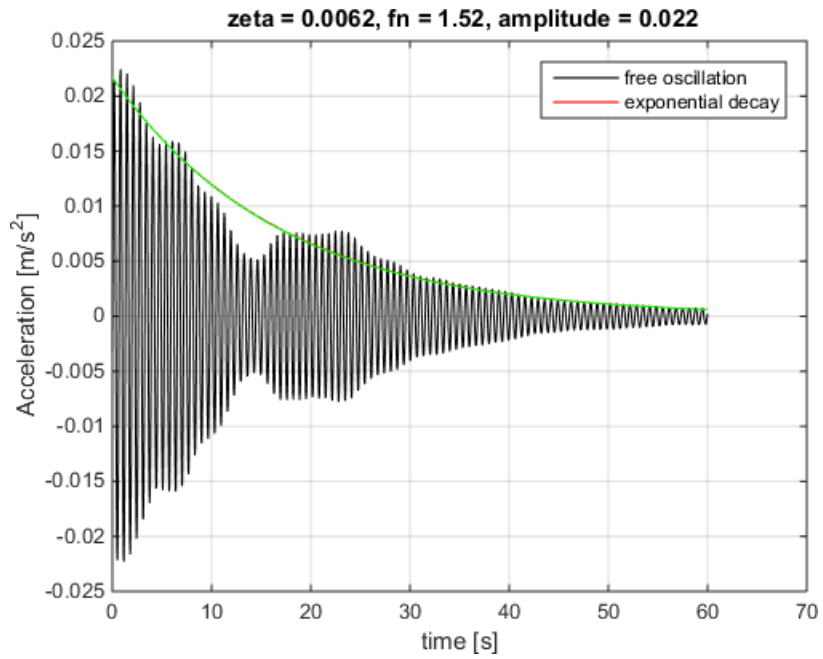


case 8, fn = 2.18, sensor 4

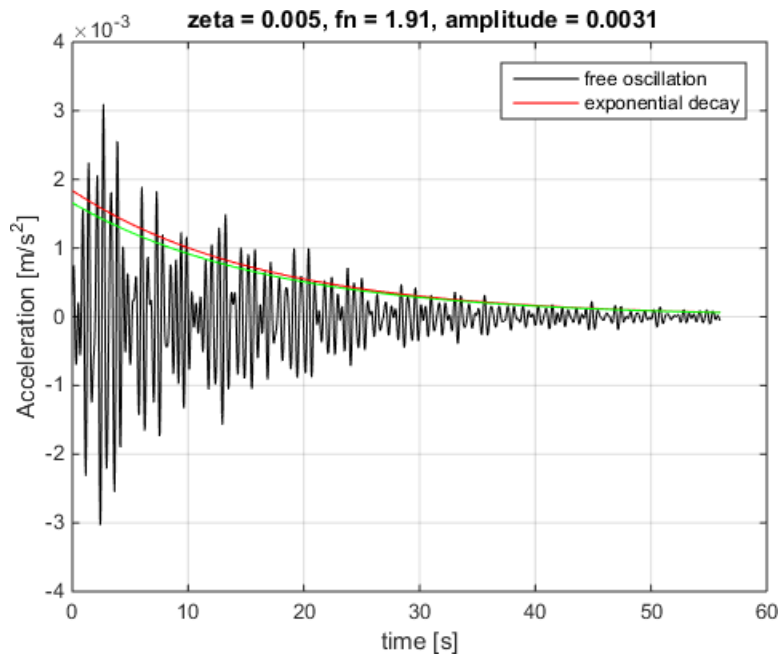


case 10, fn = 0.42, sensor 4

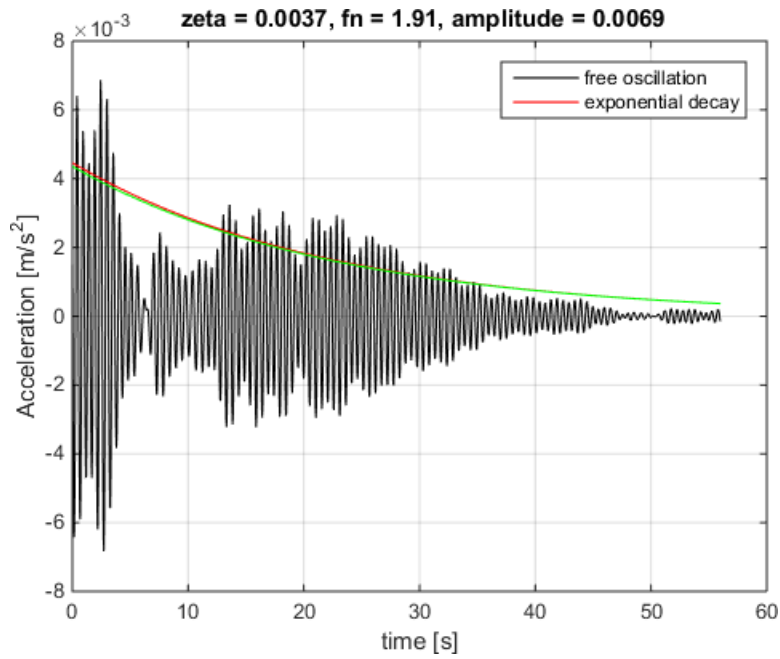




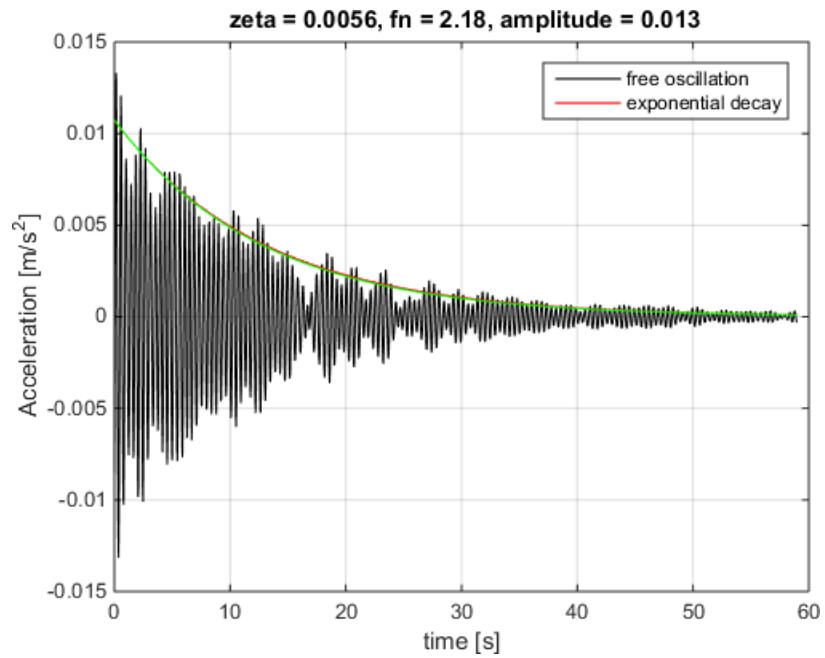
case 10, fn = 1.52, sensor 2



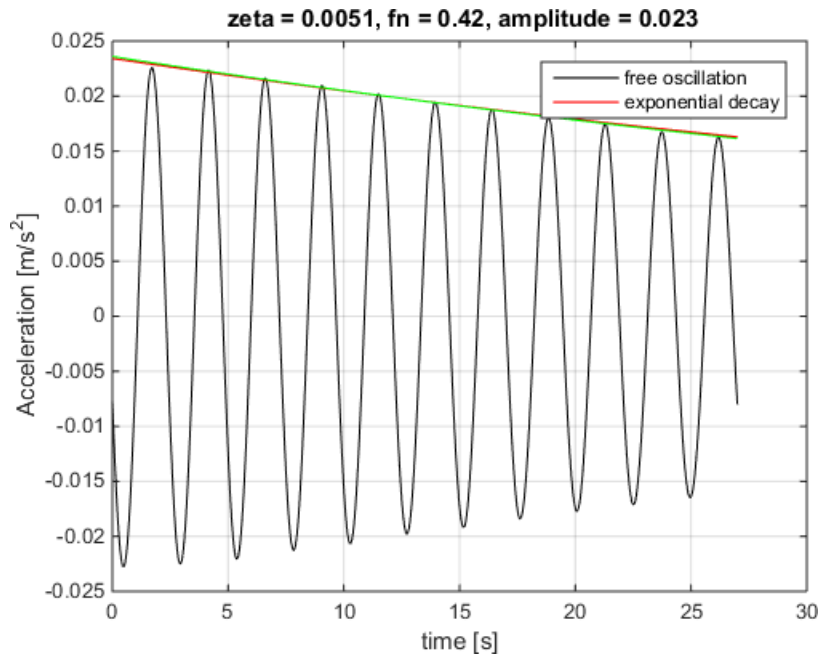
case 10, fn = 1.91, sensor 2



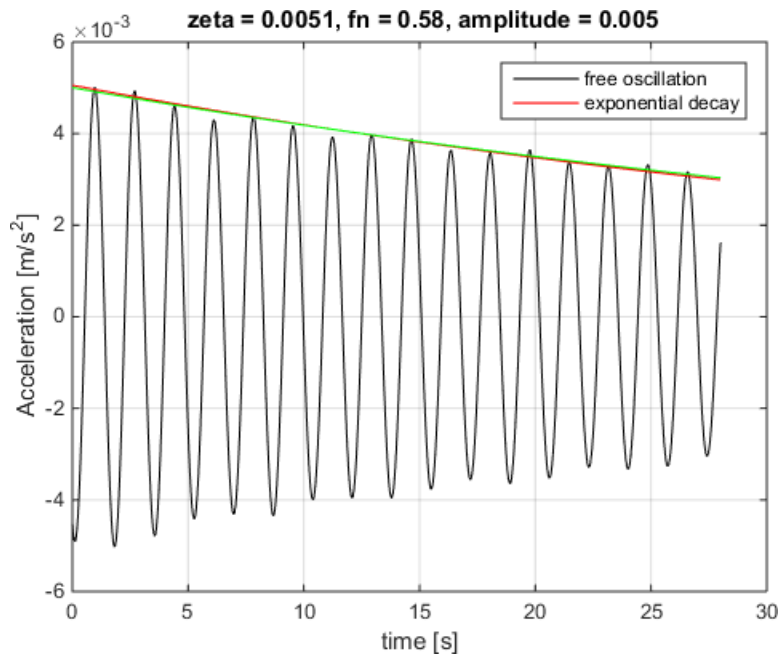
case 10, fn = 1.91, sensor 3



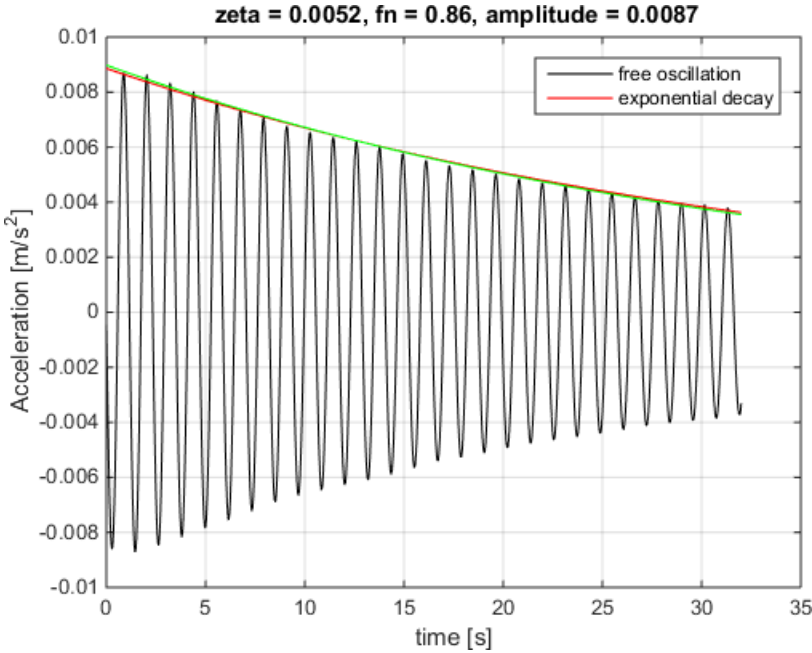
case 10, fn = 2.18, sensor 1



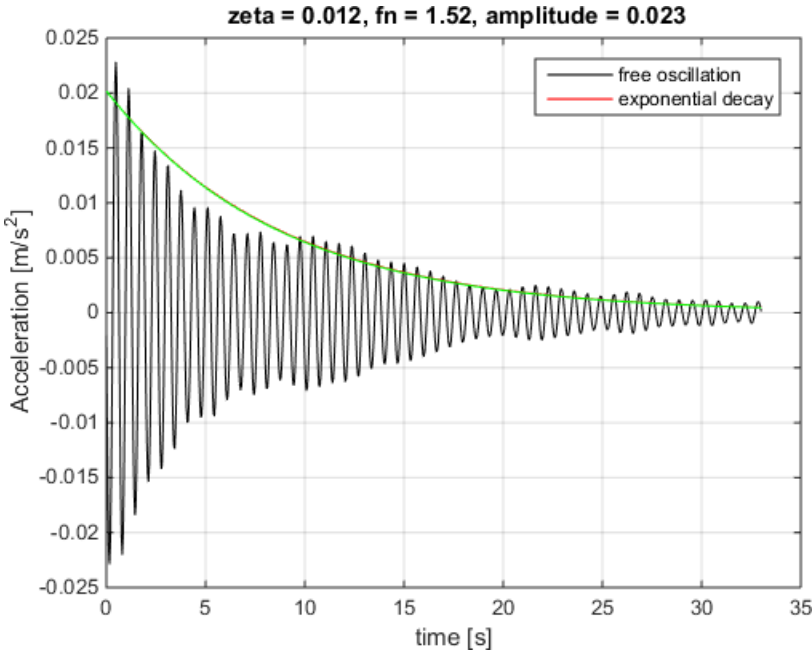
case 11, fn = 0.42, sensor 4



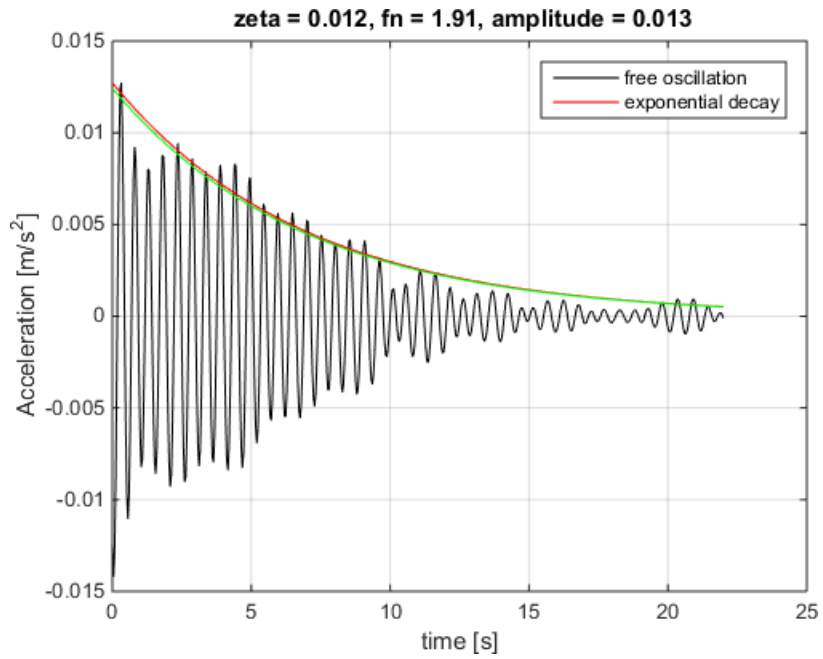
case 11, fn = 0.58, sensor 3



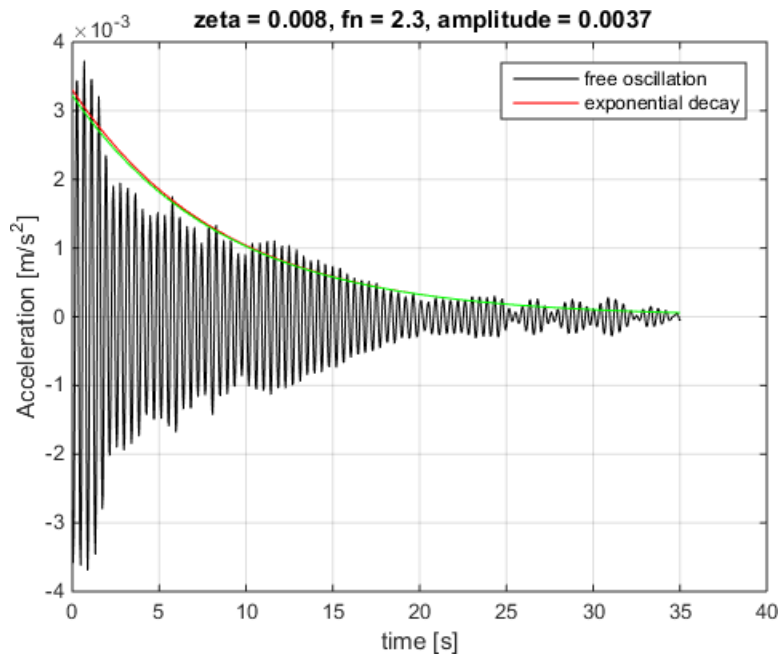
case 11, fn = 0.86, sensor 2



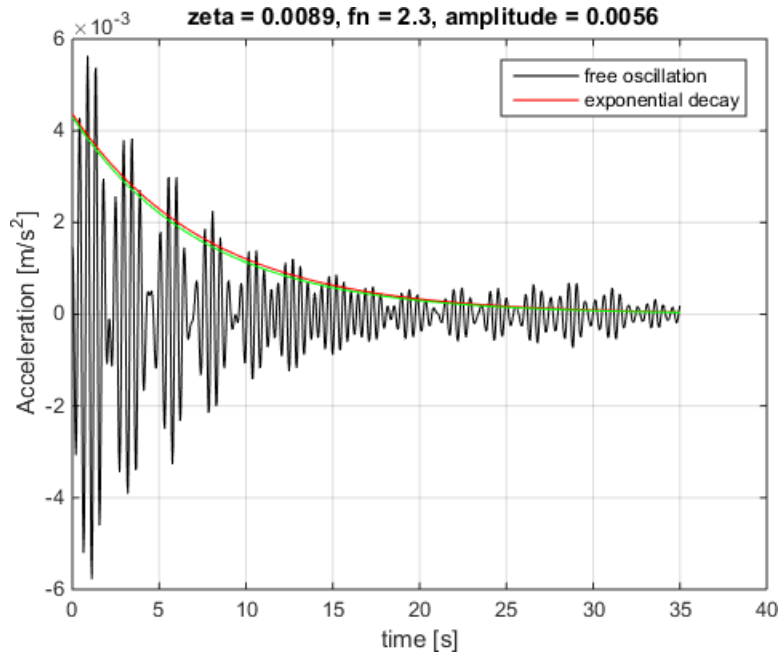
case 11, fn = 1.52, sensor 3



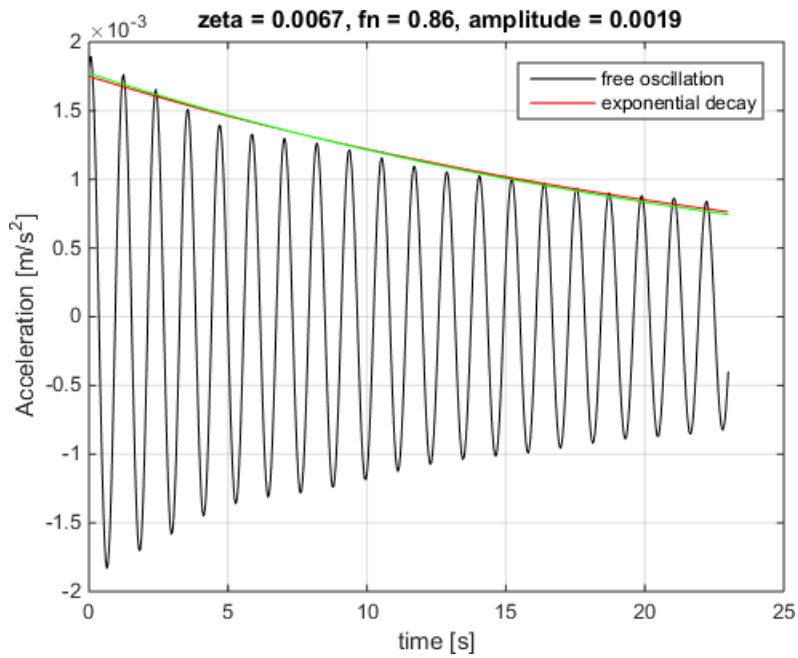
case 11, fn = 1.91, sensor 4



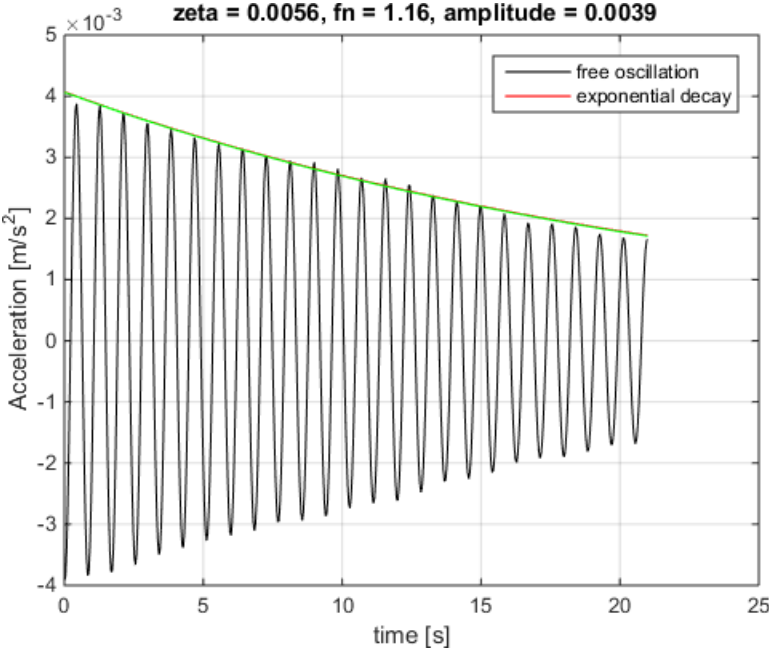
case 11, fn = 2.3, sensor 2



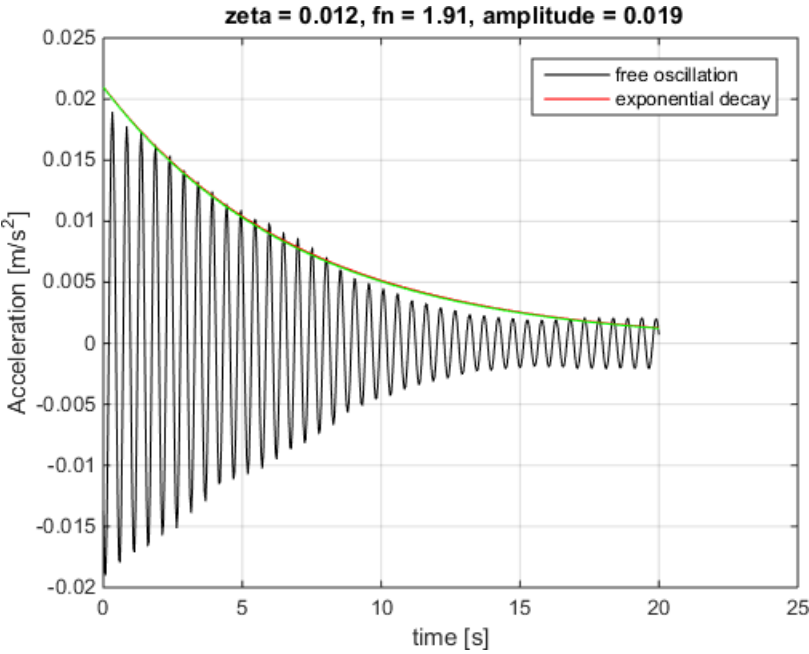
case 11, fn = 2.3, sensor 4



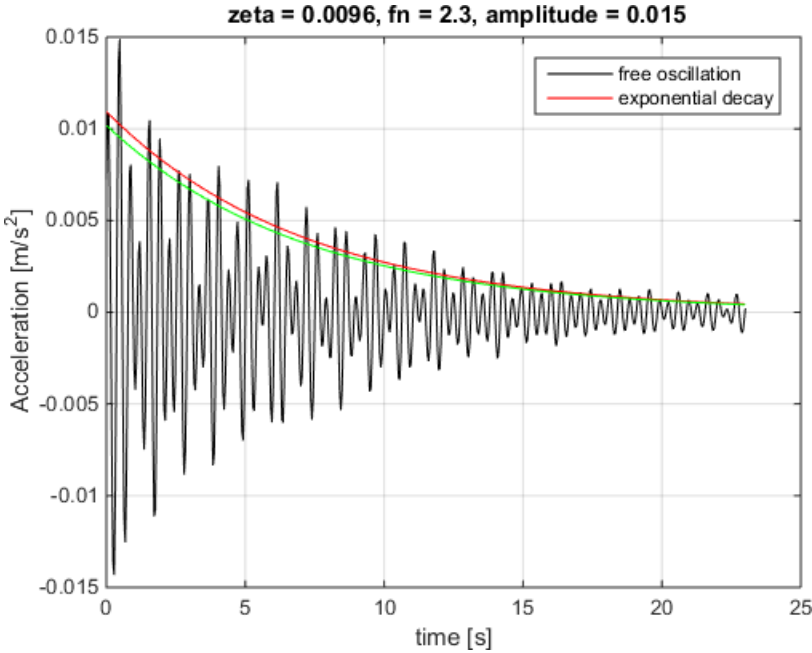
case 12, fn = 0.86, sensor 2



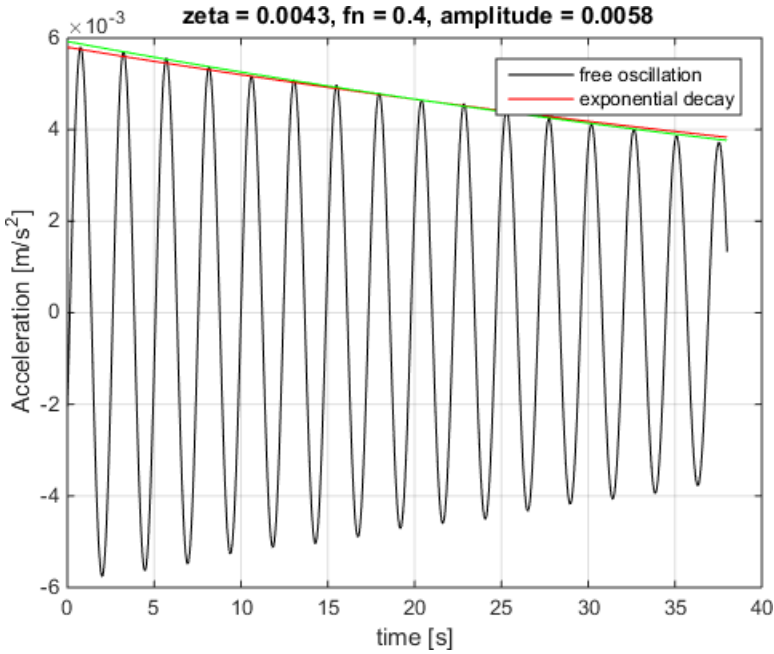
case 12, fn = 1.16, sensor 1



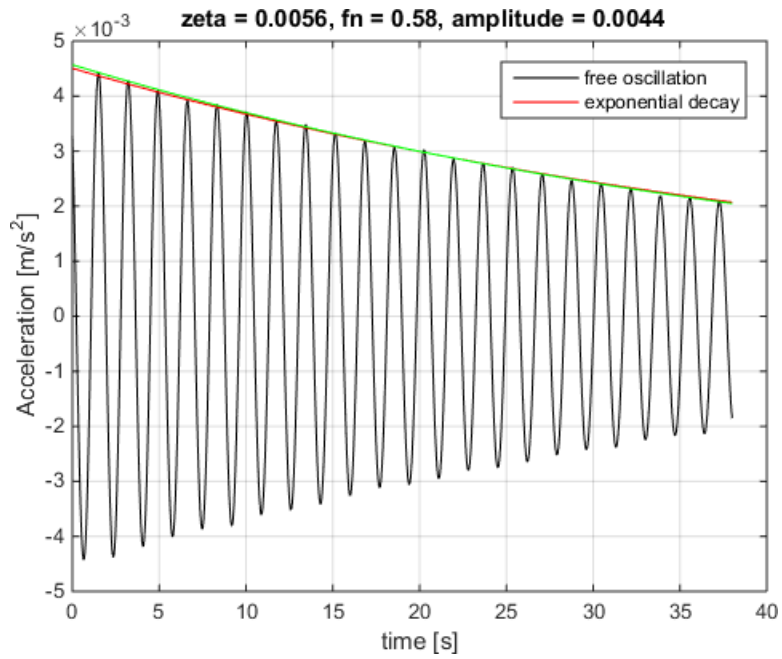
case 12, fn = 1.91, sensor 4



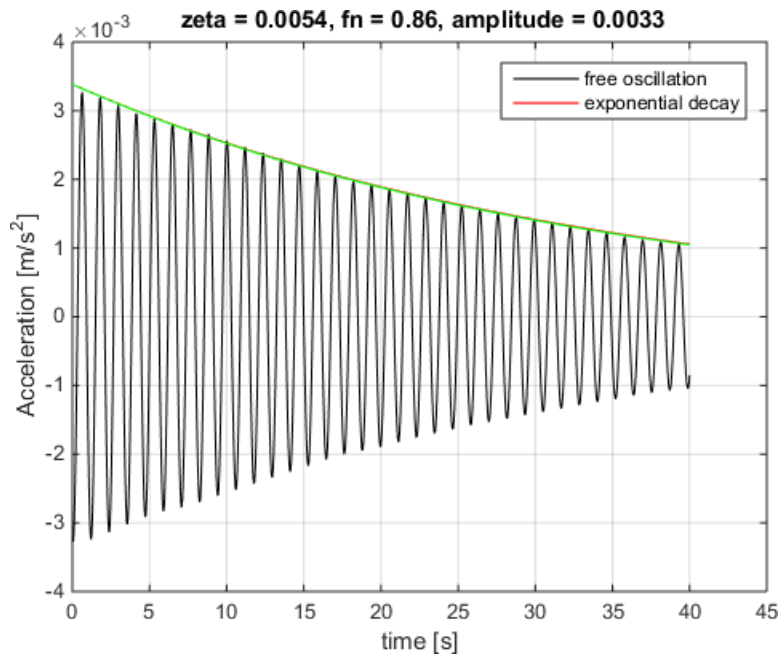
case 12, fn = 2.3, sensor 3



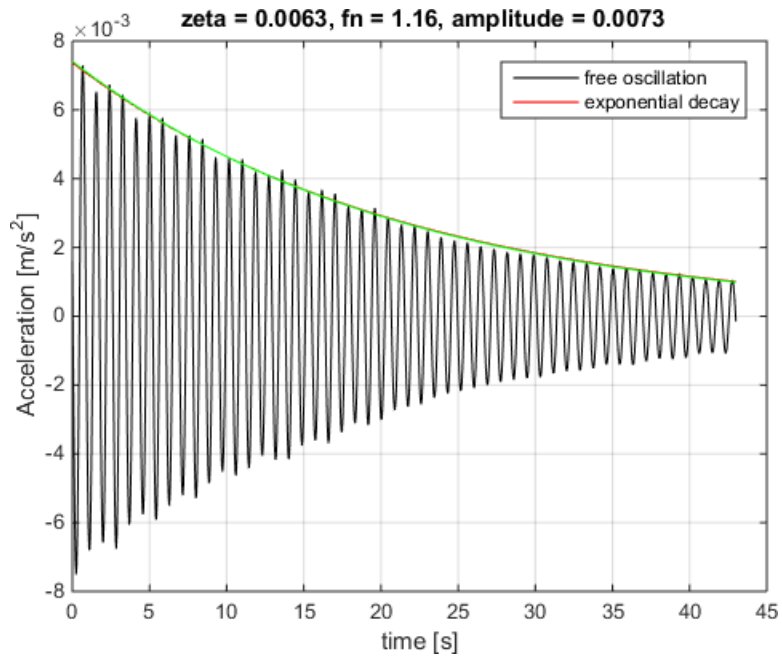
case 13, fn = 0.4, sensor 1



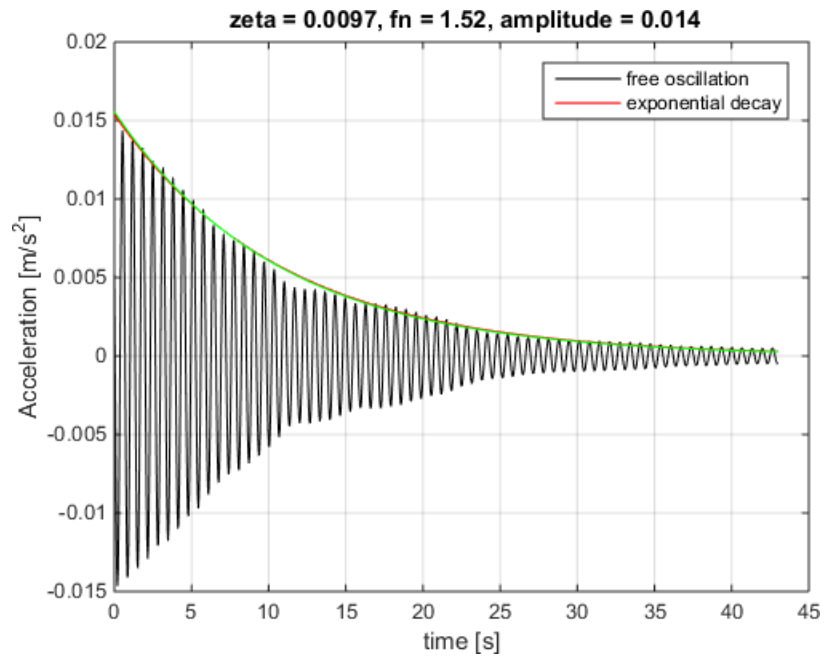
case 13, fn = 0.58, sensor 3



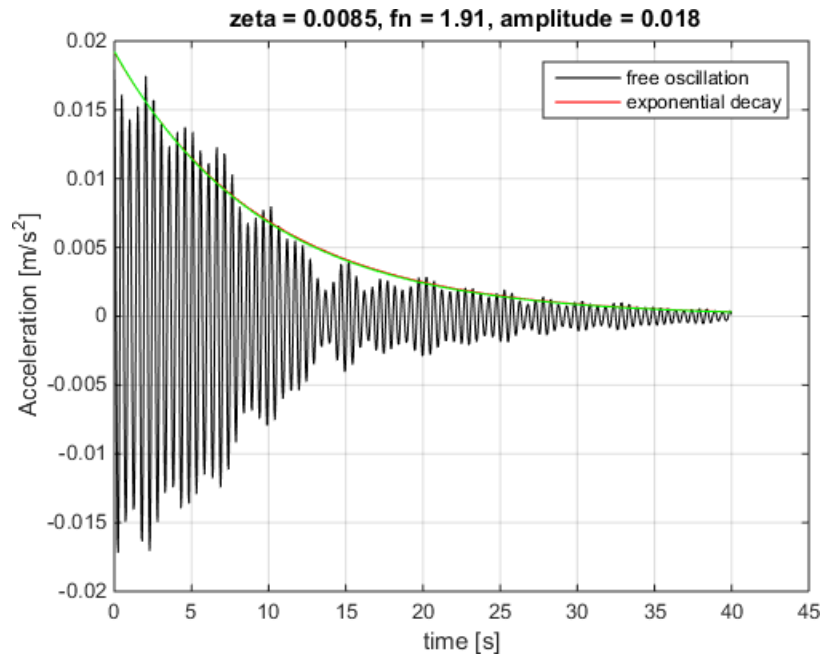
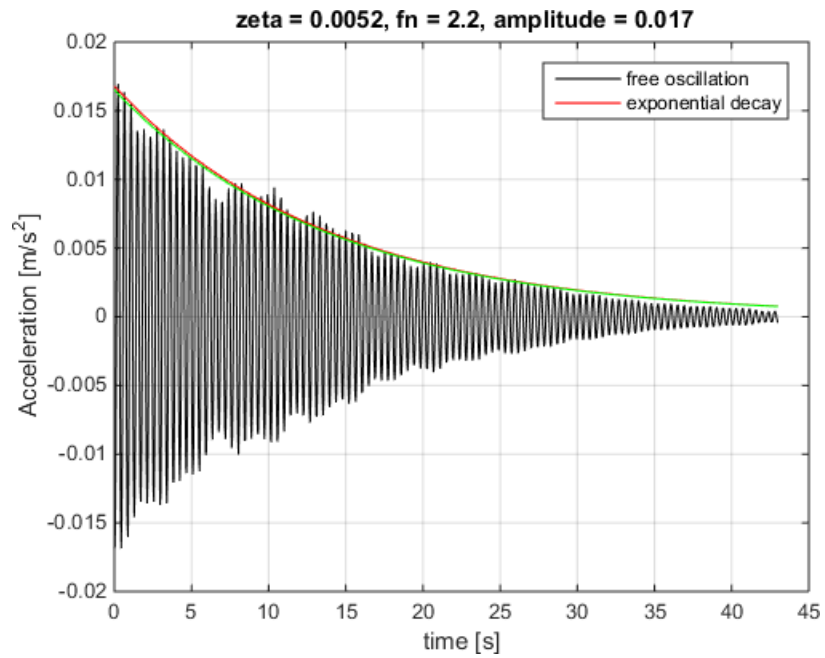
case 13, fn = 0.86, sensor 2

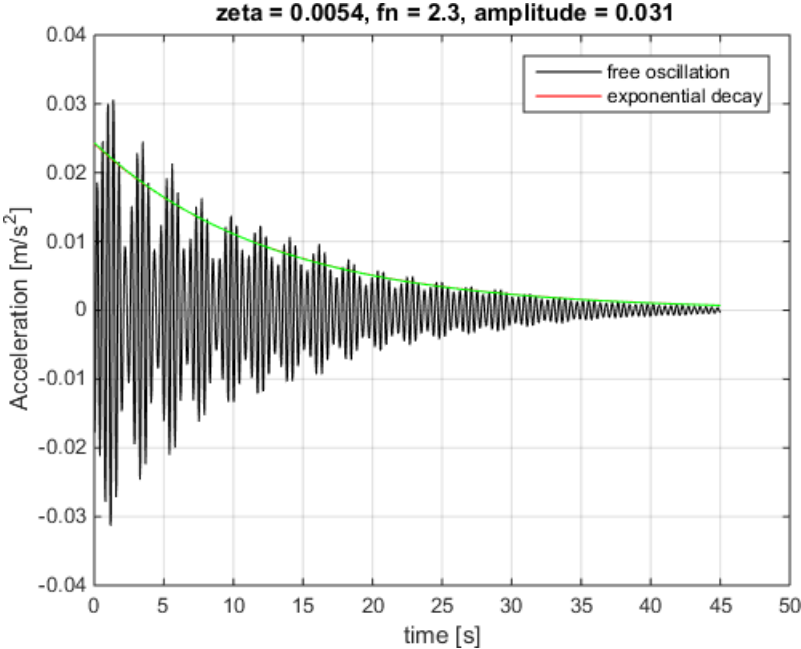


case 13, fn = 1.16, sensor 1

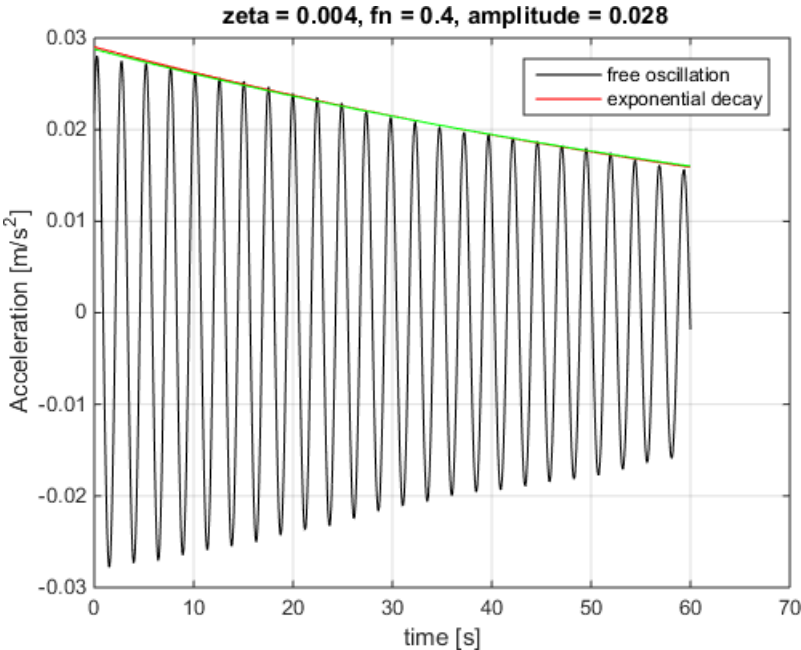


case 13, fn = 1.52, sensor 2

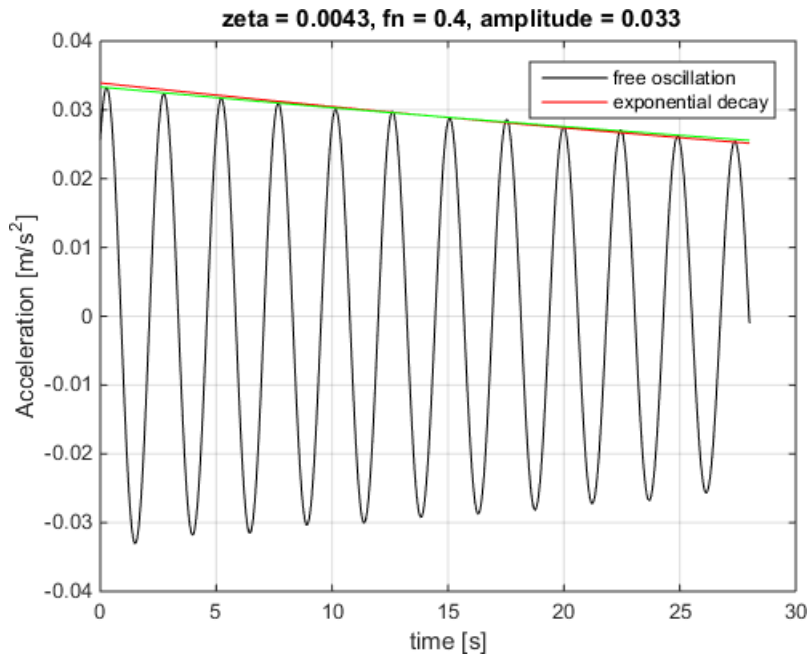
case 13, $f_n = 1.91$, sensor 4case 13, $f_n = 2.2$, sensor 2



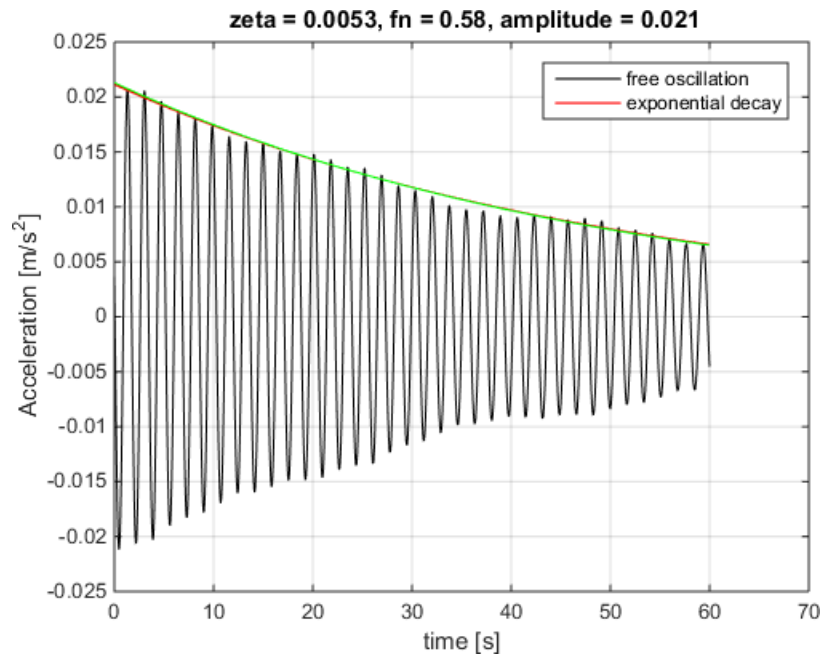
case 13, fn = 2.3, sensor 1



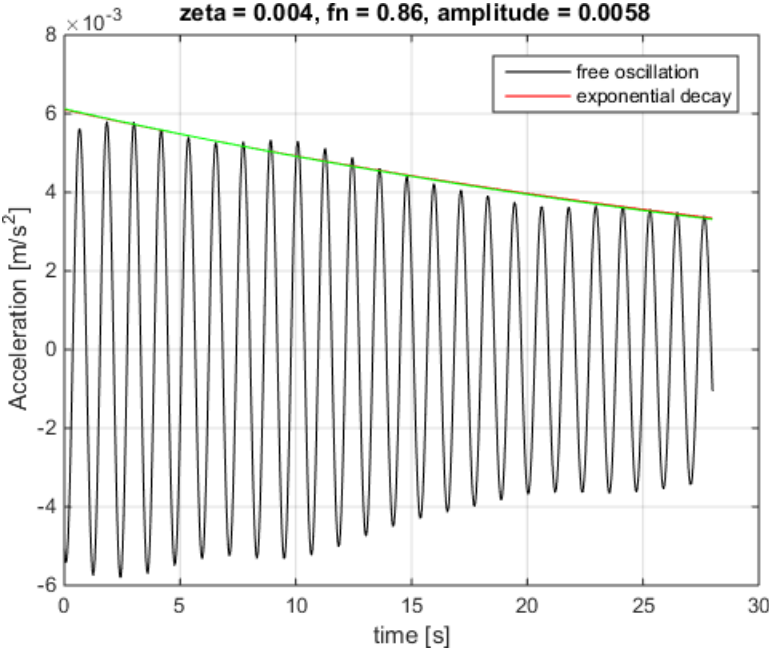
case 14, fn = 0.4, sensor 1



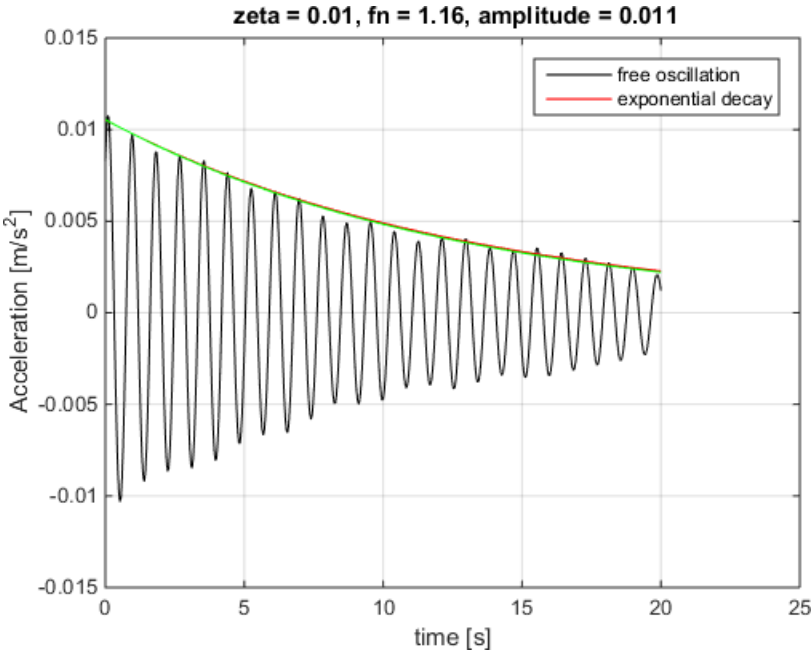
case 14, fn = 0.4, sensor 4



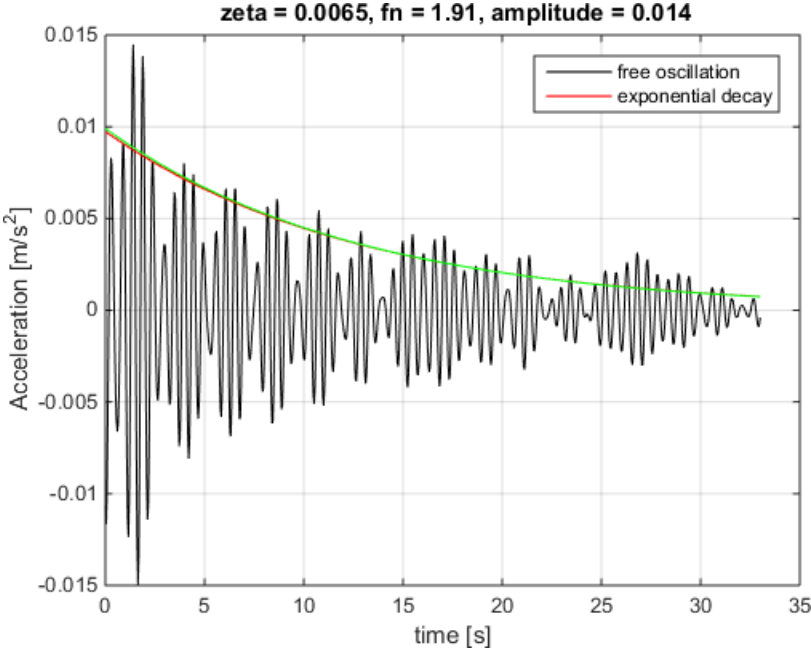
case 14, fn = 0.58, sensor 3



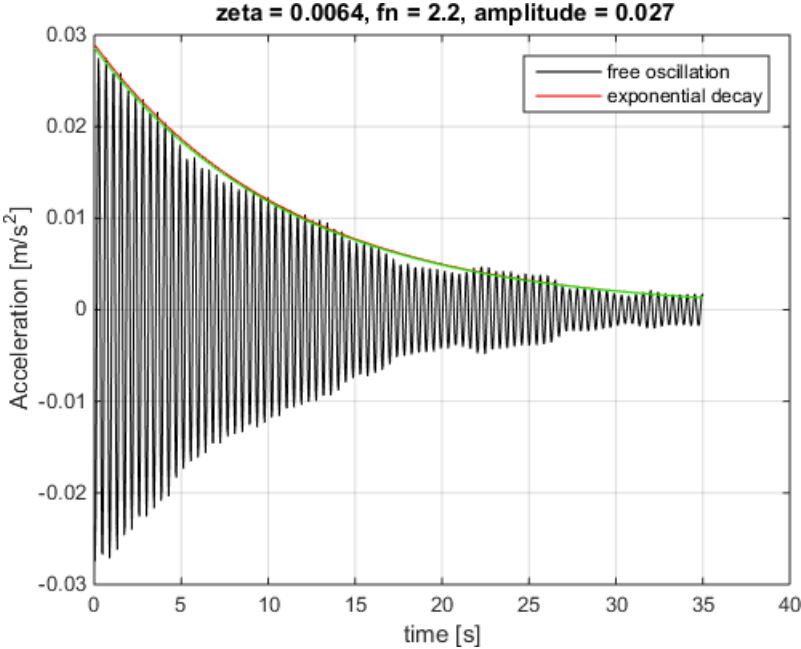
case 14, fn = 0.86, sensor 2



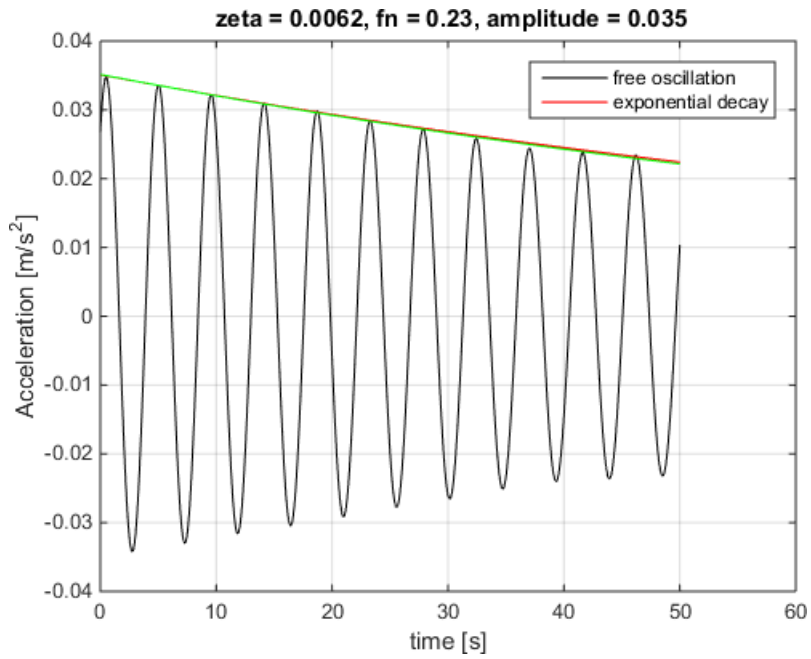
case 14, fn = 1.16, sensor 1



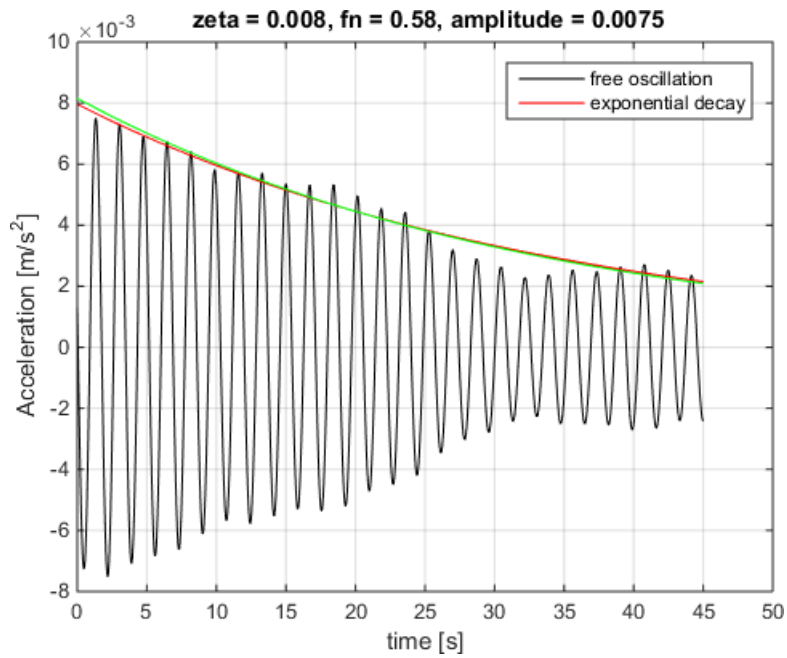
case 14, fn = 1.91, sensor 4



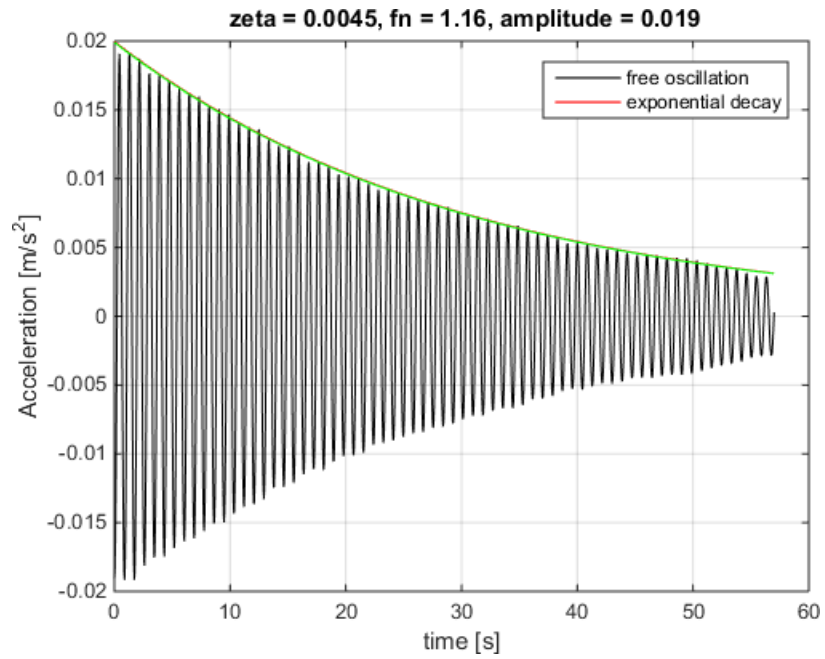
case 14, fn = 2.2, sensor 2



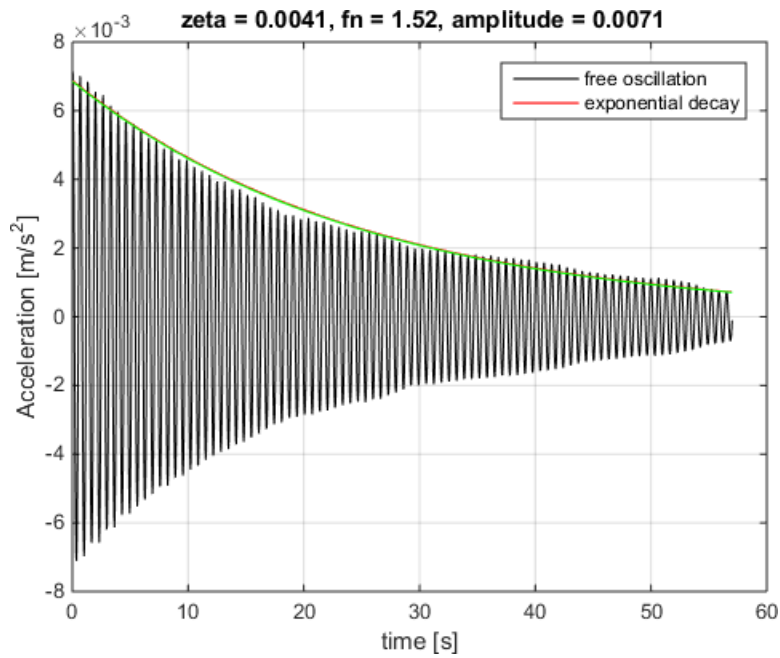
case 15, fn = 0.23, sensor 1



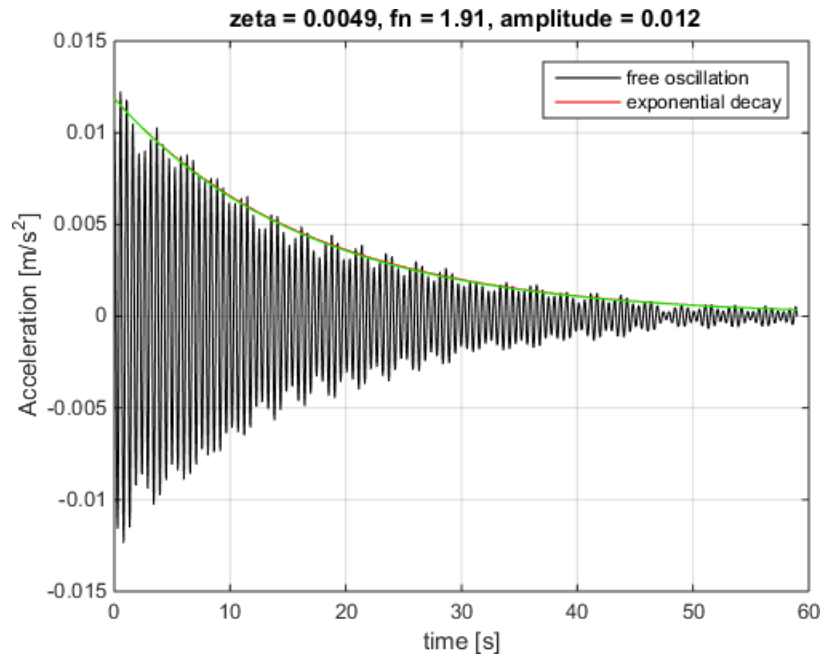
case 15, fn = 0.58, sensor 3



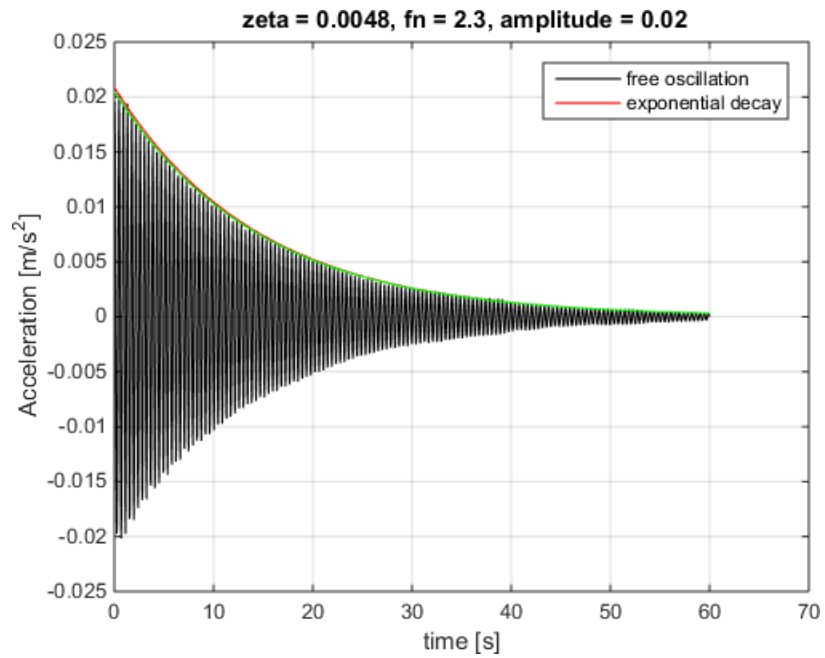
case 15, fn = 1.16, sensor 1



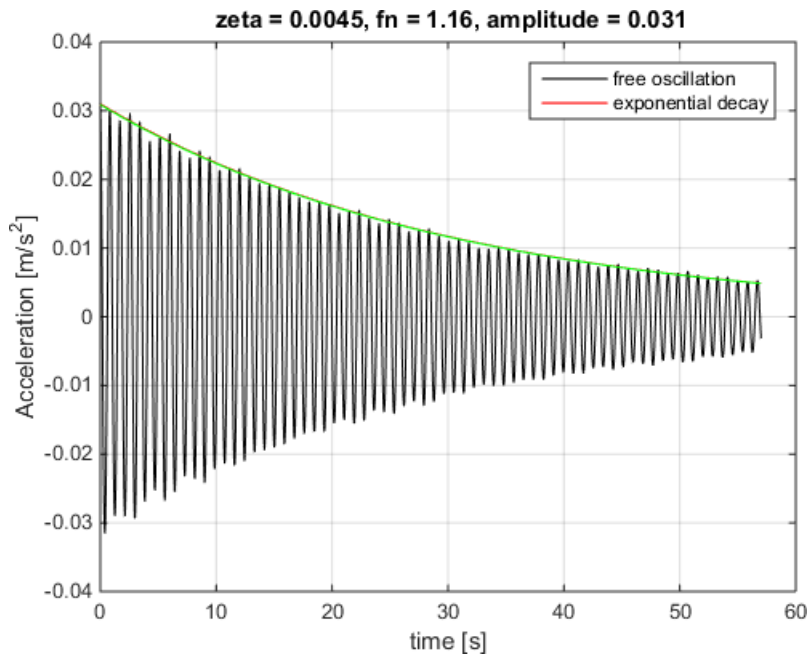
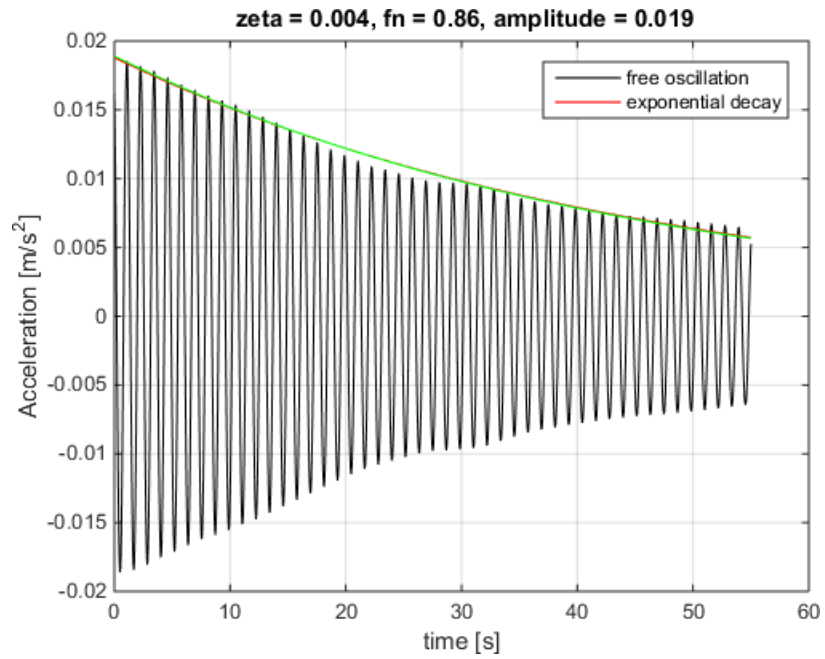
case 15, fn = 1.52, sensor 2

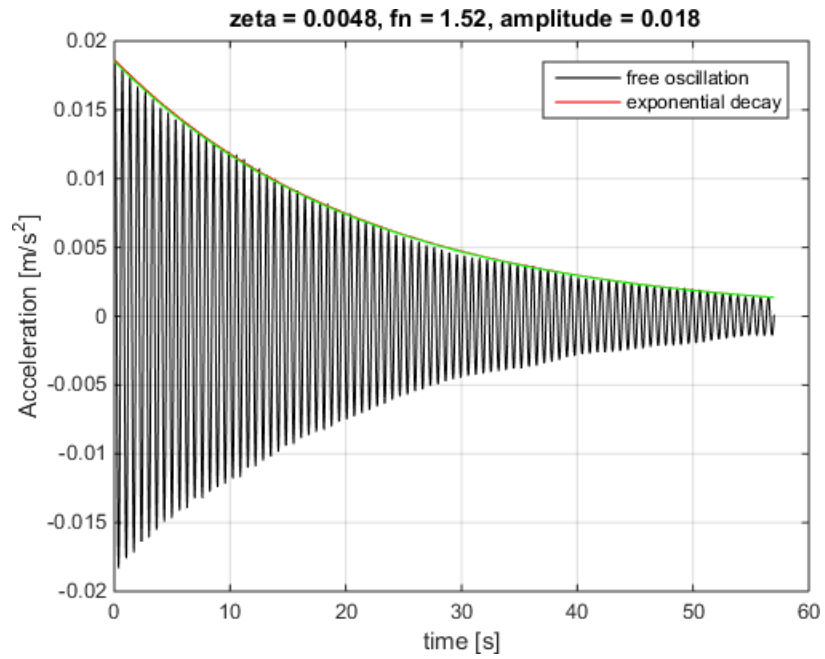


case 15, fn = 1.91, sensor 3

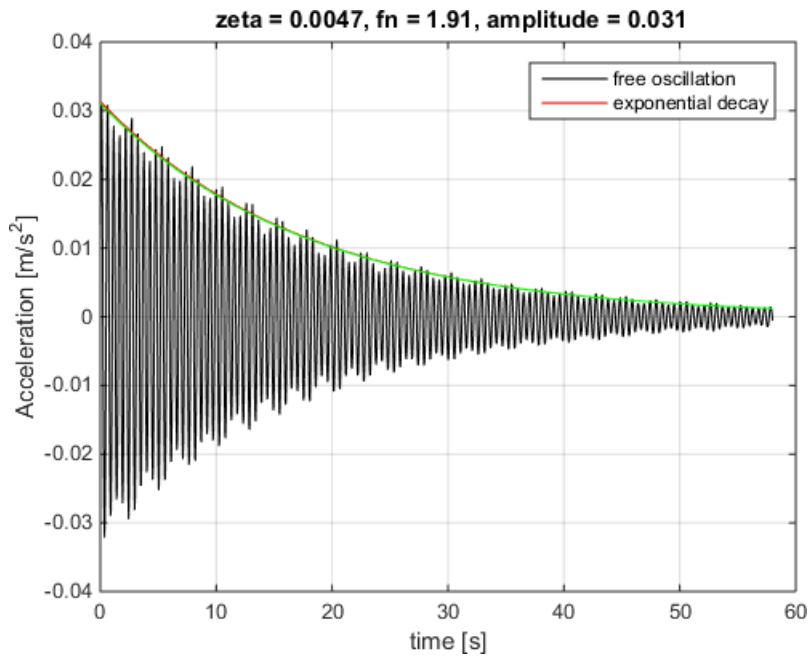


case 15, fn = 2.3, sensor 2

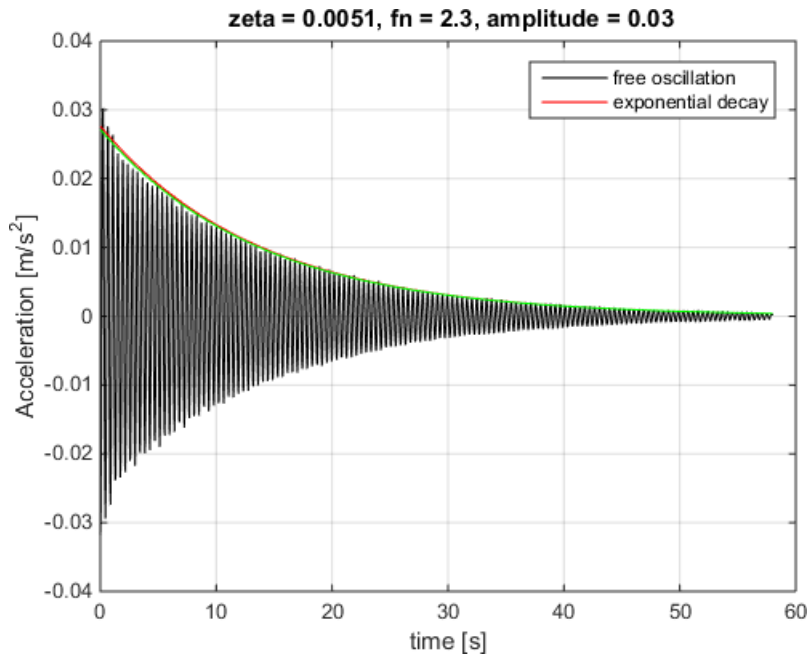




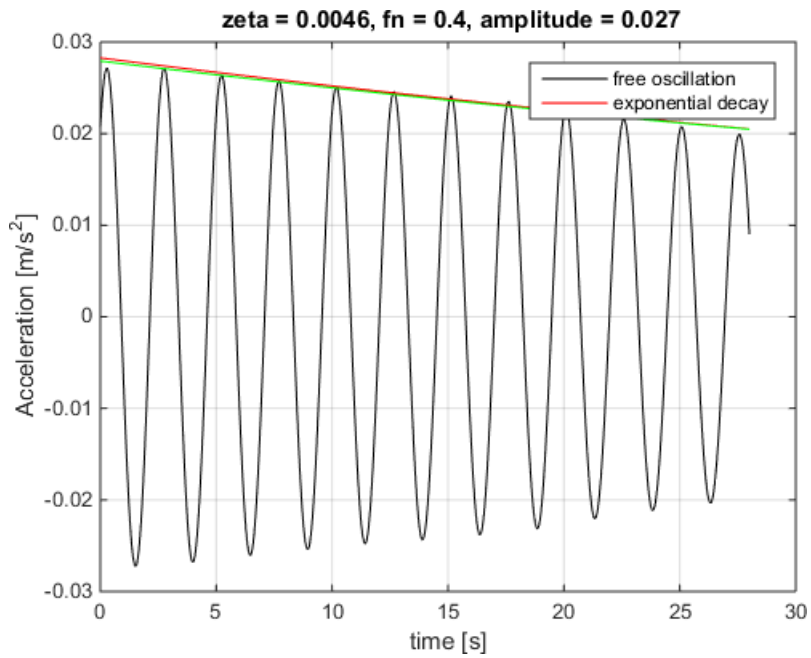
case 16, fn = 1.52, sensor 2



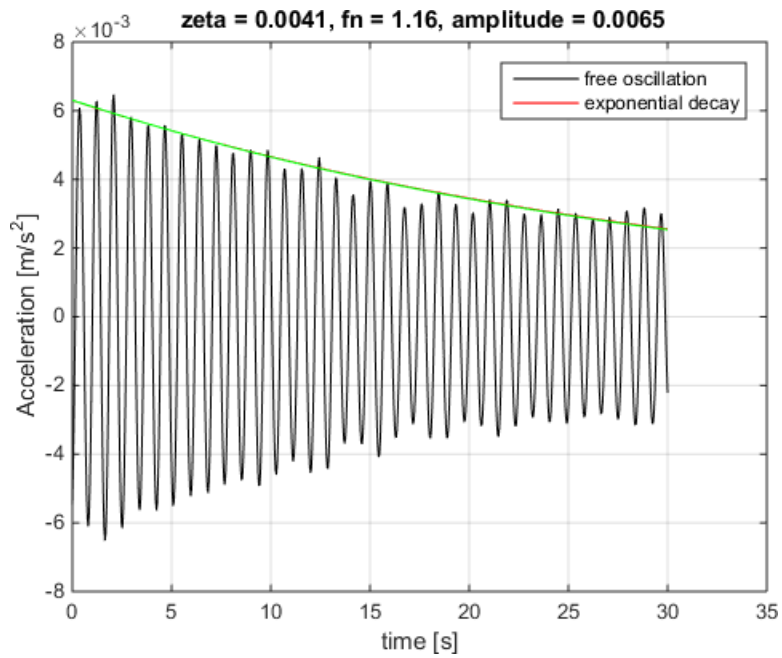
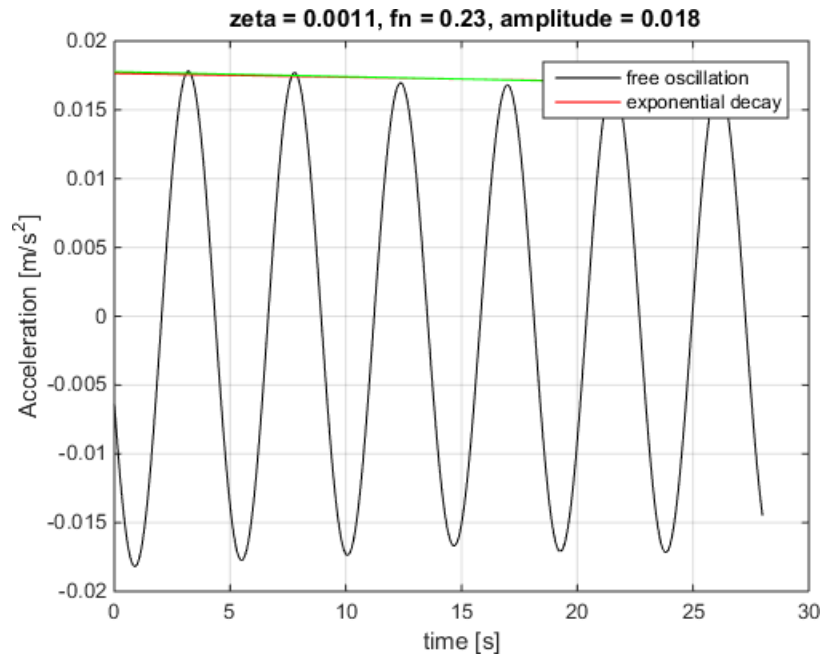
case 16, fn = 1.91, sensor 3

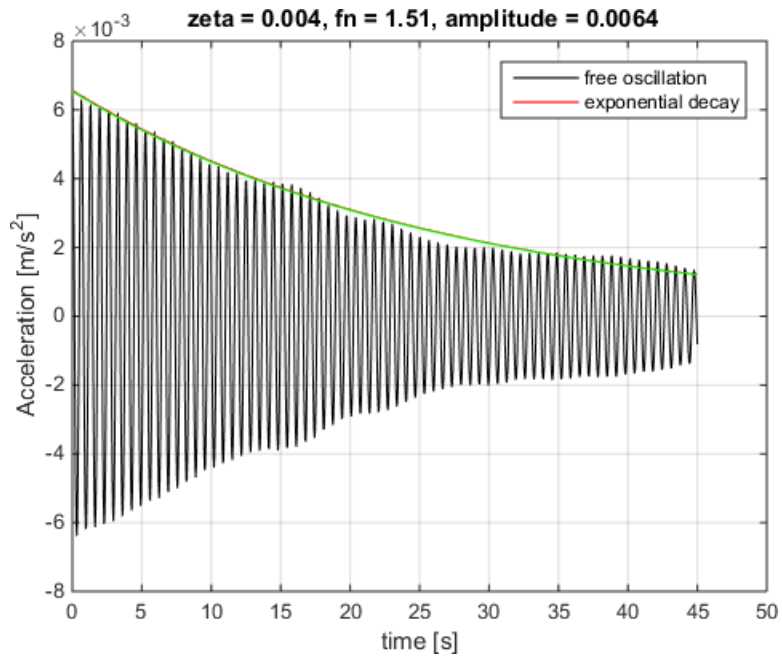


case 16, fn = 2.3, sensor 2

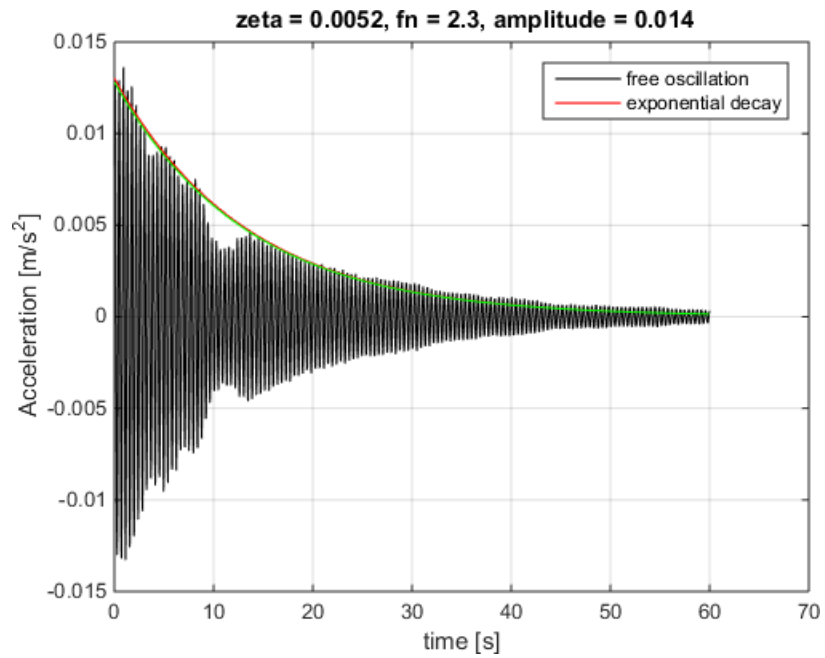


case 16, fn = 2.3, sensor 2

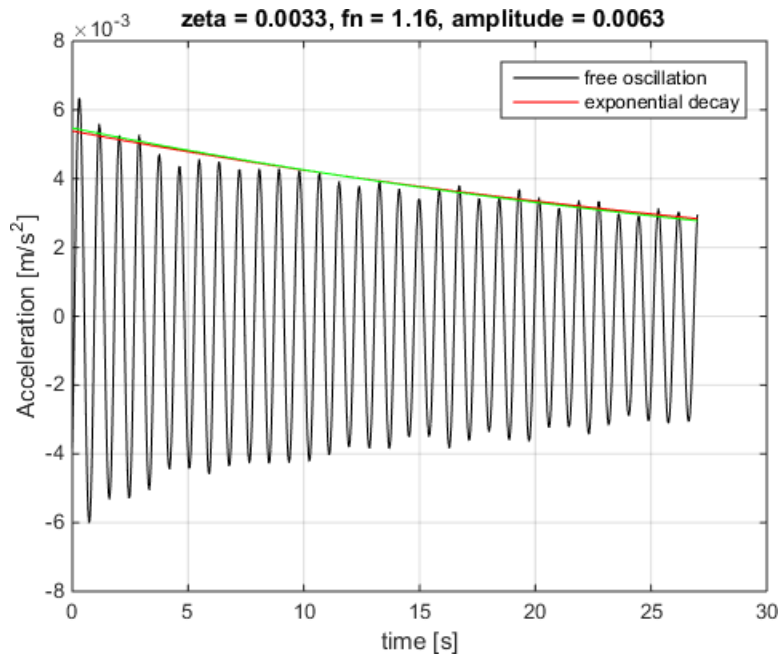




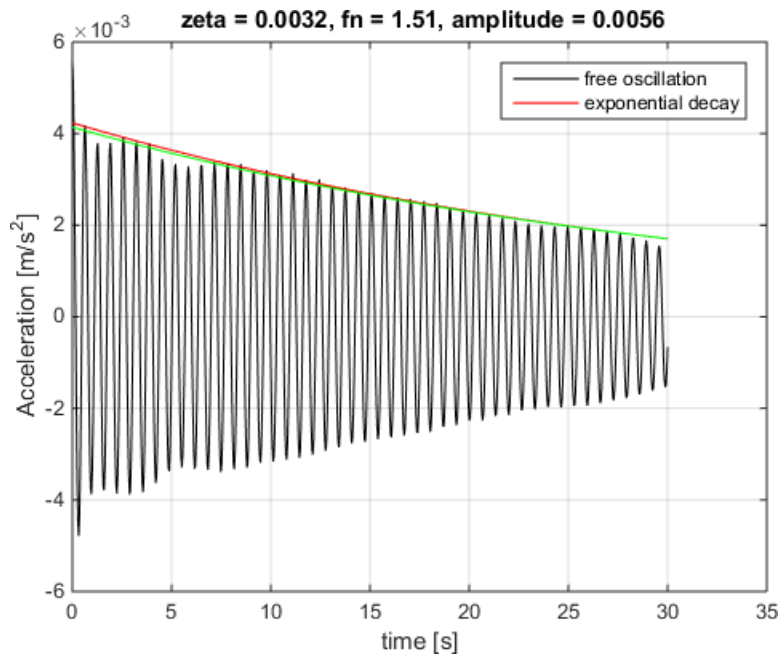
case 17, fn = 1.51, sensor 2



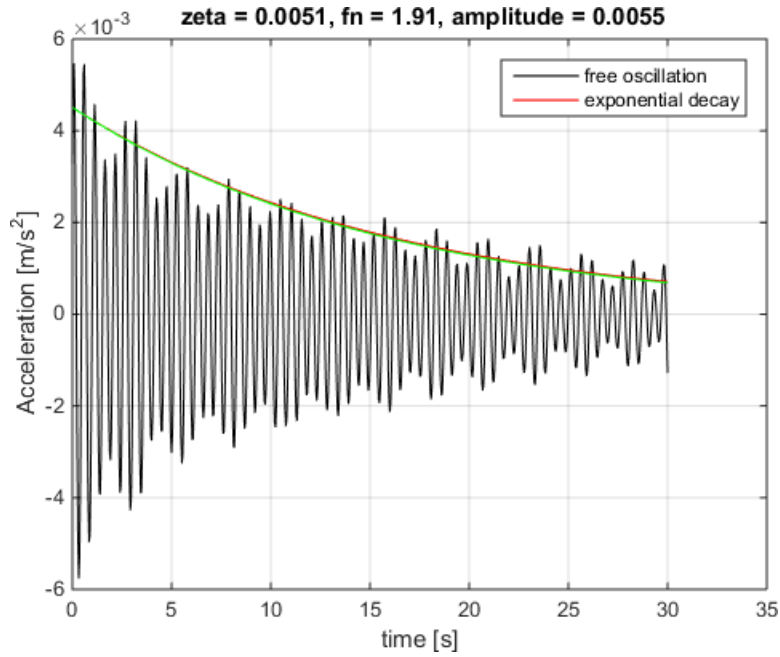
case 17, fn = 2.3, sensor 2



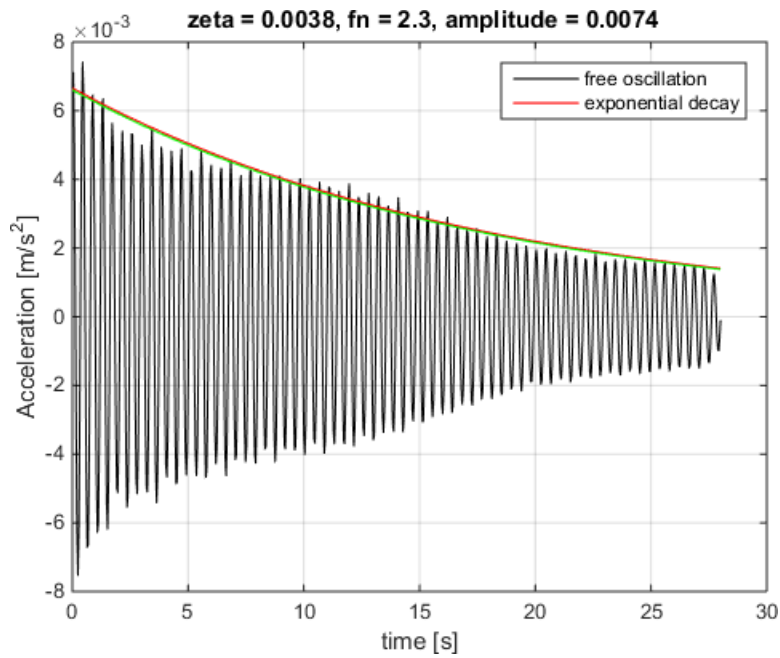
case 18, fn = 1.16, sensor 1



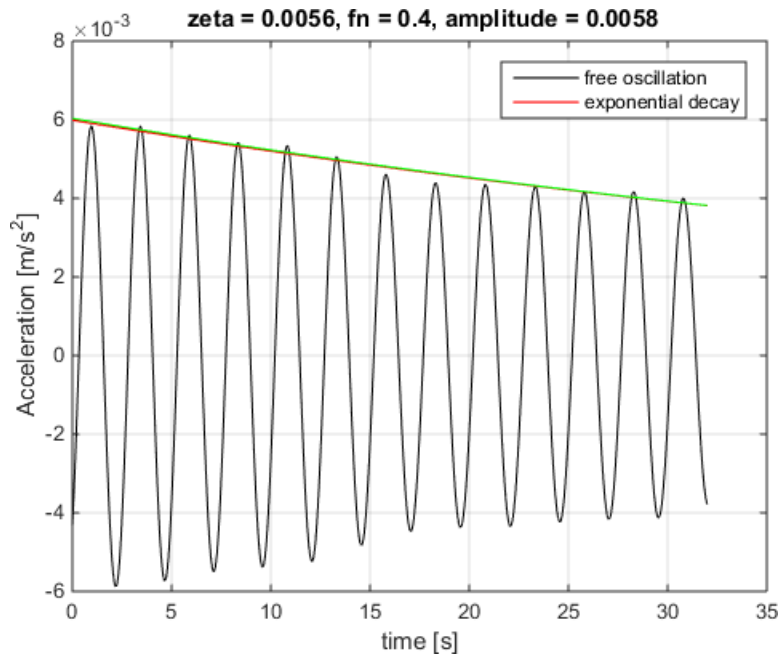
case 18, fn = 1.51, sensor 2



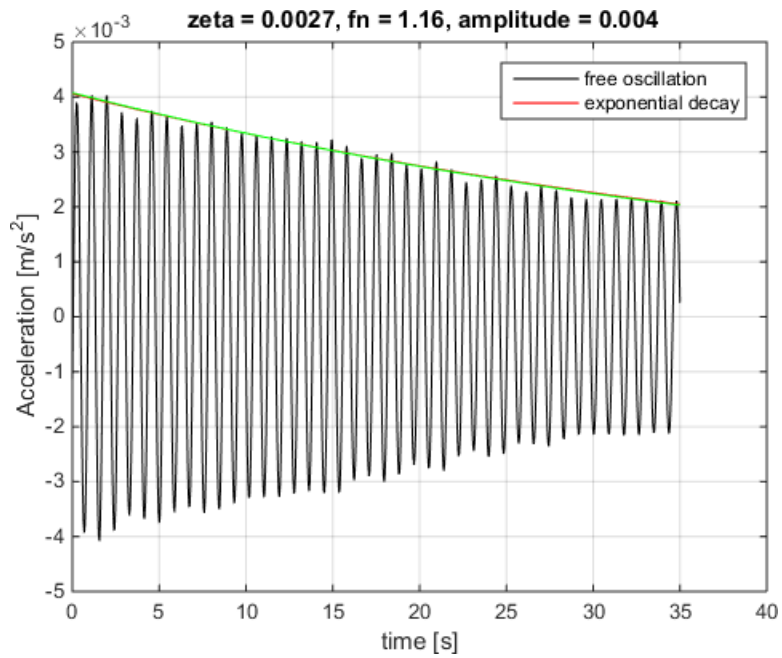
case 18, fn = 1.91, sensor 3



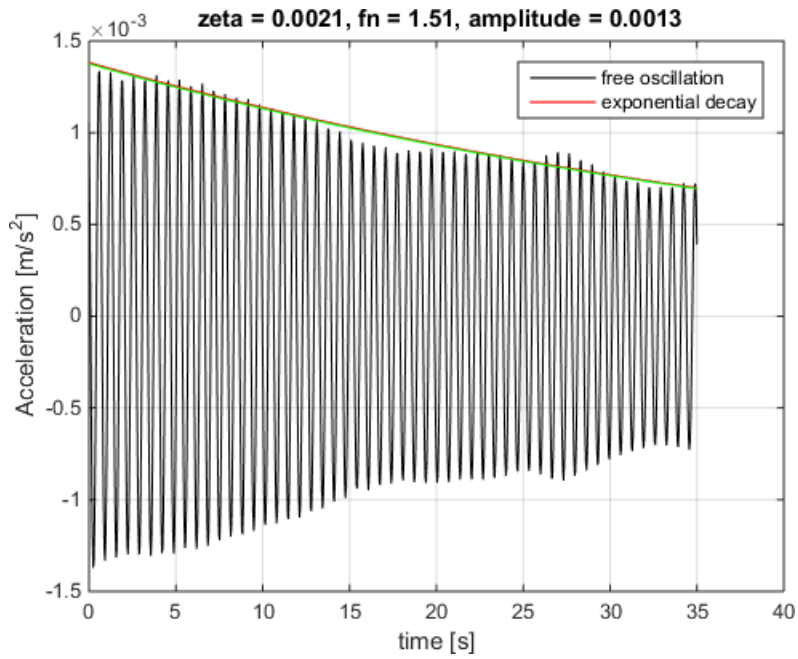
case 18, fn = 2.3, sensor 2



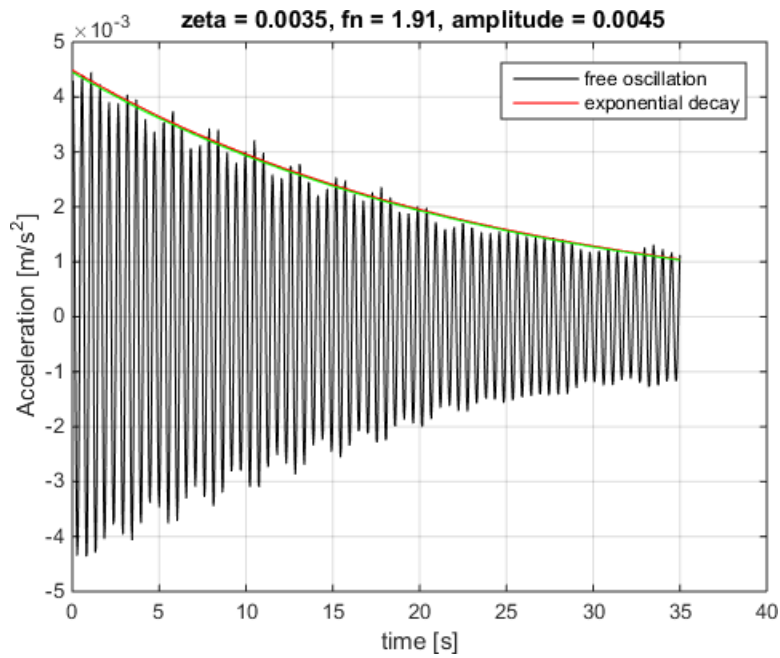
case 19, fn = 0.4, sensor 1



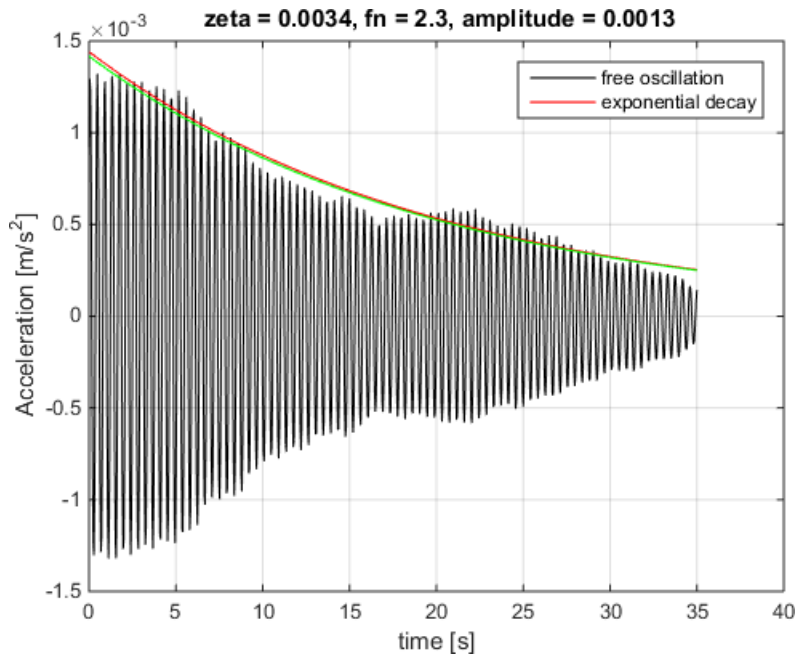
case 19, fn = 1.16, sensor 1



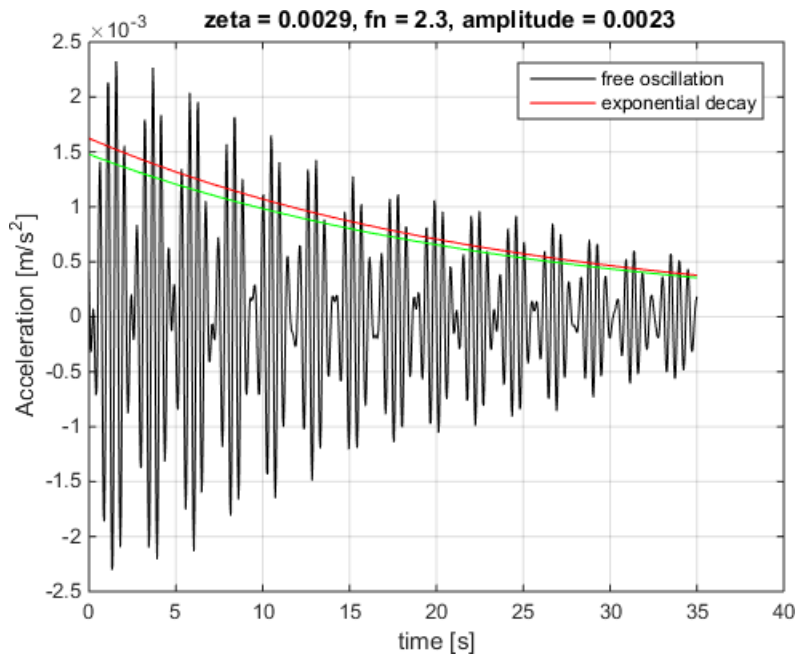
case 19, fn = 1.51, sensor 2



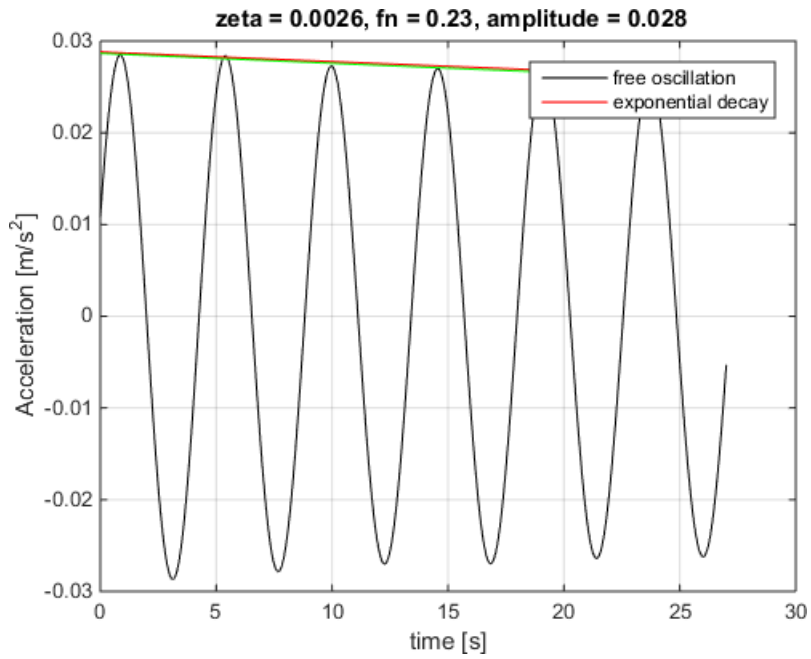
case 19, fn = 1.91, sensor 4



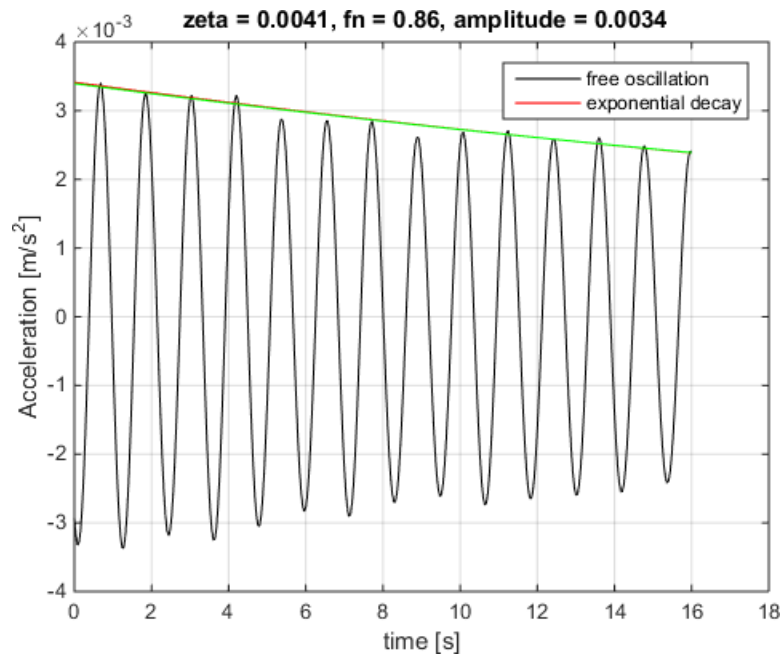
case 19, fn = 2.3, sensor 2



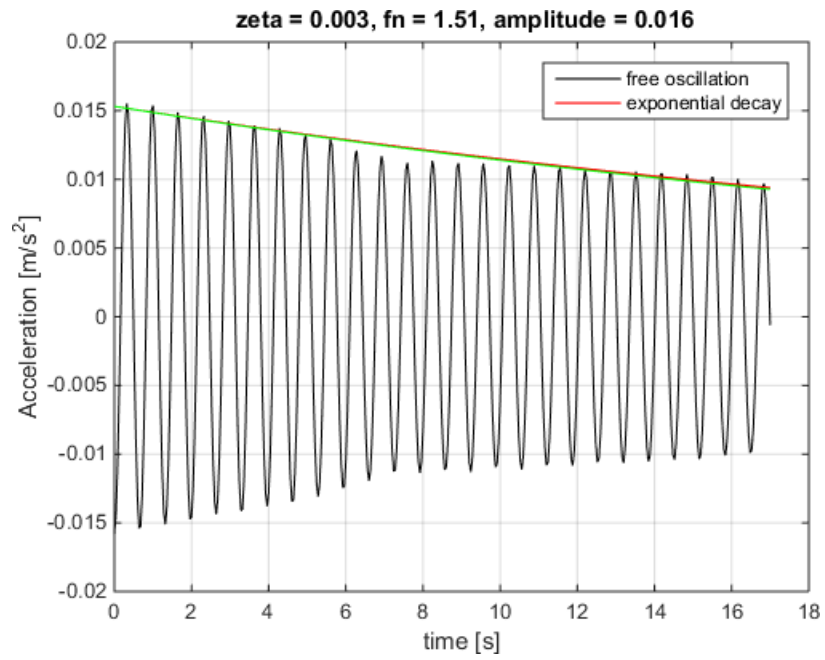
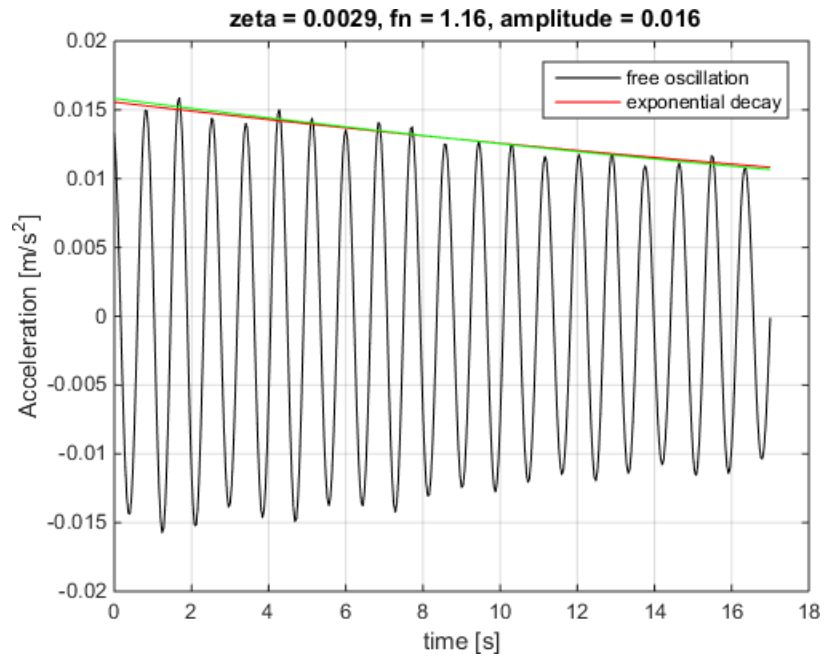
case 19, fn = 2.3, sensor 4

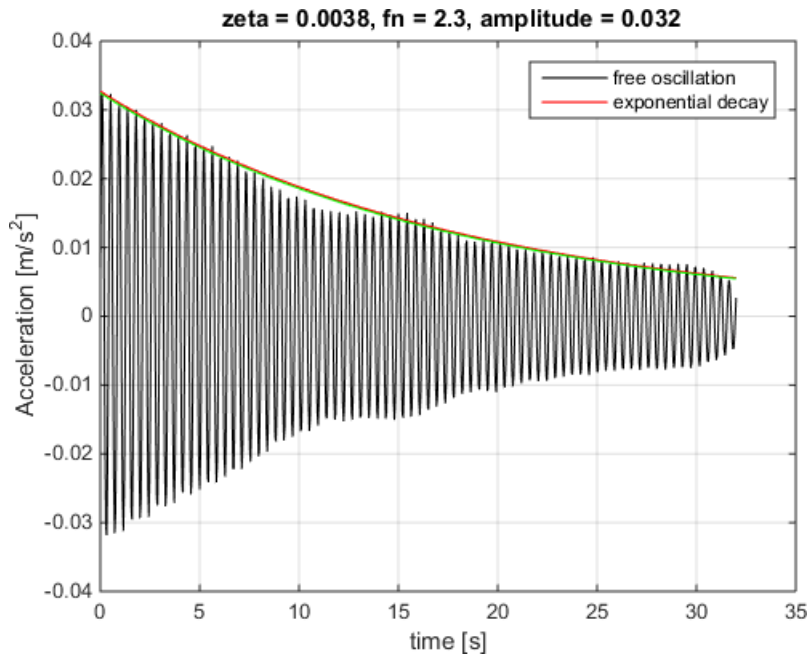


case 20, fn = 0.23, sensor 1

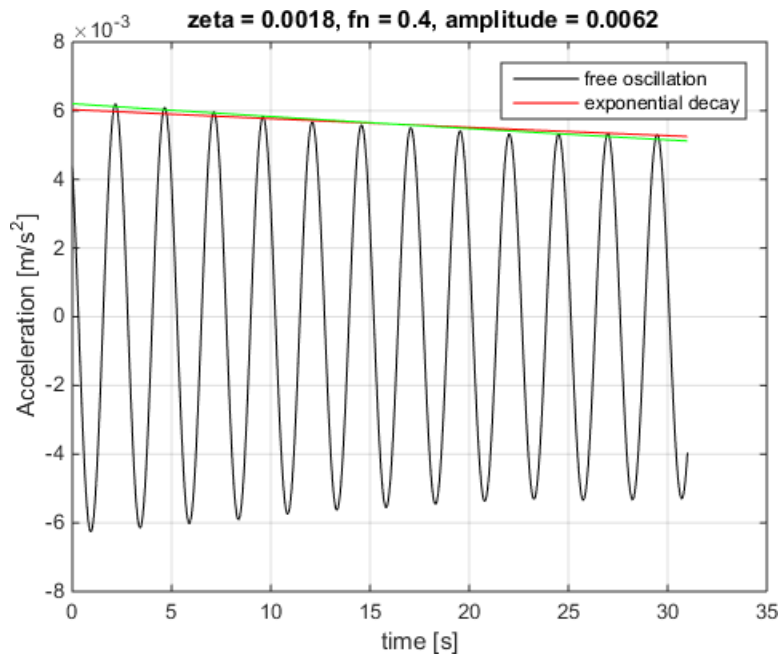


case 20, fn = 0.86, sensor 3

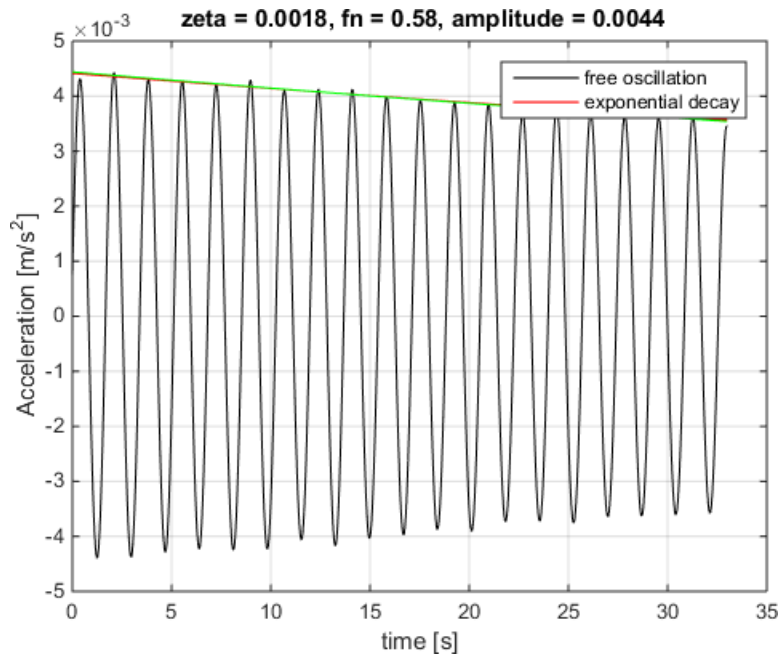




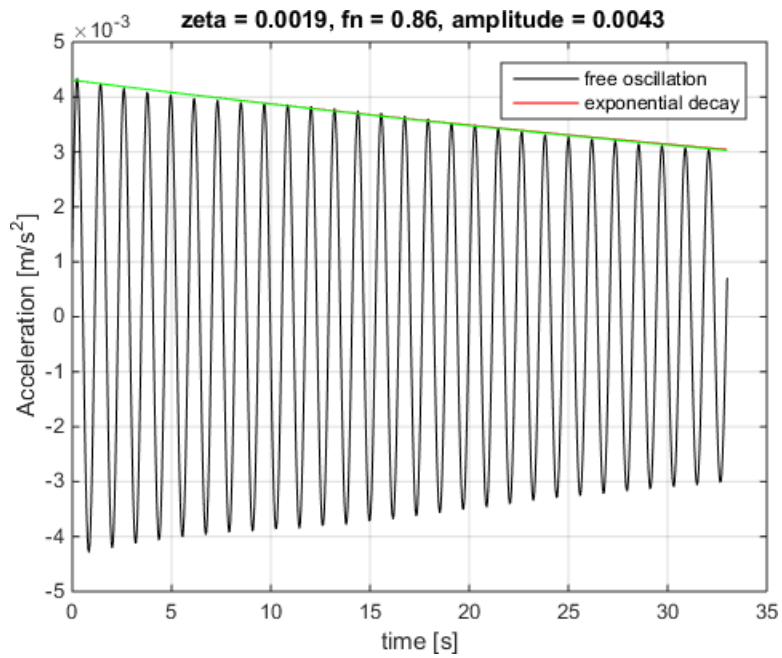
case 20, fn = 2.3, sensor 2



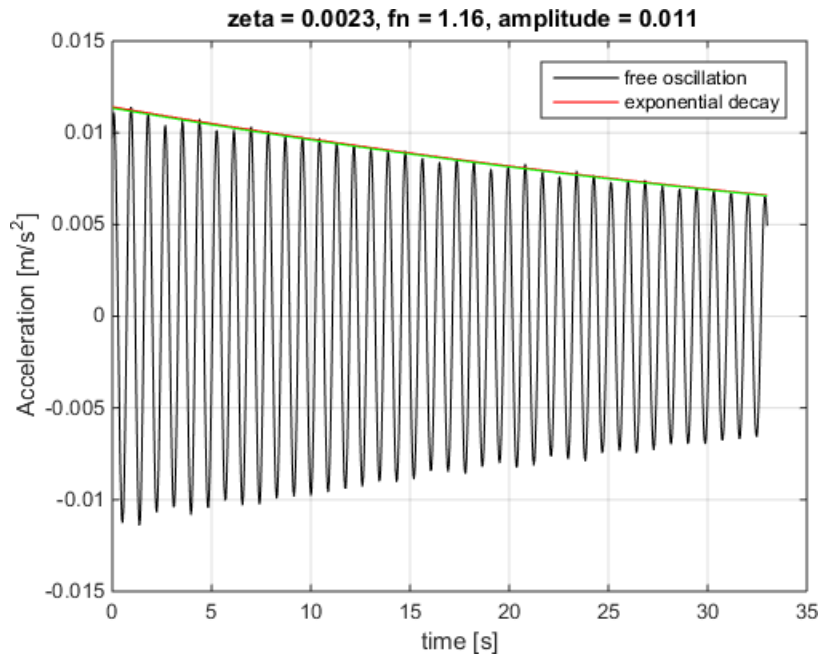
case 21, fn = 0.4, sensor 1



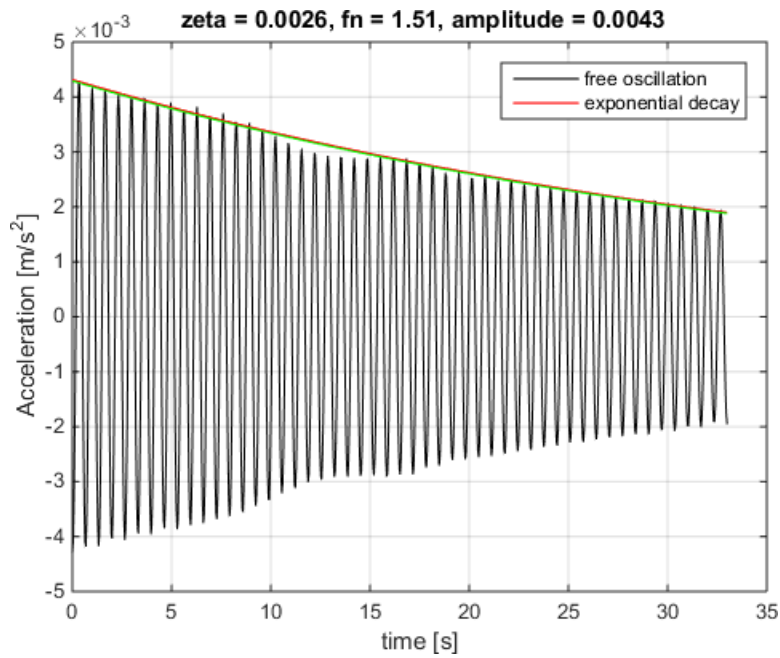
case 21, fn = 0.58, sensor 3



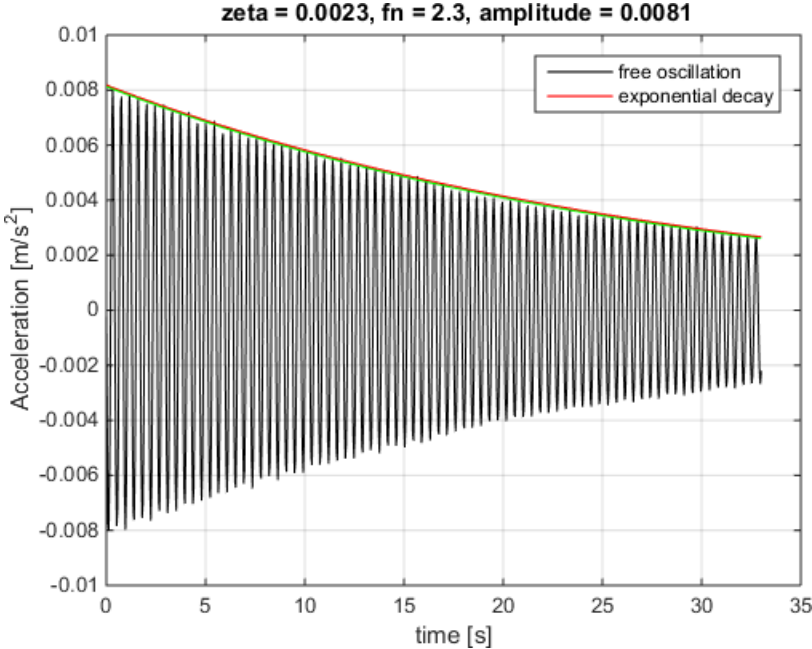
case 21, fn = 0.86, sensor 2



case 21, fn = 1.16, sensor 1



case 21, fn = 1.51, sensor 2



case 21, fn = 2.3, sensor 2